BEACHMED-e
OpTIMAL

BEACHMED-e
OpTIMAL

BEACH EROSION MONITORING

BEACH EROSION MONITORING

**Results from
BEACHMED-e / OpTIMAL Project**

Optimisation des Techniques Integrées
de Monitorage Appliquées aux Littoraux

Edited by Enzo Pranzini & Lilian Wetzel

Nuova Grafica Fiorentina

BEACH EROSION MONITORING

Results from
BEACHMED-e / OpTIMAL Project

Optimisation des Techniques Integrées
de Monitorage Appliquées aux Littoraux

Edited by Enzo Pranzini & Lilian Wetzel

Cover picture: 3D ortho-image of Mauguio-Carnon Harbour (France, Hérault Department), april 2007. Image built by a mixed of aerial photo and digital elevation model (EID Méditettanée).

Authors

Belén Alonso
Institut de Ciències del Mar, CSIC. Grup de Marges Continentals. Passeig Marítim de la Barceloneta, 37-49, 08003, Barcelona, España

Renata Archetti
Dipartimento di Ingegneria delle Strutture, dei Trasporti, delle Acque, del Rilevamento, del Territorio - DISTART Università degli Studi di Bologna, Viale Risorgimento 2, 40136 Bologna, Italia

Dan Bowman
Ben-Gurion University of the Negev, P.O.B. 653, Beer Sheva 84105, Israel

Massimo Brignone
Dipartimento di Informatica - Università degli Studi di Verona, Ca'Vignal 2, 37134 Verona, Italia

Ruggero Casacchia
CNR - Consiglio Nazionale delle Ricerche, P.le Aldo Moro 7, 00185 Roma, Italia

David Casas
Institut de Ciències del Mar, CSIC, Grup de Marges Continentals, Passeig Marítim de la Barceloneta 37-49, 08003 Barcelona, España

Nektarios Chrysoulakis
Foundation for Research and Technology – Hellas, Institute of Applied and Computational Mathematics, Vassilika Vouton, P.O. Box 1527, GR-71110, Heraklion, Crete, Hellas

Nicola Corradi
Dipartimento per lo studio del Territorio e delle sue Risorse, Università degli Studi di Genova, Corso Europa 26, 16132 Genova, Italia

Gian Luigi De Filippi
DEAM s.r.l., Via Casina 11, S. Martino a Ulmiano (PI), Italia

Nunzio De Nigris
Ingegneria Ambientale ARPA Emilia-Romagna, Vicolo Carega 3, Bologna, Italia

Cléa Denamiel
EID Méditerranée, 165 avenue Paul Rimbaud F- 34184 Montpellier Cedex, France

Claudia Dessy
Dipartimento per lo studio del Territorio e delle sue Risorse - Università degli Studi di Genova, Corso Europa 26, 16132 Genova, Italia

Eleonora Duchini
DEAM s.r.l., Via Casina 11, S. Martino a Ulmiano (PI), Italia

Ruth Durán
Institut de Ciències del Mar, CSIC, Grup de Marges Continentals, Passeig Marítim de la Barceloneta 37-49. 08003 Barcelona, España

Gemma Ercilla
Institut de Ciències del Mar, CSIC, Grup de Marges Continentals. Passeig Marítim de la Barceloneta 37-49, 08003 Barcelona, España

Ferran Estrada
Institut de Ciències del Mar, CSIC, Grup de Marges Continentals, Passeig Marítim de la Barceloneta 37-49, 08003 Barcelona, España

Marcel-lí Farrán
Institut de Ciències del Mar, CSIC, Grup de Marges Continentals, Passeig Marítim de la Barceloneta 37-49, 08003, Barcelona, España

Marco Ferrari
Dipartimento per lo studio del Territorio e delle sue Risorse, Università degli Studi di Genova, Corso Europa n. 26, 16132 Genova, Italia

Pierre Gauffres
CETMEF, 2 Bd Président Kennedy, 13097 Aix-en-Provence cedex 2. France

Anastasios N. Georgoulas
Democritus University of Thrace, School of Engineering, 67100 Xanthi, Hellas

Hugues Heurtefeux
EID Méditerranée, 165 avenue Paul Rimbaud, F- 34184 Montpellier Cedex, France

Niccolò Iandelli
Dipartimento di Scienze della Terra, Università degli Studi di Firenze, Borgo Albizi 28, 50122 Firenze, Italia

Yiannis Kamarianakis
Foundation for Research and Technology - Hellas, Institute of Applied and Computational Mathematics, Vassilika Vouton, P.O. Box 1527, GR-71110, Heraklion, Crete, Hellas

Nikolaos Aristides Kampanis
Foundation for Research and Technology - Hellas, Institute of Applied and Computational Mathematics, Vassilika Vouton, P.O. Box 1527, GR-71110, Heraklion, Crete, Hellas

Theophanis Vassilios Karambas
University of the Aegean, Department of Marine Science, University Hill 81100, Mytilene, Hellas

Nikolaos Evangelos Kotsovinos
Democritus University of Thrace, School of Engineering, 67100 Xanthi, Hellas

Alberto Lamberti
Dipartimento di Ingegneria delle Strutture, dei Trasporti, delle Acque, del Rilevamento, del Territorio - DISTART Università degli Studi di Bologna, Viale Risorgimento 2, 40136 Bologna, Italia

Giovanni Battista La Monica
DST - Dipartimento di Scienze della Terra, Università degli Studi di Roma "La Sapienza", P.le Aldo Moro 5, 00185 Roma, Italia

Audrey Lesaignoux
EID Méditerranée, 165 avenue Paul Rimbaud, F- 34184 Montpellier Cedex, France

Michalis Lipakis
Eastern Crete Development Organisation (OANAK), 3 Mahis Kritis Str., 713 03, Heraklion, Crete, Hellas

Matteo Monti
Ingegneria Ambientale ARPA Emilia-Romagna, Vicolo Carega 3, Bologna, Italia

Maurizio Morelli
Ingegneria Ambientale ARPA Emilia-Romagna, Vicolo Carega 3, Bologna, Italia

Marta Nuez
Institut de Ciències del Mar, CSIC, Grup de Marges Continentals, Passeig Marítim de la Barceloneta 37-49, 08003 Barcelona, España

Alexandros Pantazis
University of the Aegean, Department of Marine Science, University Hill 81100, Mytilene, Hellas

Elisabetta Petrocchi
DST - Dipartimento di Scienze della Terra, Università degli Studi di Roma "La Sapienza", P.le Aldo Moro 5, 00185 Roma, Italia

Enzo Pranzini
Dipartimento di Scienze della Terra, Università degli Studi di Firenze, Borgo Albizi 28, 50122 Firenze, Italia

Mentino Preti
Ingegneria Ambientale ARPA Emilia-Romagna, Vicolo Carega 3, Bologna, Italia

Didier Rihouey
CASAGEC/UPPA, 1 allée du Parc Montaury, 64600 Anglet, France

Maria Cristina Salvatore
DST - Dipartimento di Scienze della Terra, Università degli Studi di Roma "La Sapienza", P.le Aldo Moro 5, 00185 Roma, Italia

Rosamaria Salvatori
CNR - Consiglio Nazionale delle Ricerche - Istituto sull'Inquinamento Atmosferico, Via Salaria km 29.300, C.P. 10 - 00016 Monterotondo, Roma, Italia

Chiara Francesca Schiaffino
Dipartimento per lo studio del Territorio e delle sue Risorse, Università degli Studi di Genova, Corso Europa 26, 16132 Genova, Italia

Daniela Simonetti
Dipartimento di Scienze della Terra, Università degli Studi di Firenze, Borgo Albizi 28, 50122 Firenze, Italia

Paolo Tortora
DST - Dipartimento di Scienze della Terra, Università degli Studi di Roma "La Sapienza", P.le Aldo Moro 5, 00185 Roma, Italia

Lilian Wetzel
Dipartimento di Scienze della Terra, Università degli Studi di Firenze, Borgo Albizi 28, 50122 Firenze, Italia

Foreword

The *Coastal Zone* is that space in which terrestrial environments influence marine environments and *vice versa*. The *Coastal Zone* of Mediterranean countries, and in particular alluvial plains characterised by sand and gravel beaches, are territory of special interest for sustainable strategic development. In these areas social and economic interests and the protection of natural ecosystems must meet the target of Integrated Coastal Zone Management (ICZM). ICZM means a dynamic process for the sustainable management and use of coastal zones, taking into account the fragility of coastal ecosystems and landscapes.

In Madrid, Spain, on 20-21 January 2008, the *ICZM Protocol on Integrated Coastal Zone Management in the Mediterranean* was signed by fourteen Contracting Parties to the Barcelona Convention (Italy, France, Spain and Greece among the others). The Protocol will enable the countries to increase the management strategies for their coastal zones, as well as to deal with the emerging coastal environment challenges, such as the forecasted climate change.

BEACHMED-e is an INTERREG III C Regional Framework Operation (RFO) entitled "Strategic management of beach protection measures for the sustainable development of Mediterranean coastal areas". BEACHMED-e is the result of the collaboration among 9 regional partners of 4 EU Nations: Italy, France, Spain and Greece. The RFO provides for the development of 9 Subprojects with the participation of 36 public institutes (universities, institutes of research and local administrations) that have applied for a public call. The 9 Subprojects refer to the *Measures* of 3 technical *Components*.

OpTIMAL (Optimisation of Integrated Monitoring Techniques Applied to Coastlines) Subproject belongs to *Component 2* of BEACHMED-e Operation, whose general objectives are the design and implementation of technical instruments to characterise erosion at the European scale for the sustainable use of resources. A well-defined request was made by the BEACHMED-e Partner Regions following the initial Objectives Report for an in-depth analysis of monitoring processes and their suitability as a tool for assessing the morphological status of the coast.

Quantitative analysis of the morphological and sedimentary evolution of coastlines plays an essential part in the integrated management of coastal zones, and is especially critical when planning the implementation of future conservation initiatives and in assessing their effectiveness. The observation of phenomena has to take place within a limited timeframe and therefore it requires the use of extremely accurate and high-quality data gathering and processing procedures. Spatial and temporal data resolution has to adapt to all its possible variables in order to obtain a low cost/benefit ratio, which is also required for effective management to take place. Data have to be standardised and managed in order to be widely applicable to Europe.

The main goals of OpTIMAL were: the development of morphological beach survey methodologies aimed at monitoring their evolution, based on various timescales, and assessing precision based on sample sites which are characterised by different morphological and sedimentary dynamics; to define, verify and illustrate new methods for the assessment of coastal sand movements on a scale which uses several sedimentary cells; tools for determining coastline operational position after beach nourishment interventions and distribution of dumped sediments along the shoreface and nearshore in relationship with beach grain size characteristics.

The experiences gathered along the pilot sites by the 10 partners of the OpTIMAL subproject will be very useful for the National, Regional and Local Administrations participating of the BEACHMED-e Operation; in addition, the publication of this Volume in English (besides the report in French available on the BEACHMED-e website) has the specific goal to make this information available to a wider audience.

Luigi E. Cipriani
Responsibile for BEACHMED-e, Component 2 and Measure 2.1 (OpTIMAL)
Regione Toscana - Direzione Generale delle Politiche Territoriali e Ambientali

Managing Mediterranean beaches: The need for quality and standardised data in beach monitoring at different scales

Enzo Pranzini, Lilian Wetzel

Coastal zones all over the world are part of a unique and sensitive environment that is the stage of a myriad of uses – and therefore conflicts – which can be brought into pacific coexistence through a very slow but dynamic and articulated process of decision-making called Integrated Coastal Zone Management[1]. The Mediterranean, for centuries celebrated as the cradle of western civilisation, has one of the most threatened coastlines in the world, and because of its physical peculiarities and the contrasting socio-economic realities of its bordering countries it must undergo vital management challenges regarding the impacts over natural resources and the effects of coastal urbanisation (Hinrichsen, 1998). In fact, two related aspects of the developed, often urbanised, Mediterranean coasts draw the immediate attention of non-Mediterranean visitors: the economic value of the sandy stretch that we, as scientists or tourists, call *the beach*, and how strenuously this is being defended from events that in many other places of the world are just part of a balance that is allowed to proceed naturally. It is a fact that the management of such Mediterranean beaches is of key importance because of the threat they bear, the highly-priced uses they host and what such a value may represent to local, regional and national economies. This conflict gives birth to a significant line of research and specific policies on beach defence and its optimisation in terms of time and costs - beach monitoring and defence strategies imply high investments and have specific timings according to the type of environment and the scope of monitoring.

The planning and management of the coastal zone requires therefore an accurate and updated knowledge of the processes in act, and in particular of those responsible for changes to beach morphology. Shoreline evolution determines the shape and extension of the emerged beach – the part of the territory with the highest economic value – and therefore must be studied in detail by those in charge of planning and managing the different uses that are made of this part of the territory. Such is a focus of beach management as an important component of the broader coastal zone management: as beaches bear (and cause) effects that are produced (and felt) in adjacent environments, beach management is actually one "slice" of coastal management, and therefore in defining the most effective policies for the management of the beach it is necessary to frame it within the macro-scale of coastal management and sustainable use of the coastal zone.

The coastal zone subject to management can be understood as a transition space between the sea and the adjacent land, which stretches alongshore across different countries. Because of its nature many of the coastal issues that countries must face are of international scope, and the effects that coastal uses will have on nearby countries must be considered when planning them (Clark, 1998). The Mediterranean sea, due to its geographical enclosure and socio-political peculiarities, represents a particular case where the already "hard-to-define" boundaries of the coastal zone show a special blur:

---

[1]   Integration here is understood as a multi-dimensional aspect which involves, for instance, intersectoral, intergovernmental, spatial, science-management and international dimensions (Cicin-Sain and Knecht, 1998)

if the marine environment, shorelines and coastal zones are part of a cross and longshore "continuum", calling for integration also at the international level, here neighbouring countries that share such a particularly and tightly connected environment must depend deeply on transboundary policies in order to reach a coherent and effective approach to coastal management.

Coastal management and planning at international scale is in fact highly strategic and focuses on developing broad strategies and action plans to ensure common efforts between coastal nations, including programmes that are developed between groups of countries (Kay and Alder, 1999). The sustainable development of the Mediterranean coastal zone is a transnational issue, and therefore programmes that can sustain public policies on solving conflicts over the beach – and reach real change as effects – tend to be more effective if they involve different neighbouring countries.

In this context, methodologies for surveying, data processing and analysis of trends in act must take into consideration all new technologies available in order to increase accuracy and cost/benefit ratio of operative monitoring activities. Certified and shared techniques are necessary for creating regional, national and international scenarios that are capable of dealing with different realities. Such a confrontation, if using homogeneous data, allows not only to evaluate the effect that different natural and anthropogenic processes have on different realities but also to analyse the need for intervention (normative or structural) in order to plan the available resources – being aware though that the priority for interventions should not be based on physical data only.

Statistics that refer to coastal evolution processes, realised at national (e.g. for Italy - GNRSC, 2006), continental (e.g. for Europe – EUROSION, 2004) or global (e.g. for worldwide coasts - Bird, 1996), present data that are obtained with criteria and methodologies that are extremely diverse, elaborated in different forms and often with different scopes. Among the most relevant differences, we can point those that refer to time intervals, survey scales and accuracy on the positioning of the shoreline. The "perception" of how severe the phenomenon is can be highly subjective, and often influenced by local realities – minimal shoreline retreat (that could be maybe due to nearly annual oscillations) can be considered as being relevant and therefore noted wherever the general trend shows equilibrium or accretion. On the other hand, in regions that are characterised by shoreline retreat of some tens of metres per year, erosive processes of small proportions can be underestimated. In such evaluations, the economic value of the beach has an important weight, and limited erosion of beaches that are heavily used by the tourist industry will receive higher attention if compared to consistent shoreline retreat in coasts that undergo lower anthropogenic impact.

The need for developing and validating new monitoring techniques, and sharing them among countries that border the Mediterranean - where similar environmental characteristics allow an easier standardisation of the methodologies - had already been identified by the Regions who proposed Interreg III B Medocc *Beachmed* (2002 – 2004), and such approach had been developed during that project (Beachmed, 2005). The results obtained, together with the continuing technological evolution in this sector, and the need to target other competent authorities, have led Regions to propose the new Interreg III C Regional Framework Operation *Beachmed-e*[2] where a significant part of the budget was dedicated to this aspect, calling for the proposal of *OpTIMAL*.

Beachmed-e concentrated on the strategic management of beach protection for the sustainable development of the Mediterranean coastal zone, and included different 8 regions from 4 Mediterranean countries as official partners, having had participants from many other regions as observers. *OpTIMAL*, one of the nine *Beachmed-e* subprojects, aimed at the optimisation of beach monitoring, and had the participation of 10 institutes representing all those 8 regions. Each of them had to face the same problem of dealing with the reality - and complexity - of beach erosion within a different technical, social, cultural, administrative, legal and economical context. In spite of that, methodologies applied during this project at different sites have shown similar results regarding their accuracy, and this increases our hope to analyse the Mediterranean coasts in a more homogenous way in order to obtain effectively comparable results in the near future.

---

[2] In Beachmed-e, -e means *Evolution*

References

Beachmed (2005) - *Le projet Beachmed : Récupération environnementale et entretien des littoraux en érosion avec l'utilisation des dépôts sablonneux marins* (Convention 2002-01-4.3-I-028) - 3ème cahier technique (phase C). Roma, 324 pp.

Bird E.C.F. (1996) - *Beach management*. Wiley and Sons, Chichester, 292 pp.

Cicin-Sain B. and Knecht R.W. (1998) - *Integrated coastal and ocean management: concepts and practices.* Island Press. Washington D.C. 517 pp.

Clark J. (1998) - *Coastal seas: the conservation challenge*. Blackwell Science. Oxford. 134 pp.

EUROSION (2004) - *Living with coastal erosion in Europe: Sediment and Space for Sustainability*. European Commission, pp. 38.

GNRAC (2006) - *Lo stato dei litorali italiani*. Studi costieri, 10: 1-174.

Hinrichsen D. (1998) - *Coastal waters of the world: trends, threats and strategies*. Island Press. Washington D.C. 276 pp.

Kay R. and Alder J. (1999) - *Coastal planning and management*. E&FN Spon. London. 375 pp.

Beach variability and shoreline evolution monitoring

Enzo Pranzini

Beaches are one of the most variable landforms on the Earth, changing their shape from day to day, or even from hour to hour. Crest berm development, swash zone flattening or steepening, bar formation and migration, all are feed-back regulated processes, driving the beach towards configurations which are able to efficiently dissipate wave energy. Since these changes are adaptations to the different but recurring wave conditions, if no sediment loss is concerned within the profile, previous configurations can be replicated, although the "memory" of the beach for high energy events can last for several years.

Each beach has its own specific variability, related to wave climate, sediment input and coastal structures that are present alongshore: far from the sediment source and under uniform wave climate, morphological variations are limited, whereas the latter can be huge at the mouth of seasonal rivers, or with alternating storm and swell waves. Coastal structures can trigger or restrain such wave-induced changes.

Variation in wave energy and provenience is responsible for significant morphological changes and for sediment budget unbalance between the emerged and the submerged beach. Along the Mediterranean coast, where winter storms and summer calms prevail, a yearly circle can be identified, with a backshore shortening in autumn/winter and expanding in spring/summer. The "questioned" summer and winter profile terms (nowadays "erosional and accretional profile", or "storm and swell profile") fits our local condition and, as said in one of the following chapters, must cadence our monitoring activity.

Beach response to annual and seasonal variations of river discharge is less immediate, except in the very near proximity to the river mouth, where significant short term accretion can invert an erosional trend when high energy low frequency events occur (Pranzini and Rosas, 2007). Coastal landslides (Sunamura, 1992) and dune erosion (Allan et al., 2003) can trigger beach fluctuations overlapping to a longer time-scale trend, thus masking it.

Short term variations are limited when the coast is protected through hard engineering projects, but near the structures wave reflection and diffraction can induce shoreline rotation, salient development or destruction, scour trough formation and fill (French, 2001).

Timing is therefore a primary aspect in beach erosion monitoring, both to collect data that actually represent the time interval under study (which can be short for single event analysis, or longer in order to retrieve a secular trend), and to meet the need for cost-effectiveness (Beachmed, 2005).

However, time variability is not the only aspect to be considered when a shoreline evolution monitoring project is to be planned, since beaches are characterised by consistent longshore variability, which must be taken into account.

In fact, very frequently, low order curves do not fit shorelines due to distortions introduced by regularly or randomly distributed salient and concavities: therefore, each shoreline must be drawn through a continuous survey or very close points. In addition, these forms can be stable, as are cuspate forelands (Gulliver, 1896), migrate along shore (Sonu, 1968) or develop and die out in the same position in relation to 'reversing storm hotspots' (Jeffrey et al., 2006).

Coastal defence structures trigger more longhshore variability, inducing the formation of tombolos or salients, saw-toothed shorelines and terminal scour. All these coastal forms can induce local short-time shoreline displacement larger than the average shoreline evolution rate (m/yr) of the coastal segment they belong to, when analysed from medium (years) to long (decades) temporal scales (Esteves et al., 2006).

High resolution surveys (*i.e.* close profiles or small sectors where surface variations are computed) can be affected by these high frequency morphologies, showing frequent and huge shoreline displacements not important for regional analysis. On the contrary, low resolution surveys can obliterate erosional hot spots, which require monitoring and management strategies.

The following chapters deal with these problems, which arise again in other parts of this book, such as when video monitoring is analysed, or when remotely sensed images are considered in order to evaluate their efficiency in shoreline positioning.

References

Allan J.C., Komar P.D. and Priest G.R. (2003) - *Shoreline variability on the high-energy Oregon coast and its usefulness in erosion-hazard assessment*. Journ. Coastal Research, SI 38: 83-105.

Beachmed (2005) - BEACHMED, 3° Quarderno tecnico, Fase C, Rome, November 2004. pp. 278.

Esteves L.S., Williams J.J. and Dillenburg S.R. (2006) - *Seasonal and Interannual influences on the patterns of shoreline changes in Rio Grande do Sul, Southern Brazil*. Journ. Coastal Research, 22: 1076-1093.

French P.W. (2001) - *Coastal defences. Processes, problems and solutions*. Routledge, London, pp. 366.

Gulliver F.P. (1896) - *Cuspate forelands*. Geol. Soc. America Bull., 7: 399-422.

Jeffrey H.L., Amy S.F. and Charlene S. (2006) - *Reversing storm hotspots on sandy beaches: Spatial and temporal characteristics*. Marine Geology, 226: 261-279.

Pranzini E. and Rosas V. (2007) - *Pocket beach response to high energy - low frequency floods (Elba Island, Italy)*. Journ. of Coastal Research, SI 50 (Proceedings of the 9th International Coastal Symposium), Gold Coast, Australia, in press.

Sonu C.J. (1968) - *Collective movement of sand in littoral environment*. Proc.11th Conf. Coastal Eng., London. pp. 373-400.

Sunamura T. (1992) - *Geomorphology of rocky coasts*. John Wiley & Sons, Chichester, England. 302 pp.

Shoreline monitoring: review and recommendations

Dan Bowman, Enzo Pranzini

Mapping shoreline position is essential for coastal planning and management. The aim of this review is to decipher the effects of time and space, in different scales, on the shoreline behaviour in order to design an optimal coastal monitoring strategy while distinguishing between the actual shoreline trend and the noise. The uncertainties involved in locating shorelines should not be greater than the resolved trend of the shoreline change. The most common proxies for shoreline position - the high water HWL and the datum-based shoreline MHWL - are analysed and guidelines for capturing shoreline erosional hot spots are suggested. We recommend ways to increase the long-term signal/noise ratio and to determine the long-term shoreline change rate. We further discuss the short-term storm variability. We examine the effect of storm severity and post-storm recovery scenarios on the long-term shoreline behaviour. Small-scale shoreline variability should be filtered out. Transects binning, i.e., grouping together, is recommended to reduce the coastal variability. An optimal temporal sampling frequency is recommended to minimise the variability within segments. Any temporal sampling interval greater than the cyclic norm will bias the true trends. We further discuss the linear regression and the "end point rate" (EPR) methods as examples for shoreline change calculations and add examples from the Tuscany coast.

Introduction

Mapping shoreline position is essential for coastal planning and management, for establishing building setback lines and for designing coastal defence. It is for this reason that, within BEACHMED-e Operation, the OpTIMAL Project attracted the highest effort in terms of human and financial resources. Developing and testing new, more accurate and rapid surveying techniques is essential when coastal changes are rapid and the monitored coast is at regional or national scale. However, a series of reliable surveys do not guarantee the capture of the long-term evolution trend of a coast. When intending to acquire the trends and magnitudes of the spatial and temporal shoreline changes, the data-collecting strategy should take into account different considerations and monitoring schemes, in addition to the monitoring techniques. The aim of this review is to decipher the effects of time and space in different scales on shoreline behaviour in order to design an optimal coastal monitoring strategy. We refer to long-term decadal scales and to the short scales as annual, intra-annual, seasonal, non-stormy cycles and single events. We have to distinguish between the actual shoreline trend and the noise which includes, in a spatial analysis, any ephemeral shoreline irregularity like beach cusps and, in a temporal sense, any short-term variability, including the first and the last events of a data set.

Shorelines may migrate due to various factors and controlling processes:

a) The trend of the rising sea level. The latest IPCC forecasts a sea level rise of 18 - 59 cm for the year 2100. The response time of beaches to water level change becomes an important factor.

b) Difference in the alongshore sand supply, including changes in bypassing and in connectivity between coastal compartments. Down-drift sand dispersal within a compartment depends partly on the storage in shoals, on the longshore migration of shoal systems and on the behaviour and migration of bar systems.

c) Seasonal or decadal changes in storm wave conditions, including wave height, surge level, storm duration and the angle of incidence.

d) Changes in the shore-normal sediment budget, including loss to dunes and to landward recession by storm surge penetration or loss to the offshore. Storage of part of the sediments on the shore face decreases the sediment supply.

e) Long-shore variations in the wave climate.

f) Changes in the seasonal sea water level.

g) Extreme storms and surges, including the 50/100 year events, composed of super elevation of the mean water level (set up) and swash fluctuations which often prove the major control of the erosion hazard.

h) Human intervention.

Each of the above-mentioned factors contributes differently to the total shoreline migration (Allan et al., 2003). The cause-effect relationships between each trigger and beach reaction is often unclear and noisy. The response time of the shoreline to each factor may be different.

Implications of shoreline changes

The magnitude of the total uncertainty in shoreline position is a combination of the source accuracy, the shoreline interpretation and the natural shoreline variability. The uncertainties involved in locating the shorelines should not be greater than the resolved trend of the shoreline change. In order that the accumulative shoreline change will be greater than the measurement errors, the minimum time span required for monitoring a significant change T_{min} must be greater than the time interval with a shoreline change equivalent to the total measured errors (Dolan et al., 1991).

How far do shoreline changes, based on profiling, reflect trends in the coastal sedimentary budget? Profiles may show simultaneous erosional and accumulative changes (Battiau-Queney et al., 2003) which the shoreline behaviour does not express. Anti-nodes (maximum change) onshore and offshore of the MSL, separated by a nodal zone at the waterline, will result in lack of correlation between shoreline behaviour and volume changes. In another case the change of the subaerial beach and the shoreline may be small and does not reflect the subaqueous portion of the beach where the main change in volume occurred. Thus, the sites of maximum and minimum erosional/accretional changes cannot be demonstrated by shoreline behavior. Volume change may be subaerial and include the backshore or subaqueous in the upper shoreface. The migration of the sediment storages - the subaerial beach and the nearshore bars - which may propagate in the onshore direction or disappear offshore within cycles of 10 to 15 years (Guillen et al., 1999) - is not well reflected by the history of shoreline migrations.

Waterline indicators

The total water level on a beach is the sum of the tide level, the set up which is the mean water surface elevation above SWL following storm surges and is commonly viewed as the main contributor to increased water levels, and the run up which fluctuates about the set up. The most common proxy for shoreline position is the high water line (HWL) although it is not a morphological feature but a wet/dry line left by the last preceding high water event. The HWL is visible in the field and can be interpreted on aerial photographs by the colour tone (Dolan and Hayden, 1983). The HWL can be approximated by vegetation, driftwood, discoloration of rocks and tonal contrasts in air photos between the dry and the wet beach. Spectral signatures acquired within OpTIMAL project along beach transects show that the latest feature is the most evident in remotely sensed images (Carli et al., 2008). Daily variations of the HWL on gently-sloping beaches can be significant. HWL does not represent an intersection of any water surface. Well defined berms will considerably lessen the migration of the HWL. It is the manifestation of different water levels and run ups rather than an actual coastal morphology (Liu et al., 2007). Many USA agencies use the HWL. The high water line can be videotaped, field-located or photo interpreted. Video monitoring, as demonstrated by several research units joining OpTIMAL, is a cost effective technique to acquire HWL data in addition to the foreshore bathymetry, bar position and type (see Chapters 8 to 12).

In contrast to the visual, proxy-based HWL, the mean high water line (MHWL) is a datum-based shoreline derived from intersection of the mean high water tidal datum with the cross shore topography, retrieved by surveys or other altimetry data. The elevation of interest - the mean high water - is determined from local tide gauges. The MHWL eliminates variations in interpretations, varies only with morphological changes and falls lower than the HWL on beaches subject to run up. The MHWL is treated as a legal shoreline by many U.S. agencies (Liu et al., 2007).

When the visual prominence of a shoreline reference feature as the wet-dry line is masked, the toe of the beach, i.e., the base of the foreshore (Bauer and Allen, 1995) is suggested as a shoreline reference feature. An additional maximum storm surge level marker is the foredune foot which makes a 2-3 m zone of sharp break of slope (Guillen et al., 1999) and changes with tide and with the prevailing wave conditions. The beach crest is another morphological marker to be used as a water level indicator. The lower the markers on the beach the higher their variability.

In Italy, the zero isobath is generally regarded as the reference shoreline. Although invisible on the beach, it is an "objective" geodetic element, easy to be mapped with DGPS. Its positioning through aerial photographs and satellite images needs corrections based on the swash zone slope and on the astronomical and barometric tide (BEACHMED, 2005).

Hot spots

Shoreline erosional hot spots are focused coastal segments of erosion, typically hundreds of meters to a few kilometres in alongshore extent, typified by the highest shoreline shifts relative to surrounding areas. Their temporal scale may be days. In post-storm fair weather hot spots may become rapidly reversed and blurred by accretion and vegetation encroachment. A recovery of tenths of percents may occur within 12 post-storm hours. Recovery speed of hot spots may range from a few tidal cycles to a week.

Hot spots of a different temporal scale are those which persist for several decades and show historical repetition of similar maximum overwash penetrations (Dolan and Hayden, 1983). Shoreline migration at hot spots during extreme storm events may reach tens of meters. Mean shoreline excursions of storm hotspots ranged in Cape Cod and North Carolina 10.1- 27.2 m (List et al., 2006). The large change of the beach width over time at hot spots typically increases the standard deviation of shoreline migration. If vulnerable, shoreline hot spots may compose storm hazard zones.

The hot spots may be governed by different factors, as refraction over the shelf bathymetry or by the rip embayments which allow waves to propagate closer to the shore. An accretional hotspot is an area of high net accretion that may also display high variance of shoreline migration. Defining a coastal reach as a hot spot requires observations over a few years.

Structures on the beach can trigger hot spot formation when a mega cusp becomes captured and grows through the wave reflection between the structures. Such a process frequently occurs on those Tuscany coast segments, like Marina di Capalbio, where mega cusps frequently develop.

At Marina di Castagneto, in a coastal segment that is stable at time scale of decades, in the 80s a mega-cusp embayment reached a wall of a beach resort: the deepening of the swale induced the structure to collapse, while the two side horns protruded into the sea for several tens of meters.

Long-term trends

Long-terms encompass periods from decades to centuries. Minimum 10 years of monthly profiles are necessary to relatively minimise the short-term changes and delineate the true long-term trend (Eliot and Clarke, 1989). Dolan and Hayden (1983) suggest 40 years of measurements on air photos to determine long-term shoreline rates of change along the USA Atlantic coast. The available records from which long-term shoreline changes were usually determined, in most of the US and Europe, exceeds 100 years, although an accuracy of few meters is limited only to the most recent data sets. In Italy topographic maps at the scale 1:100.000 were produced by the Istituto Geografico Militare since the 1880s and during the first decades of the 20th century the 1:25.000 maps covered most of the Italian coast. For certain areas there are even older Cadastral maps in the scale 1:5.000 but the accuracy of their shoreline position is questioned.

Long-term trends may be unidirectional, cyclical, accelerating or decelerating. The most common data base used to measure long-term shoreline positions are aerial photos. Long-term slow trends may be masked by the short-term dynamic cyclic fluctuations and become immeasurable. The short-term "noise" includes: storm impacts, rip current migration, movement of nearshore rhythmic shoals, human impacts, seasonal extremes, etc. These periodic short-term, high-frequency events must be filtered out in order to resolve the slow long range trends.

Extreme erosional and accumulational shorelines can lead to erroneous calculations of long-term trends (Douglas and Crowell, 2000). Extremes may bias the long-term trends, especially when using least squares, because of their susceptibility to outliers (Zhang et al., 2002a). When determining long-term trends, the extreme shoreline positions – the outliers - should be removed from the data sets (Fletcher et al., 2003). Outliers can be identified by a priori knowledge or by residual statistics. Because erosion caused by storms is only a temporary deviation from the long-term shoreline evolution, beaches tend to recover to their long-term trends and the shoreline position should be unaffected by major storms.

The dataset of the northern Tuscany coast is based on the shorelines of 1938, 1954, 1967, 1976, 1984, 1998 and 2005. The period 1954 - 1967 demonstrates the highest erosion rates during which even traditionally-accreting beaches became stable or slowly eroding (Bartolini et al., 1989). This dramatic erosional trend was controlled by the November 1966 storms, which caused the flood in Florence, the largest high-water event in Venice and the severe erosion along the entire Italian coast.

When storm-influenced outliers are excluded, predictions based on rate improve. Adding more evenly-distributed data points and using longer time spans contribute to greater certainty of the long-term rate-of-change estimate. The linear regression is the best way to determine the long-term shoreline change rate from sparse historical shoreline data (Crowell et al., 1997). Shore sections influenced by inlets and coastal engineering projects should be excluded from the long-term analysis because they typically display nonlinear temporal behaviour. This will gradually decrease the possibility and relevance of long-term predictions, since hard and soft coastal defences are expanding. In Tuscany, out of the 191 km of continental beaches, 35 km are already artificially protected.

In order to increase the long-term signal/noise ratio special care must also be given to the temporal selections while mapping the shorelines (Zhang et al., 2002a). Records from the same season are recommended. Periods with high variability (standard deviation) are ineffective in determining the long-term shoreline trend and should be escaped. Months of low energy should be preferred, when the shoreline is most stable, standard deviations are small and the beaches steepen and minimise shoreline migration. Douglas et al. (1998) and Douglas and Crowell (2000) demonstrated the trends that were obtained using long records (>80 yr) of historical non-stormy, shoreline-position data.

Long-term (63-124 yr) mean shoreline change rates in the range of 0.58-0.64 m/y with specific sites ranging up to 1.8 m/y were reported from Maryland by Crowell et al. (1993). Long-term (1850-1990) erosional trends in North Carolina were 0.4 m/y, and erosion rates of 0.75 m/y were reported by Fenster and Dolan (1993) for the period 1852-1917 with local high accretional rates of 2.3 m/y. For the period 1845-1990 Dolan et al. (1991) reported the range + 0.5 to -1.5 m/y the most frequent rates of shoreline change.

Along the Tuscany coast these values are frequently overtaken, mostly at the river mouths: a 10.7 m/yr erosion has been documented for the beach north of the Arno River from 1978 to 2000 (Bowman and Pranzini, 2003) and 8.6 m/yr is the retreat rate measured from 1883 to 2000 at the Ombrone River mouth (Innocenti and Pranzini, 1993). Many other coastal sectors, far from river mouths, experienced erosion rates between 2 and 5 m/yr.

Short-term storm variability

Short-term shoreline variations range from days, months and seasons up to a few years (<10 yr) and usually captures shoreline changes due to storm events, seasonality of the wave climate, longshore migration of sand bodies or impacts of engineering activities as nourishment. The magnitudes of short-term shoreline changes are comparable to decades of long-term shoreline migrations.

The effect of moderate storms is often less than the seasonal variation. Storm-induced signals may, however, exceed the annual shoreline change. Storms are the most dramatic agent of short-term shoreline migration and may cause tens meters of change over days. The impression that storms dominate the coastal morphology leads to the view that erosional trends should be attributed to increased storminess.

Storm intensity can be measured by wave power (Dolan and Davis, 1992), using peak wave height squared multiplied by storm duration. Storm duration is defined as the interval of time that the wave height exceeded 2 m. In addition to individual storms, the net effect of storm clusters may have important morphological impacts. Beach erosion becomes accentuated also when storm frequency exceeds the beach recovery period. Incomplete beach recovery contributes towards an accumulative erosional effect. An increased number of storms and length of the winter season increase erosion, implying that a cumulative storm impact may often dominate. Summer storm frequency is important as well, as documented in the beach nourishment monitoring at Marina di Carrara, where continuous storm occurred after a spring fill causing losses faster than predicted by the numerical model which was based on the average wave climate (Ferri et al., 2008).

A cumulative annual or seasonal storm index, based on the mean storm wave height, was suggested by Brayant (1988) as a tool to explain beach behaviour. Indexing storm magnitude was done by weighting the wave height at the coast, after wave decay and refraction, without considering storm duration or the initial beach pre-storm state. Sallenger (2000) defined four storm impact regimes: *I. swash regime*, when the wave run up is confined to the foreshore region and the eroded material is returned to the beach. *II. collision regime,* when the maximum water level exceeds the dune base. *III. overwash regime,* when sand is transported landward. *IV. the inundation stage,* when the entire beach morphology is continuously subaqueous. A longshore mixture of these regimes may occur.

In order to record the real impact of a storm on the morphology and on the shoreline position, it is best to measure the beach width before storm by a baseline topographic survey, i.e., define the pre-storm beach state after a long period of fair weather during which the characteristic calm-weather profile was shaped. Rapid erosion and quick post-storm recovery during the days after a storm require additional measurements during the storm peak and immediately after the event. The recommended time interval during which the "pre-storm", "storm survey" and "post-storm survey" should be accomplished is a month.

Different beach recoveries have been observed. Morton et al. (1995) suggested the following four categories of post-storm beach response: 1) *continuous erosion*, 2) *partial recovery*, 3) *complete recovery*, and 4) *over-recovery*. Four stages for complete beach recovery were documented: 1) *rapid forebeach accretion*, 2) *backbeach aggradation*, 3) *dune formation*, and 4) *dune expansion with vegetation recolonisation*. Only beaches with low long-term erosion rates experience complete recovery to pre-storm conditions. Beaches with high erosion trends may not recover totally to their pre-storm state.

An important issue about the post-storm beach recovery process is timing. Although post-storm accretion may induce rapid shoreline return, storm effects may last beyond seasonal periods. After the largest storms, beaches may recover to positions consistent with their long-term (>100 yr) trend but it may take several years to more than a decade. For Delaware beaches it took about 15 years after the 1962 storm to recover to their long-term trend position.

Failure to recognise the often long post-storm recovery process can yield an erroneous estimate of the long-term shoreline movement, which could have serious consequences for coastal planning and management. Shoreline positions after the reversal following a big storm may appear to be accretional. However, this does not represent a permanent long-term shoreline trend. For trend determination this example demonstrates the need for long records of historical shoreline positions and storm activity.

The fact that shoreline positions often recover to their trend lines, no matter the storm severity, indicates that historical storm activity has often little to do with long-term beach erosion. If storms were the cause of consistent, long-term beach erosion, it would be expected that larger storms would result in more net erosion, which is not the case (Zhang et al., 2002b). Instead, long-term shoreline retreat is apparently independent of storm severity and is determined by other factors, including sea-level rise and variations in the sediment supply.

Alongshore homogeneity

In Holland, large scale, homogeneous coastal behavioural segments, in the range of 10-32 km length, have been defined (Wijnberg and Terwindt, 1995). Large scale homogeneous coastal behaviour is, however, not the rule. Coasts reveal a remarkable alongshore non-homogeneous behaviour. The reasons for the longshore variability is found in potential variability-triggering factors located alongshore. These include: inlets which have been found to influence the shoreline for as much as 10 km longshore, down-drift beach retreat which dies out from structures toward stable segments, non-uniform alongshore distribution of wave energy following refraction and longshore variable storm-induced water-levels. In addition we may find a temporal longshore rhythmicity of accretional and depositional segments. An observed periodicity of 10-15 years has been reported for such oscillations (Guillen et al., 1999). Shoreline response is thus very often neither temporarily nor spatially persistent and any longshore uniformity may become very restricted. However, comparing spatial to temporal variance showed that temporal variance of shoreline erosion can be even three to four times greater than the spatial variability. Overwash penetration may even be four to five times greater (Dolan and Hayden, 1983).

Notwithstanding the spatial and temporal variability, we should aim, as far as possible, to monitor homogeneous coastal segments, controlled by identical or similar factors and devoid of very variable site-specific shoreline behaviour. Shorelines with minimal human intervention allow studying largely the basic autonomous response, which can help understanding the evolution affecting the adjacent human-altered coastal segments, those which attract the main interest of planners.

The framework geology, including the shelf, plays a role in beach processes. Geologic units should be mapped and examined as potential shorelines zones (Honeycutt and Krantz, 2003). Outliers as capes, inlets, river mouths or other discontinuities should be taken into account and possibly regarded as morphological boundaries. The pattern of the littoral drift cells should also contribute towards the longshore partition. The longshore coherence of each coastal segment should incorporate, if possible, also nearshore sediment characteristics, source of the sediment, sediment sink and homogenaous the inner shelf characteristics.

To reduce the effect of the spatial coastal variability, transects should be binned, i.e., grouped together while searching for coastal reaches of uniform behaviour. Taking into account that correlation is inversely related to distances between transects, the spacing between transects and the length of the coastal segments analysed should be increased not beyond the limit of homogeneity.

Spatial distribution of erosion rates becomes smoother as longer time spans are monitored. Restricted time frames increase the likelihood that the alongshore variability will increase. An optimal temporal sampling frequency (Zuzek et al., 2003) should contribute to minimise the variability within segments. Finally, relative high autocorrelation is expected within each spatial coastal unit which should have its computed mean rate of change and variance, based on field data or air photos. The standard deviation of the mean rate of shoreline change can change spatially very much (>10) compared to the mean. Small standard deviations indicate the behavioural coastal homogeneity.

For the Tuscany coast, standard deviation was demonstrated to be higher on coastal segments where shore protection structures are scattered over an unprotected littoral, or where different structures alternate (see Chapter 1.2).

Rates of shoreline migration

Shoreline erosion rates are available from many coasts around the world. Short-term shoreline variability is higher in areas of low beach slopes and abundant nearshore bars, because of dynamic positional shifts. Shoreline changes of < 0.1 m/yr are regarded as being micro and shoreline migration rates of 0.1-0.9 m/yr as being meso. This range is dominating the decadal time slices along most of the world shorelines (Battiau-Queney et al., 2003) including the average shoreline regression rates in the great lakes of 0.2-0.6 m/yr. Shoreline migration rates >1 m/yr are regarded as being high to extreme.

Annual rates of shoreline migration are of course a statistical artifact and do not express the total accumulative shoreline migration nor the dynamics of the beach. An improved short-term evaluation must

sample the detailed short cyclic norms. If longer intervals are sampled the estimation of the shoreline mobility will be biased (Allen et al., 1999). The temporal time spans of monitoring should be long. The percentage of the erosional rates falling within the uncertainty range increases dramatically when shorter temporal time spans are used. The spatial erosional rates become progressively smoother as longer time spans are used. Increased time spans help to filter out short-term fluctuations (Crowell et al., 1993).

The rates of shoreline migration often change irregularly alongshore or compose a spatial quasi-sinusoidal, periodic wave phenomena with oscillations of 2.5-7 km. Most shoreline rate estimation methods assume that shoreline change is linear through time. However shorelines do not change uniformly (Douglas et al., 1998). Along the USA Atlantic coast the standard deviations of shoreline rates of change range 1.8-16.4 m/yr. i.e., greater than the mean rates of the shoreline change (Dolan et al., 1980). The standard deviation defines "beach mobility" and increases when longer time scales are considered.

High long-term shoreline migration rates of 2.4-3.3 m/yr were reported by Clarke and Eliot (1983) in Western Australia. The French Atlantic coast from Brittany to Biarritz also shows rapid long-term retreat rates in the range > 9 - 4 m/yr. Similar maximal erosional rates, in the range of meters per year, were reported by Smith and Zarillo (1990) and by Morton et al. (1995). During the last 50 years, 45.7% of the Tuscany beaches experienced a mean shoreline retreat greater than 2 m/yr which puts almost half of the Tuscany coast in the highest shoreline recessional category. The Tuscany coast should be regarded as one of the most rapidly retreating coasts of the world.

Recommendations
Data retrieval

Geology determines the shoreface, the shelf and the shoreface-inner shelf relations. The spatial variability of wave refraction, sediment supply, erodibility, nearshore morphology and lithology determine the shoreline migration rates. The nearshore geology framework should therefore be considered when monitoring shoreline changes.

Sampling intervals affect the significance of the shoreline data. Do not rely on a single or a few profile lines but preferably on series which represent a longer beach segment. The variance along the coasts may be greater, even by an order of magnitude, from the mean, because of spikes, therefore spatial sampling intervals should be appropriately made (Dolan and Hayden, 1983). Most coastal investigators call for sampling intervals smaller than 5 km. Site specific studies may include reaches of less than 1 km (Dolan and Hayden, 1983). In order to filter out the small-scale variability as mega-cusps or cyclic crescentic bars, a low pass cut-off spatial interval of 500 to 1000 meters is often recommended. Nevertheless, detailed measurements of long coastal reaches were reported with a few hundreds of meter (200-600 m) separation between transects. Hayden et al. (1979) calculated rates of change at 100 m intervals along 400 km. The distance between profiles along the Dutch North Sea coast is 200-250 m. In Hawaii a high-resolution shoreline change study was based on very short intervals of 20 m along 90 km of coast (Fletcher et al., 2003). Thus, dense data sets which cover short and very long coastal segments have been reported. However, it was suggested that decrease of spacing to 40 m decreases the variability dramatically. An additional decrease may need a too dense net of profiles.

Uniform spatial and temporal sampling scheme should be kept. Unequally-spaced data may bias the reach estimation. However, refraining from regular spatial or temporal sampling intervals will avoid being caught in along-coast or wave climate periodicities (Dolan and Hayden, 1983).

Shoreline positions should be monitored during summer under calm conditions. Random errors which are derived from shoreline interpretation, from surveying, digitation and storm induced erosion can be minimised using summertime data (Leatherman, 2003). In order to capture fair weather characteristics, daily surveys during five weeks is recommended. Daily surveys should be used when significant changes are expected, even in wave calm periods, with high degree of correlation between shoreline changes and very minor wave events.

Any temporal sampling interval greater than the cyclic norm will bias the true temporal trends. This limit should be overcome through multiple sampling. The time span of monitoring should be a few

times longer than the interested time span. Forecasts should not be made, as a rule of thumb, for periods longer than half the period covered by the data set.

In order to minimise the effect of short range variability, the time interval of measurements should be increased. In order to capture shorter term variations the temporal resolution should be at least two orders of magnitude finer than the total length of the data. So, when long-term coastal studies extend at least for several decades, we need, for short-term variation, to sample within less than one month interval. For some long-term studies bi-weekly monitoring is recommended. When biannual beach profiles are collected the surveys should be conducted in an approximately summer-winter interval. To dampen seasonal fluctuations, the interannual variability should be calculated from the same season, preferably by summer surveys. To preclude capturing the impact by storms, monthly sampling is recommended. As the temporal variance of shoreline change can be 3-4 times greater than the spatial variance, in order to maximise the sampling program samples should be collected during longer time spans rather than spatial longer.

One target of monitoring programmes often is to evaluate the effect of big storms and to follow the recovery process. This goal would need pre-storm and post-storm monitoring. Post-storm beach recovery can last even years. After hurricanes, beach profiles were obtained quarterly for two years and then once a year for ten years to follow the recovery. If a quick recovery is expected, similar to the storm erosion rate, it is recommended to monitor daily after the storm for a few days up to five weeks. Such dynamic behaviour has no implication on the long-term trend.

Data processing

The mean rate of shoreline change and its standard deviation should be computed as basic data (Dolan and Hayden, 1983). The standard deviation should be computed at fixed points along profiles and the locations of the peak standard deviations should be analysed.

The rates of beach migration can be calculated by the "end point rate" (EPR) method, in which the earliest and the most recent shorelines are compared. As these end points may be unrepresentative, i.e., product of short-term fluctuations and aberrant, the calculated rate may be misleading (Fenster et al., 1993).

The EPR system filters out all short-term variability and trend inversions. Using end point data, the potential error in the location of shorelines should be summed up and compared against the magnitude of the recorded rate of shoreline movement which must be greater (Anders and Byrnes, 1991). A minimum time span criterion for the EPR to be considered a long-term rate was suggested by Foster and Savage (1989) based on the relation of the measurement errors to the EPR.

Another possibility is to use the linear regression method which is superior to calculate erosion rates (Douglas and Crowell, 2000). Here all data points are used and the variance can be estimated. The goodness of fit and the confidence interval should be calculated. Outliers that violate the Gaussian assumption will bias the apparent trend. We may give less influence on the trend line to data points with large variance. We may also remove outliers in the data at a certain cut-off value. An additional method possible is the Minimum Description Length by which we select the best fit line, whether linear, quadratic or cubic, which best reduces the mean squared error (Fenster et al.,1993).

The beach volume history should be followed by using the shoreline migration data as a surrogate to volume changes. For this aim the spatial distribution of the sediment thickness should be surveyed and a three-dimensional isopach map of the surface sediment should be prepared. This approach may unravel the process relationship between the underlying geology and the long-term shoreline behaviour, including hot spots

Most of the effort in beach evolution monitoring is dedicated to assess and increase the survey accuracy and BEACHMED-e/OpTIMAL Project gave a valuable contribution towards this end. However, although an accurate survey is indispensable, it does not guarantee to delineate the long-term coastal evolution. For capturing the actual trend, over-sampling must be avoided, seasonal oscillations must be cut off, and surveys should be performed in the same wave climate. Nevertheless, in order to estimate the vulnerability of a specific coastal segment and locate hot spots the short-term variability must be considered as well.

References

Allan J.C., Komar P.d. and Priest G.R. (2003) - *Shoreline variability on the high-energy Oregon coast and its usefulness in erosion hazard assessments*. Journ. Coast. Res., 38: 83-105.

Allen J.R., LaBash C.l. and List J.H. (1999) - *Space and time scales of shoreline change at Cape Cod , National Seashore, MA, USA*. Coastal Sediments 99'. Am. Soc. Civ. Eng. pp. 1244-1255.

Anders F. J. and Byrnes M. R. (1991) - *Accuracy of shoreline change rates as determined from maps and aerial photographs*. Shore and beach, 59: 17-26.

Battiau-QueneyY., Billet J. f., Chaverot S. and Lanoy-Ratel Ph. (2003) - *Recent shoreline mobility and geomorphic evolution of macro-tidal sandy beaches in the north of France*. Mar. Geol., 194: 31-45.

Bauer B.O. and Allen J.R. (1995) - *Beach steps: An evolutionary perspective*. Mar. Geol. 123, 143-166.

BEACHMED (2005) - *Le projet BEACHMED : Récupération environnementale et entretien des littoraux en érosion avec l'utilisation des dépôts sablonneux marins* (Convention 2002-01-4.3-I-028) – 3ème cahier technique (phase C). Roma, 324 pp.

Bowman D. and Pranzini E. (2003) - Reversed response within a segmented detached breakwater - the Gombo case, Tuscany coast, Italy. Coastal Engineering, 49: 263-274.

Brayant E. (1988) - *Storminess and high tide beach change, Stanwell Park, Australia 1943-1978*. Mar. Geol. 79, 171-187.

Carli S., Iandelli N., Pranzini E. e Salvatori R. (2008) - L'utilizzazione di immagini telerilevate ad alta risoluzione per lo studio dell'erosione costiera: estrazione della linea d'acqua e valutazione della sua accuratezza. Studi costieri, 14: 43-54.

Clarke D.J. and Eliot I.G. (1983) - *Mean sea level and beach-width variation at Scarborough, Western Australia*. Mar. Geol., 51, 251-267.

Crowell M., Douglas B.C. and Leatherman S.P. (1997) - *On forecasting future U.S. shoreline positions: A test of algorithms*. Journ. Coastal Research, 13: 1245-1255.

Crowell M., Leatherman S.P. and Buckley M.K. (1993) - *Shoreline change rate analysis: Long-term versus short-term data*. Shore and beach, April. pp. 13-20.

Dolan R. and Davis R.E. (1992) - *An intensity scale for Atlantic coast northeast storms*. Journ. Coastal Research, 8: 840-853.

Dolan R. and Hayden B. (1983) - *Patterns and predictions of shoreline change*. In: Komar P.D. (Ed.), Handbook of coastal processes and erosion. CRC press. pp. 123-149.

Dolan R., Fenster M.S. and Holmes S.J. (1991) - *Temporal analysis of shoreline recession and accretion*. J. Coastal Research,7: 723-744.

Dolan R., Hayden B. and May S. (1983) - *Erosion of the U.S. shorelines*. In: Komar P.D., (Ed.), Handbook of coastal processes and erosion, CRC press. pp. 285-299.

Dolan R., Hayden B., May P. and May S. (1980) - *The reliability of shoreline change measurements from aerial photographs*. Shore and beach, 48: 22-29.

Douglas B.C. and Crowell M. (2000) - *Long-term shoreline position, prediction and error propagation*. Journ. Coastal Research, 16: 145-152.

Douglas B.C., Crowell M. and Leatherman S.P. (1998) - *Considerations for shoreline position prediction*. J. Coastal Research, 14: 1025-1033.

Eliot I. and Clarke D. (1989) - *Temporal and spatial bias in the estimation of shoreline rate-of-change statistics from beach survey information*. Coastal Information, 17: 129-156.

Fenster M.S., Dolan R. and Elder J.F. (1993) - *A new method for predicting shoreline positions from historical data*. Journ. Coastal Research, 9: 147-171.

Ferri S., Pelliccia F., Pranzini E., Rizzo M. and Vitale. (2008) - *Prima risposta della spiaggia di Marina di Carrara ad un ripascimento artificiale non protetto*. Studi costieri, in press.

Fletcher Ch., Rooney J., Barbee M., Lim S.Ch. and Richmond B. (2003) - *Mapping shoreline change using digital orthophotogrammetry on Maui, Hawaii*. Journ. Coastal Research, Special Issue 38: 106-124.

Foster E. R. and Savage R. J. (1989) - *Methods of historical shoreline analysis*. Am. Soc. Civil Eng., Coastal Zone '89, 5: 4434-4448.

Guillen J., Stives M.J.F. and Capobianco M. (1999) - *Shoreline evolution of the Holland coast on a decadal scale*. Earth Surf. Process. and landforms, 24: 517-536.

Hayden B., Dolan R. and Felder W. (1979) - *Spatial and Temporal analysis of shoreline variations*. Coast. Eng., 2: 351-361.

Honeycutt M.G. and Krantz D.E. (2003) - *Influence of geologic framework on spatial variability in long-term shoreline change, Cape Henlopen to Rehoboth beach, Delware*. Journ. Coastal Research, Special Issue 38: 147-167.

Innocenti L. and Pranzini E. (1993) - *Geomorphological evolution and sedimentology of the Ombrone River delta (Italy)*. Journ. Coastal Research, 9: 481-493.

Leatherman S.P. (2003) - *Shoreline change mapping and management along the U.S. East coast*. Jour. Coastal Research, S.I. 38: 5-13.

List J. H., Farris A.S. and Sullivan C. (2006) - *Reversing storm hotspots on sandy beaches: spatial and temporal characteristics*. Mar. Geol., 226: 261-279.

Liu H., Sherman D. and Gu. S. (2007) - *Automated extraction of shorelines from airborne light detection and ranging data and accuracy assessment based on Monte Carlo simulation*. Jour. Coastal Research, 23: 1359-1369.

Morton R.A., Gibeaut J.C. and Paine J.G. (1995) - *Meso-scale transfer of sand during and after storms: implications for prediction of shoreline movement*. Mar. Geol., 126: 161-179.

Sallenger A.H. (2000) - *Storm impact scale for barrier islands*. Journ. Coastal Research, 16: 890-895.

Savage R.J. and Foster E.R. (1989) - *Historical shoreline change in southern Florida*. In : Magoon O.T., Converse H., Miner D., Tobin L.T. and Clark D. (Eds.), Coastal Zone 89'. Amer. Soc. Civ. Eng., 5: 4406-4433.

Smith G.L. and Zarillo G. A. (1990) - *Calculating long-term shoreline recession rates using aerial photographic and beach profiling techniques*. Journ. Coastal Research, 6: 111-120.

Bartolini C., Cipriani L.E., Pranzini E. and Sargentini M. (1989) - *Caratteristiche geomorfologiche ed evoluzione della linea di riva del litorale toscano e criteri di lettura*. In: "Coste toscane", Regione Toscana. pp. 33-56.

Wijnberg K.M. and Terwindt J. (1995) - *Extracting decadal morphological behavior from high-resolution long-term bathymetric surveys along the Holland coast using eigenfunction analysis*. Mar. Geol., 126: 301-330.

Zhang K., Douglas B. and Leatherman S. (2002a) - *Do storms cause long-term beach erosion along the U.S. East Barrier Coast?* Jour. Geol., 110: 493-502.

Zhang K., Huang W., Douglas B. and Leatherman S. (2002b) - *Shoreline position variability and long-term trend analysis*. Shore and beach, 70: 31-35.

Zuzek P.J., Nairn R.B. and Thieme S. J. (2003) - *Spatial and temporal considerations for calculating shoreline change rates in the great lake basin*. Journ. Coastal Research, S. I. 38: 125-146.

Beach evolution monitoring:
Surface Variation Analysis
vs Transept Based Analysis

Enzo Pranzini, Daniela Simonetti

Beach evolution on two coastal segments was assessed using two different parameters extracted from the same shorelines: i) mean shoreline displacement over sectors of constant length; ii) shoreline displacement measured along transepts that are equally spaced. Short sectors and close transepts give matching results, but when reducing the analysis resolution, or studying irregular shorelines, Transept Based Analysis is not accurate in assessing beach evolution.

Introduction

The assessment of variations in shoreline position is one of the most important components of Integrated Coastal Zone Management (ICZM), both for monitoring erosion processes and evaluating the efficiency of shore protection projects.

After the acquisition of a series of shorelines (on the field, on maps or on aerial photographs), the comparison is generally performed by computing the mean shoreline displacement for stated coastal segments, *i.e.* dividing the beach surface variation by the segment length. This Surface Variation Analysis (SVA) provides the mean shoreline displacement for any sector under study (Rogers et al., 2004; Aminti et al., 2004).

A different approach is the Transept Based Analysis (TBA), which is based on the measurement and comparison of the distance between each shoreline at set points along transepts (Morton et al., 2005; Różyński, 2004). In this case beach survey can be very rapid, being limited to the direct measurement of the distance of the shoreline from a monument; or, still, on topographic maps and on aerial photographs.

Segment length and transept spacing are generally defined according to the scale of the project, ranging from tens of meters for local studies (Bowman et al., 2007; Hicks et al., 2002), to hundreds of meters (White and El Asmar, 1999) and kilometres for studies at the regional level (Anfuso and Garcia, 2005; Krause and Soares, 2004).

The results given by these two methods differ the most when shorelines are not straight, due to the presence of periodic features such as beach pads (Tanner, 1975), cusps and mega cusps (Guza and Inman, 1975) or irregular forms produced by wave convergence or divergence induced by diffraction and refraction over an uneven rocky sea bottom (Schwab et al., 1999; Schupp et al., 2006).

Artificial coastal structures intensify beach spatial variability, inducing the formation of tombolos or salients (by detached breakwaters) or of saw-toothed shorelines (by groins) which can increase the difference between SVA and TBA derived data.

Nevertheless, data retrieved through TBA are frequently taken as representative of coastal segments around the points, whereas this role is specific of data produced by SVA.

In this paper the coincidence between SVA and TBA derived data is tested in two stretches of the Tuscany coast using different scales of analysis, *i.e.* sector length and transept spacing.

Study sites

Two study areas located in southern Tuscany were selected representing different coastal types: a) a sandy beach strand which is free of shore protection structures, although undergoing beach reshaping which is driving it towards a zeta bay (Punta Ala beach); and b) a stretch of coast that is intensively protected by emerged and submerged breakwaters and groins (Follonica beach).

The beach at Punta Ala is approximately 6 km long and connects the headland of Punta Hidalgo to the jetties at the mouth of River Alma, a creek reaching the Tyrrhenian Sea, south of Punta delle Can-

nelle promontory (Figure 1). Recent studies (Pranzini and Rossi, 2000) show that this beach is evolving towards a zeta bay (Silvester and Hsu, 1993), undergoing erosion at the southern (updrift) part, and accretion at the northern (downdrift) side. On the southern part of the coast, a few beach-rock outcrops located in the nearshore create some irregularities on the shoreline.

The beach at Follonica is part of a wide gulf which extends for approximately 22 km from Piombino to Puntone Headland (Figure 2).

The beach is eroding because of the reduced sediment input by the river, due to the reclamation of wetlands that was performed in the 19th and 20th centuries, and to the river bed quarrying carried out along the last century (Bartolini et al., 1977). Since the 1960[s] the beach in front of the town has been defended by several engineering projects, comprising seawalls, groins, and emerged and submerged detached breakwaters (Aminti et al., 2002).
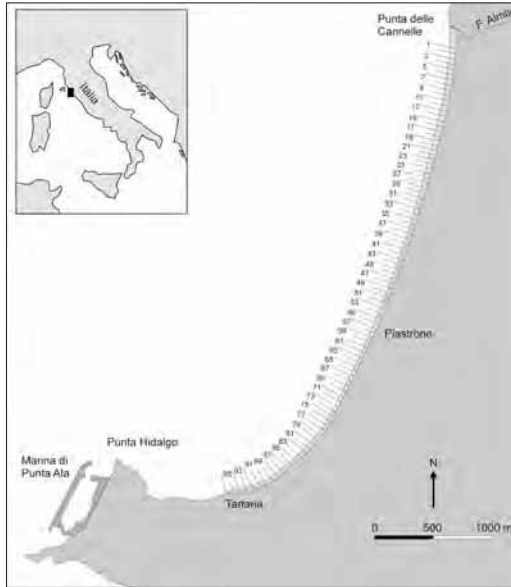
Figure 1 - Punta Ala beach location map and position of sectors.
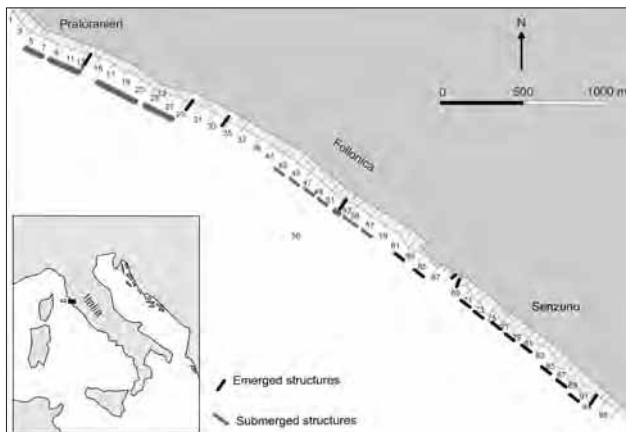
Figure 2 - Follonica beach location map and position of sectors.

Material and methods

Beach evolution was analysed at each site, comparing the two most recent shorelines available along a 4800 m long segment. These shorelines had been surveyed in 1996 and 2005 (Punta Ala) and in 2000 and 2005 (Follonica), through the acquisition of continuous shoreline position (0 m isobath) using Differential Global Positioning System/DGPS (approx. 0.2 point/m).

In both study sites, the coast was divided in 96 sectors of 50 m length for which lost or added beach surface was computed. Further, the analysis was repeated on joined sectors with lengths of 100, 200, 400 and 800 m. Transepts were then positioned in the centre of each of the sectors of different size and the displacement in shoreline position at those points was measured. Finally, the results obtained by the two methods were compared.

Results

Punta Ala beach

Mean shoreline displacement for the 96 sectors of 50 m length is -2.04 m (st.dev. = 5.44), whereas measurements performed at transept locations have a mean value of -2.12 m (st.dev. = 5.59). Absolute mean difference between pairs of values obtained through the two methods ($|\Delta_{S-T}|$) is only 0.43 m, and most of the points in the SVA/PBS graph (Figure 3) lie very near to the diagonal. Points over the bisector are optimistic
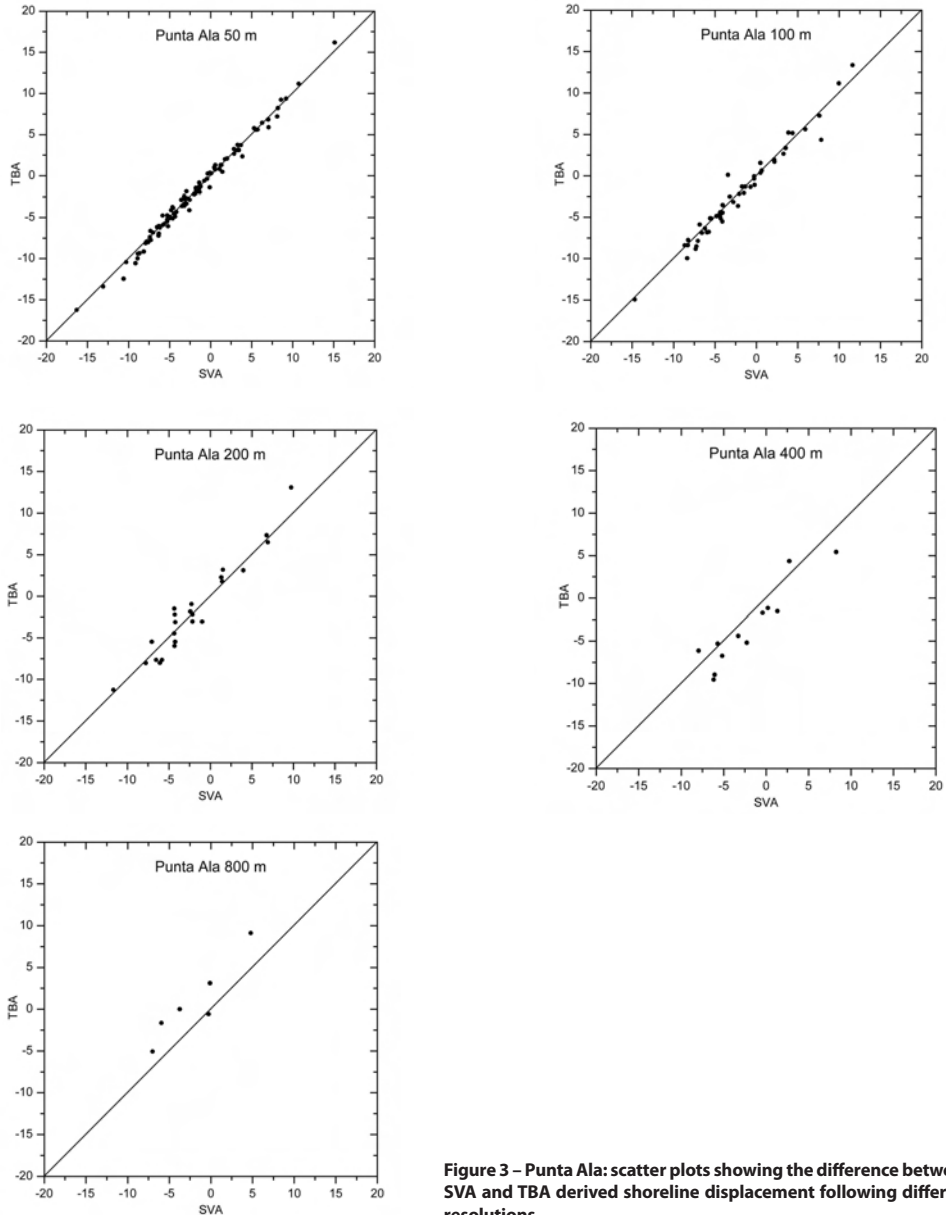
Figure 3 – Punta Ala: scatter plots showing the difference between SVA and TBA derived shoreline displacement following different resolutions.

Figure 4 – Location of sectors and transepts in the southern part of Punta Ala beach.

evaluations of the shoreline displacement given by TBA; whereas points under this line show pessimistic evaluations of it. Outliers represent peculiar cases of transepts located in points where "local" shoreline migration does not fit the shift of adjacent segments. This problem is limited to the southern part of the coast at Punta Ala, where these discrepancies are more pronounced (Figure 4).

Reducing the resolution of analysis (larger sectors and more spaced transepts), mean shoreline displacement for the whole coastal sector given by SVA does not change, whereas results by TBA are uneven, ranging from -3.42 to +0.82 m; standard deviation is more constant (Table 1 and Figure 5).

Increasing the length of sectors, points become more distant from the bisector as shown by $|\Delta_{S-T}|$, reaching a value of 2.96 m for a resolution of 800 m: TBA proved to be inaccurate in describing variations in beach surface.

Table 1 - SVA and TBA results at Punta Ala.

	Mean S	Mean T	s.d, S	s.d. T	$\|\Delta_{S-T}\|$
50 m	-2,04	-2,12	5,44	5,59	0.43
100 m	-2,04	-2,19	5,35	5,58	0.73
200 m	-2,04	-1,86	5,11	5,69	1.22
400 m	-2,04	-3,42	4,68	4,71	2.01
800 m	-2,04	0,82	4,39	4,84	2.96
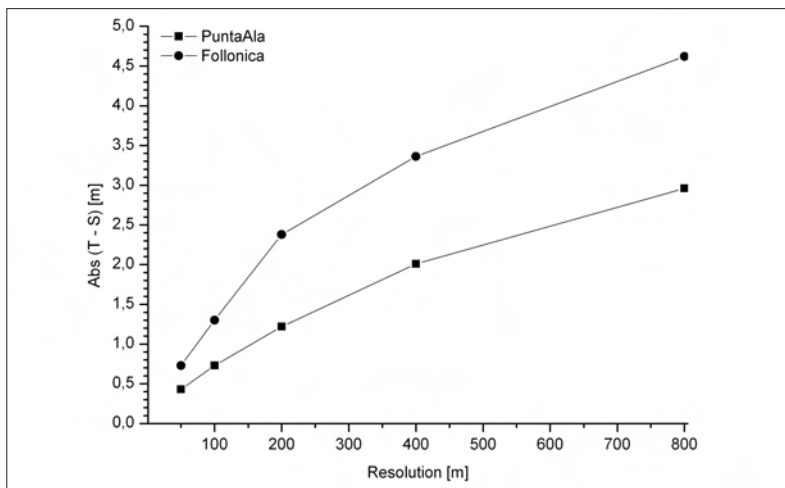
Figure 5 - Absolute mean difference between shoreline displacements obtained by SVA and TBA at Punta Ala and Follonica.

Follonica beach

At a 50 m resolution analysis, mean shoreline displacement is -1.25 m (st. dev. = 6.64) for SVA and -1.42 m (st. dev. = 6.89) for TBA. Most of the points in the SVA/TBS graphs (Figure 6) lie near the diagonal: the mean absolute difference between values ($|\Delta_{S-T}|$) is 0.73 m (Table 2). Outliers represent peculiars
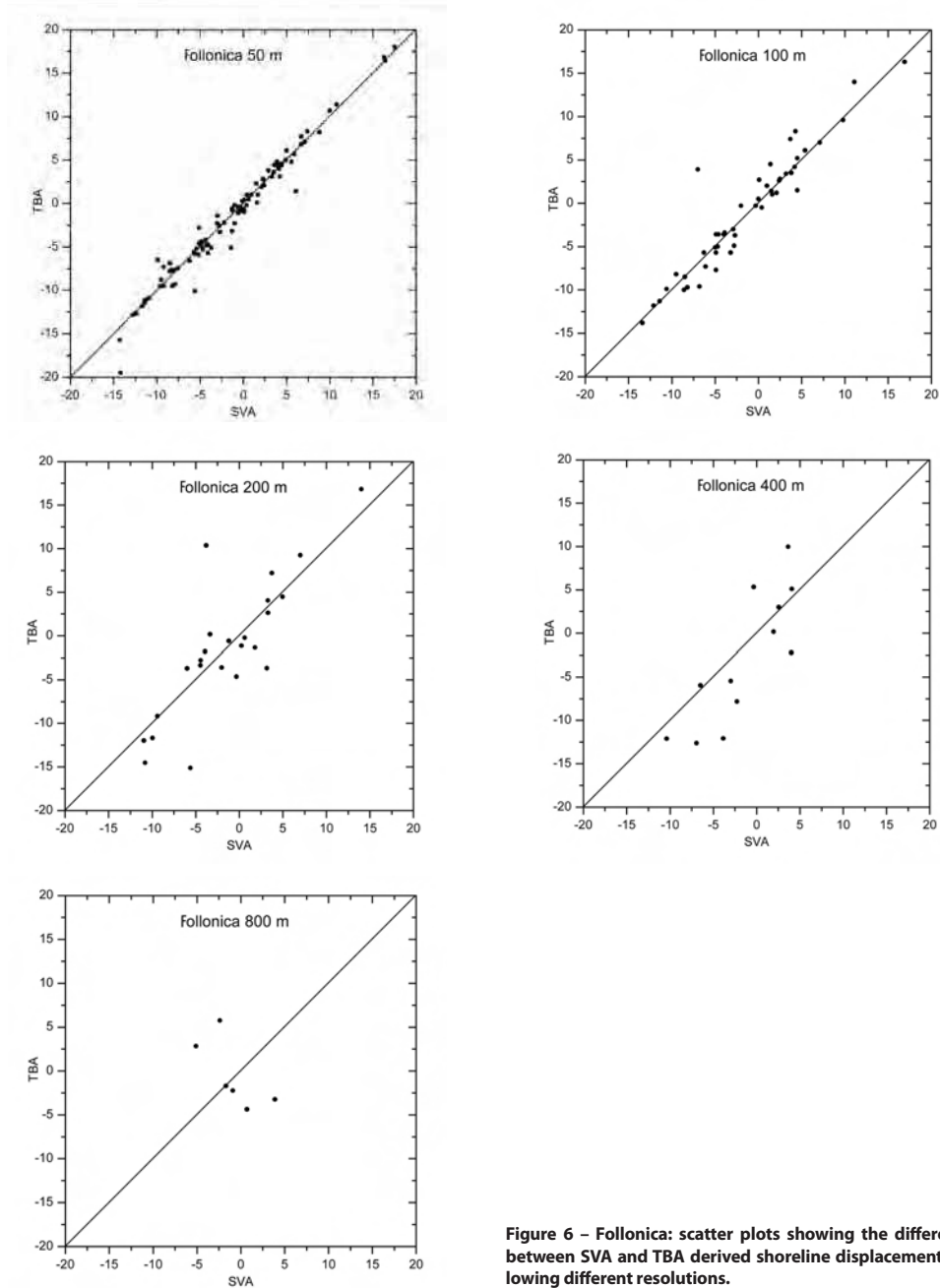
Figure 6 – Follonica: scatter plots showing the difference between SVA and TBA derived shoreline displacement following different resolutions.

cases, such as the one shown in Figure 7, where transect n. 23 is located in a stable point, and cannot document the evolution of the lobe present at the right-hand side and which is responsible for the surface variation in this sector.

Mean shoreline displacement retrieved through TBA ranges from +0.03 m to -5.85 m. At this beach, the same decrease in resolution produces more scattered points in the SVD vs. TBA graphs, as demonstrated by absolute mean differences, with $|\Delta_{S-T}|$ reaching 4.62 m at 800 m (Figure 5; Table 2).

Table 2 - SVA and TBA results at Follonica.

	Media S	Media T	s.d, S	s.d. T	$|\Delta_{S-T}|$
50 m	-1.25	-1.42	6.64	6.89	0,73
100 m	-1.25	-0.89	6.31	6.77	1,3
200 m	-1.25	-1,39	5.28	6.96	2,38
400 m	-1.25	+0.03	4.76	7.93	3,36
800 m	-1.25	-5.85	2.73	5.44	4,62
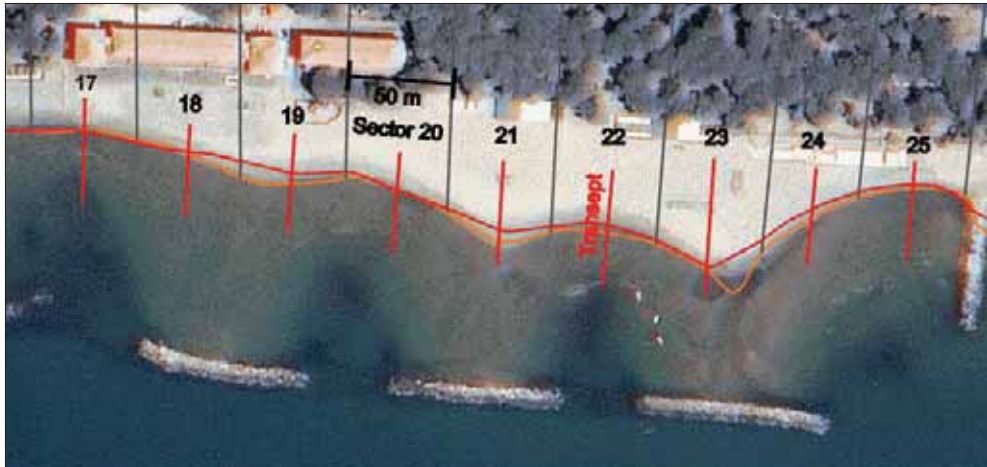
Figure 7 - Locations of sectors and transepts in the eastern part of Follonica beach. See Sector and Transept n. 20 and 22 where TBA underestimates mean beach accretion, whereas Transept 21 overestimates it.

Conclusions

Surface Variation Analysis (SVA) and Transept Based Analysis (PBA) produce different results when used to monitor shoreline evolution. As expected, differences are more pronounced when the shorelines under study are more irregular, due to the presence of natural patterns (rhythmic or not rhythmic) or to morphologies induced by coastal structures.

On average, the fitting between SVA and TBA data increases when sector length and transept spacing are reduced, but there is not a regular trend because of the random distribution and size of the irregularities.

Along the smooth shoreline at Punta Ala, there is only a small increase in mean absolute difference when resolution decreases. At this coast, the two methods give similar results for sector length (and transept spacing) up to 200 m ($|\Delta_{S-T}|$) = 1.22 m).

Along the intensively protected Follonica coast, a higher value is already verified at 100 m resolution ($|\Delta_{S-T}|$) = 1.3)., and the mean absolute difference reaches 2.38 when analysis is performed at 200 m

resolution. TBA is therefore not accurate to study coastal evolution except when profiles are extremely close (less than 100 m, at least in our case).

On average, the fitting between SVA and TBA data worsens when sector length or transept spacing increase, but there is not a regular trend because of the random distribution and size of the irregularities.

References

Aminti P., Cammelli C., Cappietti L., Jackson N.L., Nordstrom K.F. and Pranzini E. (2004) - *Evaluation of Beach Response to Submerged Groin Construction at Marina di Ronchi, Italy, Using Field Data and a Numerical Simulation Model*. Journ. Coastal Research, 33: 99-120.

Aminti P., Cipriani L.E. and Pranzini E. (2002) - *Beach erosion control along the Golfo di Follonica (Suthern Tuscany): actual hard protections vs. potential soft solutions*. Littoral 2002, 6th Int. Symp., Porto, Portogallo. pp.355-363.

Anfuso G. and Garcia F-J. (2005) - *Morphodynamics characteristics and short-term evolution of a coastal sector in SW Spain: implications for coastal erosion management.* Journ. Coastal Research, 21: 1139-1153.

Bartolini C., Pranzini E., Lupia Palmieri C. and Caputo C. (1977) - *Studi di geomorfologia costiera: IV - L'erosione del Golfo di Follonica*. Boll. Soc. Geol. It., 96: 87-116.

Bowman D., Ferri S. and Pranzini E. (2007) - *Efficacy of beach dewatering - Alassio, Italy*. Coastal Engineering, 54: 791-800.

Guza R. and Inman D. (1975) - *Edge waves and beach cusps*. Journ. Geophysical Research, 80: 2997-3012.

Hicks D.M., Green M.O., Smith R.K., Swales A., Ovenden R. and Walsh J. (2002) - *Sand volume change and cross-shore sand transfer, Mangawhai Beach, New Zeland*. Journ. Coastal Research, 18: 760-775.

Krause G. and Soares C. (2004) - *Analysis of beach morphodynamics on the Bragantinian mangrove peninsula (Pará, North Brazil) as prerequisite for coastal zone management recommendations*. Geomorphology, 60: 225-23.

Morton R.A., Miller T. and Moore L. (2005) - *Historical shoreline changes along the US Golf of Mexico: a summery of recent shoreline comparisons and analyses*. Jour. Coastal Research, 21: 704-709.

Pranzini E. and Rossi S. (2000) - *L'erosione del litorale di Punta Ala: un caso di naturale riequilibrio morfologico*. Studi costieri, 3: 3-27.

Rogers S.S., Sandweiss D.H., Maasch K.A., Belknap D.F. and Agouris P. (2004) - *Coastal change and beach ridges along the Northwest coast of Peru: image and GIS analysis of the Chira, Piura, and Colàn beach-ridge plains*. Journ. Coastal Research, 20: 1102-1125.

Różyński G. (2004) - *Long-term shoreline response of a nontidal, barred coast*. Coastal Engineering, 52: 79-91.

Schupp A.C., McNinchJ.E. and List J.H. (2006) - *Nearshore shore-oblique bars, gravel outcrops, and their correlation to shoreline change*. Marine Geology, 233: 63-7.

Schwab W.C., Theiler E.R., Allen J.S., Foster D.S., Swift B.A., Denny J.F. and Danforth W.W. (1999) - *Geologic mapping of the nearshore area offshore Fire Island, New York*. Coastal sediments '99, New York. Amm. Soc. Civil Eng. pp. 1552-1567.

Silvester R. and Hsu J.R.C (1993) - *Coastal stabilization. Innovative concepts.* PRT Prentice Hall, Englewood Cliffs, New Jersey. pp. 578.

Tanner W.F. (1975) - *Beach process, Berrien County, Michigan*. Journ. Great Lakes Res., 1: 171-178.

White K. and El Asmar H.M. (1999). *Monitoring changing position of coastlines using Thematic Mapper imagery, an example from the Nile Delta*. Geomorphology, 29: 93-105.

Closure depth estimation along the Tuscan coast aimed at short and long term coastal monitoring

Gian Luigi De Filippi, Eleonora Duchini, Enzo Pranzini

Determining the depth of closure for the scope of coastal monitoring projects is necessary due to fact that surveys must be optimised and limited to a sea bottom stretch where a significant bathymetric variation is expected to happen.

The estimated limits of beaches (i.e., the boundaries between the upper and lower shoreface) along the Tuscany coast were assessed for typical and extreme wave conditions. The littoral was divided into homogeneous areas from the meteo-marine point of view, and for each area the closure depth and set-up values were computed according to the annual wave climate and to the extreme wave heights that affect the area. To quantify the statistical uncertainties associated to the extreme values assessed, sensitivity analysis was performed considering sea level variations induced by tide and storm surge. These variations were computed by a bi-dimensional hydrodynamic barotropic model operating on true bathymetry.

The analysis of results has put into evidence how the extension of bathymetric surveys conducted in different studies is often not the most adequate.

These data permit an optimal set-up of any coastal monitoring program defining the effectiveness of beach defence projects. Moreover, morphodynamic parameters computed for the whole Tuscany coast allow a "global" analysis of the process reshaping this coast, with cross-comparisons from which new perspectives could arise.

Introduction

Closure depth (of bathymetric profiles) is defined as the depth beyond which surveys that are repeated along the years will not highlight variations in the bathymetric quote. Theoretically, it is the limit beyond which the sediment flows induced by waves are not capable of moving the sediments present. It is certainly a statistical definition, since if the period of observation is stretched, the probability that an event where waves are capable of moving sediments at higher depths is always higher. Determining the depth of closure for the scope of coastal monitoring projects is necessary due to fact that surveys must be optimized and limited to a sea bottom stretch where a significant bathymetric variation is expected to happen. Bathymetric surveys have a cost per linear meter of route (singlebeam) or per square meter of acquisition (multibeam) and any increases in the zone being surveyed determines a fast increase in costs (BEACHMED, 2005).

In addition, knowing this limit can allow evaluating if it is possible that losses towards the offshore zone happened in a certain period of time. This problem is particularly felt when the monitoring area has undergone artificial beach renourishment, since the analysis of changes in the sediment budget allow evaluating the efficacy of the renourishment project, estimate renourishment (refill) times and confirm if the baseline studies had considered correctly all the terms in the balance. The determination of closure depth is in any case necessary for calculating the volume in a renourishment project according to the larger extension of the emerged beach and the granulometry of the material.

This limit, as indicated by its definition, can be determined by overlaying bathymetric surveys that were carried along the time considered, but when it is identified using such means it can be correlated only to the period of time that was considered, and does not allow extrapolations onto longer periods.   Alternatively, it can be calculated based on the oceanographic characteristics of a certain location, which were observed during a significant numbers of years, and extrapolated to a certain period of return.

The Tuscan coast has been monitored in the past decades in order to evaluate the long term evolution trends for the sake of implementing management strategies. It was also monitored at short term at locations where defence interventions had been made, so that the efficacy of these projects could be evaluated. However, not always monitoring considered this need.

Regione Toscana has recently undertaken a more important role in the integrated management of the coastal zone due to the current administrative devolution (Regione Toscana, 2004), and has delegated to counties (Province) the power to carry out defence projects. The latter have since then initiated numerous projects for the re-equilibrium of the coastline. It is reasonable to expect that large sums of money will be needed for that aim in the near future, and therefore financial resources should be optimized. It was in accordance to this that a study on closure depth at regional scale was carried within Sub-project OpTIMAL (OCR BEACHMED-e). This study is able to provide indications that are useful to the designing and implementation of monitoring projects, as well as elements that allow having a new perception of processes under act along the Tuscan coast. A synoptic view, obtained with data of identical origins which have undergone the same processing modes, allows having a transversal confrontation among beached as never done before.

Materials and Method

The estimated limits of beaches (*i.e.,* the boundaries between the upper and lower shoreface) along the Tuscany coast were assessed for typical and extreme wave conditions. The littoral was divided into homogeneous areas from the meteo-marine point of view, and for each area the closure depth and set-up values were computed according to the annual wave climate and to the extreme wave heights that affect the area. To quantify the statistical uncertainties associated to the extreme values assessed, sensitivity analysis was performed considering sea level variations induced by tide and storm surge. These variations were computed by a bi-dimensional hydrodynamic barotropic model operating on true bathymetry.

To define meteo-marine conditions of each area, wind and wave data hindcasted respectively by the well-known ECMWF (European Centre for Medium-range Weather Forecast, 2008) and WAM (WAMDIG, 1988) models relating to the period from 1992 to 2004 were used.

The coastal bathymetry considered derives from measurements performed in 2005 by Regione Toscana; offshore bathymetry derives from nautical charts.

The method used in this study is presented below, and is based on the knowledge of the coastal processes as described in U.S. Army Corps of Engineers (1984), Massekink and Hughes (2003); Hails and Carr (1975); Svendsen and Jonsson (1980) Fredsøe and Deigaard (1992).

Research was divided into two phases.

The first phase refers to:
- assessment of the "typical" limits of the beach, *i.e* the closure depth and the level of set-up: average value, value at 95% of probability and maximum value;
- assessment of the "extreme" limits estimated starting from the extreme waves associated to a 50-year return period.

The second phase refers to:
- estimate of the wind set-up induced by extreme winds;
- estimate of the sea level variations induced by tide;
- sensitivity analysis of the extreme limits assessed in the first phase.

Beach limits

To assess the limits of the emerged and submerged beach, calculation was performed assuming the wave climate $P(H,T,\theta)$ as input. Wave climate is described by a 3-dimensional matrix where each element represents the frequency P_i of the events characterised by wave height H_i, wave period T_i, wave incoming direction θ_i. Thus, the calculation takes into account the contribution of all remarkable climate elements that are typical for each zone of the studied area.

The model used in this study is able to estimate various parameters that are useful to define the emerged and submerged beach characteristics, as well as the limits of the surf zone and the wave-induced set-up.

Closure depth

The closure depth, *i.e.*, the limit between the upper and lower shoreface that represents a seaward limit to the occurrence of significant cross-shore sediment transport, was assessed according to the original relationships of Hallermeier (1978):

$$d_{lim} = 2.28 \, H - 68.5 \, H^2/gT^2 \qquad [1]$$

Where H is the local wave height and d_{lim} is computed for each element of the matrix $P(H,T,\theta)$, obtaining a distribution of the closure depth for each section along the beach.

Thanks to the availability of the wave climate, formula [1] was preferred to the simple formula proposed by Hallermeier (1981):

$$d_{lim} = 2H_{smed} + 11\sigma \qquad [2]$$

Where H_{smed} is the significant medium wave height and σ is the standard deviation used for the general calculations along various coasts around the world.

Wave set-up

The wave-induced set-up, *i.e.*, the medium rise of the sea level due to the wave heights decreasing as consequence of the mass flux toward lower depths, is a very important phenomenon in the coastal area. For each element of the wave climate the set-up of the sea level was computed as:

$$S = 5/16\Gamma H_b \, [1-5/6\pi \, H_b/(\Gamma L_o)\sin^2\alpha_o] \qquad [3]$$

Where L_o is the deep water wave length, α_o the deep water angle of incidence, $\Gamma = H_b/d_b$, H_b is the breaking wave height and d_b the breaking depth.

In this way a distribution of the set-up values was obtained and the values corresponding to 50% and 95% of probability as well as the maximum value were assessed.

Breaking waves

The breaking waves were calculated by the well-known relationship:

$$H_b/d_b = \Gamma \qquad [4]$$

Where Γ is a function of wave steepness and bottom slope m, according to:

$$\Gamma = b-(aH_b)/(gT^2)$$

$$b = 1.56/(1+e^{-19.5m}) \qquad [5]$$

$$a = 1.36 \, g(1-e^{-19m})$$

Breaking type

The experimental results of Kamphuis and Readshow (1978) show less efficiency in the sediment uplift for the "spilling" breaking waves with respect to "plunging" or "surging".

The wave breaking conditions are defined by means of the so-called "breaking index" ε_b value, that is less than 0.4 for the spilling type, between 0.4 and 2 for plunging waves and greater than 2 for the surging mode. The breaking index is given by:

$$\varepsilon_b = \tan(\alpha)/(H_b/L_o)^{1/2} \qquad [6]$$

Where $\tan(\alpha)$ is the bottom slope and H_b/L_o is the wave steepness.

Hattori index

According to various authors, the sediment grain size distribution along a cross-shore beach profile due to cross-shore transport can be explained on the basis of the "equilibrium grain size" concept.

Therefore, given the wave conditions, for each position along the breaking zone there is a particular sediment grain dimension whereby the sediment is in equilibrium. Grains of size smaller than the "equilibrium grain size" will move seaward, while grain of larger size will move landward.

Therefore, given the wave climate and the sediment characteristics, it is possible to evaluate the predominant cross transport direction.

Moreover, Hattori and Kamawata (1980) have highlighted the importance of taking into account the wave steepness and the bottom slope with respect to the cross-shore transport, according to the relationship:

$$I_H = (H_o mgT)/[L_o W(D_{50})] \qquad\qquad [7]$$

Where H_o, L_o, T are the offshore wave height, length and period respectively.

$W(D_{50})$ is the fall velocity of a grain of D_{50} size, m is the bottom slope and g is the gravity acceleration.

Hattori index $I_H < 0.5$ means transport landward, $I_H > 0.5$ means transport seaward.

The frequency distribution of the values was calculated for each element of the wave climate by means of [7]: the result is an estimate of the beach profile evolution trend (equilibrium, erosion or accretion) due to cross-shore transport.

Sea level

Sea level variation is due to many factors. Sea level can be considered as a simple linear superimposition of several terms η_i:

$$V = \Sigma\, \eta_i \qquad\qquad [8]$$

In practice, all phenomena involved can be gathered in two fundamental categories:
1) the deterministic component and
2) the stochastic component.

Therefore the sea level can be assumed as a linear combination of these two independent quantities:

$$\eta(t) = \eta_T(t) + \eta_s(t) \qquad\qquad [9]$$

The deterministic component is mainly due to the tidal oscillation while the stochastic component is mainly due, in general, to the storm surge that is induced by wind and pressure gradient.

Tidal sea level rise

The deterministic component of the sea level, due to the tidal oscillation, can be expressed by the combination of several harmonic components with a known periodicity and can be expressed by the following equation:

$$L_D(t) = \sum_1^N A_k \cos\left(\omega_k t + \varphi_k\right) \qquad\qquad [10]$$

Where:
- Ak is the amplitude of the k-nth tidal harmonic component;
- ω_k is its angular velocity;
- φ_k is its phase;
- N is the number of the harmonic component.

Since ω_k is known, the assessment of tidal oscillation is performed by setting the tidal harmonic constants A_k and φ_k of the main tidal components.

Wind set-up

Since measured data concerning the storm surge along the coast of Tuscany are not available, the sea level due to the wind effect was computed by a hydrodynamical model.

A barotropic response is typical of the coastal zones (Elliot, 1981; Gordon, 1982). A barotropic 2D

model was applied in this study, as the coastal dynamic response in the Ligurian-Thyrrhenian Sea is barotropic in 90% of events.

Assuming as input the 50-year return period wind velocity, various simulations were performed with the barotropic model, and the sea level trend was evaluated in various coastal areas.

The model is based on the following equations (De Filippi et al., 2004):

$$U_t = -UU_x - VU_y - g\eta_x + fV + \tau_x/(\sigma H) - gU(U^2 + V^2)^{1/2}/(C^2 H) \qquad [11]$$

$$V_t = -UV_x - VV_y - g\eta_y - fU + \tau_y/(\sigma H) - gV(U^2 + V^2)^{1/2}/(C^2 H)$$

The equation of the conservation of mass is:

$$\eta_t = -(HU)_x - (HV)_y \qquad [12]$$

The index x, y, z, t refer to the partial derivatives, while the notation is:

x,y	Cartesian coordinates in the horizontal plane of the undistorted sea surface;
z	vertical coordinate, $z = 0$ on the bottom;
t	time;
η	sea surface elevation;
U,V	components of the depth-averaged current in the direction of increasing x, y respectively;
f	Coriolis' parameter $= 2\Omega\sin\Phi$;
Ω	Earth rotation speed;
Φ	latitude;
H	total depth of water;
τ_x	x component of surface stress of wind;
τ_y	y component of surface stress of wind;
C	coefficient of friction (coefficient of Chezy);
σ	water density;
g	acceleration of earth gravity;
p	hydrostatic pressure.

The depth-average currents are defined as:

$$V = \left(1/H\right)\int_h^\mu V'dz; \quad U = \left(1/H\right)\int_h^\mu U'dz \qquad [13]$$

Where V' and U' are the components of the horizontal current at depth z below the sea surface.

Stress components are calculated from surface wind components:

$$\tau_x = \sigma_a C_d W_x (W_x^2 + W_y^2)^{1/2} \qquad [14]$$

$$\tau_y = \sigma_a C_d W_y (W_x^2 + W_y^2)^{1/2}$$

Where C_d is the coefficient of friction and σ_a is air density:

$$C_d = [36.4 - 5\ln(W)]^{-2} \qquad [15]$$

The Chezy´s coefficient is calculated as follows:

$$C = 18\log_{10}(12H/r) \qquad [16]$$

Where r is the ruggedness of the bottom.

The problem of computing the water circulation is an initial boundary value problem. Thus the model requires the specification of the conditions including the shore configuration and depth contours together with the initial values of the flow parameters.

The high rate of friction dissipation in shallow areas causes disturbance to be quickly damped. The influence of initial conditions becomes negligible and after a short time a regime is established in accordance with the boundary conditions and forcing terms. This fact greatly simplified the choice of the initial conditions, assuming an initial state of rest:

$$\eta = U = V = 0 \quad \text{at} \quad t = 0 \tag{17}$$

Open sea boundary conditions must be specified for any time t>0.

The coastal boundary condition is taken to be:

$$U_n = 0 \quad \text{at} \quad H(x,y) = 0 \tag{18}$$

The numerical integration of the set hydrodynamic equations is difficult because of their intrinsic non-linear character, introduced by bottom friction and advective terms.

Several numerical finite difference schemes for non-linear equations are available which preserve the second-order accuracy required for a suitable simulation (Leendertsee-Gritton, 1971; Sielecki, Wurtele, 1970; Flather Heaps, 1975).

In the model the finite difference representation of advective accelerations is based on the "angle derivative" approach of Robert and Weiss (1966) which provides an approximation to the spatial derivatives of the advected quantity properly centred in space and time.

For the numerical integration of the equation an explicit method was used. The physical parameters η, u, v are calculated on a staggered grid.

The time integration operates according to a leap-frog method, firstly calculating the elevation at next time n+1 using variables at previous time steps n, and then calculating u and v at time step n+1 using u and v variables at previous time step n and new elevation at time step n+1. This method is needed in order to guarantee the stability of the numerical solution. The friction term is computed by a semi-implicit scheme, to improve stability.

A final remark concerns the flooding process which is important and is taken into account by the hydrodynamic model: a particular algorithm was developed which allows checking at every time step the sense of emerged or submerged points. As a consequence of the test, a mesh is allowed to be flooded or, in alternative, the velocity components leading to that grid point are automatically set to zero.

Finally, the maximum permissible time increment for stable numerical solution follows the Courant criteria valid for explicit methods:

$$D_t \leq \frac{\max\left(D_x, D_y\right)}{\sqrt{2}\left(\left|\bar{V}_{max}\right|\right) + \sqrt{gh}} \tag{19}$$

Where D_x, D_y are the dimensions of the mesh, h is the maximum considered depth and V_{max} is the maximum current.

Sensitivity analysis

To quantify the sea level rise (set-up) or fall (set-down) due to the superimposition of tide and wind effects above the extreme closure depth, the follow steps were improved:

- sea level time series were extrapolated from the hydrodynamic model outputs at each significant point along the various Phisiographyc Units, and the maximum and minimum values were analysed;
- the maximum and minimum wind set-up values calculated at each of the above mentioned locations were added to the corresponding maximum and minimum tidal set-up, according to [9];
- by adding these set-up and set-down values induced by wind and tide, an average "indetermination" was associated to the limit of the submerged and emerged beach induced by the extreme waves, previously assessed.

Partitioning of the coast

The coast has been divided into five Physiographic Units as adopted by Regione Toscana (Fig. 1). For each Unit a suitable number of points was selected to assess the coastal wave climate, according to the orientation of the coast and the exposure sector: these points, named A, B, … are shown in Figure 2. Along the whole coast 136 homogeneous (in terms of incoming wave energy) sections were selected for the study of beach characteristics.
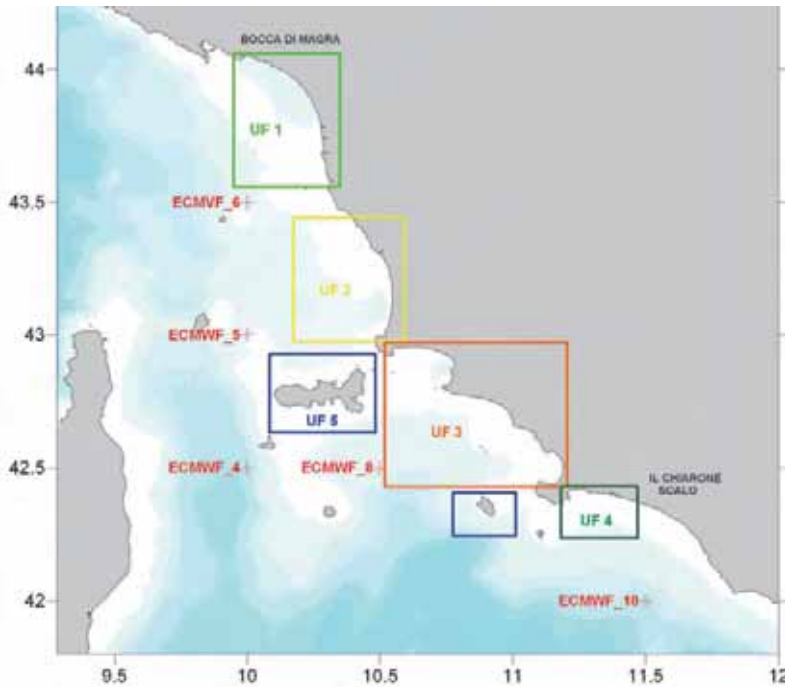
Figure 1 - Location of the Physiographic Units.
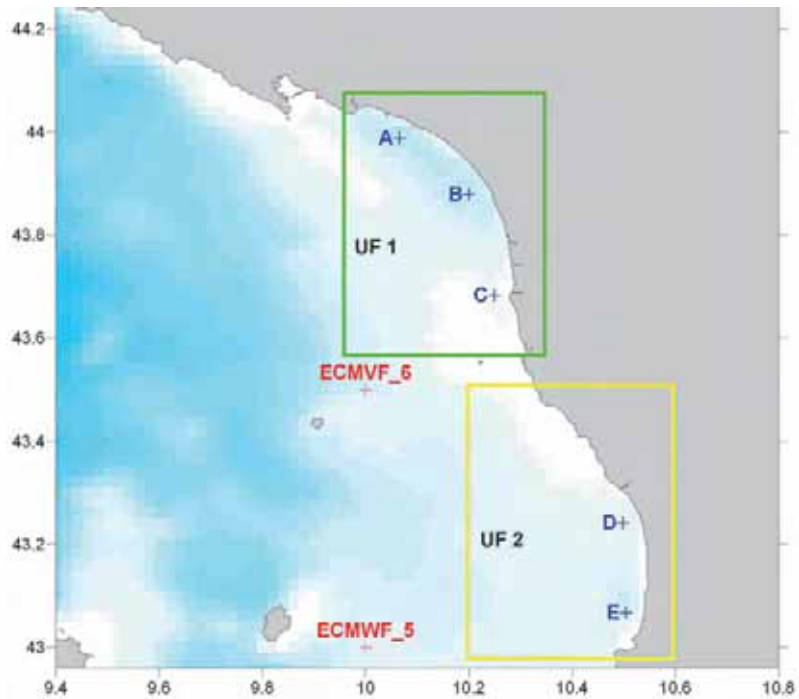
Figure 2 - Points selected to assess the coastal wave climate in Physiographic Units 1 and 2.

Results

Wind

Typical and extreme wind regimes were defined for each reference point, where frequency distributions of wind speed vs. incoming directions have been assessed (Figure 3).
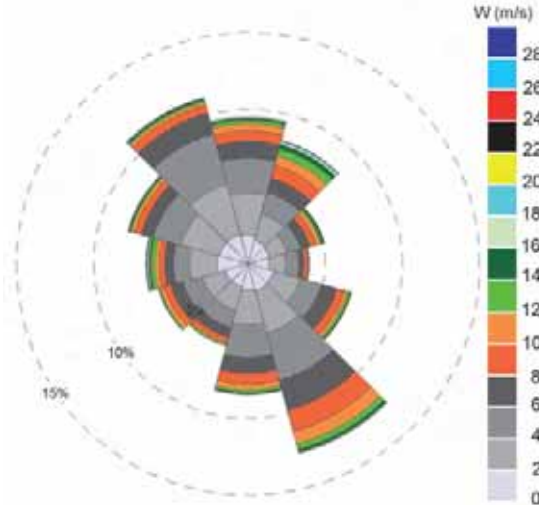
Figure 3 - Wind rose at Point 4

Table 1 reports the extreme wind speeds for the return period of 50 years, estimated by the Weibull distribution function:

$$P(W>w) = 1 - \exp[-(w/\alpha)^{\beta}] \qquad [20]$$

Where w is the wind speed, α and β the parameters of the distribution computed by the best-fit of data using the least square method.

Table 1 – Extreme values of wind speed (Return period: 50 years).

Dir	W (m/s)	W (m/s)	W (m/s)	W (m/s)	W (m/s)
(°N)	Point 4	Point 5	Point 6	Point 8	Point 10
0	23.4	22.4	24.5	24.9	22.3
30	30.6	26.1	23.2	29.7	24.0
60	25.8	24.7	23.5	26.3	17.2
90	21.5	20.6	21.5	22.2	18.3
120	24.1	21.1	22.1	24.7	20.3
150	23.7	21.5	22.1	24.7	20.0
180	23.1	22.6	19.8	23.1	19.4
210	19.8	16.1	18.2	22.3	18.9
240	21.6	25.9	28.3	23.3	20.8
270	31.9	28.7	25.8	31.0	23.9
300	25.8	20.6	23.3	26.8	18.4
330	25.2	23.1	22.6	25.0	20.1
Omni	31.9	28.7	28.3	33.2	25.8

Waves

The offshore wave climate was defined for each reference point, where frequency distributions of significant wave heights H_0 vs. incoming directions and mean wave periods vs significant waves were assessed (Figure 4).
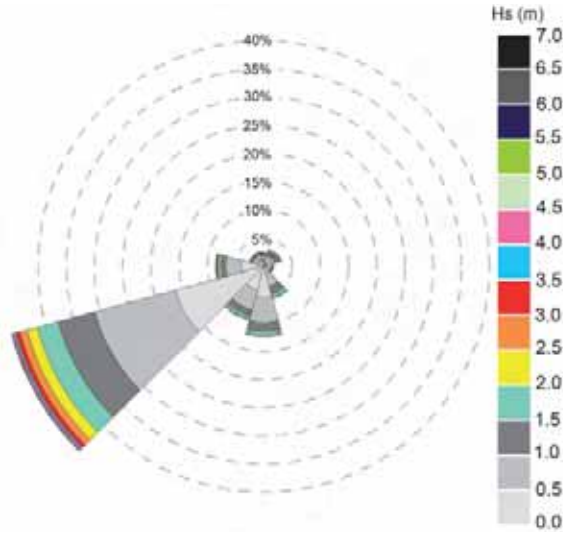
Figure 4 – Wave rose at Point 6.

Table 2 reports the extreme significant wave heights for the return period of 50 years, estimated by the Weibull distribution function, in the offshore points.

Wave propagation from the offshore to the coast was computed taking into account the refraction-friction-shoaling processes, *i.e.*, the local wave height H_i is assessed as:

$$H_i = H_o * K_r * K_s * K_f \qquad [21]$$

Where K_r K_s, K_f are the refraction, shoaling and friction coefficients respectively.

The coastal wave climate has been computed at the depth of 20m for each point, according to the expositions sectors shown in Table 3. From the analysis of the obtained wave climates, a noticeable variation was found along the coasts of Tuscany.

In Table 4 an example of the computed wave climate is reported for the Viareggio Beach.

Table 2 – Extreme values of offshore waves (Return period: 50 years).

Dir	Point 4		Point 5		Point 6		Point 8		Point 10	
(°N)	Hs (m)	Tm (m)	Hs (m)	Tm (m)	Hs (m)	Tm (m)	Hs (m)	Tm (m)	Hs (m)	Tm (m)
0	4.59	7.14	3.26	6.02	2.75	5.53	3.74*	6.45	4.28*	6.90
30	4.46	7.04	3.88	6.57	3.72*	6.43	4.17*	6.81	4.17*	6.81
60	4.64	7.18	3.44	6.18	3.47*	6.21	3.75*	6.45	3.07	5.84
90	5.16	7.57	2.43	5.20	2.06	4.78	4.59*	7.14	3.00	5.77
120	5.71	7.97	3.62*	6.34	3.59	6.32	4.01	6.67	5.22	7.62
150	5.97	8.14	3.58	6.31	3.61	6.33	5.54	7.85	5.64	7.92
180	4.50	7.07	3.81	6.51	4.30	6.91	5.95	8.13	6.19	8.29
210	3.31	6.06	3.19	5.95	4.20	6.83	4.38	6.98	6.02	8.18
240	3.51	6.24	3.66	6.38	7.54	9.15	5.36	7.72	5.97	8.14
270	4.67*	7.20	6.63	8.58	7.25	8.98	5.08	7.51	6.12	8.25
300	4.55	7.11	4.17	6.81	5.05*	7.49	5.08	7.51	5.34	7.70
330	5.39	7.74	3.97	6.64	3.81*	6.51	3.65	6.37	4.08	6.73
Omni	6.12	8.25	6.65	8.60	7.55	9.16	6.07	8.21	6.47	8.48

* = Values at the limit of validity if fetch lengths are considered

Table 3 - Wave exposure of the points where coastal climate was computed.

Computation points and Physiographics Units	Wave exposure (°N)		
	Nor.	min	Max
A – Unit 1	220	160	300
B – Unit 1	244	165	310
C – Unit 1	260	170	322
D – Unit 2	252	185	325
E – Unit 2	265	195	330
F – Unit 3	185	152	253
G – Unit 3	215	178	270
H – Unit 3	292	223	340
I – Unit 3	210	140	290
L – Unit 3	200	170	305
M – Unit 3	245	210	310
N – Unit 3	280	235	325
O – Unit 4	185	120	230
P – Unit 4	195	125	257

Table 4 - Wave climate in front of Viareggio beach, water depth 20m.

Dir.	Hs (m)										
(°N)	0.50	1.00	1.50	2.00	2.50	3.00	3.50	4.00	4.50	5.00	TOTAL
0	0.00	0.00	0.00	0.00	0.00	0.00	0.00	0.00	0.00	0.00	0.00
30	0.00	0.00	0.00	0.00	0.00	0.00	0.00	0.00	0.00	0.00	0.00
60	0.00	0.00	0.00	0.00	0.00	0.00	0.00	0.00	0.00	0.00	0.00
90	0.00	0.00	0.00	0.00	0.00	0.00	0.00	0.00	0.00	0.00	0.00
120	0.00	0.00	0.00	0.00	0.00	0.00	0.00	0.00	0.00	0.00	0.00
150	0.00	0.00	0.00	0.00	0.00	0.00	0.00	0.00	0.00	0.00	0.00
180	5.25	4.46	1.40	0.40	0.11	0.02	0.01	0.00	0.00	0.00	11.65
210	4.41	3.88	1.39	0.52	0.17	0.04	0.02	0.00	0.00	0.00	10.43
240	16.25	14.80	7.01	3.87	1.93	1.61	0.54	0.43	0.11	0.00	46.55
270	3.94	2.80	0.94	0.46	0.22	0.15	0.07	0.02	0.02	0.00	8.62
300	0.95	0.72	0.25	0.14	0.06	0.01	0.01	0.00	0.00	0.00	2.14
330	0.00	0.00	0.00	0.00	0.00	0.00	0.00	0.00	0.00	0.00	0.00
Tot.	30.80	26.66	10.99	5.39	2.49	1.83	0.65	0.45	0.13	0.00	79.39

The emerged and submerged beach

For each section the following parameters were computed assuming as input the wave climate as well as the extreme values:

- Set-up: values referred to 50-year return period, maximum and 95% of probability;
- Closure depth: values referred to 50-year return period, maximum and 95% of probability;
- Breaking depth: values referred to 50-year return period, maximum and 95% of probability;
- Breaking waves: percentage of each type of breaking (spilling, plunging, surging);
- Cross-shore transport: percentage of wave events inducing transport towards the shore, towards the sea, and alternating;
- Maximum set-up and set-down induced by extreme winds;
- Maximum and minimum sea level values induced by tides.

The behaviour of the closure depth along the whole coast, the breaking depth and the wave set-up are shown in Figure 5.
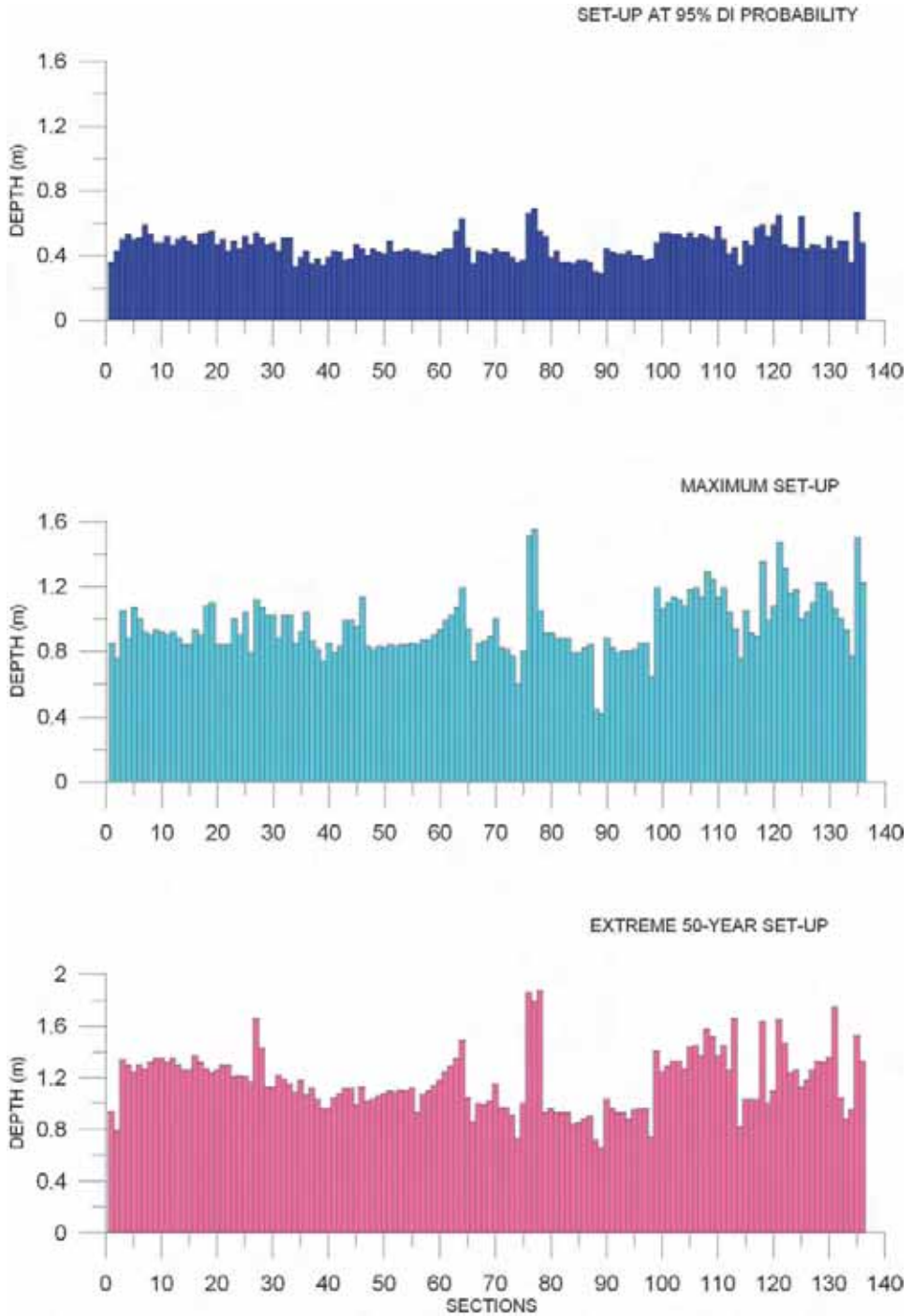
Figure 5 – Extreme, Maximum and 95% of probability of set-up along the 136 sections defined on the Tuscan coast (from North to South).

An example of the positions of closure depths (extreme, max and 95% probability) overlapping bathymetry is reported in Figure 6. The blue points along the coast indicate the position of sections where the above parameters were computed.
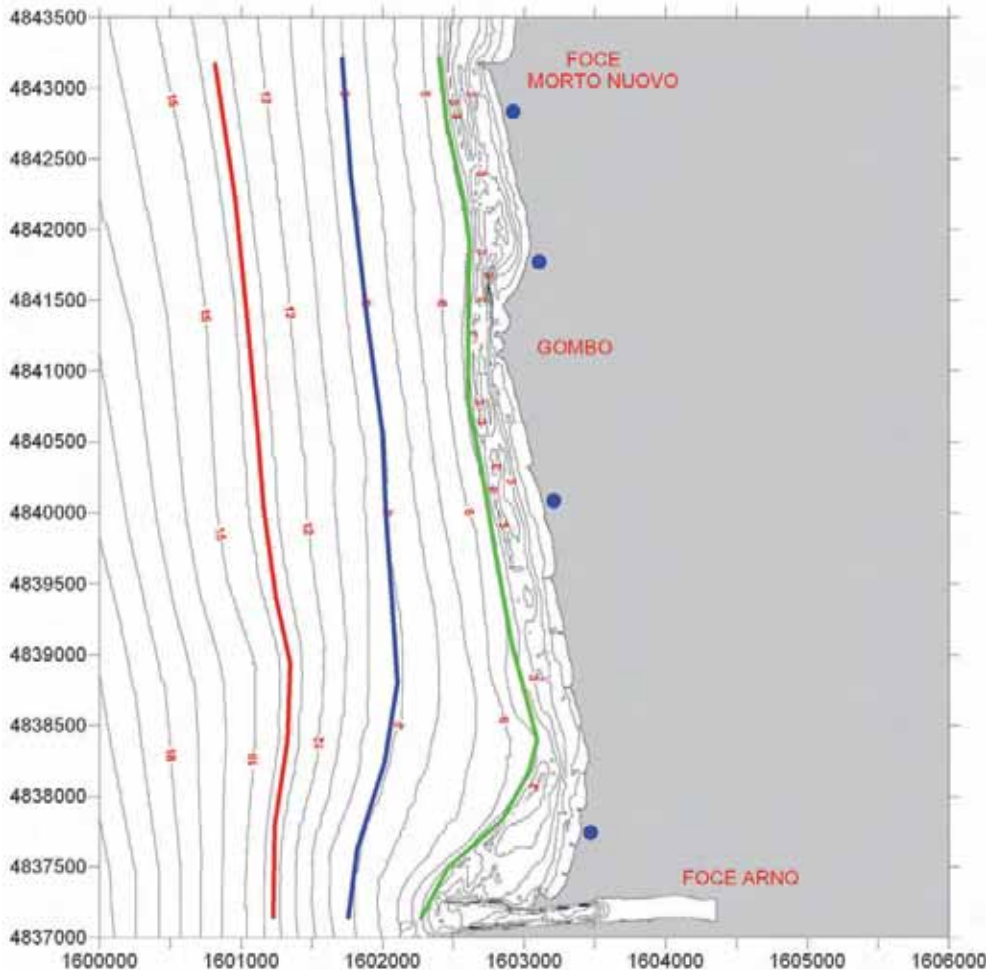
Figure 6 – Example of cartography of closure depth. Closure depth at 95% (green), maximum recorded along the 12 years of observations (blue) and for a return period of 50 years (red).

Sea level
Sea level variations must be considered: in fact, if tides are characterised by reduced values, the wind generally induces noticeable set-up values along the coasts of Tuscany.

Tidal oscillation can be represented using only the semi-diurnal components M2 and S2 and the diurnal components O1 and K1 reported in Tidal Tables.

From the harmonic constants of these components, 1-month time series were hindcasted for the stations of La Spezia, Livorno and Civitavecchia and the values were then interpolated at the different sections along the coast.

The role of the wind was assessed by a hydrodynamical model applied to a large area for 48 hours of simulation: a 24-hour wind pulse characterised by a 50-year extreme speed was supplied as input, and 24 hours in absence of wind, to evaluate the basin response.

A large number of simulations was performed in order to take into account the main wind directions affecting the coast.   An example of the results is reported in Figure 7, where the current field, represented by arrows, and the sea level, represented by isolines, are presented for the extreme wind blowing from 30°N. For each gridpoint corresponding to the closure depth, the time-series simulated by the model were analysed in order to define the minimum and maximum values of the sea level. In Figure 8, an example of these time- series for gridpoints A, B, C, generated by the extreme wind from 240°N, is presented.

Finally, in Table 5, maximum and minimum sea level elevations induced by the extreme 50-year wind are reported for the gridpoints of Physiographic Units 1, 2, 3.

Figure 7- Results from hydrodynamic model. Current field (represented by arrows) and sea level (represented by lines) for extreme wind blowing from 30°N.
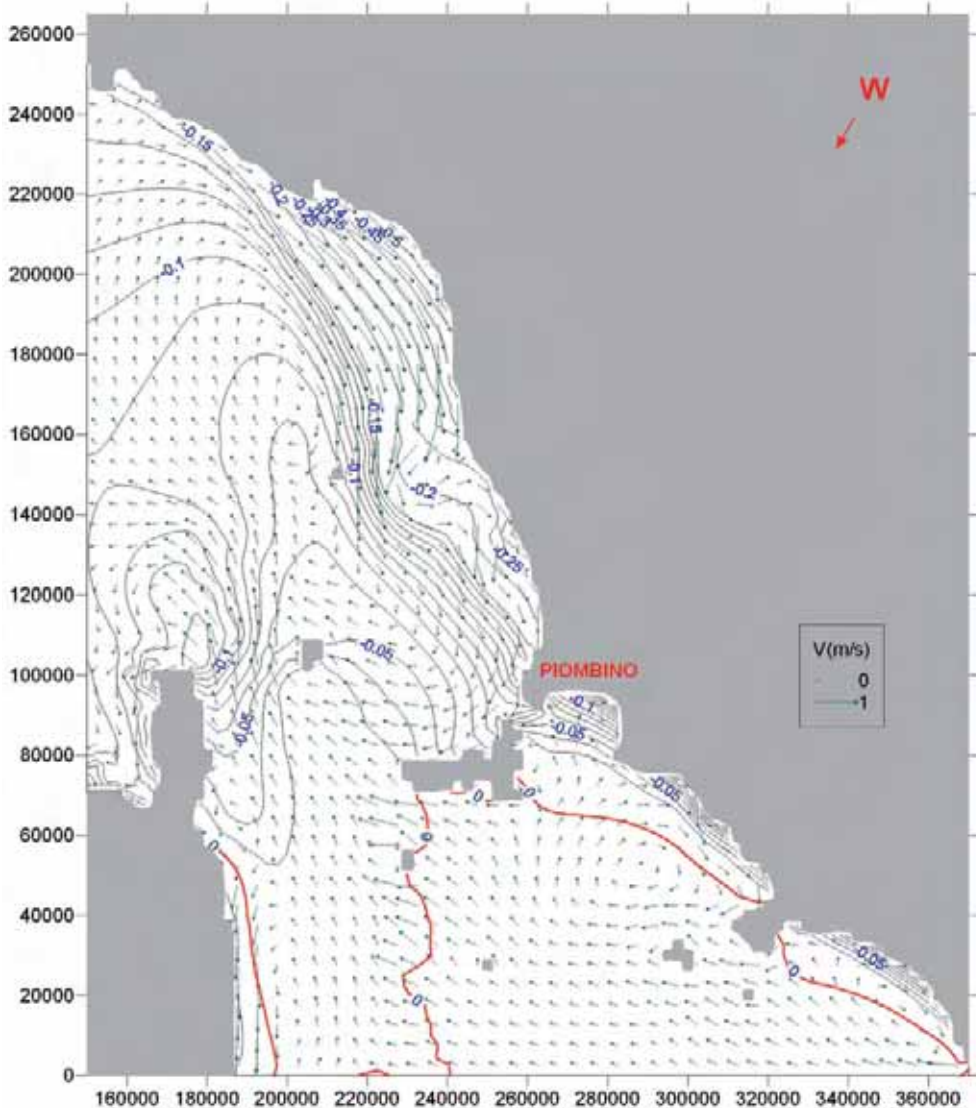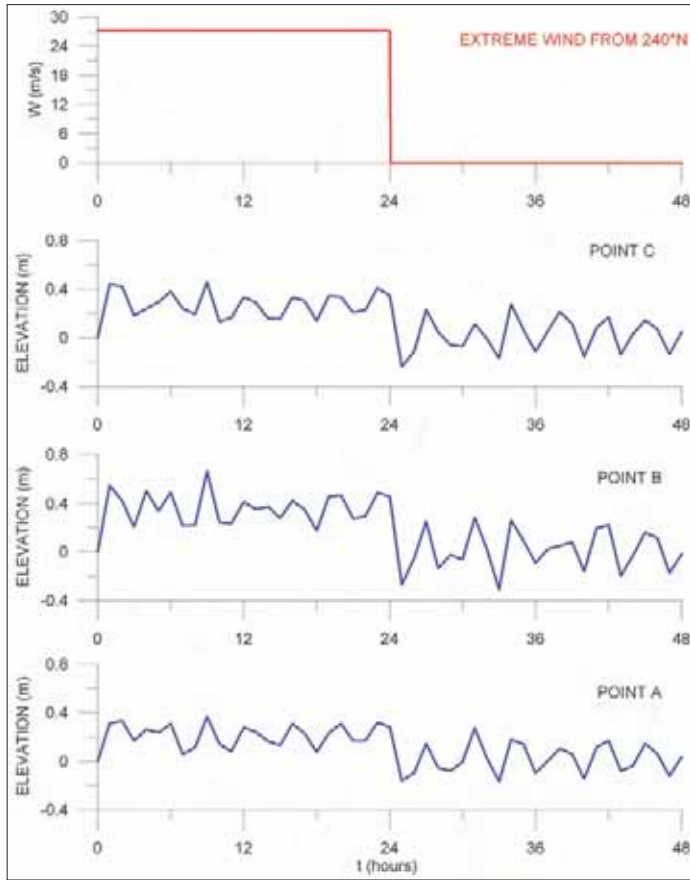
Figure 8 - Example of time-series for gridpoints A, B, C, generated by extreme wind from 240°N.

Table 5 – Max and min sea level elevations induced by the extreme 50-years wind referred to the grid-pints located at closure depth (Physiographic Units 1, 2 and 3).

Physiographic Unit 1							
Reference point	Elevation: Max and min (cm)		Elevation: Max and min (cm)		Elevation: Max and min (cm)		Elevation: Max and min (cm)
Wind direction (N)	60°		150°		240°		330°	
A	19	-32	24	0	40	-16	7	-38
B	31	-54	36	-1	67	-31	11	-45
C	27	-36	24	-5	47	-24	11	-30
Physiographic Unit 2							
Wind direction (N)	60°		150°		240°		330°	
D	22	-33	26	-1	41	-17	14	-33
E	24	-22	17	-8	28	-19	12	-17
Physiographic Unit 3							
Wind direction (N)	30°		120°		210°		300°	
F	17	-29	22	-5	17	-9	5	-27
G	19	-38	20	-6	21	-10	6	-28
H	16	-27	14	-4	15	-8	4	-19
I	11	-25	12	-1	14	-5	3	-17
L	9	-19	10	-4	10	-4	2	-13
M	9	-20	9	-6	11	-5	2	-11
N	9	-15	9	-8	8	-5	3	-8

Sensitivity analysis

The "indetermination" associated to the limit values of the submerged and emerged beach induced by the extreme waves was assessed by adding the set-up and set-down effect induced by wind and tide. The results are shown in Table 6.

Table 6 – Min and Max values of the limits of the submerged and emerged beach. Return period: 50 years.

	Closure depth (m)		Upper limit of active profile (m)	
	min	Max	min	Max
Physiographic Unit 1				
Foce Magra	-7.7	-14.0	0.25	1.88
Marina di Carrara	-13.8	-14.0	0.71	1.84
Marina di Massa	-12.9	-14.0	0.73	1.86
Marina di Pietrasanta	-12.8	-14.5	0.57	2.16
Marina di Vecchiano	-12.8	-14.8	0.55	2.14
Arno R. mouth	-12.8	-14.4	0.48	2.04
Tirrenia	-13.0	-14.3	0.62	2.28
Physiographic Unit 2				
Rosignano Solvay	-11.3	-12.4	0.61	1.74
Vada	-11.4	-12.5	0.48	1.68
Mazzanta	-11.4	-12.5	0.56	1.68
Marina di Cecina	-10.9	-12.0	0.51	1.69
Tombolo di Cecina	-11.2	-12.3	0.55	1.62
Marina di Bibbona	-11.4	-12.5	0.60	1.66
Tombolo di Bolgheri	-11.6	-12.4	0.73	1.55
Donoratico	-11.1	-11.9	0.56	1.50
Marina di Castagneto	-11.2	-12.1	0.73	1.57
San Vincenzo	-11.3	-12.1	0.81	1.68
Torraccia	-11.3	-12.1	0.92	1.92
Golfo di Baratti	-7.2	-10.7	0.49	1.48
Physiographic Unit 3				
Follonica	-7.8	-11.3	0.20	2.17
Rocchette	-9.3	-10.1	0.44	1.25
Talamone	-5.9	-10.0	0.31	1.29
Physiographic Unit 4				
Cala Galera	-5.1	-5.9	0.39	1.03
Tombolo fi Feniglia	-9.7	-10.5	0.90	1.71
Tagliata - Torba	-10.1	-10.9	1.05	1.87
Physiographic Unit 5				
Isola d'Elba	-6.7	-11.8	0.50	2.05
Isola del Giglio	-6.7	-9.4	1.12	1.74

Conclusions

In the present study the limits of the emerged and submerged beach were evaluated, for typical and extreme wave conditions, for the whole littoral of the Tuscany. For each of the five Physiographic Units of the region, a noticeable number of sections transversal to the coast were assessed: each section represents a part of the littoral characterised by homogeneous wave conditions. For each profile wave exposure and mean slopes were defined, taking into account the bathymetry measured, in order to evaluate the main parameters describing beach characteristics - assuming as input the 12-year wave climate available for the offshore region.

In the first phase closure depth and set-up level induced by waves were assessed for each section. Extreme waves for a return period of 50 years were then estimated in order to assess the corresponding extreme limits of the emerged and submerged beach at each section. In the second phase the extreme 50-year wind speeds were estimated for the main directions affecting the coast and, using a numerical hydrodynamic model, the wind set-up and set-down were computed along the coast. Minimum and maximum values of tidal oscillation were also computed, using the harmonic constant of the main tidal components derived from Tidal Tables and interpolating values among the stations. The wind- and tide-induced sea level variations, minimum and maximum, were added to closure depth and wave set-up values in order to evaluate the "indeterminations" associated to the values assessed in the first phase, *i.e.*, to quantify the range of possible variations.

To complete the information, other useful beach parameters were computed, as breaking depths, type of wave breaking and percentage of events that generate transport towards the coast or towards the offshore.

The analysis of results has put into evidence how the extension of bathymetric surveys conducted in different studies was often not the most adequate. In some cases, acquisition fields extended too much towards the sea, incurring in higher survey costs. In other cases, surveys did not reach the closure depth, and what could seem to be survey or processing errors seems to be attributable to volumes that have been lost to the offshore, entering or leaving the zone under control.

Monitoring programmes that will be developed in the future, both to understand the evolution trends of the coast and to calculate the dispersion of sediments that entered the coastal system by means of artificial renourishment, should consider the closure depth for the period of analysis: 10 years for the study of the beach response to defense works and artificial renourishment; 50 years for long term monitoring of the coastal system.

These data permit an optimal set-up of any coastal monitoring program, aimed at evaluating long term coastal evolution, and at defining the effectiveness of beach defense projects. Morphodynamic parameters computed for the whole Tuscany coast, starting from the same wave dataset and using the same processing procedures, allow a "global" analysis of the process reshaping this coast, with cross-comparisons from which new perspectives could arise.

References

BEACHMED (2005) - *Le projet Beachmed: Récupération environnementale et entretien des littoraux en érosion avec l'utilisation des dépôts sablonneux marins* (Convention 2002-01-4.3-I-028) – 3ème cahier technique (phase C). Roma, 324 pp.

De Filippi G.L., Caccavella P., Duchini E. and Guida B. (2004) – *Models validation off-shore Egypt*. Clopatra UE Project, Frascati.

Elliot A.J. (1981) - *Low frequency current variability off the West Coast of Italy*. Oceanol. Acta, 4: 47-55.

European Centre for Medium-range Weather Forecast (2008) http://www.ecmwf/.int

Fredsøe J. and Deigaard R. (1992) - *Mechanics of coastal sediment transport*. World Scientific, Advance Series on Ocean Engineering - Volume 3, World Scientific, Singapore, 396 pp.

Gordon R.L. (1982) - *Coastal ocean current response to storm winds*. J. Geoph. Research, 87: 1939-1951.

Hails J. and Carr A. (1975) - *Nearshore sediment dynamics and sedimentation*. Wiley-Interscience. 316 pp.

Hallermeier R.J. (1978) - *Uses for a Calculated Limit Depth to Beach Erosion*. XVI Coastal Engineering Conference, Hamburg, Germany.

Hallermeier R.J. (1981) - *A profile zonation for seasonal sand beaches from wave climate*. Coastal Engineering, 4: 253-277.

Hattori M. and Kawamata R. (1980) - *Onshore-Offshore transport and beach profile change*. XVII Coastal Engineering Conference, Sidney, Australia.

Kamphuis J.W. and Readshow J.S. (1978) - *A Model Study alongshore Sediment Transport Rate*. XVI Coastal Engineering Conference, Hamburg, Germany.

Massekink G. and Hughes M.G. (2003) - *Introduction to coastal processes & geomorphology*. Oxford University Press Inc., 354 pp.

Regione Toscana (2004) - *Il Piano regionale di gestione integrata della costa ai fini del riassetto idrogeologico: Erosione costiera*. Edifir, Firenze. pp. 176.

Svendsen A. and Jonsson I.G. (1980) - *Hydrodynamics of coastal region*. Technical University of Denmark DK, Lyngby.

Remote sensing in beach erosion monitoring: from the origin, to OpTIMAL and further

Enzo Pranzini

Since 1972, the year when the scientific community had access to data from the first medium-resolution satellite for the observation of the Earth (ERTS-1, later renamed as Landsat-1) we have been trying to use them for studying both the merged and submerged parts of the coastal zone (Nayak et Sahai, 1985; King et Green, 2003).

In spite of the excellent results obtained in the morphological characterization of beaches, study of estuaries and the sea floor, for shoreline extraction (both manually and automatically) and the study of erosive processes we have never had satisfying results because of the low geometric resolution of MSS sensor (IFOW = 79 m x 79 m; nominal pixel dimensions = 56 m x 79 m).

When second-generation Landsat satellites went into orbit (1982), with the TM (*Thematic Mapper*) sensor, new possibilities for littoral studies have arisen, due to the reduced pixel dimensions at the ground (IFOW = 30 m x 30 m nominal; 28.5 m x 28.5 m in georeferenced images) and also to the extension of the observation window into medium infrared, the part of the electromagnetic spectrum where the reflectivity of water and wet sand is approximately zero. With SPOT (*Système Pour l'Observation de la Terre*, from 1986), in addition to a further increase in geometrical resolution into multispectral bands (20 m), the possibility of their fusion with the panchromatic band with 10 m resolution was created; this has become possible since 1999 with Landsat ETM (*Enhanced Thematic Mapper*) data, where there is a panchromatic band at 15 m.

The accuracy that could be expected for determining the position of the shoreline could therefore arrive at *circa* ten meters, even if with the «*unmixing*» techniques it could be possible in theory to arrive at even lower values (Yates et al., 1993).

For short and long term coastal monitoring, this accuracy was not satisfactory since the displacement of the shoreline in general presents much lower rates – there are though cases of higher erosion rates in the Nile delta (39 m/year; Frihy et al., 1998) and in the Gange-Brahmaputra delta (25 m/year; Allison, 1998), where remote sensed data have therefore been successfully used.

When private operators entered the market it was possible to have high resolution sensors put into orbit, which took again into scene the issue of monitoring coastal erosion with remotely sensed data. Ikonos and Quickbird, for instance, acquire multispectral images with a resolution of, respectively, 4 m and 2.40 m, as well as panchromatic images of 1 m and 0.61 m resolution, being therefore compatible with the scale of the phenomena that are being monitored. In addition, Geo-Eye-1 is a satellite that is now operative with a panchromatic band of 0.41 m resolution, and 4 multispectral bands of 1.64 m resolution – panchromatic data are however resampled before their commercialisation, which lowers their resolution down to 0.50 m, according to restrictions made by the Northamerican government.

Sensors that operate on such satellites do not extend their observation beyond 900 nm, preventing the analysis in those wave lengths where the land-water or dry sand-wet sand contrast is more evident.

In spite of that, monitoring coastal erosion through satellite data becomes a concrete possibility, even if we have not yet developed certain and efficient methodologies for automatic shoreline extraction, which would allow the analysis and confrontation process to be completely independent from the operators.

More than an increase in spatial resolution of sensors, for our objectives it is desirable to have surveys extended onto the medium infrared, but the lower quantity of energy that arrives from the sun at such wave lengths makes it difficult to have a sensor that is able to activate unless it received energy from a larger surface. In this direction we now expect WorldView-II which, in addition to the panchromatic band at 0.41 m resolution (degraded to 0.50 m), will also host a sensor with 1.84 m resolution (multispectral), with a band within the 0.86 ÷ 1.04 nm interval.

We are not yet at the medium infrared, but in this range water has a spectral response that is quite different from that of saturated sand. The possibilities of coastal erosion monitoring using satellite data will become even more concrete.

It is in this context that the OpTIMAL activities were carried out, with the involvement of four partners in the development of techniques for processing satellite data for the scope of coastal erosion control: Università di Firenze (Toscana), Università di Roma (Lazio), OANAK (Crete) e Democritus University (East Macedonia - Thrace).

The two Italian groups have concentrated on the development and validation of algorithms for the identification of the shoreline, based on the analysis of spectral signatures acquired along crossshore profiles that intercept sand at different degrees of wetness before reaching the nearshore. Results show that the accuracy on the determination of the line that separates "water" from "nonwater" has reached a level that is acceptable for the study of shoreline evolution, even at limited time scales.

The teams from OANAK and Democritus University have applied remote sensing to extended coastal lengths, showing its efficacy and cost benefit, making available to their Regional authorities instruments that are operative for the analysis of coastal erosion.

Data produced in this project have allowed the knowledge on processes that operate along the coasts of all partner regions to be updated. They have also allowed the operativeness of such techniques to be demonstrated. These should constitute an essential instrument for the knowledge on the state of the coast, which is a fundamental element for the correct management of the coastal zone by Regional authorities.

References

Allison M.A. (1998) - *Historical changes in the Gange-Brahmaputra delta front.* Journ. Coastal Research, 14: 480-490.

Frihy O.E, Dewider K.M. and El Banna M.M. (1998) - *Natural and human impact on the northeastern Nile delta coast of Egypt.* Journ. Coastal Research, 14: 1109-1118.

King S.D. and Green D.R. (2003) - *Matching issue to utility: an hierarchical store of remotely sensed imagery for coastl zone management.* In: Green and King Ed., Coastal Systems and Continental Margin, Vol. 4, Coastal and Marine Geo-Information Systems. Kluver Academic Publishers, pp. 473-486.

Nayak, S.R. and Sahai, B. (1985) - *Coastal morphology: a case study in the Gulf of Khambhat.* Int. Journal of Remote Sensing, 6: 559-568.

Yates M.G., Jones A.R., McGrorty S and Gross-Custard J.D. (1993) - *The use of satellite imagery to determine the distribution of inter-tidal surface sediments of the Wash, England.* Estuarine, Coastal and Shelf Science, 36: 333-344.

Waterline extraction from Ikonos images for the scope of beach erosion monitoring

Niccolò Iandelli, Enzo Pranzini

Measuring the mean distance between the shoreline position obtained *in situ* using DGPS, and the corresponding shoreline position that was extracted automatically from an Ikonos image, allowed to evaluate the efficiency of different image processing techniques that are used in coastal erosion monitoring. The mean difference between the DGPS shoreline position, and the shoreline positions extracted from the B2/B4 rapport and from the NDVI were, respectively, 2.27 m and 2.89 m, being therefore smaller than the pixel dimensions at the ground. The distance between the two shoreline positions results to be very short in those coastal sections where the slope of the nearshore is high, whereas distance varies considerably where this slope is low. The accuracy of the position of the waterline extracted from remotely sensed data is able to allow erosion monitoring in coastal sections which are under severe shoreline retreat. Our results allow stating that data expected from satellites that will be put into orbit in the near future, hosting sensors at a higher spatial resolution which will have acquisition bands that are enlarged towards the IR, will allow monitoring coastal erosion even where these processes are less intense.

Introduction

Within the framework of BEACHMED (INTERREG III B) project, the operative unit of Florence had developed and tested a procedure of shoreline extraction using Ikonos data which allowed tracing the shoreline ("zero isobath") in a semi-automatic way. The procedure was based on the identification of the border between water and "non-water", done over a Near Infrared (NIR) band, extraction of the contact line by applying an *edge detection* filter (Figure 1) and its translation as a function of the beach slope (by independent ground measurements) and baric and tidal values (Figure 2). The accuracy that was archived was of circa 1-2 pixels which, corresponding to circa 4 m – 8 m, a value that was excessively high for the study of a process that in general evolve with lower annual rates in Toscana (BEACHMED, 2005).

Research has continued during Project OpTIMAL of the OCR BEACHMED-e (INTERREG III C). Several image processing algorithms have been tested in order to improve accuracy in shoreline definition. Research has been oriented towards the determination of the "waterline" through the use of high resolution images, where waterline means the whole of points where air, water and land meet (Pranzini, 2004). Certainly this line does not represent an absolute *datum*, but this can be produced using the translation techniques cited below.

The data used are those acquired by Ikonos satellite and the test zone corresponds to a part of the Follonica Gulf shore.
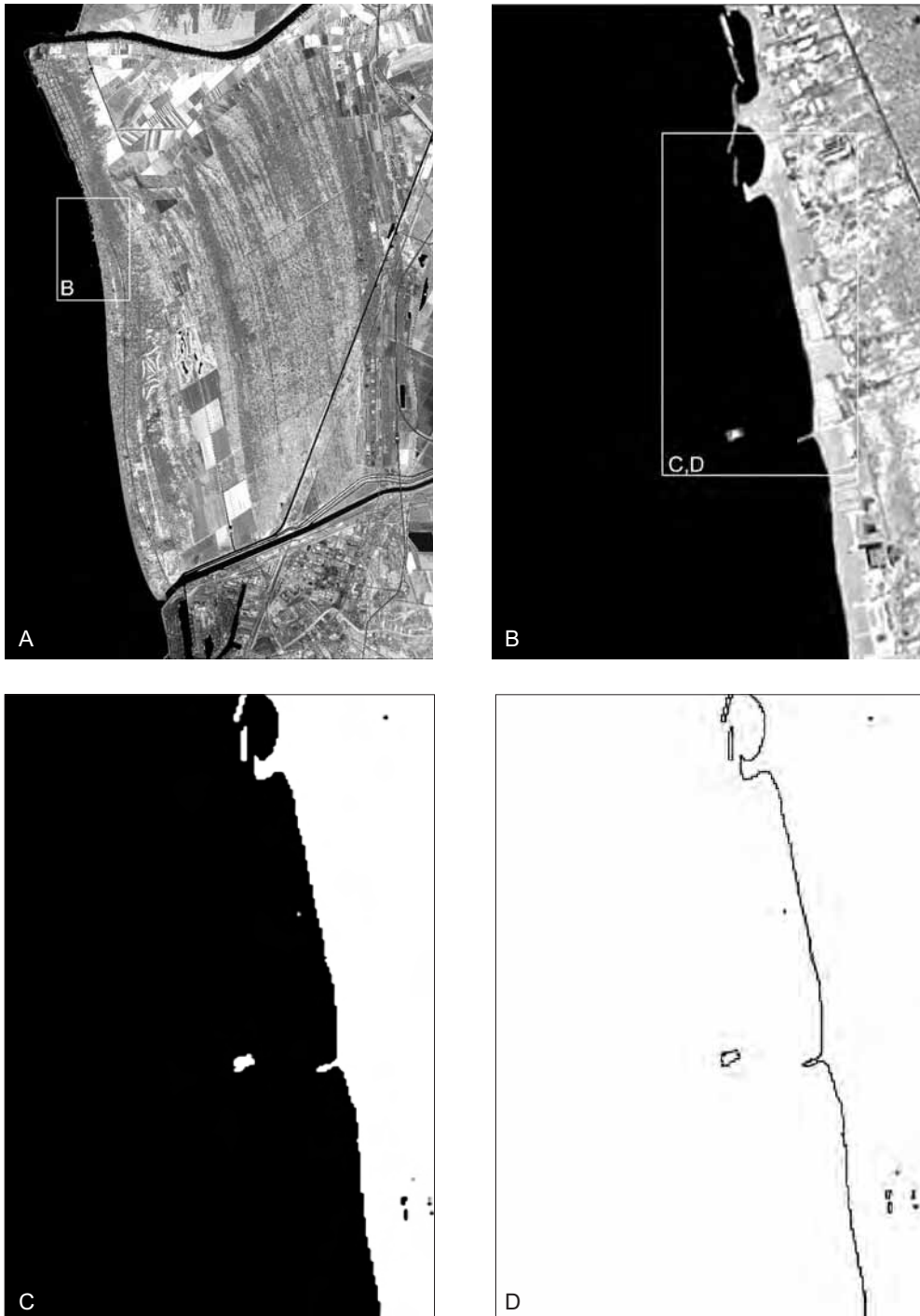
Figure 1 – Waterline extraction procedure. Original Ikonos image (top left); selection of study zone (top right); slicing in two levels (bottom left); extraction of water-land border with a high-pass filter (bottom right).
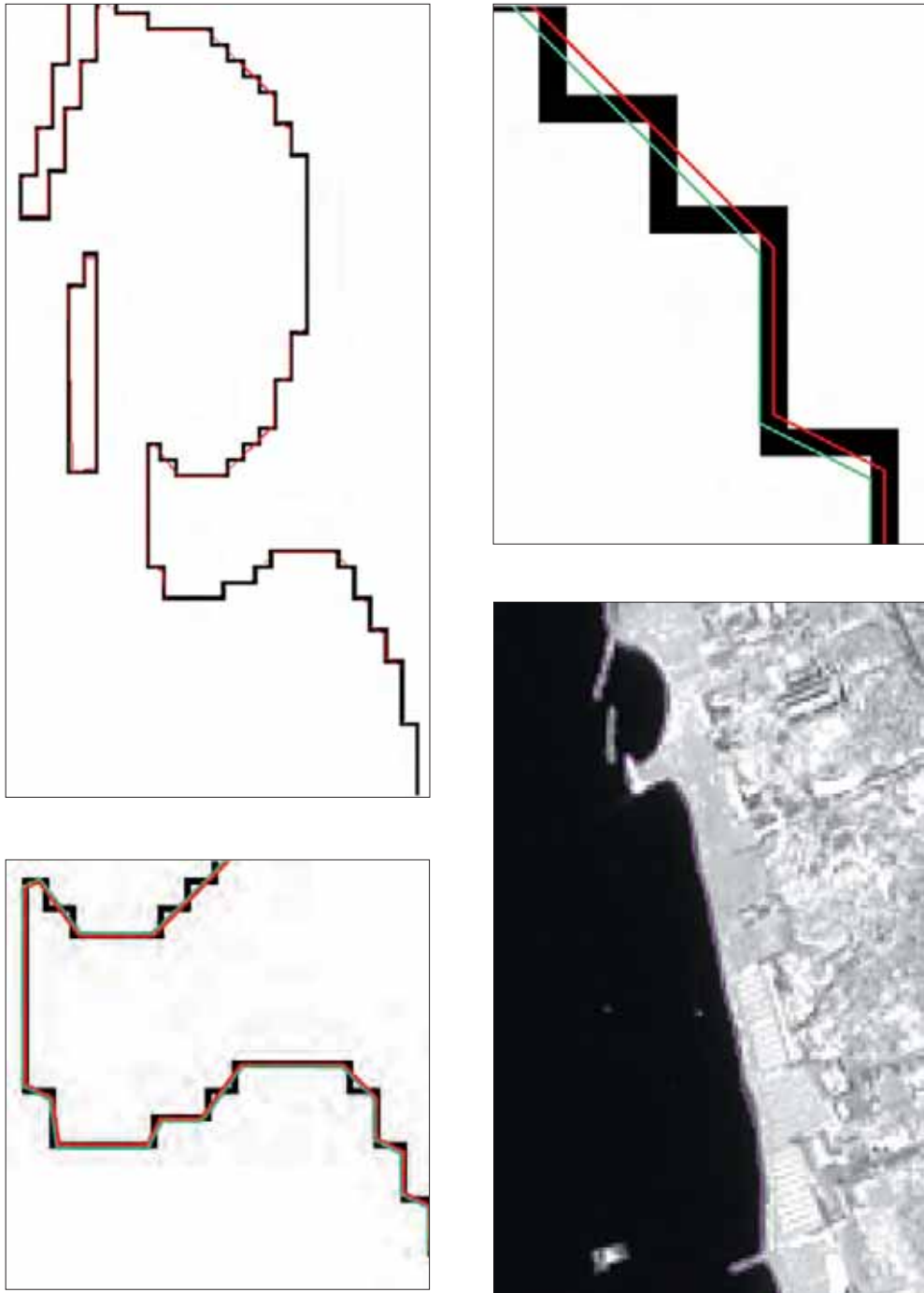
Figure 2 – Vectorialisation of the raster waterline (top left); translation of 0.5 pixel of the vectorial line in order to place it in the real water-land contact point (top right); translation of the waterline in function of astronomical and baric tides and coastline slope (bottom left); superposition of shoreline (zero isobath) over the original image.

Study area: Follonica beach

The beach in front of Follonica (Figure 3) is part of the Physiographic Unit which extends from Piombino headland to Puntone di Scarlino and is fed by rivers Cornia and Bruna, and by Fosso di Valmaggiore.

Figure 3 – Ikonos image of Follonica beach acquired on 18/04/2007 (Bands 1-2-3; B-G-R) that was later processed. In the box, the part of the beach where data in the following figures refer to.

Sediments that form this beach are constituted by *well sorted* ($0.35 < \sigma_i < 0.50$ phi) *fine sand* ($2 < Mz < 3$ phi) according to the classification proposed by Folk and Ward (1957). Mineralogical composition is mainly formed by mono-crystalline quartz (56%), carbonate lithic fragments (18%); metamorphic lithic fragments (10%), potassium feldspars (7%) and lithic terrigenes (5%). Among the heavy minerals, we find mostly augite, epidote and picotite (Gandolfi and Paganelli, 1975).

The Gulf of Follonica coast started to be eroded in the XIX century, when the main feeding watercourses were deviated for reclamation of wetlands that were present along the coast (Bartolini et al., 1977). In the XX century there were land use changes along the feeding waterbasins and the extraction of sand and gravel from the riverbeds favoured the continuation of erosion processes. This was though fought against in this part of the coast during the 60's with the construction of emerged and submerged breakwaters, seawalls and groins which today cause great variability to the shoreline position.

Ground truth

In the present study, ground truth is constituted by the waterline acquired at the same time of satellite flying-over, by two teams operating a DGPS at RTK mode.

The survey was carried during calm sea weather, and the position of the waterline could be easily recognised by the operators. Surveys were carried one hour before and one hour after the satellite cover, which kept the variations of astronomic and baric tides within 5 cm. This, considering the low average beach slope (4.76%) implies a waterline displacement of circa ±0.5 m.

At certain points the position of the limit between wet and dry sand was measured. This corresponds to the position reached by the water due to run-up a few hours before the survey, and has a mean distance of 6.0 m from the waterline.

Image processing

Images were processed by ENVI ver. 4 software, and results were compared to the ground truth within GIS environment (ESRI ArcGIS, ver. 9.1).

A first processing phase consisted in simple linear *stretching* of the different bands, two-level *slicing* and water/land extraction with an *edge detection* filter. Normalised differences and rapports between bands were later determined. This was followed by more complex processing phases, from *Principal Component Analysis* to *Ratio Transform Method* (Stumpf and Holderied, 2003). An unsupervised «ISODATA» classification into two classes, hypothetically «water» and «non-water» was also performed (Alphan, 2005).

Considering that different processing produces images with bi-modal distribution of digital values, they were object of two-level slicing putting the separation in the trough between the two modes, in order to make decision a more objective process.
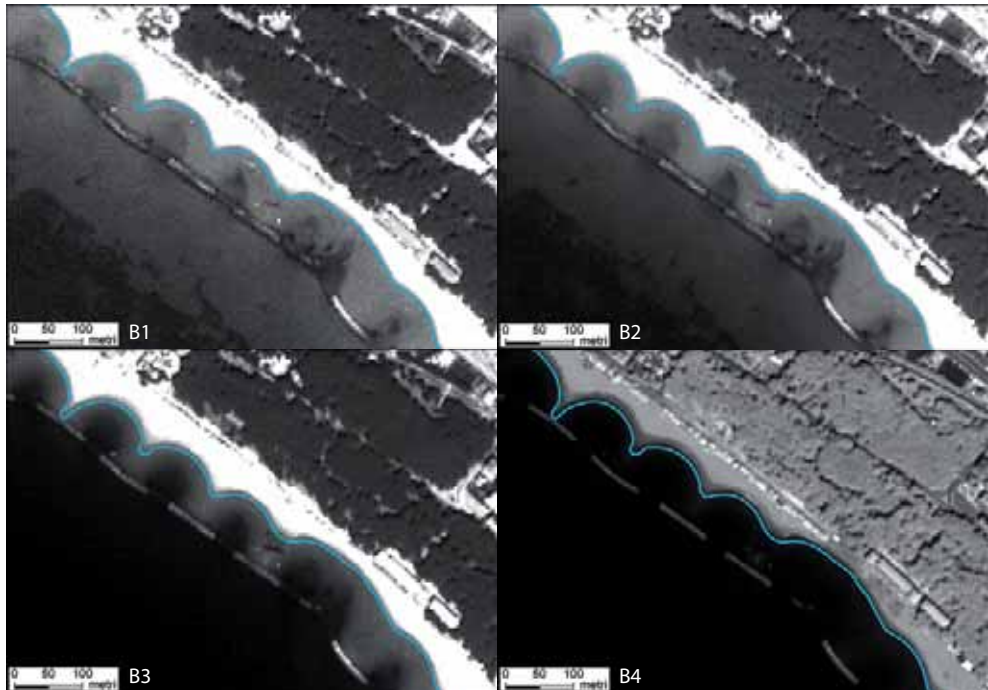
Figure 4 – The four Ikonos bands with the overlaying GPS line.

Wherever indexes led to positive and negative values, zero was used as a separation value. In order to have a better understanding of results from different processing procedures, in Figure 4 Ikonos bands are reproduced as they appear before the separation of tones.

The shorelines extracted were then compared to the position of the waterline that was measured *in situ*, calculating the distance along 33 profiles (Table 1) in which the slope of the section between 0.0 m and -0.5 m was measured, according to a bathymetric survey conducted two months before the satellite passage.

The coastal segment under study is heavily defended by parallel breakwaters, and the meteo-marine conditions verified in the two months considered allow stating that there were not significant variations in the slope of beach profiles.

Image processing was performed also over the multispectral bands after their resolution was taken to 1 m with a technique of fusion with the panchromatic band (*pan-sharpening*), but results obtained were not satisfactory due to problems relating to resampling techniques: the one based on *nearest neighbour* displaces the original pixel values at the same magnitude as the expected accuracy, and the one based on interpolation (bi-linear or cubic) reduces contrast between pixels of interest that already show differences that are very slight.

Table 1 – Average distance (m) between the shoreline extracted from Ikonos image and the one surveyed *in situ* with DGPS. Negative values indicate that the remotely sensed line is located more towards the land in comparison to the "real" one.

	GPS - B4	GPS - NDVI	GPS – NDWI	GPS - UNSUP	GPS - RWD	GPS - (B2/B4)	GPS - PCA1 (Green *vs* NIR)
Mean	-8.40	-2.89	11.85	-3.83	-7.61	-2.27	-4.75
Dev. Std.	5.42	2.11	11.57	3.01	5.66	2.21	2.59

Near Infrared
From all bands (Figure 4), band 4 is the one that allows the best discrimination among water, wet sand and dry sand. In spite of that, in the 33 profiles considered, the mean distance from the waterline that was extracted (after the two-level slicing and edge detection filter had been applied to the image) to the GPS line was of -8.40 m. This result is though strongly influenced by the gray level value which separation between "water" and "non-water" is made, a decision that is extremely subjective since the two modes are not clearly separated.

Rapport between bands
Bands ratio is generally used in order to reduce the "relief" effect from images (Crippen et al., 1988), which is useless in this case; the use we have here is based on the possibility of separating surfaces that have a different gradient of reflectivity within a certain spectral interval.

In the 450 nm ÷ 900 nm range, curves that are representative of the spectral signature of different beach surfaces are nearly parallel. However, we note that from 560 nm to 830 nm (B2 ÷ B4) the gradient is slightly different between the water and the coastline curves. In effect, from all band ratios possible (Figure 5) it is the B2/B4 rapport that leads to a better discrimination between the surfaces considered, with a distance of 2.27 m from the shoreline to the GPS line. The B2/B4 rapport makes explicit the gradient between 660 nm and 830 nm, which is slightly different between the signatures of wet and dry beach, and allows a clear definition of the upper limit of the run-up in the hours that precede the acquisition. Among the rapports, it is the only one that allows seeing parallel breakwaters, which undertake the same gray level as the sea; they are constituted by very dark blocks and have a "low crest" that keep them constantly wet. It is not surprising then that they present a response that is similar to that from the run-up zone, which, in this image processing, is associated to the sea.
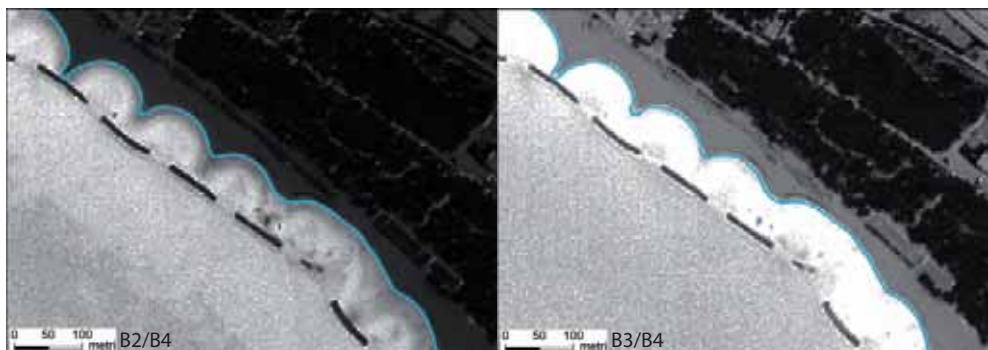
Figure 5 – Ikonos Band ratios satellite bands. In light blue, the waterline surveyed by GPS at the moment of satellite flying-over.

NDVI

The *Normalized Difference Vegetation Index* (NDVI) is a simple algorithm that is extremely robust for the evaluation of vegetation density and status. It operates over the Spectral contrast between Red and Near Infrared. In the past, it has also been used in the cartography of water surfaces, particularly in vegetated zones (Hirose et al., 2005). In our case it produced interesting results (Figure 6a) that allowed positioning of the shoreline at only 2.89 m from the "real" one.

NDWI

The *Normalized Difference Water Index* (NDWI) (McFeeters, 1996) inverts the NDVI values and uses the Green band instead of the Red one (Green-NIR) / (Green + NIR). In this type of processing, water undertakes positive values, whereas the soil and vegetation present negative values. Dry sand, with high reflectivity both in the Green and NIR bands, undertakes positive values that are though near zero.
In the study zone, the results from such image processing were unsatisfactory, with a distance of 11.85 m from the shoreline to the "real" line. In addition, it is the only type of image processing that positions the land-water contact towards the sea, in relation to the DGPS line. In effect, as shown also in Figure 6b, error is very large behind breakwaters, where beach slope is minimum and we have from shallow water up to the defence works. This algorithm has, in this study case, the tendency "not to see" the thin water layer that cover the swash zone and the nearby seafloor that is immediately in front of it.
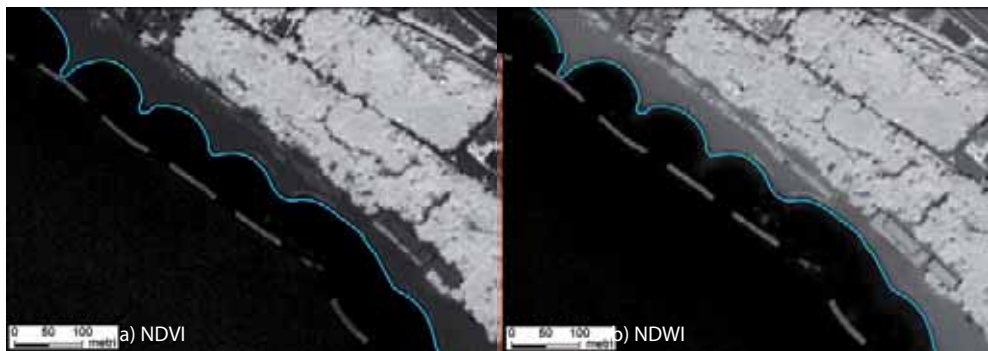
Figure 6 - NDVI and NDWI images produced by Ikonos satellite bands. In light blue, the waterline, as surveyed by GPS at the moment of satellite cover.

Principal Component Analysis

Principal Component Analysis (PCA) is a type of image processing that is often used in remote sensing in order to generate, from original bands that are highly correlated, new synthetic bands that are not correlated. It gives results that are necessarily dependent on the statistics of the dataset, and does not allow codified interpretations of the images produced. The cut of the scene influences already the
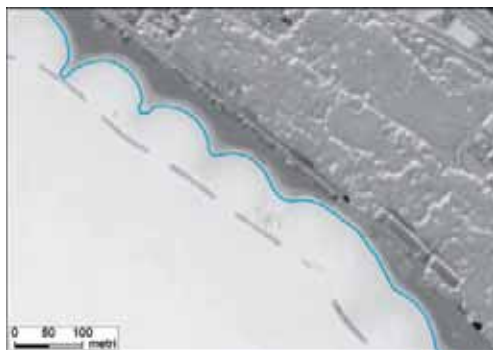
results, and all that was obtained for our subset cannot be transferred to other zones of the same Gulf of Follonica. From all the different image processing techniques possible, we show the image from the first principal component (PC 1) extracted by the dataset constituted only by bands 2 and 4, those that had produced the best rapport (Figure 7). The shoreline extracted from these images has a mean distance of 4.75 m from the "real" line.

Figure 7 - Image of PC 1, calculated with Ikonos satellite bands 2 and 4. In light blue, the waterline, as surveyed by GPS at the time of satellite cover.

Ratio Transform Method

The *Ratio Transform Method* (Stumpf and Holderied, 2003) has been developed for the sake of determining the *Relative Water Depth* between two or more zones, based on reflectivity values in Blue and Green, and contain opportune radiometric and atmospheric corrections. The use that we have in this study is therefore "atypical", since the difference in depth that we search is that between emerged and submerged zones. The image produced (Figure 8) does present a histogram with two well-separated modes. However, the two-level slicing discriminates between dry sand, on one side, and coastline + water on the other, but does not allow tracing the shoreline with accuracy (mean distance of 7.61 m).
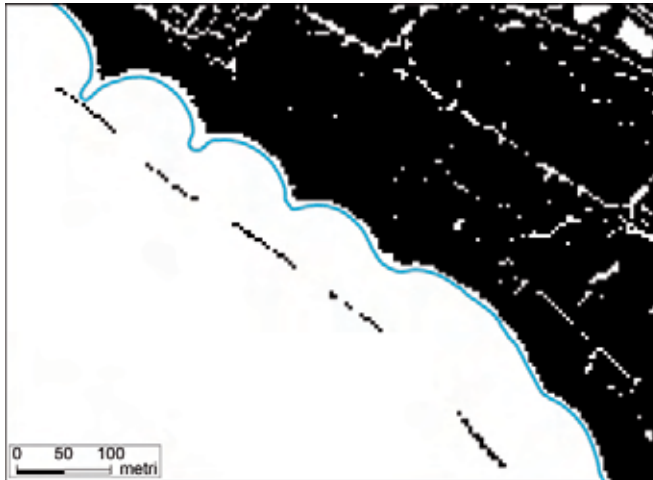
Figure 8 – Image of Relative Water Depth with slicing at 0 m. In light blue, the waterline, as surveyed by GPS at the moment of image acquisition by the satellite.

Evaluation of results as function of the slope

For the shoreline that was obtained with the best accuracy (the one produced from the B2/B4 ratio) we have analysed how error is distributed as a function of the slope of the swash zone; the parameter is the one that determines the thickness of the water layer at a determined distance from the effective waterline.

The comparison between slope and error (distance between the GPS line and the Ikonos-derived line) clearly shows this correlation: wherever slope is higher, accuracy of the derived line is much higher (Figure 9).

Dispersion of points is extremely high wherever slopes are low, where we have small and large distances (error), but with slopes over 6% the error is always under 2 m.

The stretches of coast where accuracy is lower are those directly defended by breakwaters, which form salients with very low slope along the beach profile (Figure 10).
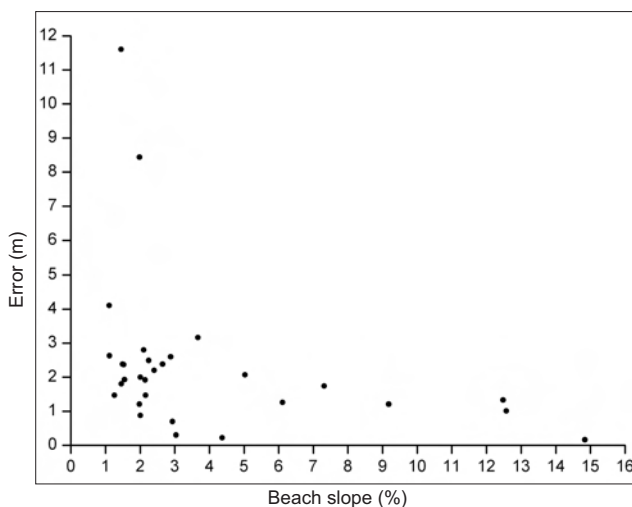
Figure 9 – Comparison between beach slope and distance (error) between the shoreline extracted from Rapport B2/B4 and the DGPS line.

Figure 10 – Shoreline extracted from the B2/B4 ratio (in red); waterline from DGPS (in light blue). The distance between these two lines is larger in the zones immediately behind breakwaters, where beach slope is lower.

Conclusions

Data provided by Ikonos satellite allows tracing with good approximation the waterline of sandy coasts – departure element for obtaining the shoreline position through astronomic and baric corrections.

The waterline extracted from image rapport B2/B4 shows an error of 2.27 m regarding the line that was acquired *in situ* at the same time of satellite acquisition. It is reasonable to think that analogue results, with rapport to the pixel dimensions at the ground, could be expected if data from satellites which carry sensors acquiring in the same spectral bands are used. In this sense, the accuracy that we can expect from Quickbird images should be of circa 1.40 m.

The good results coming out from our test are certainly related to the low reflectivity of sand in the Gulf of Follonica, which has an albedo of 0.309 within the observation range of Ikonos. We cannot affirm that such an accuracy could also be obtained in beached formed by lighter sand.

On the other hand, the beach of Follonica has low slopes in the stretches that are not defended by breakwaters. We could state that the proposed algorithm, as well as those that are not so useful to this environment, could take to much better results in beaches of higher slopes.

Aknowledgements

Part of the data presented in this chapter have been included in a paper in press on Studi costieri, n. 14, 2008, by Carli, Iandelli, Salvatori and Pranzini under the title "L'utilizzazione di immagini telerilevate ad alta risoluzione per lo studio dell'erosione costiera: estrazione della linea d'acqua e valutazione della sua accuratezza".

References

Alphan H. (2005) - *Perceptions of coastline changes in river deltas: southeast Mediterranean coast of Turkey*. International Journal of Environment and Pollution, 23: 92-102.

Bartolini C., Pranzini E., Lupia Palmieri C. and Caputo C. (1977) - *Studi di geomorfologia costiera: IV - L'erosione del Golfo di Follonica*. Boll. Soc. Geol. It., 96: 87-116.

BEACHMED (2005) - *Le projet BEACHMED : Récupération environnementale et entretien des littoraux en érosion avec l'utilisation des dépôts sablonneux marins* (Convention 2002-01-4.3-I-028) – 3ème cahier technique (phase C). Roma, 324 pp.

Caputo C., La Monica G.B., Lupia Palmieri E. and Pugliese F. (1986) - *Physiographic characteristics and dynamics of the shore of Rome*. International Geomorphology, John Wiley & Sons, Part 1. pp. 1185-1189.

Cecini C. (1998) - *Physical processes and human activities in the evolution of the Po delta, Italy.* Journ. Coastal Research, 14: 774-793.

Crippen R.E., Blom R.G. and Heyada J.R. (1988) - *Directed band ratioing for the retention of perceptually-independent topographic expression in chromaticity-enhanced imagery*. Int. J. Remote Sensing, 9: 794-765.

Folk R.L. and Ward W.C. (1957) - *Brazos river bar: a study in the significance of grain size parameters.* J. Sedim. Petrol., 27: 3-26.

Gandolfi G. and Paganelli L. (1975) - *Il litorale toscano fra Piombino e la foce dell'Ombrone (Area campione Alto Tirreno). Composizione, provenienza e dispersione delle sabbie*. Boll. Soc. Geol. It., 94: 1911-1832.

GNRAC (2006) - *Lo stato dei litorali italiani*. Studi costieri, 10: 1-176.

Hirose K., Soyji M., Hang H.T.M., Anh N.H., Triet T. Nam V.N. and Tran T.B. (2005) - *Satellite data application for mangrove management.* 16th Workshop OMISAR. pp. 7.1-7.4

McFeeters S.K. (1996) - *The use of the Normalized Difference Water Index (NDWI) in the delineation of open water features*. Int. J. Remote Sensing, 17: 1425-1432.

Pranzini E. (2001) - *Updrift river mouth migration on cuspate deltas: two examples from the coast of Tuscany (Italy)*. Geomorphology, 1-2: 125-132.

Pranzini E. (2004) - *La forma delle coste. Geomorfologia costiera, impatto antropico e difesa dei litorali.* Zanichelli editori, Bologna, pp. 246.

Stumpf R.P. and Holderied K. (2003) - *Determination of water depth with high-resolution satellite imagery over variable bottom types*. Limn. Oceanogr., 48: 547-556.

A new approach to detect shoreline from satellite images

Giovanni B. La Monica, Elisabetta Petrocchi, M. Cristina Salvatore, Rosamaria Salvatori, Ruggero Casacchia

The sensors of new-generation commercial satellites and the image processing techniques currently make possible to study and monitor shoreline variations. One of the main problems lies in locating the shoreline via a method that is not bound to the "subjectiveness" of the interpreter. A method and a software-based procedure for measuring the water/sand interface was developed to measure the position of the shoreline, based on the different spectroradiometric response of water and sand in the red and infrared wavelengths. The vegetation index (NDVI) computed as the ratio between infrared and red bands has indeed proved to be particularly suitable for the identification of the water/sand interface. This method is also applicable when analysing images acquired in different periods, as required by monitoring programmes. The method was tried out in two different sample areas along the Latium coast and was compared with traditional measuring techniques (photo interpretation), ground survey data (GPS measurements) and laboratory data (spectral signatures) that confirm that NDVI values may be successfully used to identify the water/sand interface from satellite images taken with different sensors. The procedure was tested on Quickbird and Ikonos images, using the software ENVI.

Introduction

The use of satellite images and aerial photographs to study and monitor shoreline variations is very well documented in scientific literature (Baily and Nowell, 1996). Ever since 1927 aerial photographs and photogrammetry techniques have been used to provide topographic information on coastal areas, allowing the compilation of base maps to be used in measuring shorelines in historical times (Crowell et al., 1991). Collier et al. (1995) underline the advantages of using aerial photographs with respect to traditional maps, and in particular they stress the importance of the multitemporality and repetition of image acquisition. Hesselmans et al. (1997) and Favretto et al. (2004) acknowledge that multispectral remote sensing images and remote sensing techniques are a suitable instrument for identifying shoreline variations in order to examine causes and put forward possible evolution.

One of the biggest difficulties in using remote sensing data concerns the correct identification of the shoreline on images and in relative ground checks (Battiau-Queney et al., 2003), together with the correct transfer to mapping databases (Crowell et al., 1991; Thieler and Danforth, 1995; Biasini and Salvatore, 1995).

Bergamasco and Pesaresi (1997) show the advantages of using Landsat-TM images to measure the shoreline based on the different spectral response of water and sand, but also note that the spatial resolution of these data (30 m) may be a problem.

The biggest advantage in using remote sensing data is that of being able to use images taken in the near infrared (NIR) band. When measuring the shoreline, indeed, these wavelengths are particularly useful, since in this region of the electromagnetic spectrum the reflectivity of water is practically zero (Drury, 2001; Sabins, 1987) and accordingly the identification of a separation zone between water and sand may be greatly facilitated.

In a recent paper Carli et al. (2008) show that with the use of high-resolution images it is possible to define the shoreline with an accuracy sufficient to guarantee a medium-term monitoring of beaches that have a moderate slope and low-reflectivity sand.

The sensors of new-generation commercial satellites currently make it possible to obtain multispectral images having a high spatial resolution: Ikonos and Quickbird images (which have a spatial resolution of 4 m and 2.44 m respectively in the multispectral and 1m and 0.61m respectively in the panchromatic) appear to be particularly useful not only for distinguishing the shoreline but also for classifying the vegetation of coastal zones (Fromard et al., 2004).

One of the main problems lies in locating the shoreline via a method that is not bound to the "subjectiveness" of the interpreter or of the operator. In the 2004 Beachmed report, the authors note that shorelines plotted using digital orthophotographs by different operators may be subject to positioning differences of several metres.

Image processing techniques that can be used to measure the shoreline include Principal Component Analysis (PCA) and various types of supervised classification. As Pranzini et al. (2007) indicate, these methods require the intervention of an expert operator. PCA results for instance may vary considerably depending on the percentage of pixels representing the sea contained in the original image, since this type of analysis is heavily dependent on the statistical distribution of the initial values of Digital Numbers ("scene dependent" - Lillesand and Kiefer, 1987); supervised classification procedures entail the selection of sample areas with which to "train" classification algorithms, and the selection of the classification algorithm itself, which in turn depends on the spatial and spectral characteristics of the image. Unsupervised classifications for their part require the operator to intervene on the number of classes to be recognised in the image, and this too of course varies depending on the area examined.

To guarantee the systematic monitoring of the shoreline it is however necessary to use an image processing procedure that is less bound to subjective variables, in order to optimise processing times and to enable measurements to be made autonomously by operators not highly specialised but employed in the sphere of territorial management.

This paper describes a semiautomatic procedure for measuring the water/sand interface, which is based directly on the analysis of DN values sampled from high spatial resolution satellite images, along lines perpendicular to the coastline. The procedure was tested on Quickbird and Ikonos images, using the software ENVI, release 4.3, developed by Research Systems (ITT Visual Information Solution).

Test sites

The method was tried out in two different sample areas along the Latium coast (Figure 1) characterised by sands having marked chromatic (mineralogic) differences, and was compared with traditional measuring techniques (photo interpretation), ground survey data (GPS measurements) and laboratory data (spectral signatures).

The first test area (site 1), extending for about 500 m, lies close to the town of Focene, which is intensely urbanised, and covers a stretch of beach having a breadth ranging from 50 and 90 m. The sand is light coloured, has undergone beach replenishment and is protected by spur dykes. The second test area (site 2), located about 1 km to the north of the Fiumicino canal, covers a darker stretch of beach, about 10 m in breadth, extending northwards for about 500 m. Both beaches, quite flat, are affected by "retreating" phenomena.

Figure 1 – Location map

Method

The analysis method adopted is based on the different radiometric response of water and sand (Figure 2).

The portion of energy reflected by pure water, about 3% of the radiant flux, is mostly confined to the blue and green bands, and diminishes rapidly, moving towards higher wavelengths up to complete absorption in the near IR (800 nm) (Brivio et al., 2006). The reflectance curve of a water body, despite basically retaining the same characteristics as those of pure water, is influenced by the quantity and the nature of suspended solids in the water and by the depth of the water column being observed and the characteristics of the bed.

The radiometric response of sand, the main component of coastal sediments, depends on its mineralogical composition and granulometry and on the amount of water and organic materials (fragments of algae or seashells) contained therein. Generally speaking, it can be said that the higher the wavelength, the higher the radiometric response, and that dry sand has a higher radiometric response than wet sand at all wavelengths. The spectral curve of sand, both dry and wet, is very different to that of water, especially at infrared wavelengths (Figure 2).

It follows that the infrared band is the one that best distinguishes water from sand.

In light of these considerations, a method was developed to measure the shoreline that is as objective as possible, not bound by the intervention of an operator and based on the analysis of the numerical values of single spectral bands close to the water/sand interface.

The method used was then transformed into a "semiautomatic" procedure that can be used in the ENVI-IDL environment, through the application of a routine specially written in the IDL language.
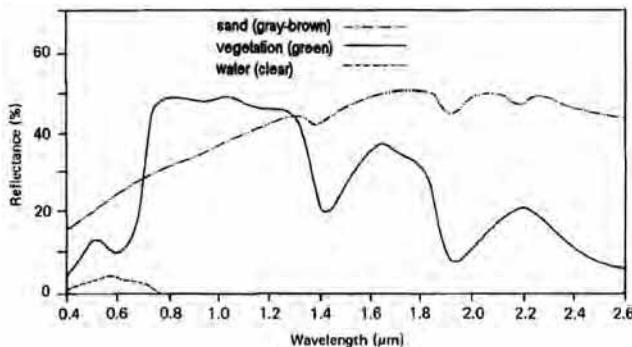
Figure 2 – Spectral signatures of water, sand and vegetation (Lillesand & Kiefer, 1987)

Data processing procedure was conceived to be done automatically, without requiring pre-processing operations such as atmospheric correction or image normalisation.
Testing was carried out using Quickbird and Ikonos high spatial resolution images (Table 1).

Table 1 – Summary of images used

Date of acquisition	Locality	Sea conditions	Sensor	Characteristics		
3/06/05	Focene - Palo Laziale	Calm	**Quickbird**	Multispectral (2.4m/pixel)	Band 1 (Blue) 0.45 – 0.52 μm	
					Band 2 (Green) 0.52 – 0.60 μm	
					Band 3 (Red) 0.63 – 0.69 μm	
					Band 4 (N IR) 0.76 – 0.90 μm	
				Panchromatic (0.5m)	0.45 –0.90 μm	
22/07/05	Fiumicino - Fregene	Rough		Radiometric resolution	11 bit	
				Re-acquisition interval	4.5-5 days	
21/12/07	Fiumicino - Focene	Calm	**Ikonos**	Multispectral (4 m/pixel)	Band 1 (Blue) 0.45 – 0.52 μm	
					Band 2 (Green) 0.51– 0.60 μm	
					Band 3 (Red) 0.63 – 0.70 μm	
					Band 4 (N IR) 0.76 – 0.85 μm	
				Panchromatic (1 m/pixel)	0.45 –0.90 μm	
				Radiometric resolution	11 bit	
				Re-acquisition interval	3 days	

For the two sample areas a preliminary analysis was carried out to identify the DN interval within which the water/sand divide could be placed. To this end, for each image a number of lines were selected (1 every 10 pixels) perpendicular to the shoreline, so as to represent a virtual line between the sea and the beach. For each line a graph was produced, giving on the vertical axis the Digital Number (DN) value and on the horizontal axis the position of the pixel in the image (column). These graphs represent spatial profiles (approximately 2,300 profiles for each of the 4 bands for both Quickbird and Ikonos), in which the evolution of reflectivity from the sea to the beach in the analysed band is clearly visible. A characteristic common to all profiles is a marked drop in DN values close to the water/sand divide.
The variation in DN values in the case of visible bands is gradual, coming in an interval of about 4-5 pixels, while in the case of the NIR (Near InfraRed) band there is a sudden change in an interval of no more than two pixels. This happens because in the infrared band radiation is completely absorbed by water, while for visible wavelengths an element of reflection is always present which, despite being small, is not negligible.

The NIR band is, accordingly, that which is best suited to identifying the water/sand divide, but for its correct use in an automatic procedure some actions are required, such as atmospheric corrections and the normalisation of images taken in different periods.

To increase the possibility of easily distinguishing the shoreline in profiles, also without operator intervention, the normalised ratio between the infrared and the red bands was calculated.

$$NDVI = \frac{\rho IR - \rho R}{\rho IR + \rho R}$$

(where ρIR is reflectivity in the near infrared band and ρR is reflectivity in the red band).

This ratio, usually known as NDVI (Normalised Difference Vegetation Index) and used chiefly to study vegetation, is particularly suited for identifying water bodies, since the reflectance curve of water shows very low values, which tend to fall as the wavelength rises. Water is the only natural element to possess this characteristic, and is thus immediately identifiable in multispectral images. Furthermore, being a normalised ratio, the NDVI value can be used to compare images taken at different times.

Following these considerations, also NDVI profiles were plotted. In these profiles (Figure 3) water always has a negative value and the contact between sand and water is characterized by a sudden drop in DN values (from 0 to -0.5) within an interval of 2 or 3 (maximum) pixels (mixed pixels).
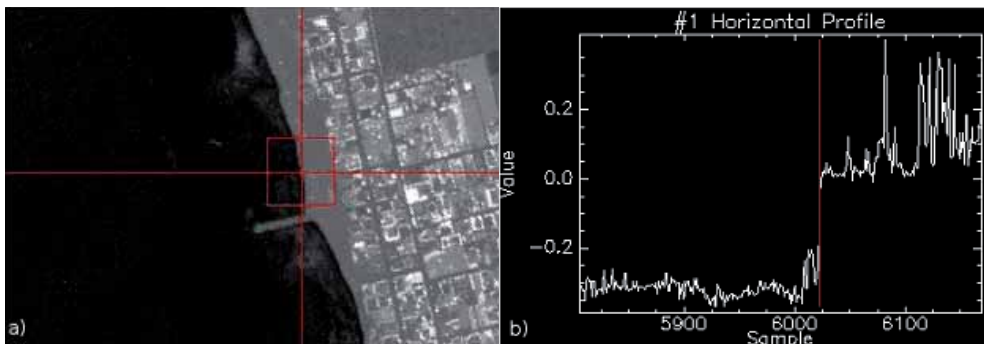
Figure 3 – Evolution of NDVI values along a profile. a) NDVI image. b) Profile. Note the sudden change in NDVI values where the beach meets the sea and the NDVI values of water, always negative.

Considering the radiometric characteristics of water and sand, their interface should be placed within this interval between the first pixel (X1) corresponding to the sea and the first pixel (X2) certainly corresponding to sand (Figure 4). It is possible to highlight these points on the image with markers.

The position of the pixels, and thus the amplitude of the interval, depends on the sea and weather conditions at the time the images are acquired and on the slope of the beach. To dectect shoreline using an automatic procedure applicable to all remote images, the best possible approximation for the positioning of the water/sand interface is the pixel X (Figure 4) placed between X1 and X2. The line joining the X markers represents the water/sand interface along the shore.

The pixel placed in an "intermediate" position does not necessarily have a corresponding "intermediate" DN value. The geometric resolution of images used represents the limiting error for this method

For the automatic positioning of markers and, therefore, for the creation of a vector file representing the shoreline, a purely geometric solution was used.

On the NDVI image, through the use of a routine written on purpose, the average value of DNs corresponding to the sea is calculated, and the value of the first pixel corresponding to sand is

identified. Two distinct lines are then plotted automatically: a third halfway line is plotted approximating the water/sand interface.

Coastal zones corresponding to sea defence works can be exlude editing manually on the nodes of the extracted vector file.

Using this routine the lines corresponding to the water-sand interface were plotted automatically on all available images, and comparisons were made with data from photo interpretation. The efficacy of NDVI images was also checked by means of *in situ* and laboratory measurements.
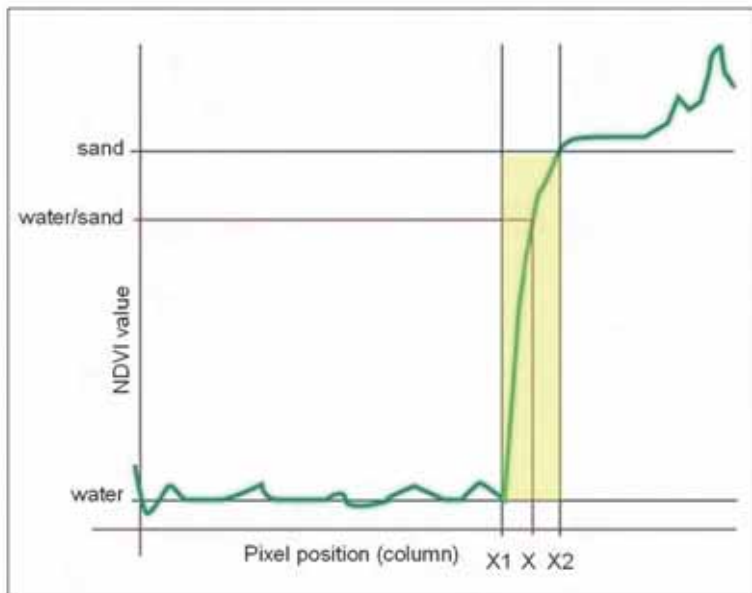
Figure 4 – Chart identifying the intervall (2-3 pixels) between water and sand. In yellow are enfatized mixed pixels.

Radiometric measurements *in situ* and in the laboratory

To analize the spectral uniformity of the studied beaches and to validate the markers representing the water/sand interface along the radiometric profile, measurements of reflectance of both dry and wet sand were taken in two test sites; samples were also collected to analyse reflectance in the laboratory (Figure 5).

In situ and laboratory measurements were carried out using a *Fieldspec* 3 spectroradiometer (ADS inc. USA), which records data in the spectral interval of between 350 and 2,500 nm with an average spectral resolution of 1 nm.

Field measurements were undertaken on 23 February 2008, under a clear sky but with a rough sea. The sensor was positioned (with a viewing angle of 25°) at the nadir point in relation to the surface target, and at a height of about 40 cm, in a sun-facing direction in order to avoid shadow effects on the target area. For each target 10 measurements were taken (with cycles of 50 acquisitions) using, as a reference for the calculation of reflectance, a *Spectralon* panel calibrated in the laboratory.

Spectroradiometric measurements were taken on both dry and wet sand targets in each test area.

At each site a reduction in reflectance at all wavelengths was recorded (Figure 6a), confirming that in the case of wet sand the higher water content reduces sand reflectivity. This change in the optical properties of sand is also due to its mineralogical composition: light-coloured sand (site 1) showed a similar behaviour, and presented a reduction in reflectance of 30-40% in the visible range, which increased moving closer to near infrared wavelengths (Figure 6b); dark sand (site 2) differed in that it presented more marked reductions in the visible range (50-60%), and consistent findings in the infrared.

Site 1   Site 2
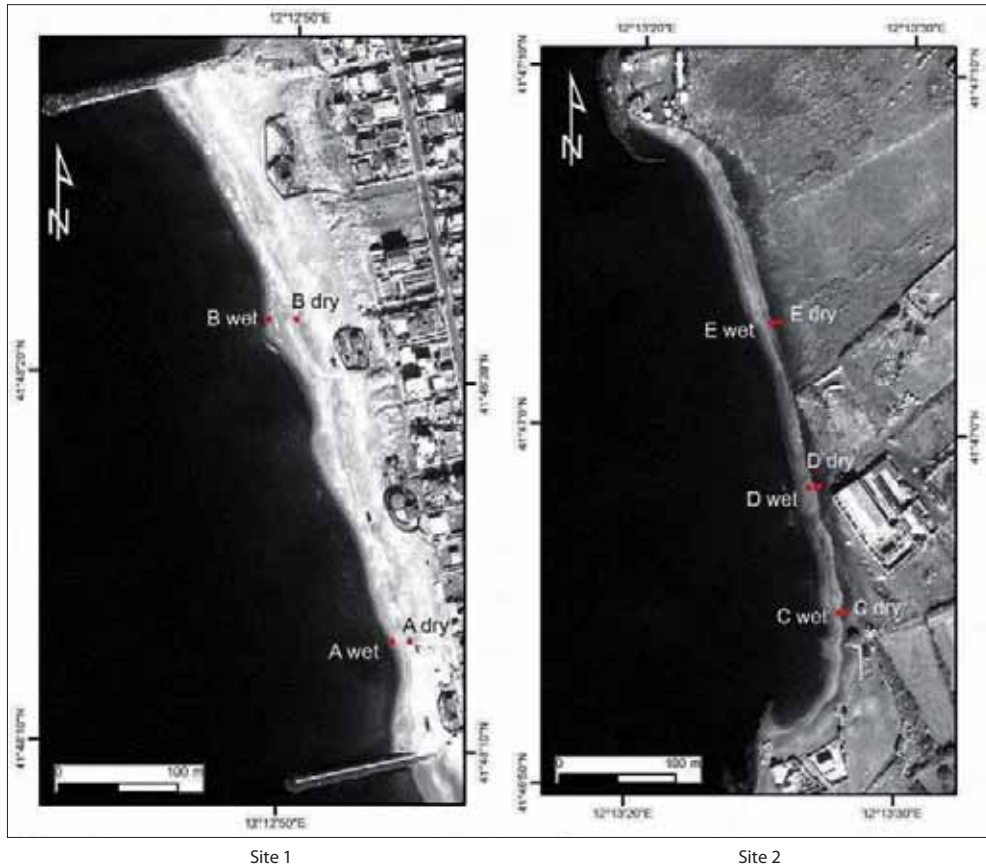
Figure 5 – Sites where reflectance was measured (© European Space Imaging GmbH - Planetek Italia).

Since the spectral range of the Ikonos and Quickbird sensors is much less broad than that of the spectroradiometer, the mean values, according to the spectral range of the 4 Ikonos bands (Figure 7) were computed. Also in this it is possible to observe a drop in reflectance going from dry sand to wet sand. Mean reflectance values for bands 3 and 4 were used to calculate the NDVI and compare it with that obtained from the images.

The light-coloured sand showed very close NDVI values, while the dry sand had slightly lower NDVI values. Dark sand presented non-uniform values, and the variation between measurements was greater. This may be explained by the changing weather conditions when measurements were taken. If one observes closely the absorption peaks of water, it can be seen that at site 2 these values are higher. To minimise these effects, laboratory measurements were taken for sand samples collected from the same sites, with the original water content preserved up to the time of measurement.

Laboratory measurements used an artificial light source (with a known emission spectrum) and the spectralon panel as reference, applying an analytical protocol deriving from that drafted by Salzano et al. (2006).

Laboratory curves, plotted at Ikonos wavelengths, presented the same spectral trends as the sand measured *in situ*, with a drop in reflectance values as the water content of sand increased. Calculating NDVI values for these curves, it is seen that the undisturbed samples had constantly higher NDVI values for wet sand (and lower for dry samples). Dry sand in band 4, indeed, always had higher reflectance values than wet sand.
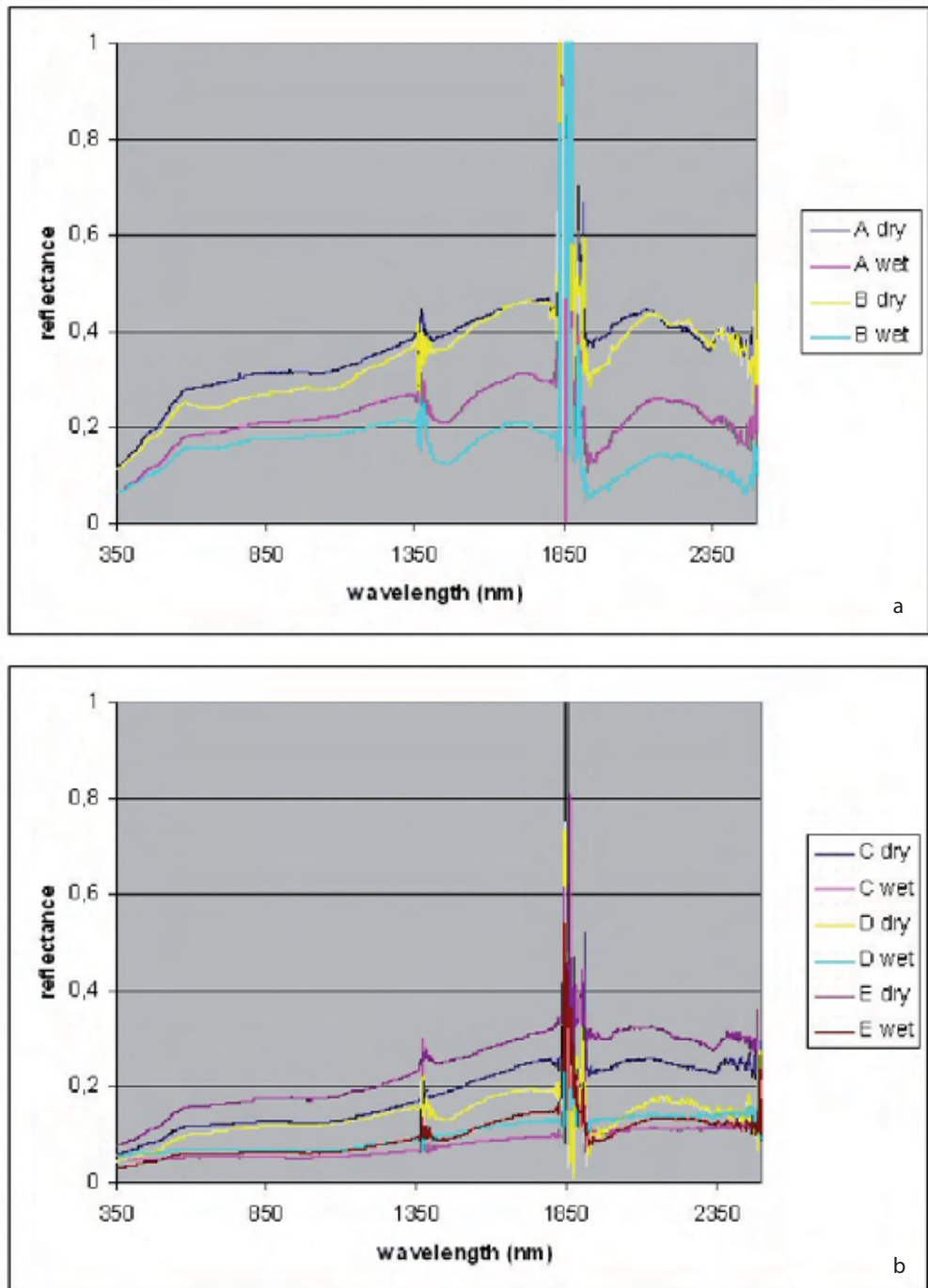
Figure 6 – Spectral signatures measured *in situ* for light-coloured sand (a) and dark sand (b). The peaks at 1350 and 1850 represent the absorption bands of water vapour in the atmosphere present when measurements were taken (wavelenght in nm).
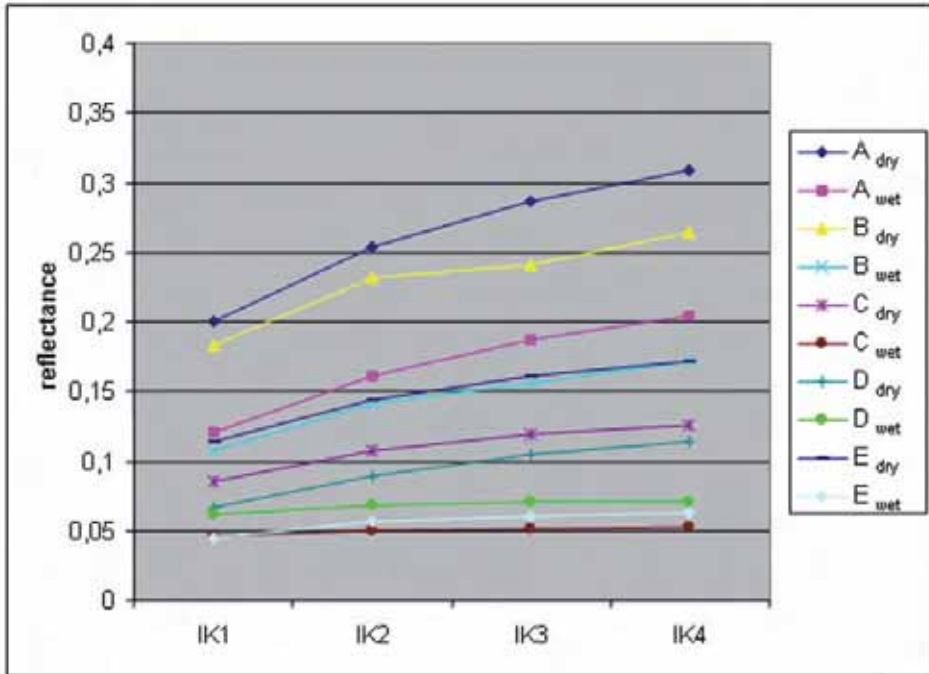
Figure 7 – Spectral signatures of sand from sites 1 and 2. Reflectance values represent the mean values calculated in the same spectral intervals of the Ikonos sensor.
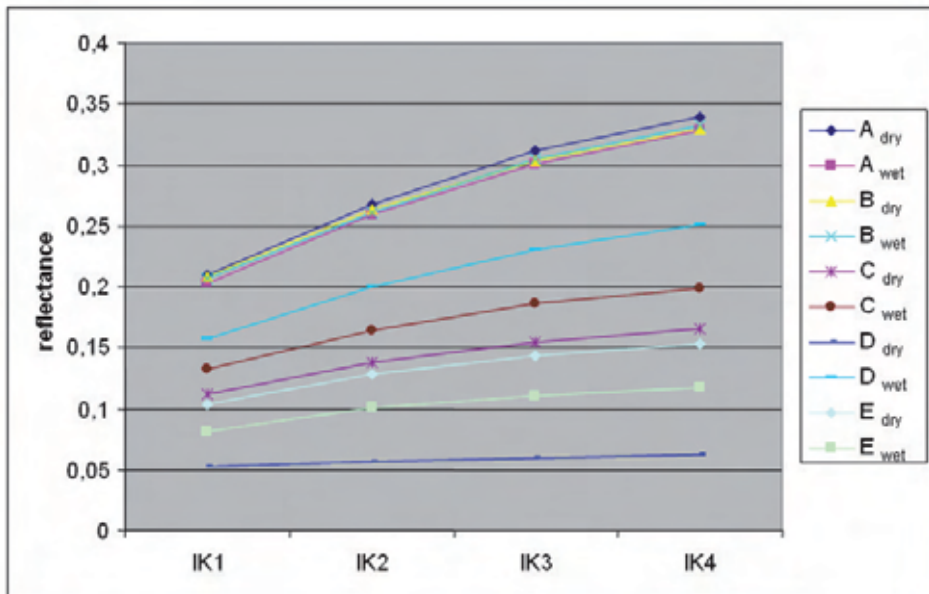
Figure 8 – Spectral signatures measured in the laboratory after sand was heated for 24 hours at 110°C of the originally dry and wet samples. Reflectance values represent the mean values calculated in the same spectral intervals as the Ikonos sensor.

Measurements on the same samples, which had been kept in an oven at 110 °C for 24 h to elimi-nate gradually all the water, showed (Figure 8) that the reflectance values of sands with a similar mineralogical composition and granulometry (sites 1) were very close. On the contrary, the sands from site 2 showed a different spectral behaviour due to granulometry and different content of femic minerals.

A similar behaviour can be osserved studing NDVI values for samples collected at site 1(Figure 9). The different pattern of NDVI data for site 2 samples points out, even more evidently, a strong disomogeneity in mineralogical and granulometric composition due to the presence of femic minerals that in site 2 E samples are distribute in policromatic aeolian ripples. This fields disho-mogenity is hidden by the laboratory preparation of samples which mix all the grains.
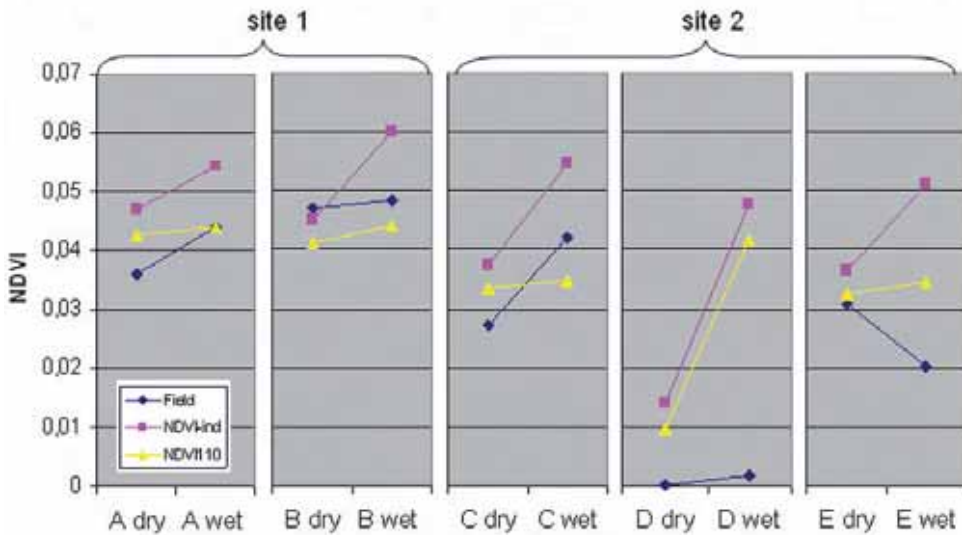
Figure 9 - NDVI values calculated using in situ and laboratory radiometric measurements. Laboratory measurements refer to both sand having a different water content (NDVI-ind) and dry sand (NDVI110).

The whole set of NDVI values shows that there is always a marked difference between dry sand and wet sand, and that sand values are in any case always greater than 0.

Field and laboratory radiometric measurements thus confirm that NDVI values may be success-fully used to identify the water/sand interface from satellite images taken with different sensors.

Comparison with photo interpretation data and ground surveys

The shoreline was detected for the same sample areas using traditional photo interpretation techniques on Quickbird images from 2005 and Ikonos images from 2007.

The photo interpretation analysis was carried out on images processed using different techniques: NDVI images for the comparison with data obtained using the previously described procedure, and panchromatic images onto which a linear stretch was applied to improve the image, and finally a false color image obtained using a color normalized sharpening (CNS) procedure.

The 2005 images were acquired in the presence of a rough sea, thus the location of the shoreline using panchromatic images proved to be rather uncertain. On the contrary, for the NDVI images, although there was a reduction in geometric resolution (2.44 m), the water/sand interface was more emphasised and better defined, even though problems remained in locating the shoreline due to the sea conditions.

Site 1

Site 2
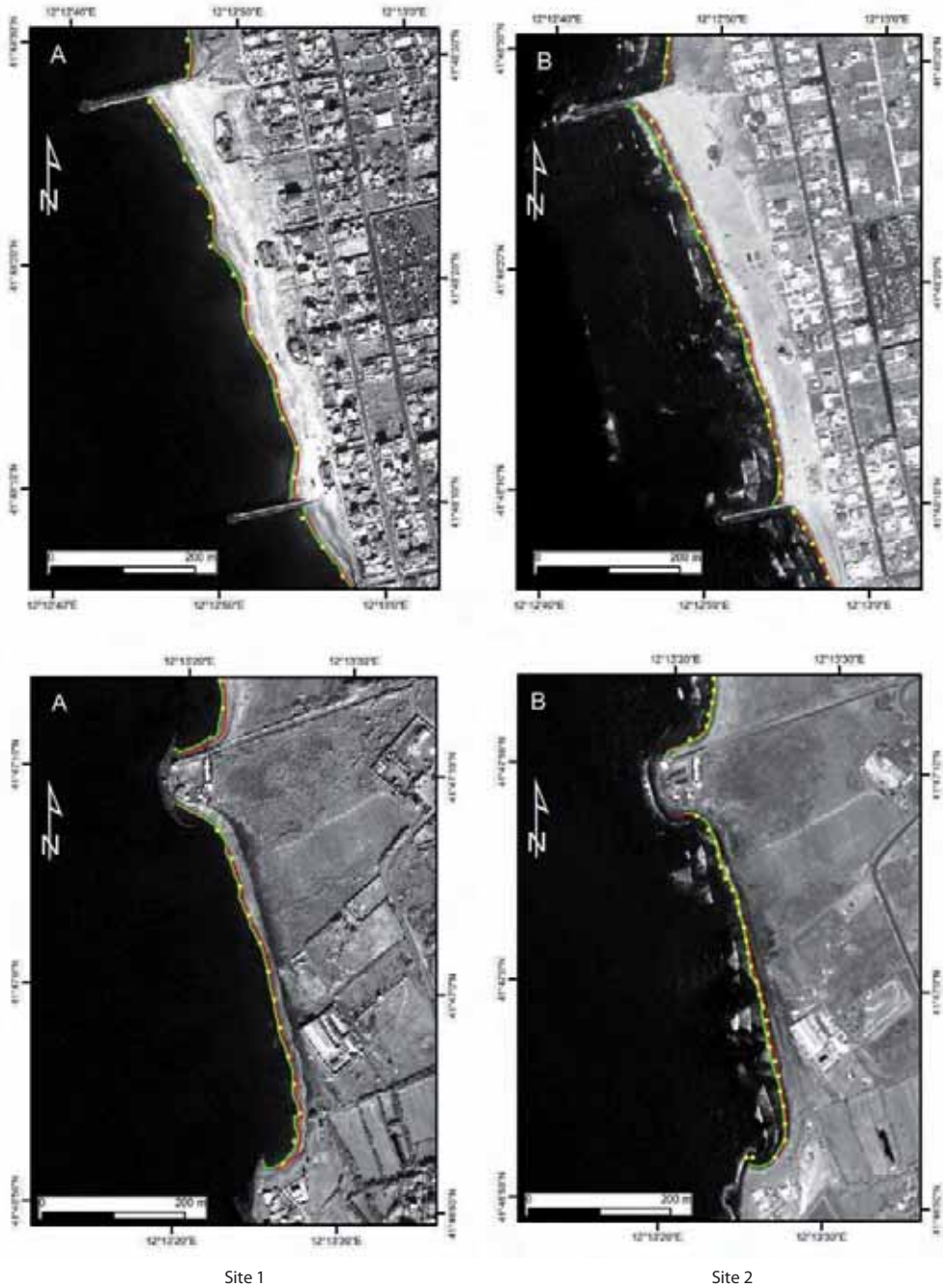
Figure 10 – Shoreline positions detected from NDVI markers (yellow points) and photointerpretation (in green using pan-sharpened image and in red using NDVI image). A= Ikonos image (© European Space Imaging GmbH - Planetek Italia); B= Quickbird image (© 2007 DigitalGlobe Inc., Telespazio per l'Italia All Right reserved).

 The 2007 images, acquired in the presence of an almost totally calm sea, allowed a better definition of the shoreline position, especially in the case of panchromatic and CNS images.

The comparison of shorelines detected in different years and using different techniques (Figure 10) showed a good match between the lines extracted from NDVI images and the shoreline photo-interpreted using the same images. There was indeed a maximum deviation of 2 pixels (max 5 m) for the Quickbird image and of 1 pixel (max 4 m) for the Ikonos image.

In the two test sites the shoreline was also compared with that obtained by means of ground surveys (GPS) undertaken about one month after the acquisition of the Ikonos image. The comparison highlighted marked differences in the beach morphology due to the different sea and weather conditions. In particular, in the stretch of coastline in front of the town of Focene (Figure 11), the image shows the presence of *sand waves* that were no longer present at the time of the ground survey. These variations may reach as much as 17 m close to deposition areas (*sand waves*), and on average they are around 5-6 m. These differences may be due to indeterminateness owing to the size of the pixel (2.44 m) or to the indeterminability of the exact position of the shoreline because of swell.
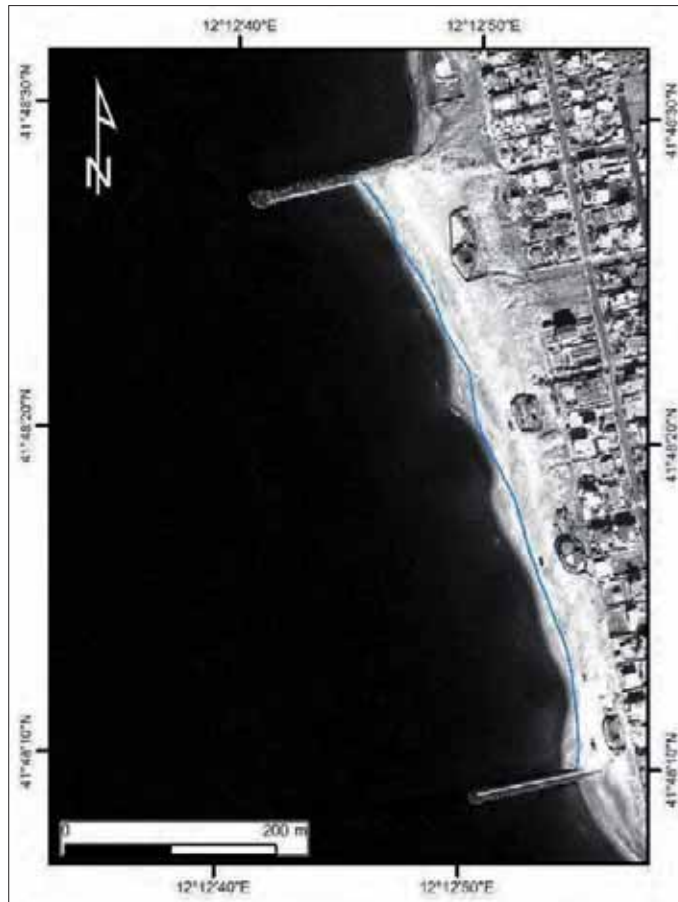
Figure 11 – Test site 1: shoreline detected by means of GPS surveys (undertaken on 23 January 2008) and the Ikonos image (© European Space Imaging GmbH - Planetek Italia - acquired on 21 December 2007). There is a marked variation in shoreline close to deposition areas (sand waves).

Swell, accordingly, is the parameter that mostly affects the correct location of the water/sand interface.

To quantify the differences in locating the shoreline caused by sea conditions, two Quickbird images of the same stretch of coastline (between Fregene and Palo Laziale), but acquired in the presence of very different sea and weather conditions (in one the sea is practically calm, in the other it is rough) were analysed. For these images (see Table 1), acquired on June 3 2005 and July 22 2005 respectively, the shoreline was detected through the manual and automatic positioning of markers. Differences were observed in locating the shoreline (Figure 10) that were of the same magnitude as those noted in the comparison between Ikonos images (December 2007) and GPS surveys (January 2008).

Conclusions

The knowledge of the evolution trend of coastlines is one of the aspects that mostly involves local administrations, having the responsability of managing the territory, also through prevention and protection actions. In this context, the use of high spatial resolution satellite images may be a valid tool for monitoring the shoreline, especially when it is possible to extract territorial elements of interest without having to use overly specialist image processing. Responding to this need, the authors developed a software-based procedure that makes it possible to detect the shoreline by identifying the water/sand interface from high spatial resolution multispectral images. The procedure is based on the clear existing difference between the radiometric response of water and that of sand in the red and infrared wavelengths. This marked difference, evident in the spatial profiles resulting from NDVI images, has made it possible to draw up a semiautomatic procedure not bound by the interpretation of an operator, consequently objective, also applicable when analysing images acquired in different periods, as required by monitoring programmes.

The shoreline, detected using this semiautomatic system, showed a good match with results obtained using the traditional photo interpretation method and other types of more complex image processing methods (i.e. Principal Component Analysis, supervised classification), which however require the intervention of an expert operator.

It is well known that the beach is an extremely dynamic morphological entity, whose changes are closely tied up with weather and sea conditions and tide variations. In monitoring coastlines using a semiautomatic system based on the use of high resolution satellite images, however, the role of sea conditions at the time of data acquisition is fundamental. Correct monitoring should therefore be based on the acquisition of satellite images taken, when possible, when the sea is calm in order to prevent the over-estimation or under-estimation of variations, not only seasonal but also shorter-term.

For the selection of images to be used, multispectral images should be preferred, even though spatial resolution is lower. The normalised ratio between the infrared and red bands (NDVI) has indeed proved to be particularly suitable for the identification of the water/sand interface. This ratio, furthermore, makes it possible to compare images taken at different times, since it minimises the effects caused by different atmospheric conditions on sand radiance, as ascertained from spectroradiometric measurements *in situ* and in the laboratory.

Of the parameters to be considered for monitoring by means of remote sensing using a semiautomatic system, the importance of the choice of image is evident, in terms of both resolution and processing method, but also in terms of sea and weather conditions. It is accordingly necessary to work on archive images after having checked sea conditions. In some localities along the Mediterranean coast, tidal conditions should also be known and taken into consideration.

References

Baily B. and Nowell D. (1996) – *Techniques for monitoring coastal change: a review and case study*. Ocean & Coastal Management, 32: 85-95.

Battiau-Queney Y., Billet J.F., Chaverot S. and Lanoy-Ratel P. (2003) – *Recent shoreline mobility and geomorphologic evolution of macrotidal sandy beaches in the north of France.* Marine Geology, 194: 31- 45.

Beachmed (2004) – *Tecniche di monitoraggio dell'evoluzione delle spiagge* – In "Il progetto Beachmed: Recupero ambientale e mantenimento dei litorali in erosione con l'utilizzo di depositi sabbiosi marini. Fase C - 3° Quaderno Tecnico: 19-92.

Bergamasco A. and Pesaresi M. (1997) – *Elaborazione di dati Landsat-TM per lo studio dell'evoluzione della linea di spiaggia: il litorale del Cavallino (Venezia)*. Rivista Italiana di Telerilevamento, 9: 35-42.

Biasini A. and Salvatore M.C. (1995) – *Fotorestituzione digitale della shoreline: area campione del Delta Tiberino*. Il Quaternario, 8: 263-266.

Brivio P.A., Lechi G. and Zilioli E. (2006) – Principi e metodi di Telerilevamento. Ed. CittaStudi, 525 pp.

Carli S., Iandelli N., Pranzini E. and Salvatori R. (2008) – *L'utilizzazione di immagini telerilevate ad alta resolution per lo studio dell'erosione costiera: estrazione della linea d'acqua e valutazione della sua accuratezza*. Studi costieri, 14: 43-54.

Collier P., Fontana D., Pearson A. (1995) – *GIS mapping of Langstone Harbour for an integrated ecological and archaeological study*. Proceeding of International Symposium on GIS and Computer Mapping For Coastal Zone management. Ed. R. Furness: 315-327.

Congalton R. G. (1991) – *A review of assessing the accuracy of classification of remotely sensed data*. Remote Sensing of Environment, 37: 35-46.

Crowell M., Leatherman S.P., Buckley M.K. (1991) – *Historical shoreline change: error analysis and mapping accuracy*. Journal of Coastal Research, 7: 839-852.

Drury S. (2001) – Image Interpretation in Geology, Blackwell Science, Nelson Thornes, UK., 292 pp.

Favretto A., Mauro G., Ramella R. and Romeo R. (2004) – *Telerilevamento e GIS per lo studio costiero: verifica di alcuni campionamenti puntuali*. Atti della 8° Conferenza Nazionale Asita – 14-17 Dicembre 2004: 1059 – 1063.

Fromard F.,Vega C. and Proisy C. (2004) – *Half a century of dynamic coastal change affecting mangrove shorelines of French Guiana. A case study based on remote sensing data analyses and field surveys*. Marine Geology, 208: 265–280.

Hesselmans G. H. F. M., Wensink G. J. and Calkoen C. J. (1997) – *Possibilities of remote sensing technologies in coastal studies*. Geojournal, 42: 65-72.

Lillesand T.M. and Kiefer R.W. (1987) – Remote Sensing and Image Interpretation. Wiley & Sons, New York, 722 pp..

Pranzini E., Carli S., Bowman D., Wetzel L., Archetti R. Torricelli E. Corradi N., Ferrari M., Schiaffino C.F. Casacchia R. La Monica G.B., Petrocchi E., Salvatore. M.C., Salvatori R., Tortora P., Monti M., Preti M., De Nigris N., Heurtefeux H., Lesaignoux A. Sire E., Koutandos E.V.m, Kampanis N.A., Karambas T.V., Kotsovinos N., Xeidakis G, Georgoulas A., Petridis D., Duran R., Barnabeu A., Alonso B., Ercilla G., Estrada F.and Farran M. (2007) – *Le Sous-projet OpTIMAL – Optimisation des Techniques Intégrées de Monitorage Appliquées aux Littoraux* – In Interreg IIIC – Beachmed-e – La gestion stratégique de la défense des littoraux pour un développment soutenable des zones cotières de la Mèditerranè – 2ème Cahier Technique Phase B, Ier Édition: 30-42.

Sabins F.F. (1986) – Remote Sensing: principles and interpretation, John Wiley, 449 pp.

Salzano R., Casacchia R., Salvatori R. (2006) - *Tecniche di spettroradiometria per lo studio dell'inquinamento urbano*. Nota Tecnica CNR-IIA, marzo 2006. 56 pp.

Thieler E.R and Danford W. (1995) – *Historical shoreline mapping: improving techniques and reducing positioning errors*. Journal of Coastal Research, 10: 547 – 563.

Maximum fluctuation of the shoreline due to tidal fluctuation

Nikolaos E. Kotsovinos, Anastasios N. Georgoulas

The advance of modern satellites (e.g. Quickbird, Ikonos) made possible to extract the "instantaneous" shoreline with a very good accuracy (1 to 3 pixels i.e. less than 2 m). The horizontal instantaneous shoreline shift, due to fluctuation of the sea surface elevation, is significant for beaches comprising fine sand and should always be taken into account when dealing with shorelines extracted from aerial or satellite images. In this paper a) we describe the methodology used to study this problem, b) we find the maximum error which is introduced when we assume that the instantaneous shoreline - extracted from satellite images - is identical to the MHWL shoreline, c) we give two empirical equations which can be used as a "rule of thumb" to calculate the maximum fluctuation of the horizontal position of the instantaneous shoreline, d) we suggest that by knowing the exact time that the image is taken, the mean grain size of the beach material and the sea surface fluctuation in the area under investigation, it is possible to correct the instantaneous shoreline to produce the MHWL shoreline.

Introduction

A part of the research carried out during the BEACHMED-e / OpTIMAL Project for the region of East-Macedonia Thrace (Greece) is based on the precise shoreline determination in order to generate an undisputable data base of the shoreline position at many time scales (short or long , i.e. hours, days or many years).

In many glossary and publications, coastline is considered equivalent to shoreline. However, according to NOAA (National Oceanic and Atmospheric Administration-USA, Public Law 31) the coastline is defined as the line of ordinary low water along that portion of the coast which is in direct contact with the open sea. This definition is different from the definition of shoreline, *i.e.*

> "Shoreline is the line of contact between the land and a body of water. On Coast and Geodetic Survey nautical charts and surveys the shoreline approximates the Mean High Water Line (MHWL). In Coast Survey usage the term is considered synonymous with coastline. "

In this paper we adopt the above definition of the shoreline. Accordingly, shore is the land bordering a usually large body of water. Coast is the land near a shore. According to NOAA, the mean sea level (sea level *datum*) is the average height of the surface of the sea for all stages of the tide over a 19 year period, usually determined from hourly readings. The MHWL is the average of all the high water heights observed over a time period of many years.

It is obvious that the instantaneous intersection of the calm sea free surface with the shore (given by satellite image and aerial photographs), determines a land-sea border line (that we may call "instantaneous" shoreline). Since the free surface of the sea fluctuates, it is obvious that in general the instantaneous "border line" between sea and land (=instantaneous shoreline at time t) is not identical with the "MHWL shoreline", which in principle is a fixed three dimensional line in space, which remains always

steady, for many years assuming that the shore has everywhere zero erosion and zero accretion, and zero increase of the mean sea level. Therefore, we must be aware that the instantaneous border line between land and sea extracted from aerial or satellite images is only an approximation of the "true" MHWL shoreline - it lies (in general) further from the shore in comparison with the MHWL shoreline, *i.e.* satellite images underestimate erosion and overestimate accretion.

With the satellite imagery we try to extract a line in space which is the instantaneous intersection at time t of the shore land with the sea free surface, by measuring the gradient of the reflectance between adjacent pixels. It is assumed that the highest gradient of the reflectance is obtained between two pixels which belong to land and water respectively. This fact introduces an uncertainty, which is due to inherent limitation of the satellite image to distinguish sharply the water from saturated with water sand. When the size of a satellite image pixel was for example 30 m, and the horizontal fluctuations of the position of the land – sea water "border line" due to tidal fluctuation is from 5 m to 20 m, it is reasonable to assume that the land - sea water "border line" extracted from satellite images determined also the shoreline, because it was by that time impossible to do better. In the past, the satellite images had horizontal resolution of about 10 m to 30 m (pixels 10 m to 30 m), and therefore the question of the tidal variation was not of practical interest for the Mediterranean Sea.

The advance of modern satellites (e.g. Quickbird, Ikonos) made it possible to extract with very good accuracy (1 to 3 pixels, i.e. less than 2 m) the instantaneous interface between land, wet sand and sea - *i.e.* it is possible to define the instantaneous "sea-land border line" with a resolution of less than 2 m.

The aim of this paper is to find a methodology to estimate the maximum error involved when approximating the shoreline from the aerially-determined border line between sea and land, and to discuss how to correct this mistake.

Vertical fluctuation of the sea free surface

It is obvious that the instantaneous land-sea border line fluctuates around a mean position, following the fluctuations of the instantaneous sea surface fluctuations. The instantaneous elevation H(t) of the sea surface is a function of the following parameters:

· Tidal fluctuation
· Barometric pressure fluctuation
· Wind surge
· Waves height
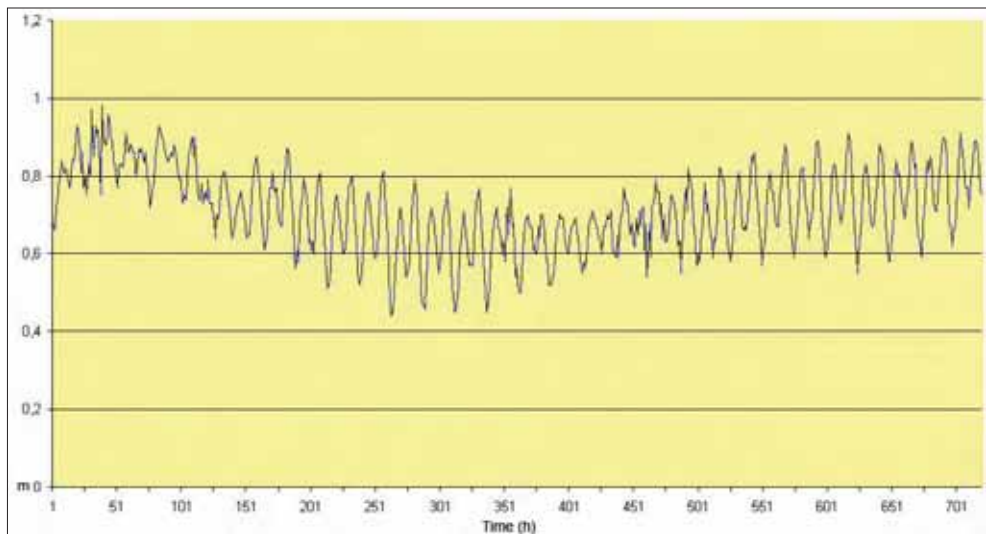
Figure 1 - Sea level fluctuation at Alexandroupolis port (0 = lowest low water level).

Typical values of sea level fluctuations in North Aegean are:
· Tidal fluctuation: about 30 cm
· Barometric pressure variability: typically 3 cm
· Wind surge: about 5 cm (for weak wind, below 1 m/s)
· Waves height: about 5 cm (for weak wind, below 1 m/s)
In Figure 1, the tidal variation of the sea level at Alexandroupolis (North Aegean) is shown for many days.

Beach profile
In the region of East Macedonia-Thrace most of the shore is characterised by sandy beaches and a sea bottom profile in equilibrium. It is assumed that the beach-profile in equilibrium is given by the following relationship (Bruun, 1954; Dean, 1977; Dean, 1991):

$$h=Ax^{2/3} \tag{1}$$

where
h = water depth at a horizontal distance (x) from the shoreline (m)
A = a dimensionless shape parameter called the 'proportionality coefficient'
x = distance from the shoreline (m)

The "proportionality coefficient" A is defined from the following relation (Cooper et al., 2000):

$$A=0.21D_{50}^{0.48} \tag{2}$$

where D_{50}= mean sediment grain-size diameter (mm).

In Figure 2, we draw the beach bed profile for various mean grain size diameters.
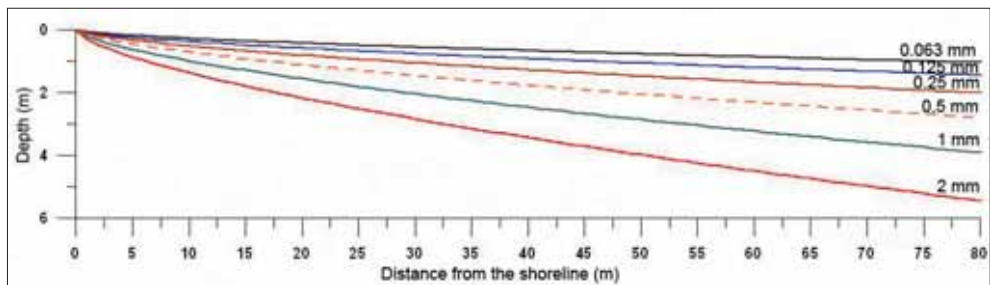
Figure 2 - Plot of the equilibrium profile for various mean grain sizes.

Horizontal variation of the instantaneous position of the land-sea water border line (instantaneous shoreline) due to tidal variations
Apparently it is useful to find a relation between the maximum horizontal variation of the position of the instantaneous shoreline and the fluctuation of the sea surface elevation.
In Figures 3, 4, 5, 6 and 7, we plot the beach profile, the line of MLWL, and the line of MHWL for tidal fluctuation equal to 50 cm, and for mean grain size equal to 0.063, 0.125, 0.25, 0.5 and 1 millimetres. It is found that the maximum fluctuation of the instantaneous shoreline position is respectively 27, 17, 10, 6 and 4 meters. Similar figures can be drawn for other values of sea surface elevation fluctuations. The mean grain size at many beaches of the region of East Macedonia Thrace varies from 0.06 mm to 0.25 mm, and therefore the above findings are useful and give a hint for the correction of shoreline extraction from satellite images. It is clear that, from the knowledge of the exact time that a satellite image is taken, we can estimate the sea surface level due to tidal fluctuation, to barometric pressure and wind.

Using the above findings, we plot in Figures 3 to 7 the maximum horizontal fluctuation of the instantaneous *shoreline position* in meters as a function of the beach *grain size D_{50}* (in mm), for tidal fluctuation equal to 0.5 m. We plot in Figure 8 the best fit regression lines for two tidal fluctuations equal to 0.3 m (blue line) and 0.5 m (brown line), and we find the following equations:

$$dx = \text{maximum fluctuation of the shoreline position} \ = \ \frac{1.73}{(D_{50})^{0.72}} \quad \text{(tidal fluctuation} = 30 \text{ cm)} \quad [3]$$

$$dx = \text{maximum fluctuation of the shoreline position} \ = \ \frac{3.73}{(D_{50})^{0.72}} \quad \text{(tidal fluctuation} = 30 \text{ cm)} \quad [4]$$
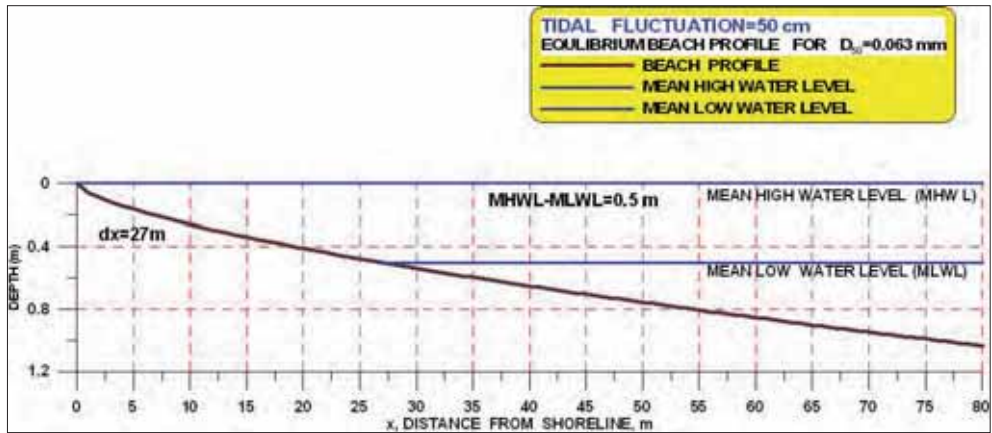
Figure 3 - The maximum fluctuation of the horizontal position of the instantaneous shoreline is about 27 m for mean grain size equal to 0.063 mm and tidal fluctuation equal to 50 cm.
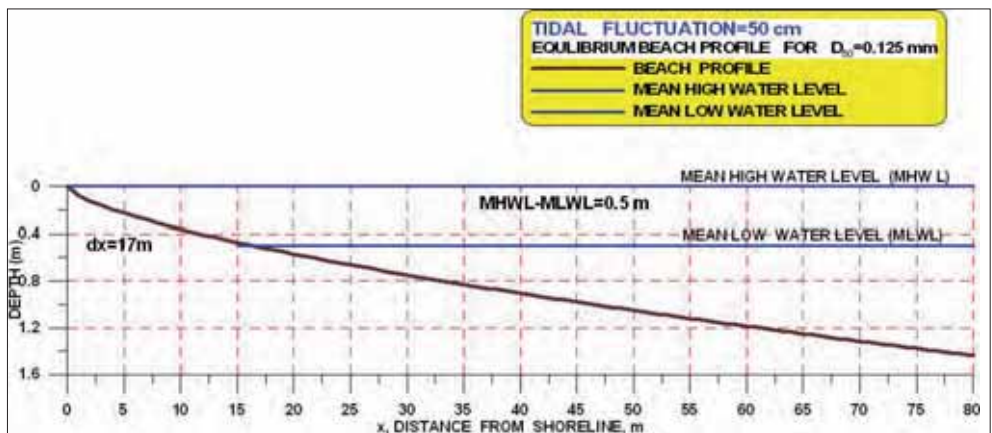
Figure 4 - The maximum fluctuation of the horizontal position of the instantaneous shoreline is about 17 m for mean grain size equal to 0.125 mm and tidal fluctuation equal to 50 cm.
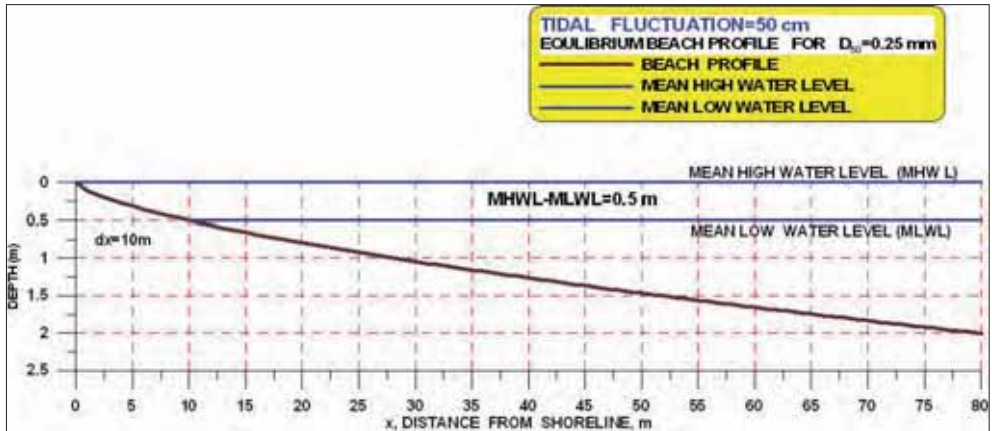
Figure 5 - The maximum fluctuation of the horizontal position of the instantaneous shoreline is about 10 m, for mean grain size equal to 0.25 mm and tidal fluctuation equal to 50 cm.
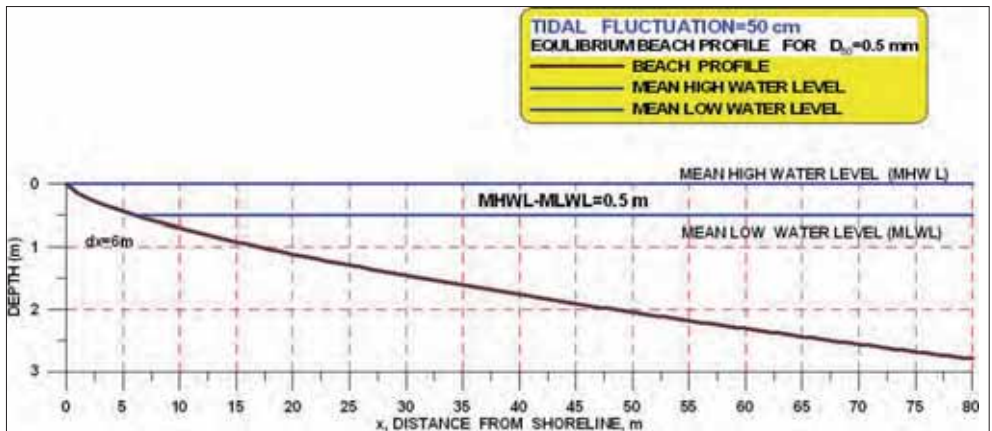
Figure 6 - The maximum fluctuation of the horizontal position of the instantaneous shoreline is about 6 m, for mean grain size equal to 0.5 mm and tidal fluctuation equal to 50 cm.
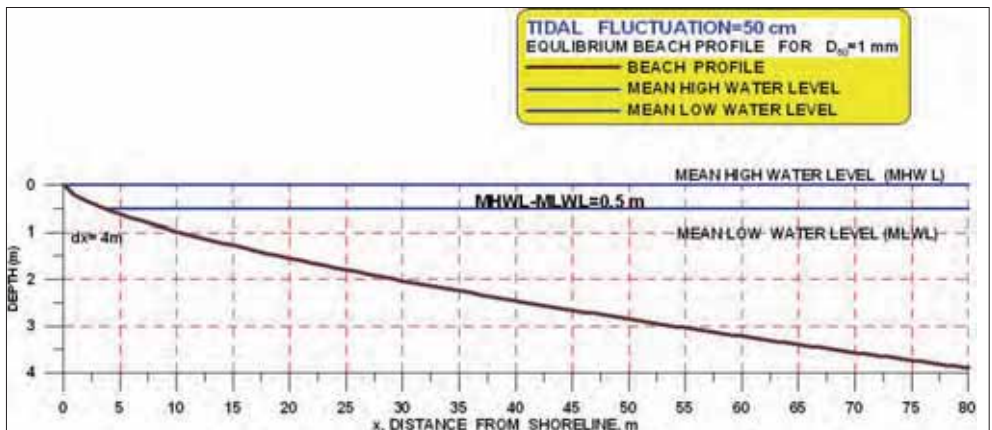
Figure 7 - The maximum fluctuation of the horizontal position of the instantaneous shoreline is about 4 m for mean grain size equal to 1 mm and tidal fluctuation equal to 50 cm.
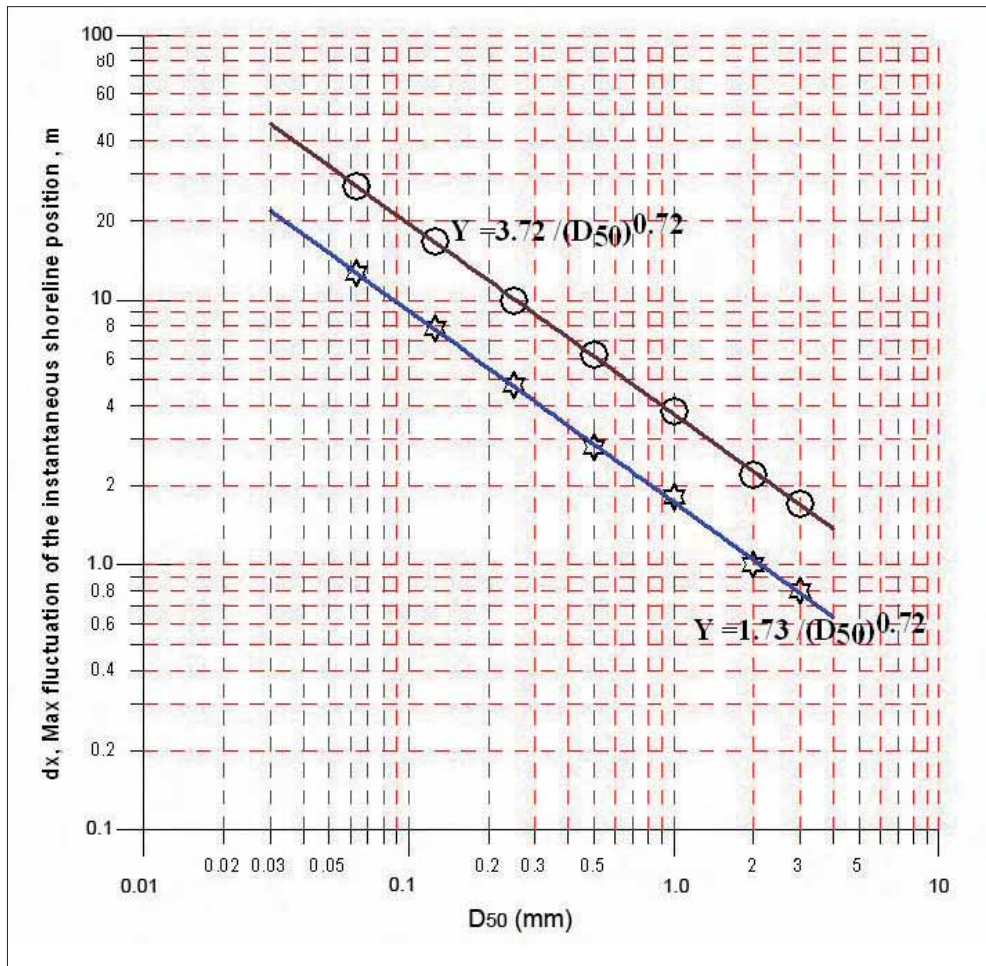
Figure 8 - The maximum fluctuation of the horizontal position of the instantaneous shoreline as a function of grain size for tidal fluctuation equal to 30 cm (blue line) and 50 cm (brown line).

Conclusions

From all the above it is obvious that the horizontal fluctuation of the shoreline is significant in the case of fine sand and should always be taken into account when dealing with shorelines extracted from aerial or satellite images.

In other words the tidal fluctuation, the barometric pressure and the wind, which influence the position of the instantaneous shoreline, can be easily taken into consideration to correct the extracted shoreline from airborne or satellite imagery, simply by knowing the exact time that the image is taken, the mean grain size diameter of the beach material and the sea surface fluctuation in the area under investigation.

This possibility for the correction of the extracted instantaneous shoreline to locate the MHWL shoreline increases the monitoring accuracy of remote sensing methods, as the dynamic fluctuation of the shoreline position is taken into consideration.

References

Bruun P. (1954) - *Coast Erosion and the Development of Beach Profiles.* US Army Beach Erosion Board, Technical Memorandum 44 .

Cooper N.J., Leggett D.J. and Lowe J.P. (2000) - *Beach-Profile Measurement, Theory and Analysis: Practical Guidance and Applied Case Studies*. J. CIWEM, 14: 79-88.

Dean R.G. (1977) - *Equilibrium Beach Profiles.* US Atlantic and Gulf Coasts. Dept. Civil Eng., Ocean Engineering Technical Report No. 12, University of Delaware, Newark.

Dean R. G. (1991) - *Equilibrium beach profiles: characteristics and applications.* Journ. Coastal Research, 7: 53-84.

Shoreline extraction using satellite imagery

Michalis Lipakis, Nektarios Chrysoulakis, Yiannis Kamarianakis

Shoreline change is considered to be one of the most dynamic processes in the coastal area. It has become important to map shoreline changes as an input data for coastal hazard assessment. In recent years, satellite remote sensing data has been used in shoreline extraction and mapping. The accuracy of image orthorectification, as well as the accuracy of image classification, are the most important factors affecting the accuracy of the extracted shoreline. In this study, the shoreline of the area of Georgioupolis was mapped for the years 1998 and 2005 using aerial imagery and Ikonos data, respectively. Ikonos data were orthorectified and a feature extraction technique was then used to extract the shoreline. This technique employed machine-learning algorithms which exploit both the spectral and spatial information of the image. Results were validated with *in situ* measurements using Differential GPS. The analysis showed that there have not been severe changes in the shoreline between 1998 and 2005, except in some locations where change was substantial.

Introduction

The coastal area is a highly dynamic environment with many physical processes, such as tidal flooding, sea level rise, land subsidence, and erosion-sedimentation. Those processes play an important role in shoreline change and development of the coastal landscape. Multi-year shoreline mapping is considered to be a valuable task for coastal monitoring and assessment. The shoreline is defined as the line of contact between land and a body of water. It is easy to define but difficult to capture, since the water level is always changing. Therefore, a problem exists in the mapping community because different public or private entities have compiled and published shoreline delineations that are based on different shoreline definitions. This has created confusion and uncertainty for those who use shoreline information daily for the sake of decision making, resource planning, emergency preparedness etc. In the USA for example, NOAA uses the tide-coordinated shoreline, which is the shoreline extracted from a specific tide water level. The MLLW (Mean Lower Low Water) and MHW (Mean High Water) are used in this way to map shorelines that can be geo-referenced. Both the MLLW and MHW are calculated from averages over a period of 18.6 lunar years (Li et al., 2001). In contrast, the U.S. Geological Survey (USGS) compiles shoreline data for the 1: 24.000 scale topographic base map series from digital orthophoto quadrangles created from photographs that are not tide coordinated, thereby making the shoreline a snapshot in time (Scott et al., 2003). It is therefore obvious that since shoreline has a dynamic nature, its definition, mapping and monitoring are complicated tasks.

Different approaches to shoreline mapping and change detection have been used in the past. Traditional shoreline mapping in small areas is carried out using conventional field surveying methods. The method used today by the American National Geodetic Survey to delineate the shoreline is analytical stereo photogrammetry using tide-coordinated aerial photography controlled by kinematic GPS techniques (Di et al., 2003). Land vehicle-based mobile mapping technology has been proposed to trace

water marks along a shoreline using GPS receivers and a beach vehicle. LiDAR depth data have also been used to map shorelines (Shaw and Allen, 1995; Li, 1997).

Automatic extraction of shoreline features from aerial photos has been investigated using neural networks and image processing techniques (Ryan et al., 1991). Photogrammetric techniques have been employed to map the tide-coordinated shoreline from the aerial images that are taken when the water level reaches the desired level. Aerial photographs taken at these water levels are more expensive to obtain than satellite imagery.

Besides aerial imagery, space-born radar and especially Synthetic Aperture Radar (SAR) have proven to be a valuable tool for coastal monitoring. SAR imagery has also been used to extract shorelines at various geographic locations (Erteza, 1998; Chen and Shyu, 1998; Trebossen et al., 2005; Wu and Lee, 2007). SAR is a very promising technology, especially for Europe since the European Space Agency (ESA) is recognized as a world leader in SAR missions (ERS1, ERS2, Envisat, GMES-Sentinel-1).

In recent years, optical satellite remote sensing data have been used in automatic or semi-automatic shoreline extraction and mapping. Braud and Feng (1998) evaluated threshold level slicing and multi-spectral image classification techniques for detection and delineation of the Louisiana shoreline from 30-meter resolution Landsat Thematic Mapper (TM) imagery. They found that thresholding TM Band 5 was the most reliable methodology. Frazier and Page (2000) quantitatively analysed the classification accuracy of water body detection and delineation from Landsat TM data in the Wagga region in Australia. Their experiments indicated that the density slicing of TM Band 5 achieved an overall accuracy of 96.9 percent, which is as successful as the 6-band maximum likelihood classification. Scott et al. (2003) proposed a semi-automated method for objectively interpreting and extracting the land-water interface, which has been devised and used successfully to generate multiple shoreline data for the test States of Louisiana and Delaware. This method was based on the application of Tasseled Cap transformation coefficients derived by the EROS Data Center for ETM+ data as described by Huang et al. (2002). The Tasseled Cap transformation was chosen over other methods primarily because of the objective and consistent manner in which it classifies pixels and because its use allowed the creation of other useful raster byproduct files. In operation, the Tasseled Cap transformation recombined spectral information of the 6 ETM+ bands into 3 principal view components through the use of coefficients derived by sampling known land cover spectral characteristics. Of the three principal view components created, i.e., Brightness, Greenness, and Wetness, the Wetness component is exploited to differentiate land from water. Zakariya et al. (2006) tried to detect shoreline changes for the Terengganu river mouth and related coastal area. Landsat data were used together with GIS capability to determine shoreline, sandy area and the changes that occur especially on sediment movement from 1996 to 2002. RGB to IHS imagery conversion analysis ISODATA (Iterative Self-Organizing Data Analysis) classification were employed. Liu and Jezek (2004), as well as Karantzalos and Argialas (2007) automated the extraction of coastline from satellite imagery by canny edge detection using digital number (DN) threshold.

Li et al. (2001) compared shorelines of the same area that were extracted using different techniques, evaluated their differences and discussed the causes of possible shoreline changes. The different shoreline products had been generated using different techniques: by digitising from aerial ortho-photos, intersecting a digital water surface with a coastal terrain model and extracting from stereo satellite images. In addition, existing shorelines digitised from USGS maps and NOAA T-Sheets were included in their analysis.

With the development of remote sensing technology, satellites can capture high resolution imagery with the capability of producing stereo imagery. The new generation of very high spatial resolution satellite imaging systems, such as Ikonos and Quickbird, opens a new era of earth observation and digital mapping. They provide not only high-resolution and multi-spectral data, but also the capability for stereo mapping. Because of their high resolution and their short revisit rate (~3 days), Ikonos and Quickbird satellite images are very valuable for shoreline mapping and change detection, therefore their data have been used in several past studies. Wang et al. (2003) investigated a novel approach for automatic extraction of shoreline from Ikonos images using a mean shift segmentation algorithm. Di et al. (2003) investigated a novel approach for automatic extraction of shorelines from Ikonos imagery:

4m and 1m resolution Ikonos images along the Lake Erie shore were used. In the first step the images were segmented into homogeneous regions by mean shift segmentation. Then, the major water body was identified and an initial shoreline was generated. The final shoreline was obtained by local refinement within the boundaries of the candidate regions adjacent to the initial shoreline. Li et al. (2003) used Ikonos stereo imagery in shoreline extraction. They presented the results of an experiment in which they attempted to improve Ikonos Rational Functions (RF) for a better ground accuracy and to employ the improved RF for 3-D shoreline extraction using 1-meter panchromatic stereo images in a Lake Erie coastal area. In this method, a 2D shoreline is extracted by manual digitising on one Ikonos image; then corresponding shoreline points on the other image of the stereo-pair are automatically extracted by image matching. The 3D shoreline is computed using photogrammetric triangulation. Chalabi et al. (2006) had used pixel-based segmentation on Ikonos image using DN threshold. The partition of the land and sea boundary was done using pseudo-colour which exhibits a strong contrast between land and water features.

Shoreline change is considered to be one of the most dynamic processes in coastal area. It has become important to map the shoreline change as an input data for coastal hazard assessment. There are many change detection techniques currently in use including visual interpretation, spectral-value-based technique (differencing, image regression, DN value analysis), multi-data composites, and change vector analysis. Visual interpretation of multi-temporal images for coastal monitoring was presented by Mazian et al. (1989) and Elkoushy and Tolba (2004). Bagli and Soille (2003) analysed DN value using slicing operation for change monitoring. In addition, Whithe and El Asmar (1999) introduced an algorithm function and DN analysis to deviate the water from the land. The DN value analysis has also been applied on Landsat images, e.g. by Frazier and Page (2000) and Marfai (2003). Fromard et al. (2004) identified coastal changes that took place over the last 50 years, and related them to natural processes of turnover and replenishment of mangrove forests. They used a combination of remote sensing techniques (aerial photographs and SPOT satellite images) and field surveys in the area of the Sinnamary Estuary, French Guiana. Mills et al. (2005) introduced the integration of the geomatics techniques to form accurate representations of the coastline. A highly accurate Digital Elevation Model (DEM), created using kinematics GPS, was used as control to orientate surfaces derived from the relative orientation stage of photogrammetry processing. Mostafa and Soussa (2006) have applied GIS and remote sensing technique to monitor the lake of Nasser including the shoreline dynamics. Three satellite Landsat images for Nasser Lake were available in a time series (1984, 1996, and 2001). Topography map of scale 1: 50.000, that is suitable to the resolution of Landsat images, was used for developing DEM. Chalabi et al. (2006) assessed multi-data sources for monitoring shoreline in Kuala Terengganu, Malaysia using Ikonos and aerial photographs. Results of time series data were combined to each other showing spatial change of shoreline. Marfai et al. (2007) illustrated the shoreline dynamics in a coastal area of Se marang - Indonesia using multisource spatial data. In spite of the technique and approach to shoreline monitoring and delineation, no single method has been implemented that is free from major disadvantages.

Therefore, shorelines of the same area may be extracted at different times using satellite data and represent changes that appeared in difference periods that are illustrated as differences among them. There are two possible interpretations of the shoreline differences. One is that the shoreline indeed changed in the real world. The other possibility is that the differences are introduced by shoreline mapping errors. The accuracy of the shoreline derived from 1 meter Ikonos imagery should be about 2m - 4m (Zhou and Li 2000; Li et al., 2001, Grodecki and Dial, 2003), considering the fact that the accuracy of 3D ground control points (GCPs) reaches 2m – 3 m, with GCPs and the accuracy of identifying and locating conjugate shoreline points is about 1.5 pixels (1m - 2m). An optimistic estimation of the shoreline accuracy derived from the 4-meter Ikonos images in this specific case is about 8.5m (Li et al., 2001).

In most of the aforementioned methods, the shoreline extraction using Ikonos orthoimagery is based on land cover classification to discriminate the pixels corresponding to water bodies from those corresponding to land. Following, the resulting thematic image is converted to vector coverage, usually

a polygon shapefile (ESRI, 2005) containing the polygons corresponding to each class. The shoreline is finally extracted from the polygon that corresponds to water by employing automatic or semi-automatic GIS procedures. Thus, the accuracy of the image orthorectification, as well as the accuracy of the image classification, is the most important factors affecting the accuracy of the extracted shoreline. The orthorectification accuracy was discussed above. Concerning classification accuracy, it depends on the spatial, spectral and radiometric resolution of the image, as well as on the classification method. Numerous studies have been carried out using satellite images to extract land cover types (Congalton, 1991; Ridd and Liu, 1998; Martin et al., 1988; Gong and Howarth, 1990; Chrysoulakis, 2003; Gallego, 2004). The majority of the past studies rely on remote sensing data to classify land cover types using either raw DN or calibrated radiance values. However, if very high spatial resolution data such as Ikonos images are used, the land cover classification of coastal areas may be problematic because of the heterogeneity and small spatial size of the surface materials, which leads to significant sub-pixel mixing (Foody, 2000; Kontoes et al., 2000). Therefore, the spatial context should be taken into account in image classification and object oriented algorithms should be used. Improvements in the accuracy of classification have been achieved using a variety of sophisticated approaches including the use of neural networks (Berberoglu et al., 2000), fuzzy logic (Bastin, 1997; Zang and Foody 1998;), texture analysis (Stuckens et al., 2000), machine learning (VLS, 2007) and incorporation of ancillary spatial data in the classification scheme (Harris and Ventura, 1995; Vogelmann et al., 1998, Stefanov et al., 2001).

Methodology

The Ikonos satellite provides global, accurate, high-resolution imagery for mapping, monitoring, and development. The panchromatic sensor with 82cm resolution and an 11.3km wide swath at nadir provides high resolution, intelligence-quality imagery. The multispectral sensor, simultaneously collecting blue, green, red, and near infrared bands with 3.28m resolution at nadir, provides natural-colour imagery for visual interpretation and colour-infrared imagery for remote sensing applications. Combining the multispectral imagery with the high resolution panchromatic results in   1-meter colour images (pan-sharpen product), which can be orthorectified afterwards. The orthorectification is needed to eliminate the geometric distortions, which will be explained below, so that image features have correct planimetric coordinates. Quantitative estimations such as shoreline detection are performed using orthorectified images.

Apart from the different techniques that can be applied for shoreline extraction and monitoring from high resolution satellite images, the processing chain consists of the following basic steps:

· acquisition of images and pre-processing;
· acquisition of the ground Control Points (GCPs) with image coordinates and map coordinates;
· computation of the unknown parameters of the mathematical functions used for the geometric correction model;
· image orthorectification using an appropriate DEM;
· automatic, semi-automatic or manual shoreline extraction from the orthorectified imagery;
· monitoring of shoreline changes by repeating the above steps at predefined time periods and comparing the relative positions of the extracted shorelines.

Thus, before the application of any algorithm for automatic extraction of shoreline from multispectral satellite images, these images should be othorectified to take into account the geometric distortions during image acquisition, as well as the effect of topography. Each image acquisition system produces unique geometric distortions in its raw images and consequently the geometry of these images does not correspond to the terrain or of course to a specific map projection. Obviously, the geometric distortions vary considerably with different factors such as the platform, the sensor and also the total field of view. However, as it has been described by Toutin (2004), it is possible to make general categorisations of these distortions. The sources of distortion can be grouped into two broad categories: the observer or the acquisition system (platform, imaging sensor and other measuring instruments, such as gyroscope, stellar sensors, etc.) and the observed (atmosphere and Earth). In addition to these distortions, the deformations related to the map projection have to be taken into account because

the terrain and most GIS end-user applications are generally represented and performed respectively in a topographic space and not in the geoid or a referenced ellipsoid. Most of these geometric distortions are predictable or systematic and generally well understood. Some of these distortions, especially those related to the instrumentation, are generally corrected at ground receiving stations or by image vendors. Others, for example those related to the atmosphere, are not taken into account and corrected because they are specific to each acquisition time and location and information on the atmosphere is rarely available. The remaining geometric distortions require models and mathematical functions to perform geometric corrections of imagery: either through 2D/3D empirical models (such as 2D/3D polynomial or 3D RF) or with rigorous 2D/3D physical and deterministic models. With 2D/3D physical models, which reflect the physical reality of the viewing geometry (platform, sensor, Earth and sometimes map projection), geometric correction can be performed step-by-step with a mathematical function for each distortion/deformation, or simultaneously with a combined mathematical function.

2D/3D physical functions used to perform the geometric correction differ, depending on the sensor, the platform and its image acquisition geometry (Toutin, 2004):

· instantaneous acquisition systems, such as photogrammetric cameras, Metric Camera or Large Format Camera;
· rotating or oscillating scanning mirrors, such as Landsat-MSS, TM and ETM+;
· push-broom scanners, such as SPOT-HRV, IRS-1C/D, Ikonos and Quickbird; and
· SAR sensors, such as JERS, ERS-1/2, RADARSAT-1/2 and Envisat.

Whatever the geometric model used, even with the RF some GCPs have to be acquired to compute/refine the parameters of the mathematical functions in order to obtain a cartographic standard accuracy. Generally, an iterative least-square adjustment process is applied when more GCPs than the minimum number required by the model (as a function of unknown parameters) are used. The number of GCPs is a function of different conditions: the method of collection, sensor type and resolution, image spacing, geometric model, study site, physical environment, GCP definition and accuracy and the final expected accuracy. The aerial triangulation method has been developed and applied with different optical and radar satellite data using 3D physical models (Toutin, 2003a, b), as well as with Ikonos data using 3D RF models (Fraser et al., 2002a, b). All model parameters of each image/strip are determined by a common least-squares adjustment so that the individual models are properly tied in and an entire block is optimally oriented in relation to the GCPs.

As it has been already motioned, shoreline extraction needs orthorectified images. To rectify the original image into a map image, there are two processing operations:

· a geometric operation to compute the cell coordinates in the original image for each map image cell, eliminating the geometric distortions as previously explained; and
· a radiometric operation to compute the intensity value or DN of the map image cell as a function of the intensity values of original image cells that surround the previously-computed position of the map image cell.

The geometric operation requires the observation equations of the geometric model with the previously computed unknowns, and sometimes elevation information. The 3D models take into account elevation distortion and DEMs is thus needed to create precise orthorectified images. DEMs impact on the orthorectification process, both in terms of elevation accuracy for the positioning accuracy and of grid spacing for the level of details. This last aspect is more important with high-resolution images because a poor grid spacing when compared to the image spacing could generate artefacts for linear features such as shorelines. For any map coordinates (x, y), with the z elevation extracted from a DEM when 3D models are used, the original image coordinates (column and line) are computed from the two resolved equations of the model. However, the computed image coordinates of the map image coordinates will not directly overlay in the original image; in other words, the column and line computed values will rarely, if ever, be integer values. Since the computed coordinate values in the original image are not integers, one must compute the DN to be assigned to the map image cell. In order to do this, the radiometric operation uses a resampling kernel applied to original image cells: either the DN

of the closest cell (called nearest neighbour resampling) or a specific interpolation or deconvolution algorithm using the DNs of surrounding cells (Toutin, 2004).

In order to accurately create or extract geographic information from raw Ikonos imagery, the Image Geometry Model (IGM) must accompany the imagery. The IGM consists of several metadata files which contain RPCs (rational polynomial coefficients). The RPCs are a series of coefficients that describe the relationship between the image as it existed when captured and the Earth's surface. Although they do not describe sensor parameters explicitly, RFs are simple to implement and perform transformations very rapidly. With the availability of RPCs, the Ikonos interior and exterior orientations are very accurate. Therefore Ikonos imagery can be orthorectified if the IGM, an accurate DEM and some GCPs are available by employing any photogrametric software such as Orthoengine (PCI, 2003) or Leica Photogrammetry Suite (Leica, 2005).

The next step for shoreline extraction is the water-land separation; therefore the orthorectified image should be classified or a polygon corresponding to water (or land) area should be extracted. Taking into account the aforementioned land cover mapping constraints for very high spatial resolution satellite data, a machine learning classifier approach seems the best solution for Ikonos multispectral image classification. This type of classifier uses an inductive learning algorithm to generate production rules from training data. As with a neural network, there are several advantages to using a machine-learning approach. Since ancillary data layers may be used to help improve discrimination between classes, fewer field samples are generally required for training. This machine learning model is non-parametric and does not require normally-distributed data or independence of attributes. It can also recognize nonlinear patterns in the input data that are too complex for conventional statistical analyses or too subtle to be noticed by an analyst. Feature Analyst software (VLS, 2007) was selected for shoreline extraction from Ikonos imagery, since it employs machine-learning techniques which have the potential to exploit both the spectral and spatial information of the image. It provides a paradigm shift to automated feature extraction since it: (a) utilises spectral, spatial, temporal, and ancillary information to model the feature extraction process, (b) provides the ability to remove clutter, (c) incorporates advanced machine learning techniques to provide unparalleled levels of accuracy, and (d) provides an exceedingly simple interface for feature extraction. It works by taking a small and simple set of training examples, learns from the examples, and classifies the remainder of the image. When classifying the contents of imagery, there are only a few attributes accessible to human interpreters. For any single set of imagery these are: Shape, Size, Colour, Texture, Pattern, Shadow, and Association. Traditional image processing techniques incorporate only colour (spectral signature) and perhaps texture or pattern into an involved expert workflow process. The shoreline extraction steps using Feature Analyst are shown in Figure 1.
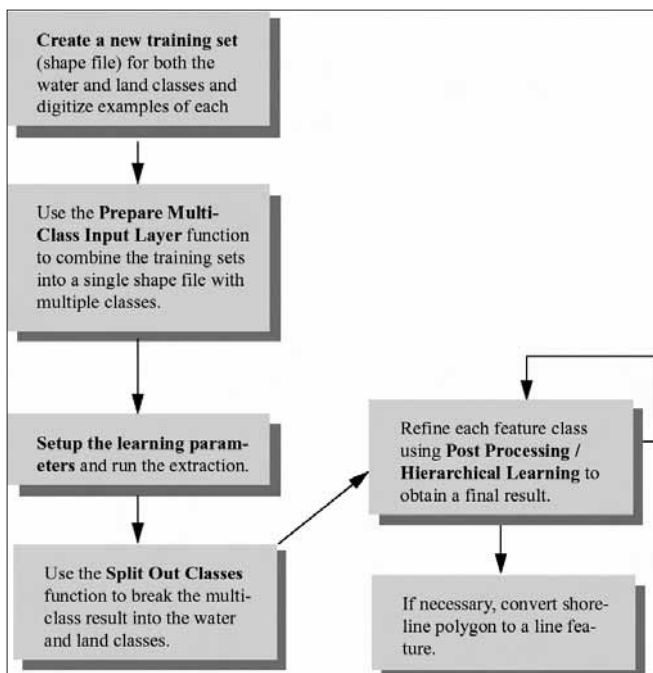
Figure 1 - Shoreline extraction work flow (adapted from VLS, 2007).

Case Study: Shoreline extraction in the area of Georgioupolis, Crete

The Shoreline extraction for the area of Georgioupolis was performed for the years 1998 and 2005 using aerial imagery and Ikonos data, respectively. The results validated with *in situ* measurements with Differential GPS (DGPS) provided by OANAK. The Hellenic Geodetic Reference System of 1987 (EGSA87) was used in all cases.

Shoreline extraction using an aerial image acquired in 1998

An orthorectified aerial image and a DEM of the broader area of Georgioupolis were available to OANAK as past project products. The aerial image has the spatial resolution of 1m, whereas its positional accuracy was better than 2 m (RMSExy < 2 m). It is shown in Figure 2, where the road network (produced by DGPS measurements) of the area has been superimposed (red lines). Feature Analyst was employed to classify the aerial orthoimage into 2 classes: land and water. The extraction of the shoreline was afterwards straightforward from the polygon corresponding to water class, using the ArcGIS software (ESRI, 2005). The latter will be also applied to Ikonos image, so it will be described in more detail below. The 1998 shoreline as extracted from the aerial image is also shown in Figure 2 (yellow line).

Figure 2 - Orthorectified aerial image acquired in 1998. The road network (red) and the extracted shoreline (yellow) have been superimposed.

Shoreline extraction using an Ikonos image acquired in 2005

The 2005 shoreline was extracted from an Ikonos multispectral image. ERDAS Imagine (Leica, 2005) was used to pre-process the image; LPS (Leica, 2005) was used to orthorectify the image; Feature Analyst (VLS, 2007) was used to extract the shoreline and ArcGIS (ESRI, 2005) was used to fine-tune the extracted shoreline. The processing chain included the following steps:

Step 1: Acquisition of images and pre-processing.

A panchromatic (PAN) and a four band (R, G, B, NIR) multispectral Ikonos image together with IGM and RPCs was provided by the image vendor as Raw Geo Product. The four channels are shown in Figure 3. ERDAS Imagine was used to merge the panchromatic and the multispectral images to provide a four-band pan-sharpen product with spatial resolution of 1m. The Wavelet Resolution Merge function (Leica, 2005) was used. The resulting pan-sharpen product is shown in Figure 4 as a pseudocolour composition RGB: 4-3-2.

Figure 3 - Ikonos spectral channels of the 2005 acquisition over the area of Georgioupolis: a) blue band; b) green band; c) red band; d) near infrared band. The strong absorption of water in the near infrared band is obvious in d), therefore this band is the most useful for the discrimination between land and water.

Step 2: Acquisition of GCPs.
A field campaign was organized by OANAK and 15 GCP's were selected using a differential GPS. The location of these points (circles) superimposed to the road network of the study area is shown in Figure 5. Their positional accuracy was better than 1m (RMSExy < 1m). Several other GCPs were randomly selected to be used for validation of the orthorectification procedure.
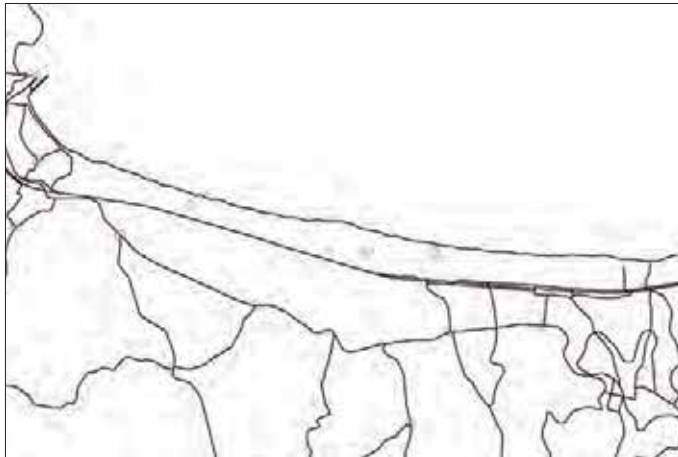
Figure 5 - Location of the measured GCPs superimposed to the road network of the study area.

Step 3: Computation of the unknown parameters of the mathematical functions used for the geometric correction model.
The interior and exterior orientations were automatically computed using LPS since the IGM and the GCP's were available. The aerial triangulation procedure (Leica, 2005) was followed. This procedure eliminated the geometric errors which have been previously discussed, except for the effect of topography. This effect was taken into account by using a DEM of the study area available at OANAK's. This DEM had been produced photogrammetrically using a stereo-pair of aerial images from the 1998 campaign. The vertical accuracy of the DEM was better than 1m (RMSEz < 1m). The DEM with the road network of the area superimposed is shown in Figure 6.
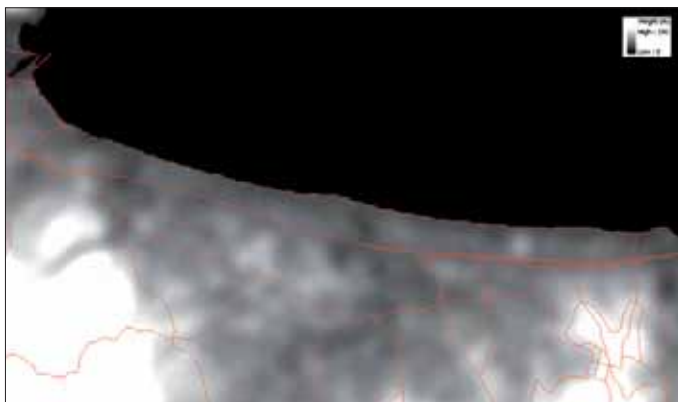
Figure 6 - The photogrammetrically derived DEM with the road network and the shoreline extracted from the aerial image superimposed.

Step 4: Orthorectification of images.
Since an accurate DEM was available and the aerial triangulation parameters were computed by LPS, the orthorectification procedure was also straightforward as a geometric and a radiometric operation,

as it has been already described. The orthorectification result is shown in Figure 7 as a pseudocolour composition RGB: 3-2-1, with the road network of the area (red lines) and the shoreline extracted from the aerial image (yellow line) superimposed. The spatial resolution of the othorectified image is 1m, whereas its positional accuracy is better than 2m (RMSExy < 2m), therefore, as it has been explained, the expected accuracy of the shoreline to be extracted is around 4m.

Figure 7 - Pseudocolour composition RGB: 3-2-1 of the orthorectified Ikonos pan-sharpened image with the road network (red lines) and the shoreline extracted from the aerial image (yellow line) superimposed. Differences in shoreline between 1998 and 2005 are obvious.

Step 5: Semi-automatic shoreline extraction using Feature Analyst.
The extraction of the shoreline using Feature Analyst is a semi-automatic procedure, as shown in Figure 1, involving:
·   the creation of a new set containing two training classes;
·   the preparation of a multi-class input layer;
·   the setup of the learning parameters and the execution of the algorithm;
·   the splitting of the two classes into a final polygon;
·   the post processing, for smoothing of the result polygon;
·   the conversion of the polygon into a line.
The first action is to create the training set of polygons. This is the most important action, because the quality of the results is dependant on the quality of the training sets. The training set will consist of two classes, one that corresponds to water elements and another one that corresponds to land elements. At this point, these two classes are indicated as two separate sets of polygons and then combined into a multi-class input layer. Creating the water set of polygons, includes a number of trials, to finally deicide and conclude to the most representative set. The result of these trials is a set of four polygons,

three of which are located at the edge of the water mass, extending through the inshore, as shown in Figure 8 (purple). The same procedure is followed to decide about the land set. The result is a corresponding set of six polygons (blue).

Figure 8 - Pseudocolour composition RGB: 3-2-1 of the orthorectified Ikonos pan-sharpened image with the water (purple) and land (blue) training polygons superimposed.

In order to run a multi-class extraction, the two different classes of water and land have to be combined into a single, multi-class layer. There is a built-in function of Feature Analyst for this. The produced two-class layer is the input of the algorithm.

Having the input, the next action is to set the algorithm's parameters (VLS, 2007). All four image bands are about to be included and the image resolution is set to 1m. The spectral information is derived from this multispectral image, whereas the spatial context for each pixel is taken into account by adjusting the input representation of the classification algorithm. The input representation, that determines how each pixel is looked at in relation to its neighbours, is set to "Manhattan" representation (VLS, 2007). Manhattan is a pre-defined input pattern, used mainly for water mass and land cover features, like oceans, lakes, floods, wetland, impermeable surfaces, etc. The pattern width is set to 5. This means that considering that the "decision pixel" (red in Figure 9) is in the centre of a 5×5 grid, according to the Manhattan input representation, the algorithm will take into account 13 pixels (blue in Figure 9), located as shown in Figure 9. Computing 13 pixels of each band, there is a total of 52 pixels that will be computed to make a decision for a single pixel. The minimum aggregate area is set to 500 pixels. That is to maintain relative feature characteristics, while trying to find a large area.
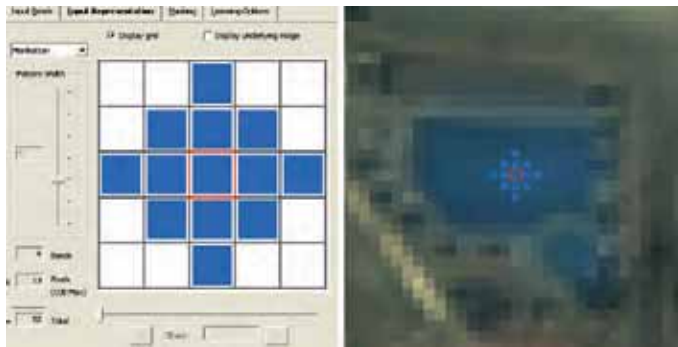
Figure 9 - The 'Manhattan' input representation that is used, with pattern width set to 5.

The classification result is shown in Figure 10. It is again a multi-class layer, which needs to be split. Although the border of both result classes is the same line (the shoreline), the water class is chosen for the extraction. The built-in function in Feature Analyst that splits out classes was used to split the classes and keep only the water class as a separate set. Since only one polygon has been left its border was smoothed in order to extract the shoreline. The "Bezier Smooth Algorithm" (VLS, 2007) was used, with the following parameters: the number of vertices to each side set to 2 and the maximum distance each vertex is allowed to move set to 3m. The result of the smoothed polygon is shown in Figure 11.
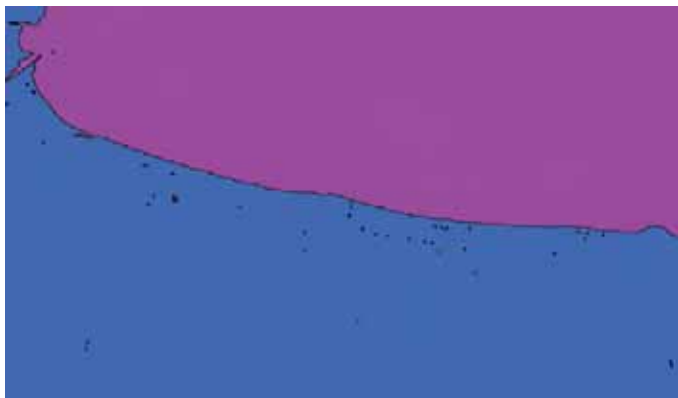
Figure 10 - The land – water classification result: a two class result corresponding to the two-class input. Both spectral and spatial information have been taken into account.

Figure 11 - The extracted – smoothed polygon corresponding to water.

Finally, the border of the water polygon was automatically extracted and converted to a line shapefile following a standard GIS procedure (VLS, 2007; ESRI, 2005). This line shapefile is the final result of the shoreline extraction procedure as it is shown in Figure 12, where the extracted shoreline has been superimposed on the orthorectified Ikonos image.

Figure 12 - Pseudocoloured composition RGB: 3-2-1 of the orthorectified Ikonos image with the extracted shoreline (yellow line) superimposed.

Step 6: Comparisons - Validation.
The produced shorelines (1998 Shoreline, and 2005 Shoreline) were compared and a Root Mean Square Error (RMSE) was computed to reflect the shoreline change during this 7 years period. RMSE is a global measure, thus the maximum change was highlighted and it is presented below. The RMSE was used as a quantitative evaluation of the extracted shorelines accuracy. RMSE encompasses both systematic and random errors and is defined as [1]:

$$\text{RMSE} = \sqrt{\frac{1}{n} \sum_{i=1}^{n} \delta s_i^2} \qquad [1]$$

Where:
δs_i = minimum distance of the two lines at a pre-defined location i (x, y),
n = number of measuring locations in this study.

Finally, both the image-derived shorelines were compared with an *in situ* derived shoreline which was produced by OANAK with the use of differential GPS. The three lines are shown in Figure 13, where a part of the study area has been extracted (scale 1: 2.000): The *in situ* derived shoreline is presented in red, the 1998 Shoreline is presented in green and the 2005 Shoreline is presented in yellow. The RMSE calculated using the *in situ* line as baseline, as well as the RMSE between the extracted shorelines for 1998 and 2005, are shown in Table 1.

Figure 13 - Part of the study area as a pseudocolour composition RGB: 3-2-1 of the orthorectified Ikonos image (scale 1:2000). The in situ derived shoreline is shown in red, the 1998 Shoreline is shown in green, whereas the 2005 Shoreline is shown in yellow.

The analysis showed that there were not severe changes in shoreline between 1998 and 2005, except in some locations where the change was substantial. The most important change is shown in Figure 14, where a part of the study area around the river which is close to the town of Georgioupolis has been extracted (scale 1: 2.000): both lines have been superimposed on the Ikonos orthorectified image. The 1998 Shoreline is presented in green and the 2005 Shoreline is presented in yellow, as before. It is obvious from Figure 14 that the outfall of the river has been modified during this 7 year period. A shift of about 50m to the ESE direction can be observed in Figure 14.

Table 1 - RMSE between a) in situ and aerial image derived shoreline (1998); b) in situ and Ikonos derived shoreline (2005); c) aerial image and Ikonos derived shoreline.

Pair of Lines	RMSE (m)
In situ – 1998 Shoreline	3.01
In situ – 2005 Shoreline	5.65
1998 Shoreline– 2005 Shoreline	6.46

Figure 14 - Part of the study area as a pseudocolour composition RGB: 3-2-1 of the orthorectified Ikonos image (scale 1:2000). The 1998 Shoreline is shown in green and the 2005 Shoreline is shown in yellow. A shift of about 50m to the ESE direction of the river outflow is observed.

References

Bagli S. and Soille P. (2003) - *Morhological automatic extraction of Pan-European coastline from Landsat ETM+ images*. International Symposium on GIS and Computer Cartography for Coastal Zone Management. Genova, Italy.

Bastin L. (1997) *Comparison of fuzzy c-means classification, linear mixture modeling and MLC probabilities as tools for unmixing coarse pixels*. International Journal of Remote Sensing, 18: 3629 – 3648.

Berberoglu S., Lloyd C.D., Atkinson P.M. and Curran P.J. (2000) - *The integration of spectral and textural information using neural networks for land cover mapping in the Mediterranean*. Computers & Geosciences, 26: 385 – 396.

Braud D.H. and Feng W. (1998) - *Semi-automated construction of the Louisiana coastline digital land/water boundary using Landsat Thematic Mapper satellite imagery*. Department of Geography & Anthropology, Louisiana State University. Louisiana Applied Oil Spill Research and Development Program, OSRAPD Technical Report Series 97-002.

Chalabi A., Mohd-Lokman H., Mohd-Suffian I., Karamali K., Karthigeyan V. and Masita M (2006) - *Monitoring shoreline change using Ikonos image and aerial photographs: a case study of Kuala Terengganu area, Malaysia*. In: Proceedings of the ISPRS Mid-term Symposium Proceeding. Enschede, The Netherlands.

Chen L.C. and Shyu C.C. (1998) - *Automated Extraction of Shorelines from Optical and SAR Image*. In: Proceeding of Asian Conference on Remote Sensing (http://www.gisdevelopment. net/ aars/acrs/1998/ ps3/ps3013a.asp).

Chrysoulakis N. (2003) - *Estimation of the all-wave urban surface radiation balance by use of ASTER multispectral imagery and in situ spatial data*. Journal of Geophysical Research, 108: 4582 (DOI:10.1029/ 2003JD003396).

Congalton R.G. (1991) - *A Review of Assessing the Accuracy of Classifications of Remotely Sensed Data*. Remote Sensing of Environment, 37: 35-46.

Di K., Wang J., Ma R. and Li R. (2003) - *Automatic shoreline extraction from high-resolution Ikonos satellite imagery*. In proceeding of the Annual ASPRS Conference. Anchorage, Alaska.

Elkoushy A.A. and Tolba R.A. (2004) - *Prediction of shoreline change by using satellite aerial imagery*. In: Proceeding of the XX ISPRS Congress. Istanbul, Turkey.

Erteza I.A. (1998) - *An automatic coastline detector for use with SAR images*. SANDIA Report SAND98-2102. Sandia National Laboratories, California.

ESRI (2005) - *ArcGIS 9. What is ArcGIS 9.1?* Environmental Systems Research Institute, California.

Foody G.M. (2000) - *Estimation of sub-pixel land cover composition in the presence of untrained classes*. Computers & Geosciences, 26: 469 – 478.

Fraser C.S., Hanley H.B. and Yamakawa T. (2002a) - *Three-dimensional geopositioning accuracy of Ikonos imagery*. Photogrammetric Record, 17: 465–479.

Fraser C.S., Baltsavias E. and Gruen A. (2002b) - *Processing of Ikonos imagery for sub-metre 3D positioning and building extraction*. ISPRS Journal of Photogrammetry and Remote Sensing, 56, 177–194.

Frazier P.S. and Page K.J. (2000) - *Water body detection and delineation with Landsat TM data*. Photogrammetric Engineering and Remote Sensing, 66: 147–167.

Fromard F., Vegaa C. and Proisy C. (2004) - *Half a century of dynamic coastal change affecting mangrove shorelines of French Guiana. A case study based on remote sensing data analyses and field surveys*. Marine Geology, 208: 265–280.

Gallego F.J. (2004) - *Remote sensing and land cover area estimation*. International Journal of Remote Sensing, 25: 3019-3047.

Gong P. and Howarth P.J. (1990) - *The use of structural information for improving land-cover classification accuracies at the rural – urban fringe*. Photogrammetric Engineering and Remote Sensing, 56: 67-73.

Grodecki J. and Dial G. (2003) - *Block adjustment of highresolution satellite images described by rational polynomials*. Photogrammetric Engineering and Remote Sensing, 69: 59-68.

Harris P.M. and Ventura S.J. (1995) - *The integration of geographic data with remotely sensed imagery to improve classification in an urban area*. Photogrammetric Engineering and Remote Sensing, 61: 993 – 998.

Huang C., Wylie B., Homer C., Yang L. and Zylstra G. (2002) - *Derivation of a tasseled cap transformation based on Landsat 7 ETM at-satellite reflectance*. International Journal of Remote Sensing, 23: 1741-1748.

Karantzalos K. and Argialas D. (2007) - *Automatic shoreline mapping from panchromatic satellite images*. In: Proceedings of 8th Pan-Hellenic Geographic Conference. Greek Geographical Society (in Greek).

Kontoes C.C., Raptis V., Lautner M. and Oberstadler R. (2000) - *The potential of kernel classification techniques for land use mapping in urban areas using 5 m-spatial resolution IRS-1C imagery*. International Journal of Remote Sensing, 21: 3145–3151.

Leica (2005) - *ERDAS Field Guide*. Leica Geosystems. Atlanta, Georgia, USA.

Li R., Di K. and Ma R. (2001) - *A Comparative Study of Shoreline Mapping Techniques*. In: Proceeding of the 4th International Symposium on Computer Mapping and GIS for Coastal Zone Management. Halifax, Nova Scotia, Canada.

Li R., Di K. and Ma R. (2003) - *3-D Shoreline Extraction from Ikonos Satellite Imagery*. Marine Geodesy, 26:107–115.

Li R. (1997) - *Mobile mapping: An emerging technology for spatial data acquisition*. Photogrammetric Engineering and Remote Sensing, 63: 1165-1169.

Liu H. and Jezek K.C. (2004) - *Automated extraction of coastline from satellite imagery by integrating canny edge detection and locally adaptive thresholding methods*. International Journal of Remote Sensing, 25: 937–958.

Marfai M.A., Almohammad H., Dey S., Susanto B. and King L. (2007) - *Coastal dynamic and shoreline mapping: multi-sourcesspatial data analysis in Semarang Indonesia*. Environ Monitoring and Assessment, DOI 10.1007/s10661-007-9929-2.

Marfai M.A. (2003) - *Monitoring of the coastal zone dynamics by means of multi-temporal Landsat TM*. In: Proceedings of the annual scientific meeting XII, Indonesian remote sensing society. Bandung.

Martin L.R.G., Howarth P.J. and Holder G. (1988) - *Multispectral classification of land use at the rural-urban fringe using SPOT data*. Canadian Journal of Remote Sensing, 14: 72 – 79.

Mazian H.I., Aziz I. and Abdullah A. (1989) - *Preliminary evaluation of photogrammetric-remote sensing approach in monitoring shoreline erosion*. In: Proccedings of the 10th Asian Conference on Remote Sensing Proceeding. Kuala Lumpur.

Mills J.P., Buckley S.J., Mitchell H.L., Clarke P.J. and Edwards S.J. (2005) - *A geomatics data integration technique for coastal change monitoring*. Earth Surface Processes and Landforms, 30: 651–664.

Mostafa M.M. and Soussa H.K. (2006) - *Monitoring of Lake Nasser using remote sensing and GIS techniques*. In: Proceedings of the ISPRS Mid-term Symposium. Enschede, The Netherlands.

PCI (2003) - *OrthoEngine User Guide*. PCI Geomatics. Ontario, Canada.

Ridd M.K. and Liu J. (1998) - *A comparison of four algorithms for change detection in an urban environment*. Remote Sensing of Environment, 63: 95 – 100.

Ryan T.W., Sementilli P.J., Yuen P. and Hunt B.R. (1991) - *Extraction of shoreline features by neural nets and image processing*. Photogrammetric Engineering and Remote Sensing, 57: 947-955.

Scott J.W., Moore L.R., Harris W.M. and Reed M.D. (2003) - *Using the Landsat 7 Enhanced Thematic Mapper Tasseled Cap Transformation to Extract Shoreline*. Open-File Report OF 03-272 U.S. Geological Survey.

Shaw B. and Allen J.R. (1995) - *Analysis of a dynamic shoreline at Sandy Hook, New Jersey, using a geographic information system*. In: Proceedings of ASPRS/ACSM. pp. 382-391.

Stefanov W.L., Ramseyc M.S. and Christensen P.R. (2001) - *Monitoring urban land cover change: An expert system approach to land cover classification of semiarid to arid urban centers*. Remote Sensing of Environment, 77: 173 – 185.

Stuckens J., Coppin P.R. and Bauer M.E. (2000) - *Integrating contextual information with per-pixel classification for improved land cover classification*. Remote Sensing of Environment, 71: 282 – 296.

Toutin Th. (2004) - *Review article: Geometric processing of remote sensing images: models, algorithms and methods*. International Journal of Remote Sensing, 25,1893–1924

Toutin Th. (2003a) - *Block bundle adjustment of Ikonos in-track images*. International Journal of Remote Sensing, 24: 851–857.

Toutin Th. (2003b) - *Error tracking in Ikonos geometric processing using a 3D parametric modelling*. Photogrammetric Engineering and Remote Sensing, 69: 43–51.

Trebossen H., Deffontaines B., Classeau N., Kouame J. and Rudant J.-P. (2005) - *Monitoring coastal evolution and associated littoral hazards of French Guiana shoreline with radar images*. Comptes Rendus Geosciences, 337: 1140-1153.

Vogelmann J.E., Sohl T. and Howard S.M. (1998) - *Regional characterization of land cover using multiple sources of data*. Photogrammetric Engineering and Remote Sensing, 64: 45 – 57.

VLS (2007) - *Feature Analyst Version 4.1 for Imagine*. Reference Manual. Visual Learning Systems Inc. Missoula, USA.

Wang K.D.J., Ma R. and Li R. (2003) - *Automatic shoreline extraction from high resolution Ikonos satellite imagery*. In: Proceedings of the ASPRS Annual Conference. Anchorage, Alaska.

Whithe K. and El Asmar H.M. (1999) - *Monitoring changing position of coastline using thematic mapper imagery, an example from the Nile Delta*. Geomorphology, 29: 93–105.

Wu T.D. and Lee M.T. (2007) - *Geological Lineament and Shoreline Detection in SAR Images*. Proceedings of IEEE Geosciences and Remote Sensing Symposium (IGARSS 2007). Barcelona, Spain.

Zakariya R., Rosnan Y., Saidin S.A., Yahaya M.H., Kasawani I. and Lokman H. (2006) - *Shoreline detection and changes for Terengganu river mouth from satellite imagery (Landsat 5 and Landsat 7)*. Journal of Sustainability Science and Management, 1: 47-57.

Zang J. and Foody G.M. (1998) - *A fuzzy classification of sub-urban land cover from remotely sensed imagery*. International Journal of Remote Sensing, 19: 2721 - 2738.

Zhou G. and Li R. (2000) - *Accuracy Evaluation of Ground Points from IKONOS High-Resolution Satellite Imagery*. Photogrammetric Engineering and Remote Sensing, 66: 1103-1112.

Applications of remote sensing video systems for coastal erosion monitoring: the experience during OpTIMAL Project

Renata Archetti

Monitoring of nearshore systems for both coastal zone management and scientific purposes has traditionally relied on *in situ* measuraments of waves, currents, sediment transport and morphological changes. These traditional technologies provide data of high quality, but have limited resolution in time and space, and can be restricted due to the high costs involved. Remote sensing from satellite and aircraft has improved the spatial coverage of measurements, but can also be extremely expensive. Remote sensing systems based on the use of video cameras offer on the other hand a good opportunity to monitor the coastal environment at relatively low costs.

The use of video for coastal monitoring has been introduced by the Coastal imaging Lab from the Oregon University at the beginning of the 90s. They have developed a complete system, with hardware and a sophisticated software well known as Argus, which now compose a widely used technology all over the world for research and management of the coastal zone.

With the increasing offer of video cameras and video technologies several systems have been developed in the past years for coastal monitoring purposes.

Sophisticated, operational methods of video analysis now enable the quantification of:

- Shoreline evolution and beach width, to evaluate the potential for recreation or to assess the morphological impact of a storm event.
- Erosional and accretional sediment volumes at the intertidal beach, to evaluate the morphological impact of coastal structures, and investigate seasonal fluctuations in beach dynamics and beach nourishments, for instance.
- Wave run-up, to evaluate the stability of coastal structures such as seawalls, harbour moles and revetments.

OpTIMAL activities are inserted in this context, with the work of four partners who develop and test techniques for setting up video systems and for processing video images for the purpose of monitoring coastal erosion. Results obtained by the Universities of Bologna (Emilia Romagna) and Genova (Liguria) are presented in this book. OANAK (Crete) developed a low-cost effective system which is operative since March 2008 whose validation has not yet been completed. The University of Florence, after using a video system to study an artificially drained beach at Alassio, monitored a beach nourishment at Marina di Carrara; both studies have already been published (Bowman and Pranzini, 2007; Ferri et al., 2008). Moreover, during BEACHMED-e, the Conseil Général de l'Hérault (France) has planned to install a new video system on Valras Plage, and Regione Lazio has planned to install two video monitoring stations in the south of the region (Fondi and Terracina).

DISTART (Università di Bologna) managed two video systems. The first is an Argus video station, located at Lido di Dante (Ravenna, Italy) and which was already available at the beginning of the project. A second video station was installed in the framework of OpTIMAL project in Igea Marina (Rimini, Italy) in October 2006. Both beaches that are monitored by Università di Bologna are protected by a system of structures: parallel low-crested structures and boundary groins. In the study

case of Lido di Dante, from where a 4 years dataset is available, a medium-term shoreline trend is described by Archetti and Lamberti (2006) and Archetti et al. (in press). At Igea Marina the analysis of video data during an 18 month period has allowed the dynamics of the beach and its relation-ship with the forcing mechanisms of waves (and tides) to be investigated (Archetti et al., 2008). A software for video analysis aimed at coastal studies, called Beachkeeper, was developed by Dip. Te.Ris. (Università di Genova) and applied to the images taken by a webcam installed in Levanto (La Spezia), where a pocket gravel beach is observed and studied with the use of image analysis.

The first paper, "Video systems for coastal monitoring", gives a reference to video technology and aims at a brief description of the different systems used during the project, offering a comparative analysis among them. In particular, Argus, SVM-EVS and Beachkeeper video systems are briefly pre-sented and their installation characteristics are described. The following papers describe the scien-tific results from each study site.

References

Archetti R. and Lamberti A. (2006) - *Studio della evoluzione di una spiaggia protetta da opere a cresta bassa mediante videomonitoraggio*. Proc. XXX IDRA2006 vol. 1. pp. 99.

Archetti R., Torricelli E. and Lamberti A. (in press). *Study of the evolution of a beach protected by low crested structures using video monitoring*. Journal of Coastal Research.

Archetti R., Torricelli E., Erdman R. and Lamberti A. (2008) - *First application of a new imaging system for the coastal monitoring*. Proc. of Coastal Structures 07. In press.

Bowman D., Ferri S. e Pranzini E. (2007) – *Efficacy of beach dewatering - Alassio*, *Italy*. Coastal Enginee-ring, 54: 791-800.

Ferri S., Pelliccia F., Pranzini E., Rizzo M.G. and Vitale G. (2008) - *Prima risposta della spiaggia di Marina di Carrara ad un ripascimento artificiale non protetto*. Studi costieri, 15 (in press).

Video systems for coastal monitoring

**Renata Archetti, Chiara F. Schiaffino, Marco Ferrari,
Massimo Brignone, Didier Rihouey**

The use of video cameras for coastal management is now a valuable system for the control of morphodynamics and hydrodynamics in the coastal environment, and also for the control of ship traffic, tourist flow, etc. The aim of this paper is to present the video systems developed for the videomonitoring of the coastal zone in Europe, and applied during the BEACHMED-e project. Videosystems are briefly presented and their installation characteristics are described.

Introduction

Remote monitoring of coastal conditions in locations of high public usage is a fast growing application of information technology. Video camera systems provide a potentially rich source of information on the state of the coastal zone.

Following the wide diffusion of video cameras, also at good prices, the use of video cameras and of video images analysis for environmental control has increased in the past years. The use of video for coastal monitoring was introduced by Rob Holman in the early 90s, and now is a widely used technology all over the world for research and management of the coastal zone (Lippmann and Holman, 1990). The aim of this paper is twofold: to present the video monitoring technologies used during BEACHMED-e and to present a comparison analysis among the different video systems.

The video monitoring stations often consist of a few digital cameras oriented obliquely along the coast. The field of view can cover up to 180°, corresponding to a long stretch of coast from 3 km to 6 km, depending on the camera height and on the focal length of the lens. The video cameras are connected to a local computer housed near the station, which is responsible for managing image acquisition and to perform preliminary analysis, connecting through a phone line to a second server located in the laboratories for analysis.

The snapshots are taken several times during daylight hours by the cameras and the system is programmed to process different types of images. Images are acquired from video-cameras with varying dimensions, depending on the type of the camera, at intervals of one hour.

The hardware is programmed to extract different types of images consisting of traditional frames (snapshot) images and statistics of the snapshots: the time-exposure (or timex) images are the primary and most popular product of the Argus protocol, which is now a consolidated protocol for image acquisition and analysis. Each image represents the mathematical time-mean of all frames collected at 1 Hz or 2 Hz over a 10-minute period of sampling (Figure 1). Non-moving objects onshore are rendered as they appear in a snapshot. However, moving features such as waves are averaged out and only their mean brightness returns. The principle feature of time-exposure images is the delineation of areas of preferred wave breaking in the surf zone as white bands. Timex can also be created by taking long exposure snapshots (this second methodology has been developed by the EVS-SVM system and is presented later). Following a similar approach, the variance is an image where the mathematical time-variance of all frames collected in 10 minutes can be estimated (Figure 2). On a

variance image, static pixels are black and moving pixels are bright. The mean of the timex is the day-timex. Another type of image that can be collected is the timestack, the timeseries of pixel intensities located on defined arrays (Figure 3). Not all systems collect daytimex, variances and timestacks. Images are then sent to an archive. Standard post-processing of images regards merging and rectification. Planview images allow detecting features of the coastal environment that are of interest (such as shoreline and bar positions) in a real coordinate system. Besides time-averaged video data, data sampling schemes can be designed to collect time series of pixel intensities, typically at 2 Hz, with which wave and flow characteristics can be investigated (Chickadel et al., 2003; Archetti and Lamberti, 2007). This image is called timestack, and is collected by Argus, EVS-SVM and KOSTA systems.

Figure 1 - Example of timex image.   Figure 2 - Example of variance image.
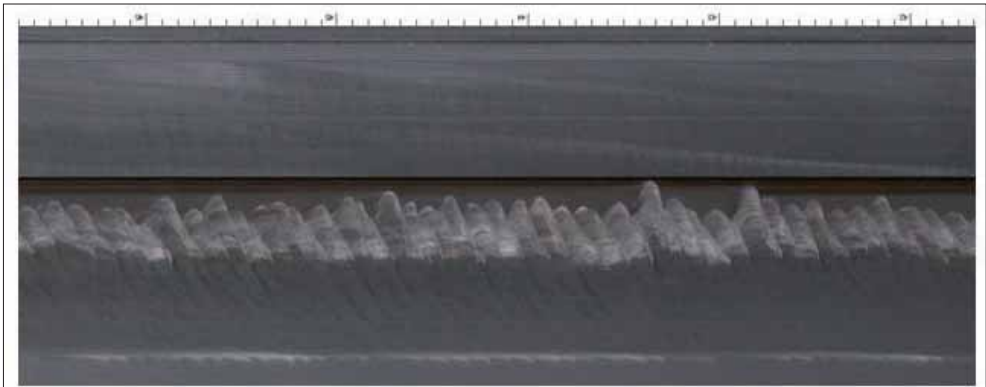
Figure 3 - Example of timestack image – time is on the x axis and space is on the y axis.

The Argus Video system

The Argus video system is the first video system developed for coastal research and monitoring and now its basic image analysis is considered a standard for the more recent video systems. Several references are available about the description of Argus system and its applications. The system has now reached the third generation, which is well described in Holman and Stanley (2007) where a review of previous technologies and applications is also provided. A short review and application of Argus is also available on the wikipedia website (http://www.encora.eu/coastalwiki/Argus_video_monitoring_system). The international Argus network involves collaborators who have deployed cameras in a wide range of radically different environments world-wide, including the east and west coasts of mainland America, Hawaii, Australia, New Zealand, UK, the Netherlands and Spain.

The first and only Argus video station in Italy has been installed in Lido di Dante (Ravenna) in 2003. The system is provided with an image analysis software running in Matlab environment called ARE2007. Argus Toolbox comprises: *DBOrganizer,* which allows organising database entries; *GeomTool*, which allows solving geometries to orthorectify images; *Argus Merg Tool*, which allows merging images (pan and plan); *IBMapper,* which allows the automatic detection of shorelines on the video image; and *PIX Tool*, which controls the acquisition of timestacks.

Typical applications are the quantification of storm-driven shoreline changes, impact of beach nourishment, long-term shoreline changes and bar migrations (Armaroli et al., 2007). On timex images it is easy to identify the position of the shoreline and of the bars - the detection tool *IBMapper* is based on the principle of clustering of pixels belonging to the different areas (wet/dry, breaking/not breaking). Examples are available in Kroon et al. (2007), Aarninkhof et al. (2003), Turner and Anderson (2007).

More recent applications regard the quantification of wave run-up, evaluation of the stability of coastal structures such as seawalls, harbour moles and revetments or the flooding risk of a beach, and the measure of wave direction, wave period and longshore currents (Chickadel et al., 2003; Archetti and Lamberti, 2007).

The Lido di Dante Argus Video Station

Lido di Dante is a small tourist area in the Emilia Romagna region on the Adriatic Sea, located 7 km South of Ravenna. The Lido di Dante beach has a combination of a protected and an unprotected beach - the Northern part of the study area is protected by three groins and a parallel semi-submerged barrier, while the Southern part is not protected. The system of groins and barriers forms two cells. Therefore, the site is of particular interest since it gives the opportunity to simultaneous study the dynamics of a protected and an unprotected beach from the same point of observation.

The video monitoring station installed in 2003 in Lido di Dante is a 3rd generation Argus station (Holman and Stanley, 2007) and consists of a system of four digital video cameras placed on a wooden tower of 18 m of height. Pixel resolution of the images is 1024 x 768.

Images taken by the four cameras are not simultaneous: the first camera (C1 directed to the South) takes pictures during the first ten minutes of every daytime hour, C2 during minutes from 10 to 20 and so on (Figure 4). The final 20 minutes are used several times to collect timestacks, high frequency time series of pixel intensities located in an appropriate position of the image (Holman et al., 1993).

All images are merged and ortorectified. Images are made available on line at the site http://argus-data.wldelft.nl/index.html.

Figure 4 - Lido di Dante Argus station - images taken by camera 1, camera 2, camera 3 and camera 4.

The analysis carried out in Lido di Dante regards the quantification of storm-driven shoreline changes of the beach protected by structures, the long term evolution (Archetti and Lamberti, 2007), bar migration (Armaroli et al., 2007) and the longshore currents induced by waves breaking over the parallel structures (Archetti and Lamberti, 2007).

The EVS Video system

The EVS system is a high resolution digital camera system used to take, archive, and upload pictures onto the Internet. Designed for construction and environmental monitoring and documentation, the system has a number of features and characteristics such as: photo-quality images, automatic creation of time lapse movies, extensive image archiving, weather station support, easy installation. The system is controlled by an embedded Pentium computer running on Windows. The control software has been designed over eight years to be very flexible and easy to program for handling both the Webcam and image archiving needs you may have.

The Video Monitoring Station Software VM95 is at the heart of video monitoring stations. The software offers many sophisticated operations that are not available in other software packages.

VM95 allows unattended image acquisition, labelling, archiving, and optionally uploading to the Internet at programmable intervals. Available features include exposure time, image quality/dimension, daily on/off times, graphic overlays, and many more. Setting up the software to capture images, graph weather data, and make slideshows to upload to the Internet is done by setting up scenes. Up to 80 different scenes may be programmed. All scenes have a daily hour on/off and sample interval.

A difference from the Argus system is that the EVS-SVM software (VM95) can control high resolution digital still cameras from Olympus and Canon (in addition to video). These cameras provide very high quality images, and a technique has been developed using neutral density filters to take long exposures during daylight, sufficient to generate averaged images. Variance images and time stack plots are not possible though. The same high resolution camera can be used to take 'tourist' or promotional shots and upload those images to other websites, serving a completely different sector.

In addition, the EVS system also allows adding a pan/tilt to the system, and offers Sony video cameras with up to 35x zoom. Using the built-in video server in the EVS system, it is possible to pan/tilt and zoom the camera remotely over the Internet through either a web interface (activex) or through a custom application that runs on Windows. Also through the web interface, it is possible to snap high resolution digital still shots and display them in a matter of seconds.

Details on the EVS SVM video system are available at the website: http://www.svm.it/.

Igea Marina EVS Video Station

The video station has been installed on the roof of a building in the front of the beach. The station is composed by two video systems. The first video system consists of a high resolution Super HAD CCD 1/2" video camera with 3.6 mm -18 mm zoom, looking to the North (Figure 5). The second video system, looking towards the South, is composed of two 8 Megapixel digital still cameras Olympus SP500UZ (maximum resolution 2816 X 2112) mounted in a single housing. One of the digital cameras is set to take snapshot pictures at daylight and long time exposures during the night, while the other, covered by a suitable filter, is set to collect long time-exposures (15 s) during the day.

The camera control software allows a remote operator to schedule image collection of specified types of images at different desired intervals. Thus, for example, with the video camera we can plan to collect, on an hourly basis, a continuous stream of video images that are then averaged together to form a single averaged image (the timex image). With the digital camera, timex images will be obtained by averaging many of the 15 second (exposure time) images, covering 600 seconds. The associated PC-based controller performs camera control and image collection, creates the time-averaged images (thereby sharply reducing data transmission overhead) and transmits the results to the remote data collection centre.

Images are made available on the web site: http://videomonitoring.eu.org/igea.

Two SVM-EVS video stations configured with Olympus cameras have been installed in Terracina and Fondi by Regione Lazio.

Figure 5 - The EVS SVM Video system. The left-hand side is a videocamera and the right-hand side is a still camera.

The Beachkeeper video system

Beachkeeper video system is a software for the management and elaboration of images acquired by a webcam. The peculiarity of this software is its applicability to all acquisition features independently of its scope. In this context studies have highlighted its applicability to webcams installed for tourist purposes, with limited functions.

The image elaboration system of Beachkeeper has been developed at Genoa University in cooperation between Dip.Te.Ris. (Dipartimento per lo studio del Territorio e delle sue Risorse) and Di.Ma. (Dipartimento di Matematica), which delivered the Matlab® 2006b support. It has been applied for coastal morphology evolution analysis.

Beachkeeper allows, through some basic features, georeferencing and rectifying images as well as obtaining averaged time-exposure e variance images.

The mathematical procedure deployed for producing time-exposure and variance images (Figure 6) uses the average colour for all colour levels that characterise single pixels of RGB images. In order to obtain variance images, the elaboration takes into consideration the standard deviation (σ).

a)   b)

Figure 6 – a) Timex image, 2 November 2005, 12 a.m. ; b) Variance image, 2 November 2005, 12 a.m.

All elaborated frames and images were georeferenced by means of an *ad hoc* Matlab code. This application is based on the classical approach used by Abdel Aziz and Karara (1971) which allows changing the reference system from 3D to 2D (Holland et al., 1997). Through this system, it is possible to find the corresponding geographic coordinates of each pixel of the webcam image.

After georeferencing, the images can be ortorectified (Figure 7). Many existing studies have used detailed analysis of the intrinsic camera parameters for rectification (Monti et al., 1999): in Beachkeeper georeferencing is used instead and rectification is the result of the application of an algorithm to the georeferenced image.

a)   b)

Figure 7 – a) Timex image, 2 November 2005, 12 a.m. ; b) Timex rectified image, 2 November 2005, 12 a.m.

Levanto video station

The video station installed in Levanto by Ge.Co. s.r.l. was operative from June 2005 to June 2006. The video system consisted of 2 high resolution webcams (maximum resolution 1280 x 960 pixel) located at 16 m height above sea level, in the eastern sector of Levanto beach. Both webcams were pointed at NW-direction and allowed a panoramic view of the beach as well as a detailed view of the central and western sector, where nourishment took place between 2004 and 2005 (Figure 8).

a)   b)

Figure 8 – a) Zoomed panoramic snapshot image; b) Zoomed snapshot image.

In order to guarantee homogeneous data acquisition in time, 4 photos were taken every 2 minutes, for a period of 8 minutes, 3 times a day: at 8 a.m, at 12 a.m. and at 4 p.m.

All acquired photos were georeferenced, rectified and averaged using Beachkeeper in order to assess the morphological evolution of the beach under different hydrodynamic conditions during the 12 months following the completion of nourishment operations.

The KOSTA Video system

KOSTA Coastal video monitoring is based on a photogrammetric technique which allows transforming 2D image coordinates into the corresponding 3D real world coordinates (Trucco and Verri, 1998). CASAGEC and AZTI Tecnalia joined to develop a coastal video system: the Kosta System. Since September 2006, 6 stations have been installed: 5 in France (2 in Anglet, and 3 in Biarritz) and 1 in Spain (Mundaka). Details on the system are available at the website http://web.univ-pau.fr/CASAGEC/3921/).

In September 2007, a new video station has been installed on the top of a 47 m building located in front of Valras Beaches, as a part of the European project MEDDOOC INTERREG BEACHMED-e. This station is composed of 6 cameras, covering a 180° field of view (Figure 9).
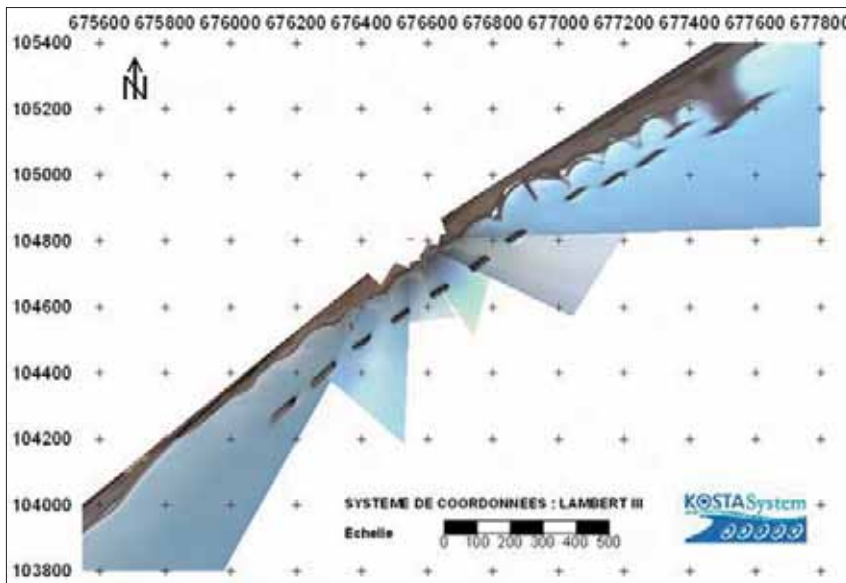
Figure 9 - Merging and rectification of the images taken at Valras.

Comparison analysis

A synthetic comparison among the systems for coastal video-monitoring is presented in Table 1. The most recent systems (EVS and KOSTA) have some capabilities comparable to the Argus system. They can provide you with averaged images, variance images, time stack plots and data, and can upload to any ftp site, using file names consistent with the Argus system. Beachkeeper, a recent system in developing, has comparable capabilities to the others, except the possibility to obtain time stacks. EVS can also upload using its own conventions for the archive, which allow the use of efficient slideshows for image delivery over the web.

Conclusions

The present study shows four systems for coastal video-monitoring used during the Beachmed-e project. The first three systems presented, Argus, EVS and KOSTA, are videomonitoring stations, complete with hardware and software. The main difference among them lies in the type of camera used, while the types of images that are produced are similar. Argus is undoubtedly the most validated system, as it was the first to be developed for research in the coastal zone, and it is now widely spread throughout the world. The three systems are equipped with software that is more or less advanced and sophisticated for standard processing, such as the production of timex and variance images and timestack. In addition, other softwares have been developed for georeferencing and ortho-rectification of images and automatic detection of the shoreline. The Beachkeeper system, however, is a software applica-

ble only for standard image processing (production of timex and variance) and orthorectification and georeferentiation. It can be used with various types of acquisition support and images. During the project it was used to process images taken by a webcam which had been previously installed for the control of tourist flows.

The article presents a comparative table providing a first comparison among the 4 systems proposed. The choice will depend on the budget available and on the characteristics of the site to be monitored. In addition, the article gives the reader a basic reference on the main videomonitoring techniques in use in Europe.

Table 1 - Comparison among video systems characteristics.

	Argus	EVS	Beachkeeper	KOSTA
Year of development	Established, well known and internationally accepted system for video acquisition and analysis. Developed since the early 90s.	System developed since 1998 mainly used for environmental control	System developed in 2006 for coastal monitoring during the BEACHMED-e OCR	System developed in 2006 for coastal monitoring
Stations	More then 50 Argus Station in USA, Europa and Australia	Some installation equivalent to Argus are available: Puleo at Delaware Univ. USA. Igea Marina UNIBO. *Installation for beach monitoring:* Boca Raton FL Boca Inlet Boynton Inlet Lake Worth Inlet Jupiter Inlet Monty county FL Saint Lucie Inlet Sebastian Inlet Pocomac River Santa Cruz CA San Francisco CA USGS Lerici I Sarzana I Terracina Fondi	Levanto, June 2005 – June 2006	Adour (September 2006) Mundaka / Espagne (February 2007) Sain Juan de Luz France (February 2007) Biarritz France (2007).
Software	Software for database man-agement Software for image rectifica-tion and merging, shoreline identification	Software for Timex and variance images Post processing software: Lens calibration Ortho-rectification Geo-referencing * Shoreline detection Intertidal beach bathymetry * In progress	Software for Timex, Day Timex and variance images Post processing software : Ortho-rectification Geo-referencing Shoreline detection* *In progress	Software for Timex and variance images Post processing software: Lens calibration Ortho-rectification Geo-referencing
Image resolution	Max resolution 1024 x 768 pixels	Max resolution 10MPixel (3264 x 2488)	Max resolution 1280 x 960	Max resolution 1024 x 768 pixels.
Timestack images	YES	YES	NO	YES
Acquisition possible during the night	NO	YES	Information not available	Information not available
	Rigid	Flexible	Flexible	Flexible
Type of cameras:	Digital video cameras (Low resolution)	Video-cameras and still-cameras (up to 10MP resolution)	Webcam	Digital cameras

References

Aarninkhof S.G.J., Turner I.L., Dronkers T.D.T., Caljouw M. and Nipius L. (2003) - *A video-technique for mapping intertidal beach bathymetry*. Coastal Engineering, 49: 275-289.

Abdel-Aziz Y.I. and Karara H.M. (1971) - *Direct linear transformation from comparator coordinates into object space coordinates in chose-range photogrammetry*. In Proc. ASP/UI Symp. Close-Range Photogrammetry, Urbana, IL. pp.1-18.

Archetti R. and Lamberti A. (2007) - *Study of hydrodynamic induced by low crested structures through image processing*. In: McKee Smith J. (Ed.) Proc. of the 30th International Conference. On Coastal Engineering. /San Diego, California, USA 3-8 Sept. 2006. World Scientific Publishing Co.Pte.Ltd. pp. 5021 - 5033.

Armaroli C., Ciavola P., Caleffi S. and Gardelli M. (2007) - *Morphodynamics of nearshore rhythmic forms: an energy-based classification*. Proceedings of International Conference on Coastal Engineering (ICCE 2006), San Diego, CA, USA, Settembre 2006. vol. 4: 4009-4021.

Chickadel C.C., Holman R.A. and Freilich M. (2003) - *An optical technique for the measurement of long-shore currents*. Journal of Geophysical Research, 108: 3364.

Holland K.T., Holman R.A, Lippmann T.C., Stanley J. and Plant N. (1997) - *Practical use of video imagery in nearshore oceanographic field studies*. IEEE Journal of Oceanic Engineering (special issue on image processing for oceanic applications) 22: 81-92.

Holman R.A. and Stanley J. (2007) - *The History, Capabilities and Future of Argus*. Coastal Engineering, The CoastView Project special issue, 54: 477-491.

Holman R.A., Sallenger Jr. A.H., Lippmann T.C. and Haines J. (1993) - *The application of video image processing to the study of nearshore processes*. Oceanography, 6: 78-85.

http://argus-data.wldelft.nl/index.html.

http://videomonitoring.eu.org/igea.

http://web.univ-pau.fr/CASAGEC/3921/

http://www.encora.eu/coastalwiki/Argus_video_monitoring_system

http://www.svm.it/.

Kroon A., Aarninkhof S.G.J., Archetti R., Armaroli C., Gonzalez M., Medri S, Osorio A., Aagaard T., Davidson M.A., Holman R.A. and Spanhoff R. (2007) - *Application of remote sensing video systems for coastline management problems*. Coastal Engineering, 54: 493-505.

Lippmann, T.C. and Holman R.A. (1990) - *The spatial and temporal variability of sand bar morphology*, Journal of Geophysical Research, 95: 11575-11590.

Monti C., Guerra F., Balletti C. and Miniutti D. (1999) - *Geometric operations in digital images*. Proceedings of XVI International Symposium CIPA. Olinda, Brazil.

Trucco E. and Verri A. (1998) - *Introductory Techniques for 3-D Computer Vision*. Prentice Hall, Inc.

Turner I.L. and Anderson D.J. (2007) - *Web-based and 'real-time' beach management system*. Coastal Engineering, 54: 555-565.

Study of beach evolution due to storms and nourishments by video monitoring

Renata Archetti

The purpose of this study is to present the results of shoreline monitoring for the period October 2006 - March 2008 of a beach, using the tools developed during the OpTIMAL project for video image processing. The study was carried out in Igea Marina, where a video monitoring station EVS-SVM was intalled in September 2006. During the period of observation the beach was widened by nourishment, and an intensive field campaign was carried out for measuring waves and currents at the site by two ADCPs. The dynamics of the beach and its relationship to the forcing mechanisms of waves and tides are presented.

Introduction

The collection of data representative of the state of the coastal environment, essential for the proper management of coastal areas, is a challenging and expensive task.

Remote sensing techniques using video cameras have been developed in recent years in order to monitor the hydrodynamic processes (Chickadel et al., 2003; Archetti and Lamberti, 2007, Jimenez et al., 2007) and coastal morphodynamics (Aarninkhof et al., 2003; Kroon et al., 2007). The most common application in the processing of images for coastline management is the detection of the shoreline position on timex. The main advantage of the detection of the shoreline on video images is the possibility to obtain the information with high frequency in time. It has been shown how the sporadic shoreline detection performed occasionally (1 or 2 times a year) through traditional methods (GPS) or satellite imagery can lead to misleading results in respect to the real evolutionary trend of a beach (Kroon et al., 2007; Archetti et al., in press).

The purpose of this work is: a) to present the experience of monitoring a beach with a video system, designed with low-cost digital cameras and installed in Igea Marina, Rimini (Preti et al., 2005) and b) to show a new technique for shoreline detection, at an hourly frequency, based on a type of image called timestack, which represents the intensity of pixels on cross-section arrays in time and c) to describe the evolution of a shoreline that was monitored for over a year and the correlation of the shoreline evolution to meteomarine conditions. The paper ends with a discussion on future developments.

The study site

Igea Marina is located on the Northern Adriatic Sea, 15 km North of Rimini (Figure 1). The beach was protected until 2002 by a system of parallel emerged structures. The same system protects the littoral zone from Rimini to Cesenatico, as we can see in Figure 1. In 2003, a pilot intervention aiming at improving water quality (Preti et al., 2005) was carried out, and consisted of lowering the crest of 6 adjacent detached barriers just above m.s.w.l., building two lateral partially submerged groins and realising some renourishment. The installation of the imaging station was implemented in order to monitor coastline evolution and hydrodynamics at the groin heads and at the barrier gaps beyond the area of the intervention.

The video station installed in Igea Marina in September 2006 is described in Archetti et al. (this issue).

Figure 1 - Location map.

Video image Analysis

The study of various shoreline features and processes is facilitated by transforming the images into real world coordinates. This process of geo-referencing an image is carried out in the following manner. First, lens distortion is corrected by lens calibration. Then, with the use of ground control points, the image is rectified and placed in a geo-referenced system. The processes has been implemented and carried out for both imaging systems at Igea Marina.

In order to estimate the parameters for camera calibration, image series of a planar checkerboard were taken. The corner position is automatically extracted and calibration parameters are estimated with the Matlab camera calibration toolbox. The tool allows the estimation of the so-called camera intrinsic parameters and the non-linear distortion introduced by the lens. The lens distortion is shown in Figure 2, where each arrow represents the effective displacement of a pixel induced by lens distortion, higher for the still camera than for the video camera. Observe that for the video camera (Figure 2a) there is high radial distortion at the right side of the shoreline. For the still camera the maximum radial distortion reaches 20 pixels, but is located in a position of reduced interest for our analysis.

The second step is the image rectification. This process consists of projecting the entire image captured, or a portion of it, from the image reference system on a user specified horizontal plane.
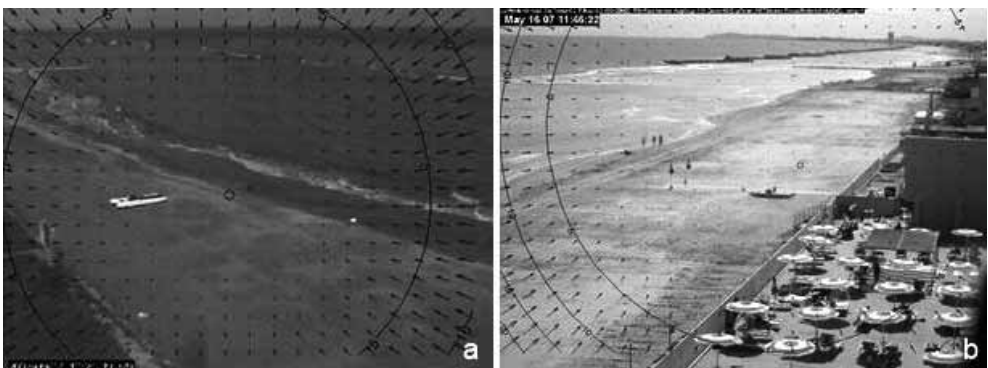
Figure 2 - The impact of the complete distortion model (radial and tangential) on each pixel of the images for both video systems: videocamera (a) and still camera (b).

By image rectification we mean the transformation from image coordinates to world coordinates of the entire captured scene or a portion of it. We have used a projective transformation of a plane at the sea water level. The matrix of transformation from image coordinates (U, V) to geographic coordinates (x, y, z mswl) is called the geometry. The process involves the establishment of pairs of ground control points (GCP) which are visible in the images and in the real world.

In order to extract useful information for analysis, ground control surveys were carried out and included the identification and location of permanent and temporary ground control points (GCP) placed on the beach and in the sea (*i. e.*, poles showing the roundhead structures) in the field of view of each camera (Figure 3).

Figure 3 - Timex image by still camera during the GCP survey with RTK-GPS in Igea Marina. The points show the GCPs location.

The accuracy of the RTK-GPS (Real Time Kinematic GPS) was assessed by surveying 4 benchmarks at the site: the first 2 located on the street behind the beach and the others on the beach (these points were surveyed at the beginning of our measurements). All four measurements were within the stated accuracy of the RTK-GPS, yielding a horizontal root mean square error (erms) of 0.04 m.

The reference system of the survey had its origin at the video camera location, and was rotated 36° in order to have the orientation of the x-axis normal to the shoreline, with the positive x-axis pointing in seaward direction. The y-axis is directed perpendicular to the x-axis, such that the co-ordinate system obtained is positive in a mathematical sense. The latter means that the rotation from the x-axis towards the y-axis indicates the counter-clockwise (or 'positive') turning direction. In this reference the structures parallel to the shore are y-oriented and the groins x-oriented (Figure 4).
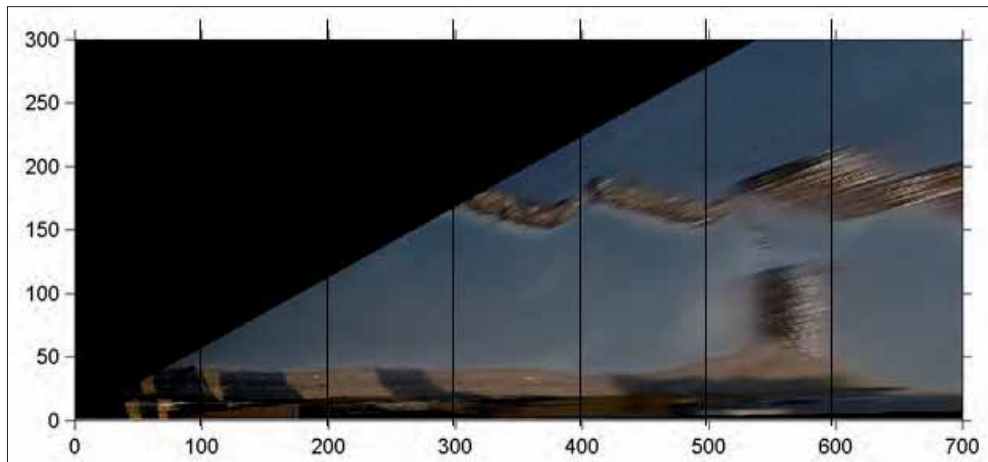
Figure 4 - Rectified plan-view image in the local coordinate system. The vertical lines are seven shore-normal transepts.

For every GCP image, coordinates are associated with the xy coordinates in the local reference system. The geometry (relationship between UV and xy coordinates) has been calculated several times, about once a month, as the FOV and the zoom of the cameras have had some minor excursion in time. These changes are mostly due to the temperature excursion, which causes minor movements of the systems and of the lens focus.

A rectified image is shown in Figure 4. The error in the rectification process estimated by comparing RTK-GPS GCP with video derived GCPs is 1.28 ± 1.30 m and increases with a linear trend with the distance from the origin. It has been estimated that for position at the distance of the order of 100 m O(100), the error is O(0.10), increasing up to O(1.0) at 400 m distance. Following the data presented within the area of interest the error in the image rectification is acceptable.

As a preliminary analysis and first application using this imaging station in order to quantify changes in coastal features and nearshore processes, we have developed two approaches to detect the shoreline evolution. The first consists of making timestacks in selected sections on the beach: a timestack image is obtained by sampling image intensities along a fixed cross-shore array and stacking them over time. The second approach consists in the detection of the shoreline on the entire image at selected times.

Timestack analysis

For several longshore transects (see Figure 4 for reference) data of usable imagery in timestack were compiled for the period 1 October 2006 – 28 February 2008. Examples of timestacks are shown in Figure 5: on the y axis is the cross-shore distance from the beach and on the x axis is the time. On the image in Figure 5 it is possible to detect by eye the limit sea/beach (or dry/wet). The shorelines keep constant during winter 2007 with the same small fluctuation of the order of a few meters in coincidence with storm events. In April 2007, the beach nourishment carried out by the Regione Emilia Romagna produced an advance in the shoreline position varying from 20 m to 25 m in different sections of the beach. The beach width kept constant for the whole summer and in fall it was possible to observe some fluctuations in correspondence to storms. On the same image the measured sea water level (swl) and the wave height Hs are shown. The significant wave height sources are the hindcasted wave data from SWAN (courtesy provided by ARPA SIM, in blue on the plot), the wave data measured by the directional wave buoy installed offshore from Cesenatico, on a depth of 10 m (in red), and the measures during the field campaign carried out in winter 2007 – 2008 by two ADCP installed at the site (black line).

Through this technique the limit dry/wet is detectable during all the day-light hours. With the help of this timestack image, the behaviour of the shoreline can be monitored in a very simple way. A similar analysis has been presented in Elko et al. (2005).

The shoreline was detected in an automatic way, as follows: The Red band was divided by the Blue band (hereafter R/B), in this way it was possible to obtain an image where the boundary wet/dry is easily detectable. For each line (each hour) of the R_B image the threshold between wet/dry has been estimated as the mean R_B in the whole image plus the mean of R_B in the wet part of the image, previously selected.
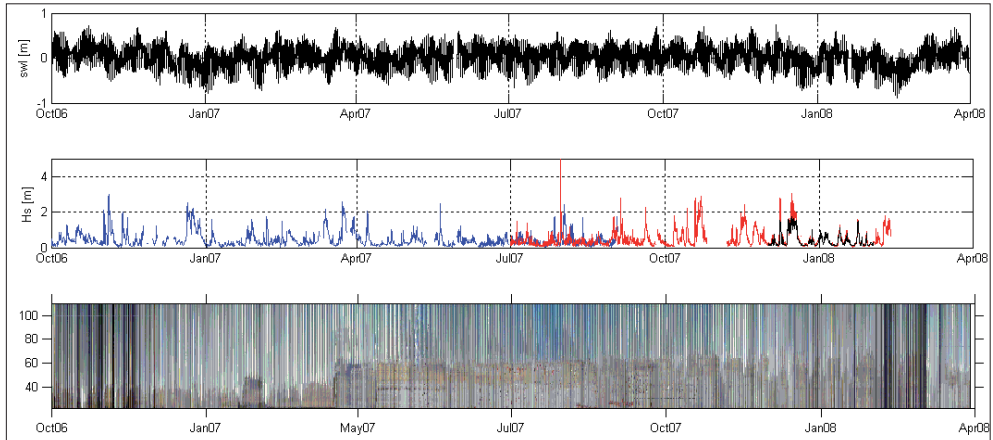
Figure 5 - SWL time-series (top panel); Hs time-series (mid panel); A 1.5 year timestack taken from the section y=200 m in Igea Marina (bottom panel).

The shoreline position is then estimated for each section as the maximum R_B < threshold. The signal has been detrend with a low pass filter, in order to filter the daily tidal excursion. An example of the automatically detected shoreline is shown in Figure 6. When the shoreline decreases the beach width decreases.
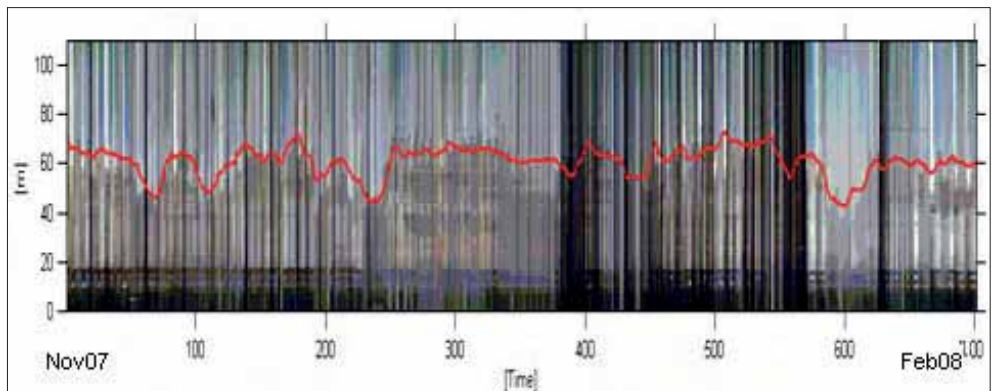
Figure 6 - Example of timestack image and automatically detected shoreline.

Figure 7 shows the shoreline evolution for the period December 2007- March 2008. During the period two ADCPs have been installed inside and outside the low-crested structures. In Figure 7 the Hs, Tp and SWL measured during the field campaign are shown. The blue line refers to the measure taken by the ADCP installed outside the LCS and the red line refers to the data measured by the ADCP installed inside the area protected by the structure.
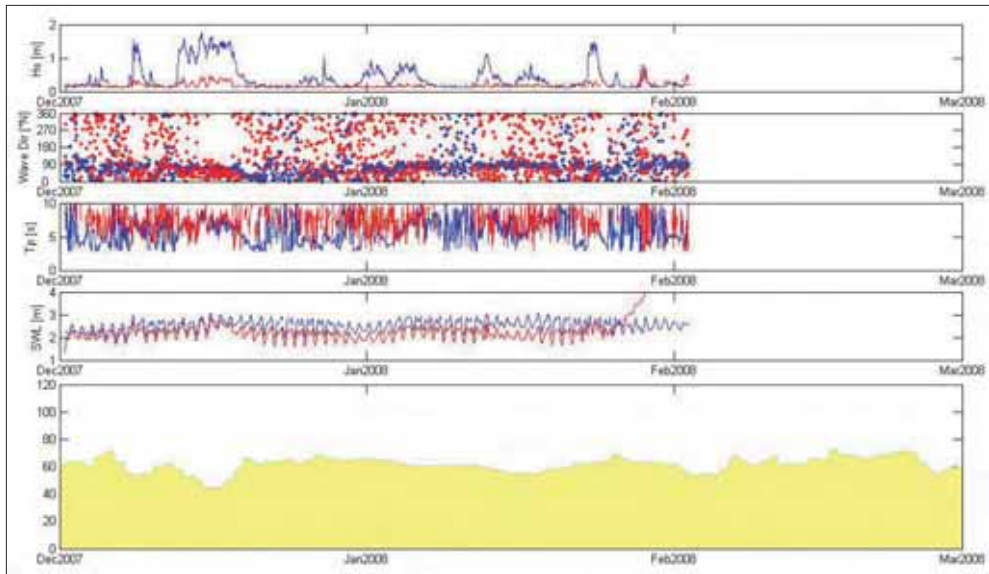
Figure 7 – Wave height, wave peak period swl measured by the ADCP (blue located outside and red inside the structure) during the field campaign (Top panels). Shoreline detected in section 200 during the field campaign.

A severe storm from the North occurred in December 2007. The shoreline shows a retreat, mostly due to the increase of the swl. After the storm, in the end of December 2007, the beach width goes back to the original dimension. During the storm the waves have been strongly reduced by the structures, as we can observe in the plot regarding the Hs (top panel). At the end of March 2008 the beach width is still at the same dimension as before the summer. This means that the low crested breakwaters work well in the reduction of wave height.

Shoreline position detection
The shorelines have been detected on the entire image in order to follow the evolution along the beach. The first step consisted of selecting the most appropriate images for the analysis: good quality images taken during very calm days (and after periods of calm conditions), at the time in correspondence to the sea water level equal to approx. zero. The shoreline was detected on oblique images and then rectified and interpolated in order to have the shoreline position at 1m spatial resolution. A total of 50 shorelines were detected. Figure 8 shows 19 shorelines detected in the period 5 October 2006 – 5 February 2008.
The shorelines closer to the back of the beach (to the x axis in Figure 8b) refer to the "surveys" carried out before nourishment, whereas the others relate to the "surveys" carried out after or during nourishment. The behaviour of different sections is comparable, except for sections at y=400 m and y=150 m which show more evident retreat. The mentioned sections are located just in front of the gaps of the parallel low-crested structures. The strong currents that are generated at the gaps are responsible for greater erosion of the beach.
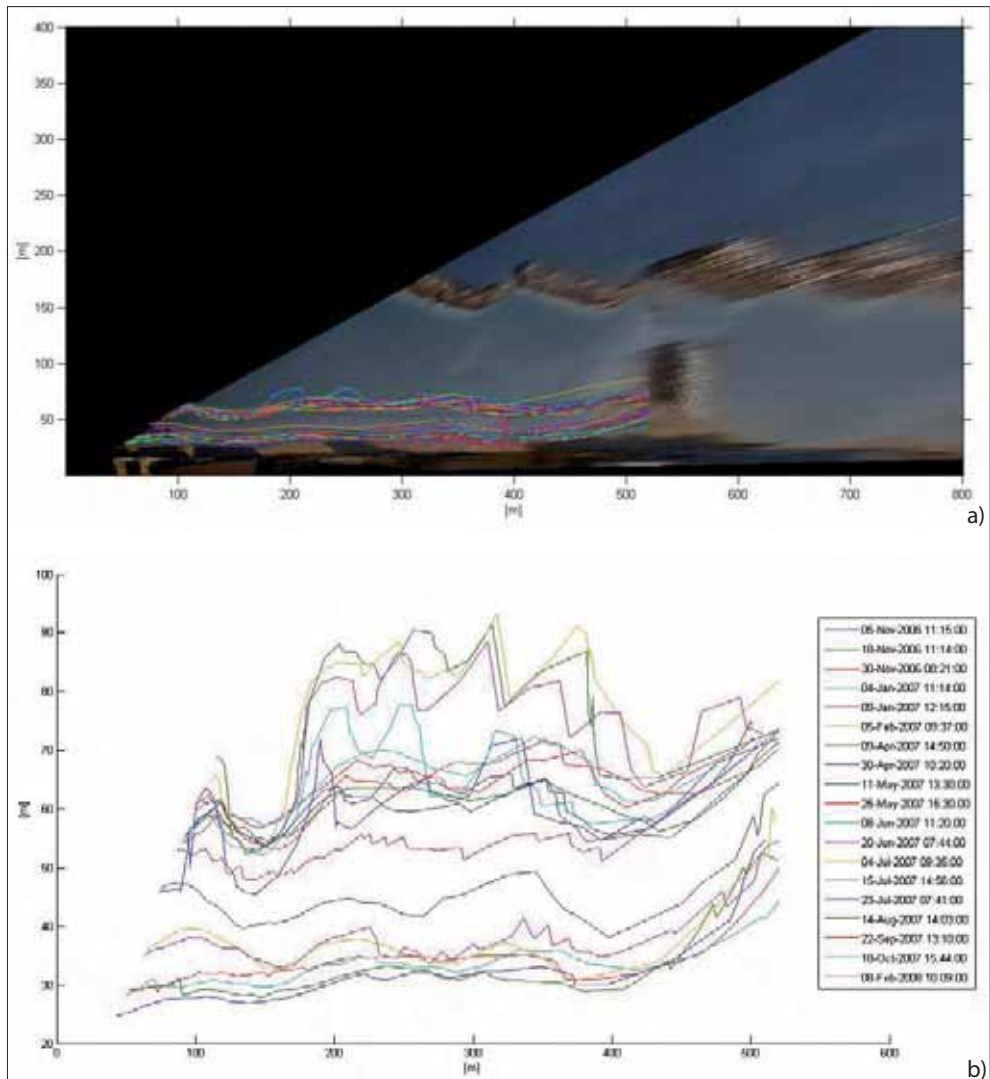
Figure 8 - A total of 19 shorelines plotted on plan-view images during the study period.

Conclusions

The use of the EVS-SVM image monitoring system at Igea Marina beach has provided effective means to describe the variability in morphology before and after storm events and sand nourishment. Analysis of video data during an 18-month period has allowed investigating the dynamics of the beach and its relationship to the forcing mechanisms of waves (and tides). The evolution of the shoreline before nourishment (carried out in April 2007) shows a small accretion of the beach probably due to seasonal variability. The shoreline position and the beach dimension seem to maintain constant in time until the end of the analysis, in March 2008, despite the storms that occurred in Autumn and Winter. The study of Igea Marina beach shows that beach evolution can be successfully analysed using a low cost technique that allows an increase in sampling frequency and provides the opportunity for a detailed study of beach behaviour, identifying relevant events and their effect on coastal evolution.

References

Aarninkhof S.G.J., Turner I.L., Dronkers T.D.T., Caljouw M. and Nipius L. (2003) - A video-technique for mapping intertidal beach bathymetry. Coastal Engineering, 49: 275-289.

Archetti R. and Lamberti A. (2007) – Study of hydrodynamic induced by low crested structures through image processing. Proc. XXX ICCE, San Diego CA, 2-7 Sep 2006.

Archetti R., Torricelli E., Lamberti A. - Study of the evolutio of a beach protected by low crested structures using video monitoring. Journ. Costal Research, in press.

Chickadel C.C., Holman R.A. and Freilich M. (2003) - *An optical technique for the measurement of long-shore currents.* J. Geophys. Res., 108 : 3364.

Elko A.N., Holman R.A. and Gelfenbaumm G. (2005) - Quantifying the rapid evolution of a nourishment project with video imagery. Journal of Coastal Research, 21 : 633 – 645.

Jimenez A., Osorio A., Marino-Tapia I., Davidson M., Medina R., Kroon A., Archetti R., Diavola P. and Aarninkhof S. (2007) – *Beach recreation planning using video-derived coastal state indicators*. Coastal Engineering, 54: 1 – 40.

Kroon A., Aarninkhof S.G.J., Archetti R., Armaroli C., Gonzalez M., Medri S, Osorio A., Aagaard T., Davidson M.A., Holman R.A. and Spanhoff R. (2007) - *Application of remote sensing video systems for coastline management problems*. Coastal Engineering, 54(6-7): 493-505.

Preti M., Lamberti A., Martinelli L., Albertazzi C. and Sammarini S. (2005) - *An effort toward renaturalisation of Igea Marina beach: transformation of 6 emerged barriers into a single low crested structure.* Proc. MedCoast 2005 (Kusadasi, Turkey). E. Özhan Ed. pp. 919-930.

Nourishment of Levanto (Italy): a webcam-aided evaluation of a mixed sand and gravel beach fill

**Claudia Dessy, Chiara F. Schiaffino,
Nicola Corradi, Marco Ferrari**

Aim of this study is to evaluate the effectiveness -in terms of erosion mitigation- of beach nourishment for Levanto mixed sand and gravel beach.

The beach of the town of Levanto, located between the promontories of Punta Gone and Punta Picetto, is a pocket beach. Two groins divide the beach into three separated sectors. The evolution of the coastal morphology is moreover influenced by a submerged breakwater, located in the central sector.

During 2004-2005 nourishment of the western and central sectors was carried out using about 16.000 m^3 of gabbros and basalts from a quarry. No nourishment took place in the eastern sector since its conditions have proven stable over the year. Immediately after nourishment completion an operation of maintenance and adaptation of the groins followed, in order to retain and stabilise the sediment in the central and western sector, thus avoiding the significant losses recorded in previous years.

In order to evaluate the short and mid-term effectiveness of the nourishment, the shoreline variations were video-monitored until June 2006.

The shorelines in the rectified Timex images of the period between May 2005 and June 2006 were determined and then compared with a reference situation.

The results show a general stabilisation of beach morphology and an increased sedimentary budget, as a consequence of the 2005 nourishment, sufficient for creation of seasonal profiles. In particular, the management scheme seems more successful in the western sector, while the central sector was subject to modest erosion. Finally, the shoreline of the eastern sector, which has been stable over the years and where no nourishment took place, retreated in comparison with the previous year. This is probably due to reduced sediment inputs to this cell as a consequence of groins re-location used alongside nourishment for stabilisation of the other two sectors.

Introduction

Gravel sediment is currently largely used in coastal engineering works for both coastal protection and replenish of eroded beaches. Past morphodinamic and sedimentary beach evolution research focussed upon sandy beaches. During the 90s there was an increase in scientific studies focussing upon mixed sand and gravel beaches.

Sediments characterised by coarse grain-size are used for nourishment of eroded beaches because of their high water permeability (Van Wellen et al., 2000). This results in gravel beaches being more stable if compared with sandy beaches, because sediment erosion by backwash flow is reduced.

Aim of this study is to evaluate the evolution of the gravel beach of Levanto (La Spezia, Italy) after its nourishment. Since in gravel beaches the main morphological changes occur in the swash zone

(Pedrozo-Acuña et al., 2006) the focus of this study is the shoreline evolution during the 12 months after nourishment completion and under different hydrodynamic conditions.

The study was carried out through a video-monitoring system and, within BEACHMED-e / OpTIMAL Project, it was also addressed to the evaluation of the efficiency of this technique.

A comparison of the elaborated images allowed reconstructing the seasonal cycles of Levanto beach and thereby assessing the efficiency of the nourishment intervention for morphological stabilisation.

Study area

Levanto beach is part of the alluvional plain of the Ghiararo torrent, belonging to the littoral cell Punta della Madonna - Punta Picetto. The beach of Levanto is located between the promontories of Punta Gone (W) and Punta Picetto (E), which limit sediment transport to and from nearby locations, and so it can be classified as a pocket beach (Silvester et al., 1980).

Two groins divide the ca. 800 m long beach, into three separated cells (Figure 1). Over the years the western e central sectors have undergone coastal protection measures aiming at reducing their documented erosion, while the eastern sector has shown no erosion trend. The protected sectors present maximum width of about 35 m and their extension is, respectively 150 m for the western one and 250 m for the central one; the eastern sector, about 400 m long and maximally 43 m wide, is the largest.

Sediment dimensions vary across the beach both in cross-shore and long-shore direction. In the intertidal area the sediment grain-size ranges between medium sand and pebble, decreasing in offshore direction to fine sand. Beach grain-size decreases from W to E due to the longhsore drift.

Since the beginning of the century, coastal protection schemes have been applied in order to mitigate coastal erosion. The groins are, respectively, the western one 30 m long, and eastern one 40 m long. In November 2005, those two structures have been reinforced at the basis with the aim of reducing return current flow thus helping sediment retention. In the central sector, about 65 m off the shoreline, there is a submerged breakwater (length 100 m, width 7 m), which reaches 2 m below water surface. Two gaps of about 30 m and 40 m width are created between the two groins and the barrier. The last beach nourishment of the central and western sectors was realised between fall 2004 and spring 2005, using about 16.000 m³ of gabbros and basalts from a quarry in the hinterland. The material used had a mean grain-size (D_{50}) of 30 mm.

Figure 1 - Location map (Aerial photograph, Regione Liguria)

Wave conditions

The hydrodynamic conditions used for Levanto were derived from data collected by a buoy (43° 55′ 41.99″ N; 09° 49′ 36.01″ E) belonging to the Rete Ondametrica Nazionale (Hydro-Marine National Network) and located off La Spezia coast at a depth of about 90 m. The considered shoreline has a prevailing wind sector between 190°N and 280°N, therefore is exposed to waves and currents generated from SW and partly from the S and SE.

The maximum tidal excursion for the site of Levanto, interpolated from data relative to La Spezia, is about 30-40 cm (IIM), and thereby is considered irrelevant for this study.

Beach monitoring video-station

The video station was installed in Levanto by Ge.Co. s.r.l. in May 2005 and was operative until June 2006. The video system consisted in 2 fixed digital webcams equipped with internal memory, allowing to acquire images of the beach at a definition of 1280x960 pixel. The webcams were located at 16 m height upon sea level, on the top of a building near the eastern sector of the beach. The data were transmitted via ADSL. Both webcams were pointed in NW-direction and allowed a panoramic view (Figure 2a) of the three sectors of the beach as well as a detailed view (Figure 2b) of the central and western sector, where last nourishment took place in 2005.

The system was set for automatic periodic data acquisition. Three acquisitions per day took place at 8 a.m., at 12 a.m. and at 4 p.m., in order to guarantee homogeneous data acquisition during daytime. During every acquisition cycle photos were taken every 2 minutes for a period of 8 minutes.

a)   b)
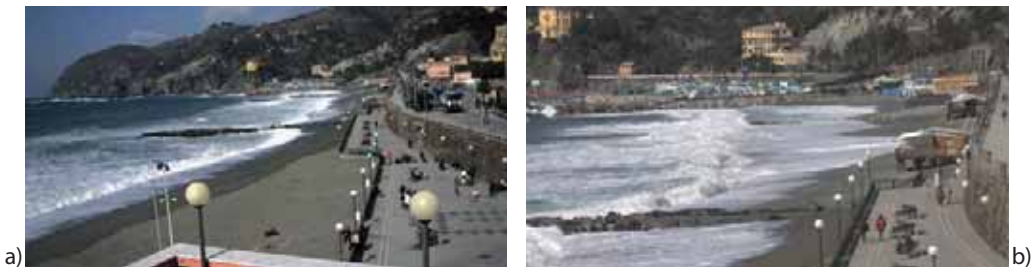
Figure 2 – a) Panoramic snapshot image; b) Zoomed snapshot image.

All acquired photos were sent to a dedicated ftp site. The Beachkeeper software, supported by Matlab® 2006b, has been developed for image management and elaboration by a cooperation of Dip.Te.Ris and Di.Ma., within the Genoa University.

The software allows producing timex and variance images (Holland et al., 1997; Monti et al., 1999), that highlight morphological features of the beach. Among the basic features, there is also the possibility to georeferentiate images using the approach of Abdel-Aziz et al. (1971).

Since the webcam images entail some perspective view, which could hinder morphology recognition, a function of the software allows to simulate a plan view (Figure 3).

a)   b)

Figure 3 – a) Timex image, 1 May 2006, 8.00 a.m.; b) Rectified timex image, 1 May 2006, 8.00 a.m.

The procedure deployed, which uses georeferentiation, represents an innovation with respect to methods reported in existing literature, which take into account intrinsic characteristics of the cameras in order to perform this transformation (Holland et al., 1997).

Monitoring of the effects of nourishment

Aim of this study is to evaluate the effects of Levanto beach nourishment upon coastal morphology. The evaluation of the efficiency of this intervention for erosion mitigation has been carried out based upon the time-evolution of the shoreline as recorded in time exposure and variance images (Plant & Holman, 1997; Guillén et al., 2003). It was possible to daily and monthly delineate the shorelines and thereby to reconstruct the seasonal shoreline evolution. Such a study allows to trace a general evolutionary trend of the coastal system and therewith to evaluate the efficiency of the nourishment scheme.

The shoreline changes until June 2006 were analysed in order to determine the mid-term coastal evolution.

The shoreline was determined based on the methodology of Aarninkhof et al. (2003), Plant et al. (1997) Ojeda et al. (2005) e Lippmann et al. (1989), who define the shoreline as the contact line between still water level and the beachface. For this reason the images acquired during minimum wave conditions were selected in order to minimize errors in the determination of the shoreline.

For each selected rectified time-exposure image the shoreline was traced and those were successively compared with the shoreline of 13 May 2005 –date of webcam installation– in order to analyse the morphological evolution of the beach.

Moreover, seasonal comparisons were carried out in order to gain a more detailed and complete overview of the beach behaviour.

June 2005 – September 2005

Shoreline evolution during the first four months after nourishment (June 2005 – September 2005) is shown in Figures 4 and 5.

Due to the littoral drift, which transports sediments towards the East, the eastern part of the shoreline advances in all three sectors of the beach.

During this period only minor changes are observed, which highlight a general stability of the beach and modest redistribution of the nourishment material.
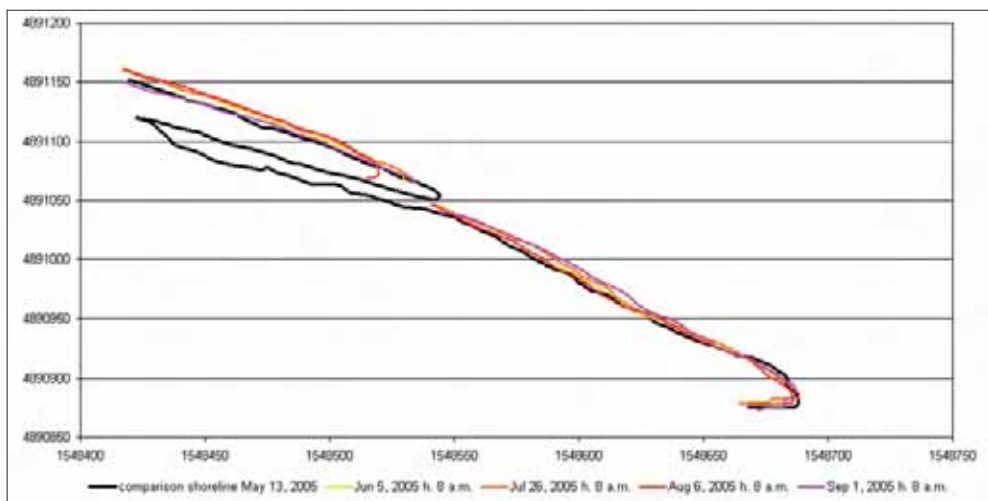
Figure 4 – Comparison of shorelines in the western and central sectors during the period June 2005 – September 2005.
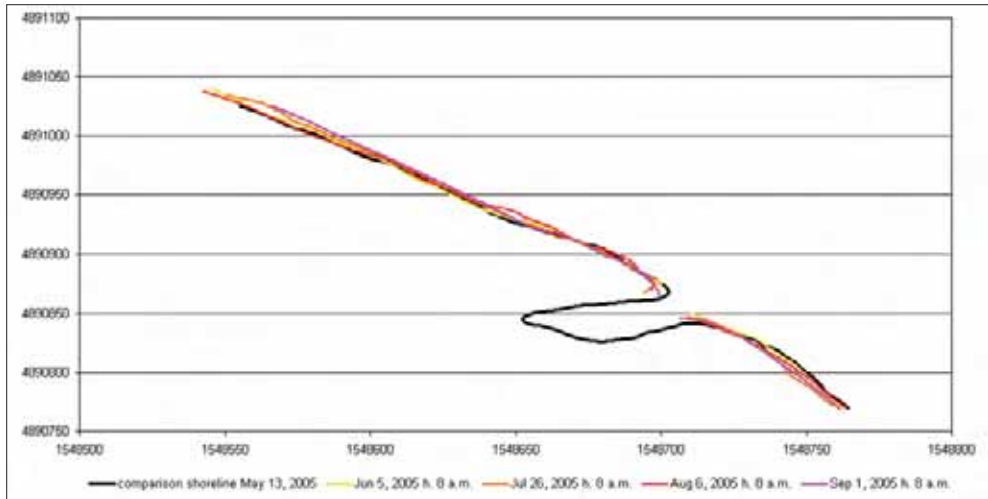
Figure 5 – Comparison of shorelines in the central and eastern sectors during the period June 2005 – September 2005.

September 2005 – December 2005

During fall most significant changes of the shorelines were observed (Figures 6 and 7). The central sector showed a marked retreat if compared with the adjacent sectors. In this area, where no nourishment was carried out, retreat of the shoreline is particularly evident on the lee of the groin.

The observed changes are related to the more intense wave dynamics and the consequent sediment transport from backshore to foreshore.
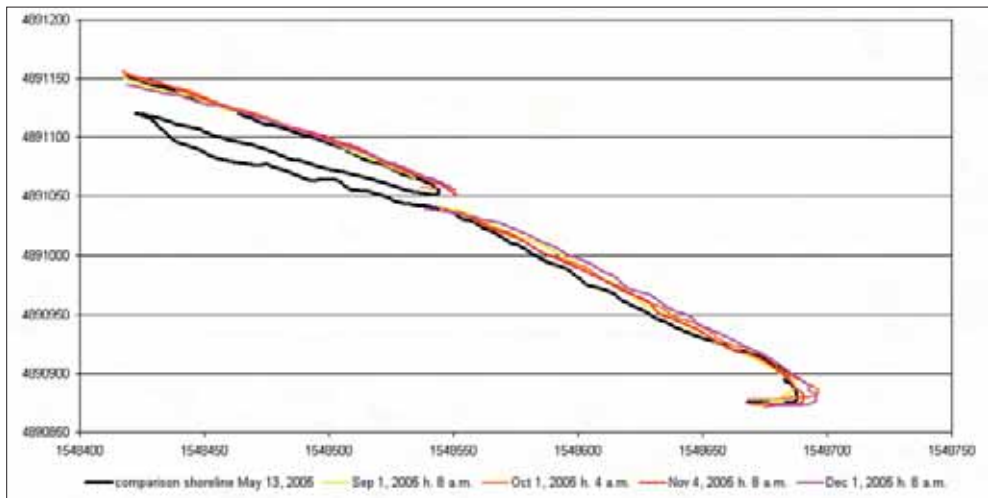
Figure 6 – Comparison of shorelines in the western and central sectors during the period September 2005 – December 2005.
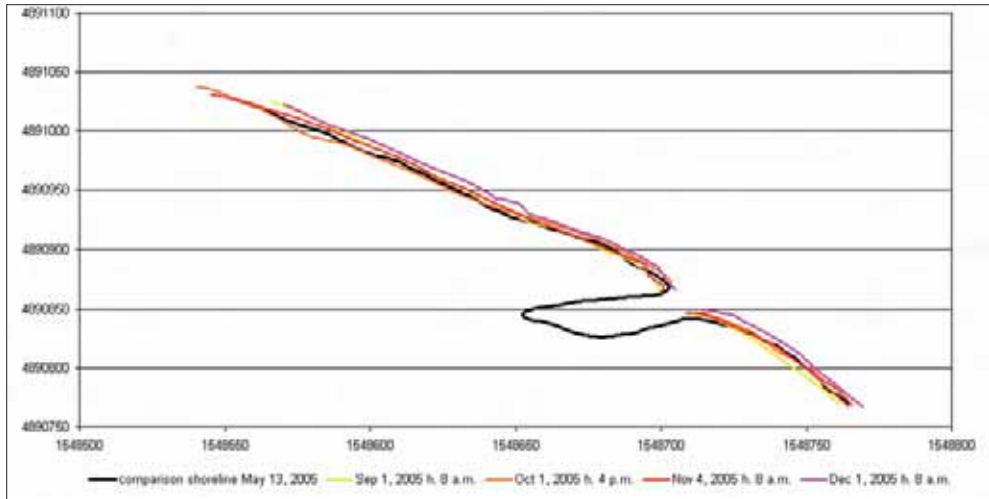
Figure 7 - Comparison of shorelines in the central and eastern sectors during the period September 2005 - December 2005 .

December 2005 – March 2006

A general retreat is observable in all three sectors and particularly in the central one (Figures 8 and 9). In March a shoreline advance within the eastern sector is observed, thereby reaching the position of the previous summer. This advance is not observable in the middle area of the central sector, probably due to the action of the submerged breakwater.

In the eastern sector the shoreline shows a slight retreat from December 2005 until January 2006, while it is stable during the following months.
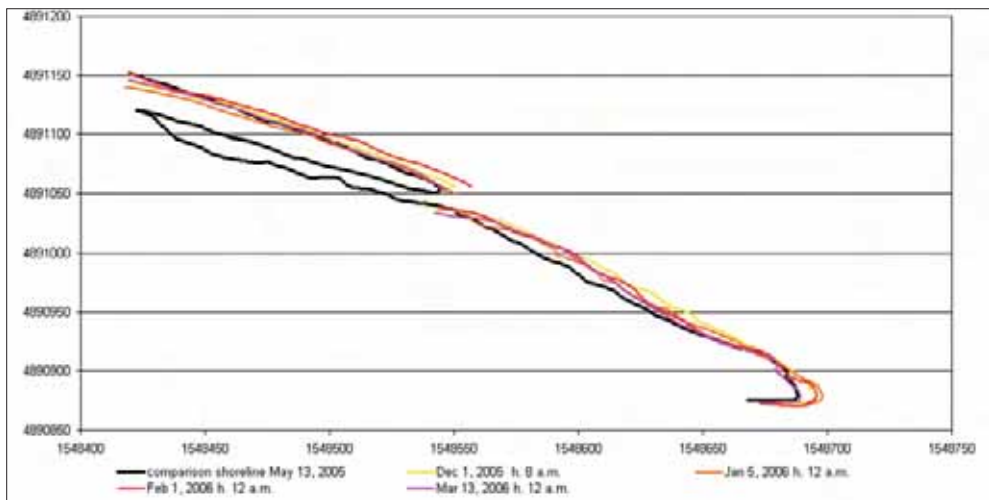
Figure 8 – Comparison of shorelines in the western and central sectors during the period December 2005 - March 2006.
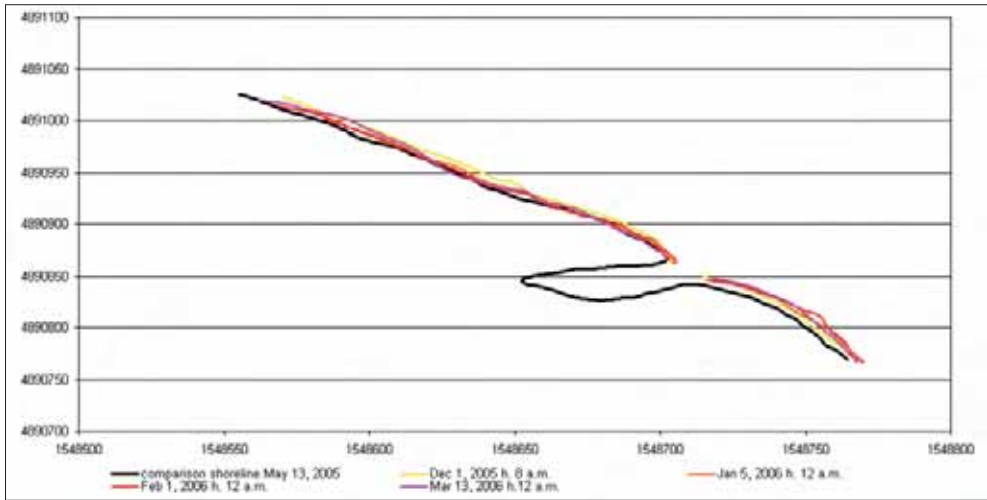
Figure 9 – Comparison of shorelines in the central and eastern sectors during the period December 2005–March 2006.

March 2006 – June 2006

During the period March - June 2006 (Figures 10 and 11) both the central and western sectors are stable. In particular in the western sector the morphodynamic profile realised in March is maintained with some oscillations. In the eastern sector a slight accretion with respect to the previous months is noticeable.
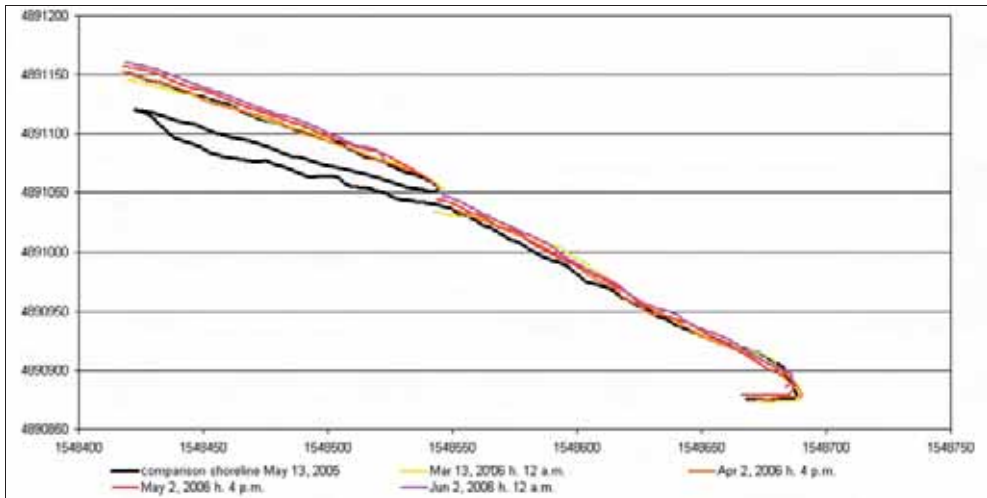
Figure 10 – Comparison of shorelines in the western and central sectors during the period March 2006 – June 2006.
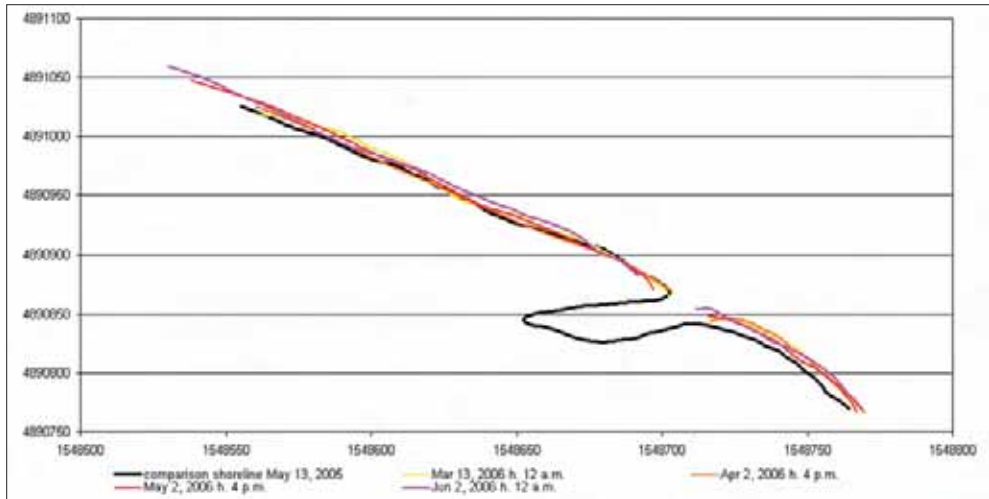
Figure 11 – Comparison of shorelines in the central and eastern sectors during the period March 2006 – June 2006.

Shoreline dynamics in one-year time

Figure 12 shows the different shorelines of the western and central sector in one year time after the nourishment occurred between fall 2004 and spring 2005.

The analysis of the images relative to June 2005 and December 2005 highlights a retreat of the shoreline in the western sector. Such change can be due partly to redistribution of nourishment material and partly to the construction of the seasonal profile. The input of new sediment altered the morphodynamic state of the beach, wave energy elaborated the discharged sediments and transported them to the submarine beach.

However, in June 2006 the shoreline assumed a similar position to that in June 2005, therefore it can be affirmed that no substantial loss of material took place during 12 months of monitoring.

In the central sector, the shoreline in June 2006 retreated if compared with its position in June 2005.
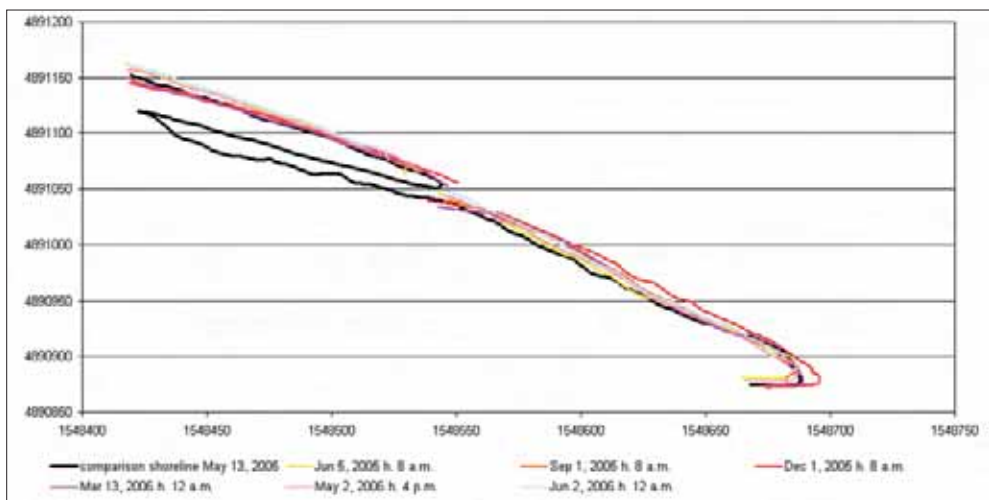
Figure 12 – Comparison of the shoreline in a time-interval of one year.

On the one side this could be due to a loss of material, on the other side such retreat could be compensated for during summertime, and could therefore represent a delay in the building of the seasonal profile.

In the eastern sector (Figure 13), which did not undergo any nourishment intervention, a modest retreat can be noticed in comparison with June 2005. This sector, located on the lee of the groin, had no input of nourishment material, which leads to the hypothesis that the groins efficiently trapped the material in the western and central sectors.
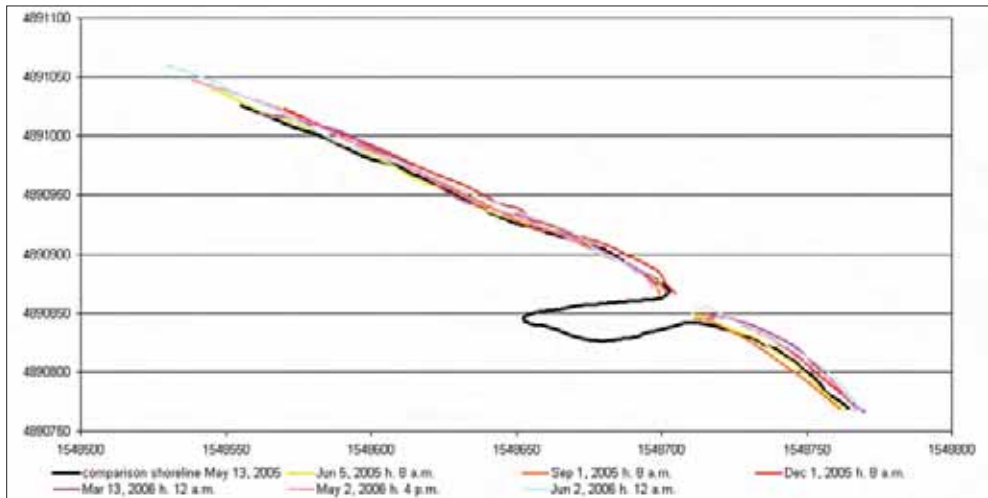
Figure 13 – Comparison of the shoreline in a time-interval of one year.

Conclusions

This study has presented results of 12 months monitoring of Levanto shoreline, where nourishment in presence of coastal protection works took place.

From the analysis of the dynamics of the shoreline results that the beach has maintained a stable condition. Its sedimentary budget, increased by the material discharged during the nourishment in spring 2005, was sufficient for the realisation of the seasonal profiles and, therefore, for coping with different hydrodynamic conditions. The nourishment seems to be particular effective in the western sector, while the central sector shows signs of sediment losses. The sector where no nourishment took place shows some shoreline retreat with respect to the previous year. Although one-year time is not sufficient to analyse in detail the morphodynamics of the beach, this study allowed determining the probable development trend and the consequences of the nourishment upon the littoral asset.

Video monitoring proved to be a valuable technique to analyse short term beach response to shore protection projects.

Acknowledgements

The authors would like to tank the government of the Ligurian Region and in particular Corinna Artom and the Dipartimento Pianificazione Territoriale staff for the support.

References

Aarninkhof S.G.J., Turner I.L., Dronkers T.D.T., Caljouw M., Nipius L. (2003) - *A video based technique for mapping intertidal beach bathymetry*. Coastal Engineering, 49: 275-289.

Abdel-Aziz Y.I., Karara H.M. (1971) - *Direct linear transformation from comparator coordinates into object space coordinates in chose-range photogrammetry*. In Proc. ASP/UI Symp. Close-Range Photogrammetry, Urbana, IL, pp.1-18.

Guillen J., Chic O., Ojeda E., Palanques A., Aarnikhoff S. (2003) - *Monitorización de las playas de la ciudad de barcelona utilizando imágenes de video: evolución de la línea de costa en respuesta a temporales y regeneración artificial (2001-2002)*. VII Jornadas Españolas de Ingeniería de Costas y puertos, Libro de resumenes; M. Lasada y M. Castillo Ed., 254-256.

Holland K.T., Holman R.A, Lippmann T.C., Stanley J., Plant N. (1997) - *Practical use of video imagery in nearshore oceanographic field studies*. IEEE Journal of Oceanic Engineering (special issue on image processing for oceanic applications) 22(1): 81-92.

Lippmann T.C. and Holman R.A. (1989) - *Quantification of sand bar morphology: a video technique based on wave dissipation*. Journal of Geophysical Research, 94(C1), pp.995-1011.

Monti C., Guerra F., Balletti C., Miniutti D. (1999) - *Geometric operations in digital images*. Atti XVI International Symposium CIPA. Olinda.

Ojeda E. and Guillén J. (2005) - *Movilidad de la linea de costa en playas urbanas muy encajadas*. En: Tendencias actuales en geomorfología litoral. Editores: Hernández, L., Alonso, I., Mangas, J. y Yanes, A., Universidad de Las Palmas de Gran Canaria: 25-30.

Pedrozo-Acuña A., Simmonds D.J., Otta A.K., Chadwick A.J. (2006) - *On the cross-shore profile change of gravel beaches*. Coastal Engineering, 53: 335-347.

Plant N.G., Holman R.A (1997) - *Intertidal beach profile estimation using video images*. Marine Geology 140: 1-24.

Silvester R., Tsuchiya Y., Shibano T. (1980) - *Zeta bays, pocket beaches and headland control*. Proceedings of 17th International Conference of Coastal Engineering, ASCE 2: 1306–1319.

Van Wellen E., Chadwick A.J., Mason T. (2000) - *A review and assessment of longshore sediment transport equations for coarse-grained beaches*. Coastal Engineering, 40: 243-275.

A video system application to assess the morphological evolution of the Levanto gravel beach (La Spezia, Italy), protected by defence work

**Chiara F. Schiaffino, Claudia Dessy,
Marco Ferrari, Nicola Corradi**

Video monitoring is an efficient aid for analysing beach morphological asset and its evolution in time. Moreover, video monitoring allows evaluating the efficiency of management actions for coastal protection. Aim of this study is to assess the effects of a submerged breakwater upon the morphological evolution of a selected coastal region. As known, this kind of protection work can cause sediment accumulation and the consequent formation of a beach salient in the protected area. The evolution in time (erosion/accretion) of such salient, related to the intensity of wave conditions, allows determining the efficiency of the breakwater.

The pocket beach of the town of Levanto (La Spezia, Liguria), is mainly constituted by mixed sand and gravel sediments; it is divided into three separated cells by two transversal groins; moreover, the central sector is protected by a submerged breakwater.

Between 2004 and 2005 the western and central cells were nourished with gravel ($D_{50} = 30$ mm). For this study images were acquired in regular intervals by two webcams during the 12 months following nourishment completion. The acquired data were related to hydrodynamic data recorded by the R.O.N. buoy of La Spezia, in order to evaluate the evolution of coastal morphology in relation to wave conditions.

The evolution of the morphological asset of the littoral was studied by jointly analysing the acquired images and the relative wave conditions. There are basically three different evolutionary phases of the salient: (1) under minimal wave heights the shoreline morphology shows scarce variability; (2) under moderate wave intensity sediments accumulate and form the salient; (3) under intense wave conditions the morphology is destroyed and the shoreline is uniform.

Introduction

Submerged breakwaters are widely used worldwide (Dally & Pope, 1986; Tomalla & Vincent, 2003; Lamberti & Zanuttigh, 2005; Iskander et al., 2007). Those structures protect the coastline from direct wave impact. The dispersion of wave energy, realised through wave breaking further offshore, diffraction, refraction and reflection of waves, is among the main functions of such protection works (US Army Corps of Engineers, 2002). In general the flux of water related with waves approaching the coast overtops the barrier, while the backwash concentrates in the gaps (Johnson et al., 2005). Some studies show that submerged breakwaters offer very effective protection for coasts characterised by moderate wave energy (Pylarczyk et al., 2003).

Experimental data show that a typical impact of a submerged breakwater upon the shoreline is the development of a salient (Hsu & Sylvester, 1990; Dean et al., 1997; Zyserman & Johnson, 2002). There are a few data available about the evolution of gravel beaches protected by artificial barriers (Van Gent, 1995; Pranzini & Farrel, 2006). The aim of this study is to analyse the effects of a submerged breakwater upon the morphological evolution of the mixed sand and gravel beach of Levanto. The effects of this structure on the foreshore were assessed through a video monitoring system, which allowed continuous analysis in time of the morphodynamic state of the beach, therefore representing a versatile tool for coastal process analysis (Aarninkhof & Roelvink, 1999).

Study area and coastal protection works
The beach of Levanto, located in the eastern Liguria and included in the littoral cell of Punta della Madonna and Punta Picetto, was analysed in this study (Figure 1).
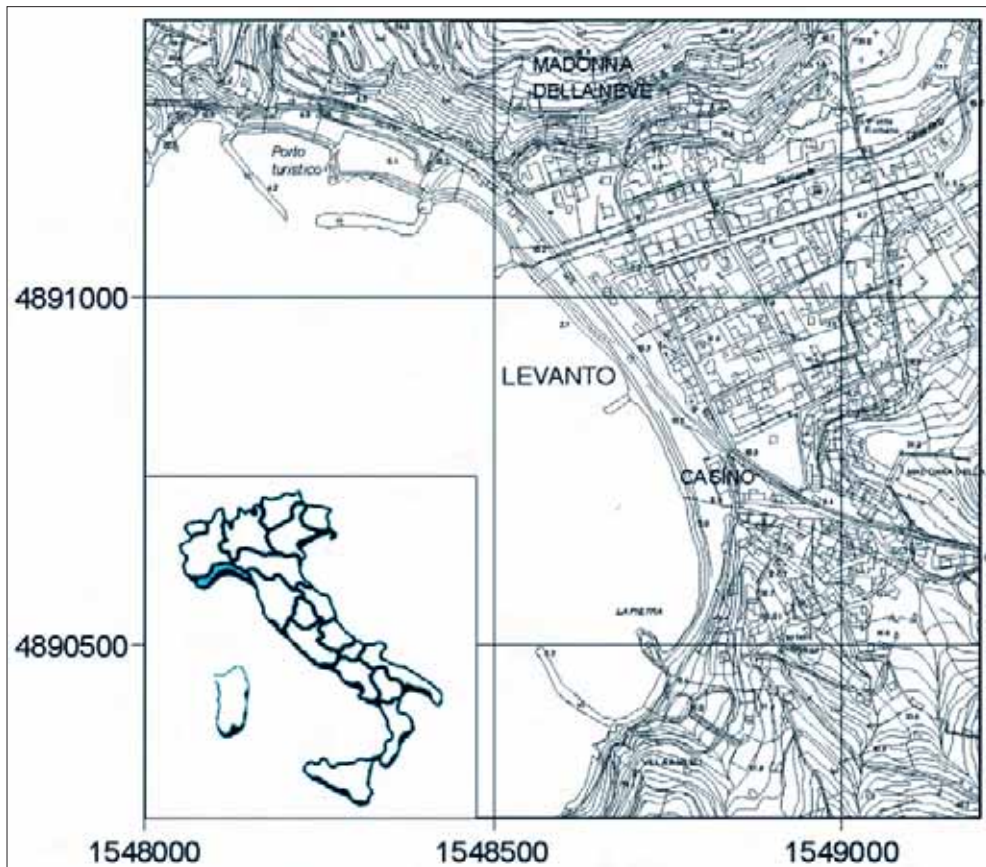
Figure 1 - Location map (CTR vettoriale, Servizi Informativi Territoriali e Ambientali Regionali, Regione Liguria).

This coastal region is NNW-SSE oriented and the beach, located between the promontories of Punta Gone (W) and Punta Picetto (E), can be classified as a pocket beach (Silvester et al., 1980).
The sediment grain-size of the intertidal area ranges between 0.30 mm and 11.30 mm and decreases in off-shore direction until 0.12 mm.
Beach grain-size decreases from W to E, from a gravel fraction of 70% to less than 30% due to the longshore drift towards the East.

The beach length is ca. 800 m and it can be divided into three separated sectors (Figure1) due to the presence of two groins. The western sector (150 m length and 35 m depth) and the central sector (250 m length and 35 m depth) show a moderate erosive trend, while the eastern sector (400 m length and 43 m depth) has been stable over the years. Coastal protection in this area is the result of multiple successive management schemes started in the beginning of last century.

The groins, which subdivide the beach, have, respectively from W to E, a length of 30 m and 40 m. In November 2005 those two structures have been reinforced at the basis with the aim of reducing backwash around them. The submerged breakwater built between the groins, 65 m off the shoreline, is 100 m long and 7 m wide and reaches 2 m below water surface. Two gaps of about 30 m and 40 m width are created between the two groins and the barrier. The last soft-protection management scheme of the central and western sectors was realised between fall 2004 and spring 2005. The used material, about 16000 m^3 of gabbros and basalts from a quarry in the hinterland, were crushed in order to obtain a mean grain-size of 30 mm.

Wave conditions

Levanto beach can be considered a microtidal area, being ordinary tidal excursions about 30-40 cm. The considered shoreline has a prevailing wind sector between 190°N and 280°N, therefore is exposed to waves and currents generated from SW and partly from the S and SE.

Since 1999 the hydrodynamic conditions have been registered by a buoy (43° 55' 41.99" N; 09° 49' 36.01" E) belonging to the Rete Ondametrica Nazionale (Hydro-Marine National Network) and located off La Spezia coast at a depth of about 90 m.

From the acquired data can be seen that dominant wave as well as frequent wave originate from SW, while secondary wave originate from W and S, according with data included in MEDATLAS (2004). R.O.N. data (http://www.idromare.com a service provided by APAT) for the period 2005 - 2006 provide a significant wave height lower than one meter in 83% of the cases (Figure 2). During the considered year there were 20 storms (H_s > 1.5 m) lasting on average about 2-3 days.
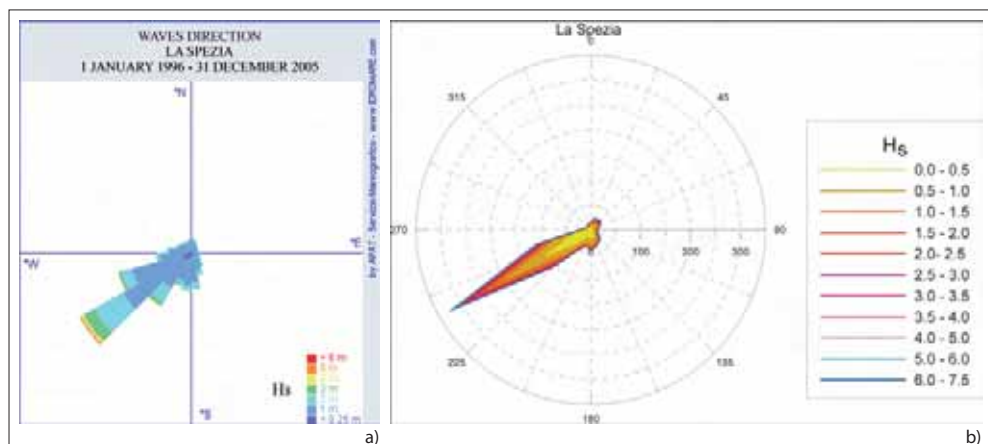
Figure 2 – a) Average direction of origin of waves on a ten-year basis (1996-2006), data from APAT; b) Polar Plot of wave height during the period 1996-2004, data from MEDATLAS.

Video-monitoring

The video station, operative between June 2005 and June 2006, consisted in 2 webcams located on the top of a building near the eastern sector of the beach, at height of 16 m upon sea level. Both webcams were pointed in NW-direction: the first allowed a panoramic view of the three sectors of the beach, while the second recorded exclusively images of the central and western sectors last nourished in 2005 (Figure 3).

Figure 3 – a) Panoramic snapshot image; b) Zoomed snapshot image.

Three acquisitions per day took place at 8 a.m., at 12 a.m. and at 4 p.m., in order to guarantee homogeneous data gathering during daytime. During every acquisition-cycle photos were taken every 2 minutes for a period of 8 minutes.

The registered images, having a resolution of 1280x960 pixels, were elaborated using common image processing techniques (Holman et al., 1993; Aarninkhof et al., 1999; Alexander et al., 2004; Davidson et al., 2004). All images were georeferentiated, rectificated and averaged by means of a dedicated software.

In total 4300 images were used for evaluating the morphological evolution of the beach face influenced by the submerged breakwater; the data derived from the video monitoring have been integrated with available hydrodynamics data for the study area.

Results

Information derived from video-monitoring was integrated with wave condition analysis in order to define the processes that characterise the evolution dynamics of the shoreline.

Numerous hydrodynamic models have been used in literature for investigating evolution processes of sandy beach shorefaces influenced by parallel barriers (Hanson & Kraus, 1991; Zyserman & Johnson, 2002; Jhonson et al., 2005; Pilarczyk, 2003).

According to Ranasinghe & Turner (2006) water fluxes generated by waves approaching the coastline overtop the barrier until they interact with the longshore current. The meeting of those two currents generates a decrease of sediment transport capacity and the deposition of material along the beach face. Water accumulates nearshore and successively generates fluxes in opposite direction at both ends of the barrier. The barrier creates therefore significant changes in the coastal dynamics.

In Levanto gravel beach circulation within the central cell is strongly influenced by the presence of the two groins and the submerged breakwater. The analysis of available snapshot images allows determining the presence of a salient (Figure 4).

Figure 4 – Morphodynamic model of Levanto beach based upon empiric data.

The deposition of this accumulation structure and its evolution in time are strictly connected with wave conditions and influenced by the direction of wave origin as well as the velocity of increase or decrease of wave height.

$H_s < 0.5\ m$

If significant wave height is lower than 0.5 m the salient is in a maturity state independently of the wave origin direction. Due to low wave energy, the accumulated sediment is not elaborated and its form is not modified. In Figure 5 a well developed salient is shown. This picture was recorded during a calm day characterised by waves from SW and wave height about 0.5 m.

Figure 5 – Snapshot image 23 July 2005, 8.05 a.m., waves from SW; H_s = 0.5m.

$0.5\ m < H_s < 1\ m$

If wave height range is in this interval, the submerged breakwater cannot completely disperse wave energy. Different salient evolution states were determined in relation with wave conditions.

If wave height increases within 12 hours, from values below 0.5 m to values greater than 1 m, the salient is destroyed. However, if H_s oscillatory increases the morphology of the salient is maintained.

When a gradual decrease of wave height occurs and the direction of waves is constant, the images show a continuous and slow accretion of the shoreline until the salient is formed. Figure 6 shows a

Figure 6 – a) Snapshot image 13 September 2005, 8.01 a.m., wave origin: W and H_s = 0.4 m.; b) Snapshot image 14 September 2005, 12.03 p.m., wave origin: SW and H_s = 0.32 m.

Figure 7 – a) Snapshot image 21 May 2006, 12.03 p.m., wave origin: SW and H_s > 2.5 m.; b) Snapshot image 22 May 2006 12.03 p.m., wave origin: SW and H_s = 0.6 m.

case in which wave originate from W-SW; although wave height slowly decreased from 0.90 m on September 12th 2005 at 8.00 a.m. to about 0.35 m on September 14th 2005 at 8.00 a.m., the morphology of the salient was not formed yet. The salient started appearing only after 12.00 a.m. on September 14th 2005, when wave height was about 0.30 m.

When an abrupt decrease of wave height occurs (within 12 hours), it is not common to observe salient formation. This is due to the lack of time for waves to rearrange sediments transported to the foreshore during the storm. In Figure 7 a salient in formation is to be seen. In this case wave height was about 0.6 m originating from S. During the preceding days a very intense storm with waves from SW occurred; wave height were initially greater than 2.5 m and quickly decreased.

$H_s > 1\ m$

Under this conditions the submerged barrier can not efficiently break waves, which overtop it without significant changes. High wave energy causes the redistribution of salient material in the shoreface thus completely destroying the morphology.

Under wave conditions originating from SW, very rapid salient destruction can occur (within 12 hours). A similar evolution takes place, although less rapid in time, under wave conditions originating from other directions.

The image in Figure 8 shows a condition where wave height is 1.10 m and the shoreline is uniform. The salient was destroyed due to intense wave energy during the previous days: wave originated from SW reached heights greater than 2 m.

Figure 8 – Snapshot image 15 August 2005, 8.07 a.m., wave origin: SW and H_s = 1.10 m.

Conclusions

Based on the presented analysis three evolution phases of the salient have been determined in relation with wave conditions:

– If wave height is lower than 0.5 m sediment transport is limited and no change to salient occurs, which is always present.
– If wave height ranges between 0.5 m and 1 m, different salient evolution patterns take place in dependence of different wave conditions.
– Under very rough wave conditions and wave height greater than 1 m the salient is destroyed and the shoreline is uniform.

The hydrodynamic behaviour of the mixed sand and gravel beach of Levanto, empirically determined in this study, is similar to those modelled for sandy beaches in existing literature.

On this basis of the presented study, a wave height of 1 m can be assumed as the upper limit for efficient coastal protection by means of the existing barrier. Lower waves are easily diffracted, forming the salient, while higher waves possess enough energy to redistribute the sediment previously accumulated, which is dispersed along the shoreface.

References

AA.VV (2004) - *Wind and wave atlas of the Mediterranean sea*. Western European Union, Western European Armaments Organisation Research Cell, pp. 386.

Aarninkhof S.G.J. and Roelvink J.A. (1999) - *Argus-based monitoring of intertidal beach morphodynamics*. Coastal sediments: 2429-2444.

Aarninkhof S.G.J. and Roelvink J.A. (1999) - *Argus-based monitoring of intertidal beach morphodynamics*. Coastal sediments: 2429-2444.

Alexander P.S. and Holman R.A. (2004) - *Quantification of nearshore morphology based on video imaging*. Marine geology, 208: 101-111.

Davidson M.A., Aarninkhof S.G.J., Van Koningsveld M. and Holman R.A. (2004) - *Developing coastal video monitorino system in support of coastal zone management*. Journ. Coastal Research, S.I. 39.

Dean R.G., Chen R. and Browder A.E. (1997) - *Full scale monitoring study of a submerged breakwater, Palm beach, Florida, USA.* Coastal Engineering, 29: 291-315.

Hanson H. and Kraus N.C. (1991) - *Numerical simulation of shoreline change at Lorain, Ohio*. Journal of Waterway, Port, Coastal, and Ocean Engineering, 117: 1-18.

Holman R.A., Sallenger A.H., Lippmann T.C. and Haines J.W. (1993) - *The application of video image processing to the study of nearshore processes*. Oceanography, 6: 78-85.

Hsu J.R.C. and Sylvester R (1990) - *Accretion behind single offshore breakwater*. Journal of Waterway, Port, Coastal, and Ocean Engineering, 116: 362-380.

http://www.beachmed.com.

http://www.idromare.com a service provided by APAT.

Istituto Idrografico della Marina - *Tavole di marea (Mediterraneo – Mar Rosso) e delle correnti di marea (Venezia – Stretto di Messina)*. Divisione Editoriale- Istituto Idrografico della Marina, pp. 112.

Johnson H.K., Karambas T.V., Avgeris J., Zanuttigh B., Gonzalez-Marco D. and Caceres I. (2005) -*Modelling of waves and currents around submerged breakwaters*. Coastal Engineering, 52: 949-969.

Pranzini E. and Farrel E.J. (2006) - *Shoreline evolution and protection strategies along the Tuscany coastline, Italy*. Journal of Coastal Research, S.I., 39: 843-848.

Pylarczyk K.W. (2003) - *Design of low-crested (submerged) structures - an overview*. 6th International Conference on Coastal and Port Engineering in Developing Countries, Colombo, Sri Lanka.

Ranasinghe R. and Turner I. (2006) - *Shoreline response to submerged structures: a review.* Coastal Engineering, 53: 65-79.

Silvester R., Tsuchiya Y. and Shibano T. (1980) - *Zeta bays, pocket beaches and headland control*. Proceedings of 17th International Conference of Coastal Engineering, ASCE 2: 1306–1319.

US Army Corps of Engineers (2002) - *Harbor hydrodynamics*. Coastal Engineering Manual, CEM II (7): 3-30.

Van Gent M.R.A. (1995) - *Wave interaction with berm breakwaters*. Journal of Waterway, Port, Coastal, and Ocean Engineering, 121: 229-238.

Zyserman J.A. and Johnson H.K. (2002) - *Modelling morphological processes in the vicinity of shore-parallel breakwaters*. Coastal Engineering, 45: 261-284.

Long trend shoreline evolution of a beach protected by structures

Renata Archetti, Alberto Lamberti

The purpose of this study is to analyse the shoreline response of a beach protected by a system of low-crested-structures (LCS) and to apply the results to the management of coastal stability problems. These aims are achieved by selecting and monitoring the appropriate Coastal-State-Indicator (CSI) to describe the state of the beach. The CSI used is the Mean-Intertidal-Position (MIP), which has been detected by the Argus system installed in Lido di Dante, Italy.

The error in the shoreline estimation from video was assessed by comparing shorelines detected with GPS and image analysis over a large number of cases. The horizontal error in the shoreline detection is estimated to be on the order of 0.90 ± 0.74 m, which is acceptable because it is on the same order of magnitude as the swash width.

The MIP, which has been monitored over a four-month period with elevated spatial and temporal resolution, was monitored in several transects of the beach protected by a system of LCS and boundary groynes, creating two cells. The behaviour of the section in the middle of the cell was comparable to the behaviour of the total beach. Results were analysed with respect to the fixed beach state of the initial beach position (January, 2004). The MIP regression rate is around 2.3 m/year, which is modest considering the local subsidence magnitude (1.8 cm/year). Therefore, the actual data do not show any evidence of immediate risk either for the present structures on the beach or for the infrastructure immediately behind; however, the results do show a risk for the sustainability of the characteristics that permit tourist development. The use of video-derived CSIs is confirmed to offer a valuable tool for coastal management.

Introduction

The coastal zone is an important economic, social and environmental resource. One of the principal problems that coastal managers frequently have to deal with is the erosion of the shoreline. Numerous reasons have been argued to be the cause of this problem: fluvial regulation and the subsequent loss of sediment arriving to the coastal environment, rising sea levels, and human activities like coastal engineering work that blocks the littoral drift.

Compared to the emergent breakwaters used in the past, submerged parallel breakwaters or low crested structures for shoreline protection are becoming more popular due to their low aesthetic impact, their capability of allowing more water recirculation, and their offer of beach protection from a more sustainable method. Their construction is often combined with sand nourishment schemes.

The primary functions of these structures are: (1) to reduce wave energy at the shoreline, (2) to redistribute the sediment transport pattern and create desirable beach features, and (3) to provide toe support for beach slopes as perched beaches.

Several recent studies and research programs have evaluated the environmental impact of low crested structures (LCSs), but little literature is available on the response of beaches protected

by this kind of structure. The Delos Project (www.delos.unibo.it) studied the hydrodynamic processes induced by LCSs (Cáceres et al., 2005; Van der Meer et al., 2005; Archetti and Lamberti, 2006), and the morphodynamic changes close to roundheads have been described both by Zyserman et al. (2005) and by Zanuttigh (2007). Recently, Cáceres et al. (2007) quantified current intensities induced by wave overtopping around LCSs.

The present study focuses on the quantification of coastal state information from a video monitoring technique and the interpretation of that information in an end-users context. This paper adopts a predictive approach by discussing the role of video imagery in predicting coastal evolution where the coastline is defended by a LCS system.

The observation of shoreline changes is routinely carried out not more than twice a year. The "Regione Emilia Romagna" (the Regional Authority), which is one of the most up-to-date institutions in Italy and is committed to elaborating guidelines for integrated coastal management, commissions one general bathymetric survey of the regional coast every five years and a low elevation flight to monitor the position of the shoreline once a year at most. A survey carried out with such a low frequency loses a great deal of important information, such as the seasonal variability of morphodynamic behaviour. Results based on an infrequent survey can lead to a completely different understanding of coastline evolution trends. For example, traditional surveys monitoring a transect in Egmond, the Netherlands, where the beach volume was collected 6 times in 2 years, did not show the large variability of the mean shoreline position and were not able to point out seasonal variations. On the contrary, a daily survey with video observation showed much greater variability (Kroon et al., 2007) and a different trend in coastal evolution.

In 2003, an Argus video monitoring station for high spatial and temporal resolution of coastal processes was installed in Lido di Dante beach in the northern Adriatic Sea (Italy) in the framework of the 5th European Funded Project CoastView (www.TheCoastViewProject.org), and maintained during the Beachmed-e OpTIMAL project. A description of the Argus Video system and of the study site is given in the paper in this volume by Archetti et al. This work aims to document the mean shoreline evolution of a beach protected by LCSs.

The study site of Lido di Dante
Lido di Dante is a small tourist area in the Emilia Romagna region on the Adriatic Sea, 7 km South of Ravenna, delimited by the river mouth of Fiumi Uniti to the North and Bevano river to the South (Figure 1). The use of the beach for tourist purposes and its problems of erosion began in the 1970s, and made it a site of scientific interest for researchers and coastal managers. Lido di Dante has been, in fact, one of the study cases during the research project DELOS (Lamberti et al., 2005) and during the CoastView project. Lido di Dante is a combination of a protected and an unprotected beach, in fact the northern part of the study area (Figure 1) is protected by three groins and a parallel semi-submerged barrier, while the southern part is not protected. The site therefore is of particular interest, as it gives the opportunity to study the dynamics of the protected beach and those not protected simultaneously, from the same point of observation.

The system of groins and barriers form two cells that are called the North Cell and the South Cell. The beach has been artificially maintained by nourishment almost constantly in the past few years, with around 8,000 m^3/year generally filled in spring before the beginning of the tourist season.

Argus data analysis
The shoreline detection
The shoreline is defined as the intersection curve between the beach surface and the sea surface. It moves up and down, but its position at any fixed elevation is constant over the short term. The detection interval has to be sufficiently long to filter out the effect of rapid variability of wave elevation on the beach due to wave run-up and run-down, but also sufficiently short to be referred to as a contemporary water level. The timex image is averaged over ten minutes, and the seawater level measured by the local tide gauge is also measured with a ten-minute interval.

The shoreline is associated with a contemporary sea level and, in any given instant, represents an isodepth as defined by Boak and Turner (2005). The procedure to quantify the intertidal beach is generally based on two steps: first, the position of the shoreline is detected on rectified timex images, and second, the associated vertical elevation is estimated from the available data (tide gauge) and hydrodynamic conditions during the image acquisition time. These procedures produce a sequence of isodepths in the intertidal beach. The temporal series of such contour lines (isodepths) detected during a tidal cycle allow for interpolation and plotting of the three-dimensional beach surface between low tide and high tide. This procedure is described in Aarninkhof et al. (2003). The intertidal bathymetry was used as a significant indicator in several studies, and was also detected with other remote sensing technologies, for example with the use of radar (Takewaka, 2005). In the following analysis, the Argus IBM toolbox, developed following the Pixel Intensity Clustering (PIC) methodology (Aarninkhof and Roelvink, 1999; Aarninkhof, 2003), is applied to detect the shoreline position. Feature (wet/dry) discrimination is performed on timex images according to the principle of the intensity distribution in the Hue Saturation Value domain (HS and V). Pixels are clustered into two dominant categories (wet/dry) separated by the beach shoreline.

An example of two intertidal beach bathymetries is shown in Figure 2. The red bathymetry was "surveyed" on 25 Jan 2005, and the green one on 08 February 2005.
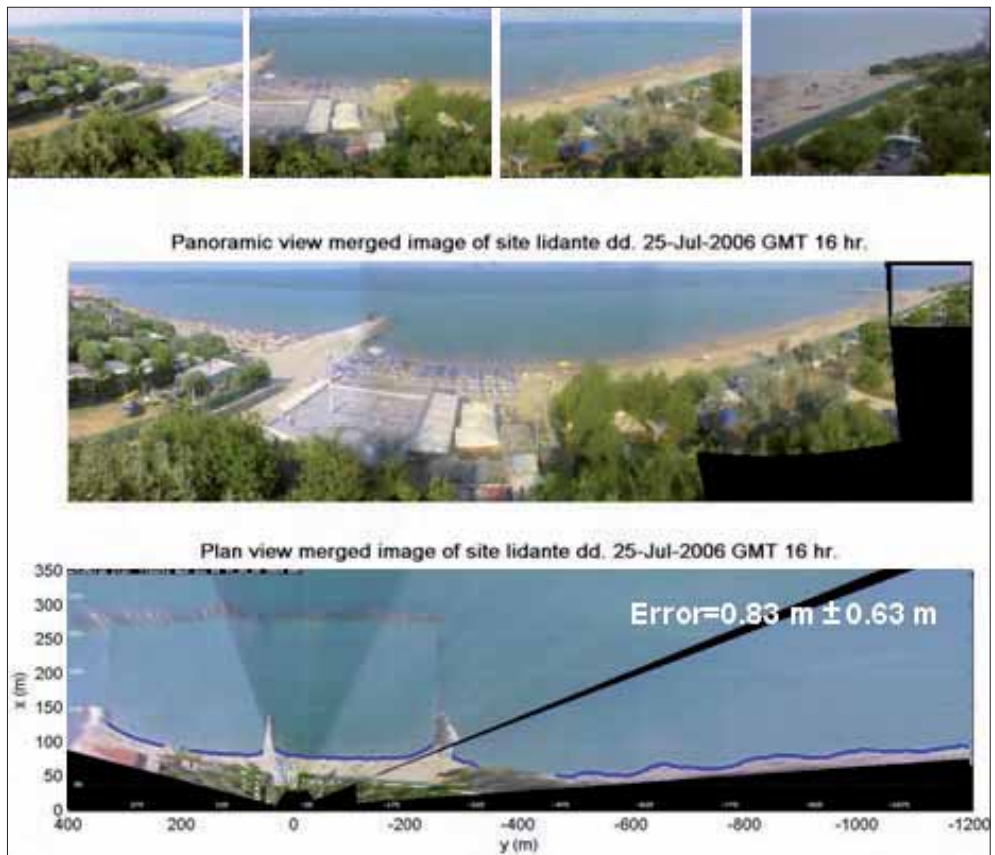
Figure 1 - Images taken by the Argus station in Lido di Dante; Merge image; plan view image of Lido di Dante and shoreline detected (blue line)
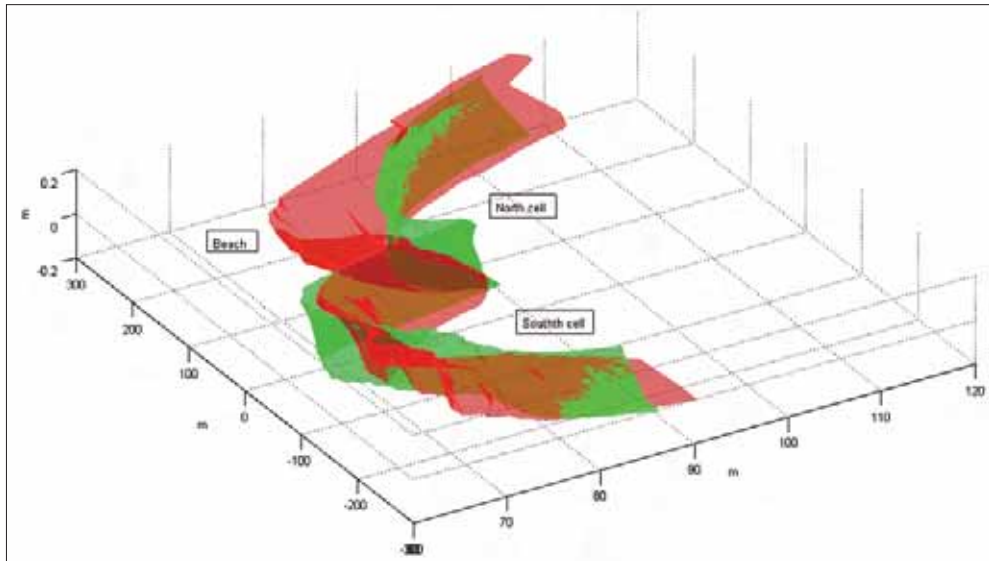
Figure 2 - Two intertidal beach bathymetries "surveyed" on 21 January 2005 and on 08 February 2005.

Error estimation

The accuracy of the image-derived survey method was assessed by comparison with a beach survey regarding the beach protected by LCS. The survey was obtained with a GPS (Global Positioning System) used in Differential Kinematic mode.

The error of the topographical survey of the shoreline and of the intertidal beach is attributable to the following factors: the horizontal uncertainty induced by the ortho-rectification process; the uncertainty due to the shoreline detection process and the vertical uncertainty due to the transfer of the sea level data from the tide gauge at Porto Corsini (Ravenna) to Lido di Dante (approx. 10 km distant).

A data set of 41 shoreline measurements was collected at Lido di Dante from 15 to 22 July 2004. The shoreline surveys were carried out by moving a GPS in the kinematic mode: measurements were done by walking on the beach, at the centre of the swash zone, at constant velocity of approx. 0.5 m/s, over a distance of about 800 m alongshore, in the protected area delimited by the external groins. The climate conditions during the survey were extremely calm: measured offshore waves were lower than 0.15 m and the water in the protected zone was extremely still (the survey dates had been chosen appropriately). During the experiment, the tidal level spanned a range between -0.5 m and + 0.3 m with respect to the mean sea water level.

The survey was carried out on an hourly basis, simultaneously with the recording of time-averaged (Timex) video images by the Argus station: we have started from South, in the field of view of *camera 2* at 10 minutes past hour, *camera 3* at 20 minutes past hour and the last *camera 4* at 30 minutes past hour. The post-processing correction of the single frequency GPS (model SR510 by LEICA Geosystems) data through the data collected simultaneously by a close Continuously Operating Reference Station (CORS) produced data with centimetre precision. The RINEX file used comes from the CORS managed by the Department of Geophysics of the University of Bologna located in Marina di Ravenna, about 8 km from the survey area.

Video derived shorelines were detected on the video-images using the IBM tool and all shorelines were interpolated to regular intervals (1 m) in the longshore.

The deviations between Argus-derived data and GPS-surveyed shorelines in alongshore position y (see Figure 3 for local geographic reference) at time t were defined as:

$$\delta_d(y,t) = x_G(y,t) \, \delta \, x_A(y,t) \qquad\qquad [1]$$

where $x_A(y,t)$, $x_G(y,t)$ represent the shoreline position at alongshore position y and time t as detected from the Argus video analysis and the GPS survey, respectively and interpolated in order to have data at 1m spacing alongshore. When $\delta_d(y,t)$ is negative, it means that the shoreline detected using Argus system was landward with respect to the GPS survey and vice versa, when $\delta_d(y,t)$ is positive it means that the shoreline detected by Argus was seaward with respect to the GPS survey.

The shoreline is not detectable with Argus around section 200 as it is masked by a small building located in the Northern cell of the beach.

Figure 3 shows the mean (over the 41 surveys) of the deviation between the Argus-based and GPS-surveyed in the alongshore position y $\delta_d(y,t)$ (central panel), and the mean of the absolute value of $\delta_d(y,t)$ at each alongshore coordinate.

We observe high deviation between measurements close to the central groin (coordinate x = 60 m in Figure 5) and at the boundary groins, due to the difficulty in the survey of the shoreline with Argus, as the groin masks the shoreline.

The following zones were selected: the Northern cell (395 < y < 220 and 190 < y < 60) and the Southern cell (30 > y > -220) (Figure 4); in the selected zones, the groins were excluded from the analysis. Except for these outlier data, the $\delta_d(y,t)$ ranges between 0.46 m to 1.33 m, within a distance of ± 300 m from the Argus station. The $\delta_d(y,t)$ is in most cases positive, so in general the shoreline detection made by GPS is seaward. Lowest error of 0.46 ± 0.50 m is in section 120.

The mean of the absolute $\delta_d(y,t)$ is equal to 0.90 m; the mean of standard deviation is 0.74 m. The greater errors are estimated in the shoreline comparison during the early morning, when the sunrise leads to difficulty in detecting the shoreline position.

The value of 0.90 ± 0.74 m can be assumed as the horizontal uncertainty induced by the ortho-rectification process and due to the shoreline detection process (e_HShoreline).

The cross-shore pixel resolution within a length of ± 300 m from the Argus station ranges from 0.1 m to 1 m, being of the same order of the error found. We expected that the error increased with the distance, in reality we do not see any clear linear trend of the error with the distance.

A first comparison between video-derived and GPS surveyed shoreline measurements in the unprotected zone of Lido di Dante is described in Armaroli et al. (2004), but an estimation of the error is not provided.

Shoreline evolution

To enable observation of the changes in the shoreline mobility, the mean intertidal beach position has been estimated in reference to an initial configuration in order to study its behaviour over time. The MIP, mean intertidal position, is defined as a mean intertidal volume position in a meter strip of the coast.

The MIP is similar to the consolidated indicator used in the Netherlands, the momentary intertidal coastline (MICL) (Van Koningsveld and Mulder, 2004), which is defined as the mean position of the coastline between the dune foot and the lower limit of the intertidal beach. In the case of Lido di Dante, the MICL cannot be defined since there are no dunes in the back-beach; therefore, we decided to describe the mean intertidal coastline position with respect to an initial bathymetry in the intertidal zone (08 January 2004), which was located approx. 55 m from the back of the beach, where a wall (1m of height) is placed to prevent water that reaches the back of the beaches, during extreme events, from flooding streets and houses. Risk of flooding of the urban area behind the beach exists in the case where beach width reaches 20 m or less. In Lido di Dante, and in general in the beaches of the Romagna littoral, the intertidal beach has a tidal range of approximately 0.5 m - 1.0 m with an average intertidal slope of 1:15 and extends in a cross-shore direction for approximately 7.5 m – 15 m.
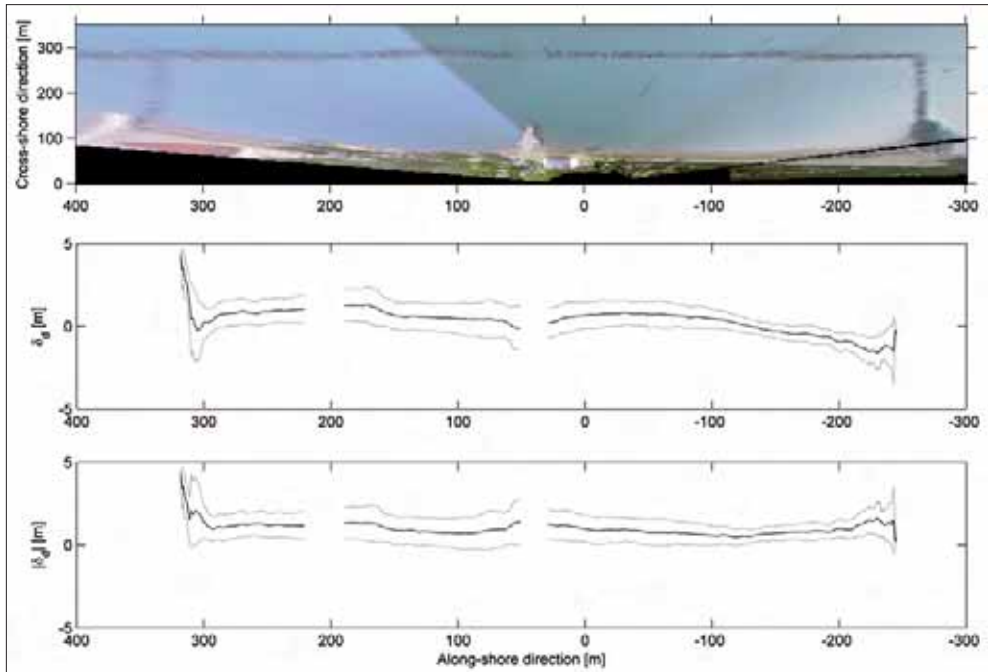
Figure 3 - Deviation between the Argus-based and GPS-surveyed in the alongshore position y δ_d (y,t)(central panel) and the mean of the absolute value of δ_d (y,t) at each alongshore coordinate.

The selected CSI MIP was detected using the technique explained in the previous paragraphs for the years 2004, 2005, 2006 and 2007 (until April) in the protected beach at Lido di Dante. The frequency of the video survey was determined by the periodic variations in the amplitude of the tidal excursion (which determine the extension of the measurable area) and by the meteorological conditions, so we detected 72 intertidal bathymetries during approximately 3.5 years. In this analysis, we carried out a video "survey" only during days with very calm sea and a wide tidal excursion. Surveys carried out with such a frequency allow for the observation of beach evolution in a continuum.

An interval of tidal excursion corresponding to ± 0.20 m, centred on the mean sea-water level, is common for all 72 intertidal bathymetries. The vertical intertidal beach ranging within ± 0.20 m represents, therefore, a monitorable zone of the intertidal strip of Lido di Dante beach.

All bathymetries in the intertidal zone were compared with the initial bathymetry from 08 January 2004 at the beginning of this study.

Figure 4 shows the Mean Intertidal Position in time, in respect to the initial intertidal position in the Lido di Dante beach protected by the LCS system; the plot is a measure of how the mean intertidal position goes forward and retreats in the whole studied area and represents the average behaviour of the whole zone. On the same plot, the sea-water level recorded in Porto Corsini (top panel) and the off-shore significant wave height (central panel) are shown.

The vertical lines in Figure 4 represent the sand nourishment events or sand rearrangements during the study period.

This study reveals that the sporadic survey of the shoreline carried out a tantum (at annual or biannual sampling frequency, for example) can be misleading, because it creates a photograph that is too dependent on the time of acquisition.
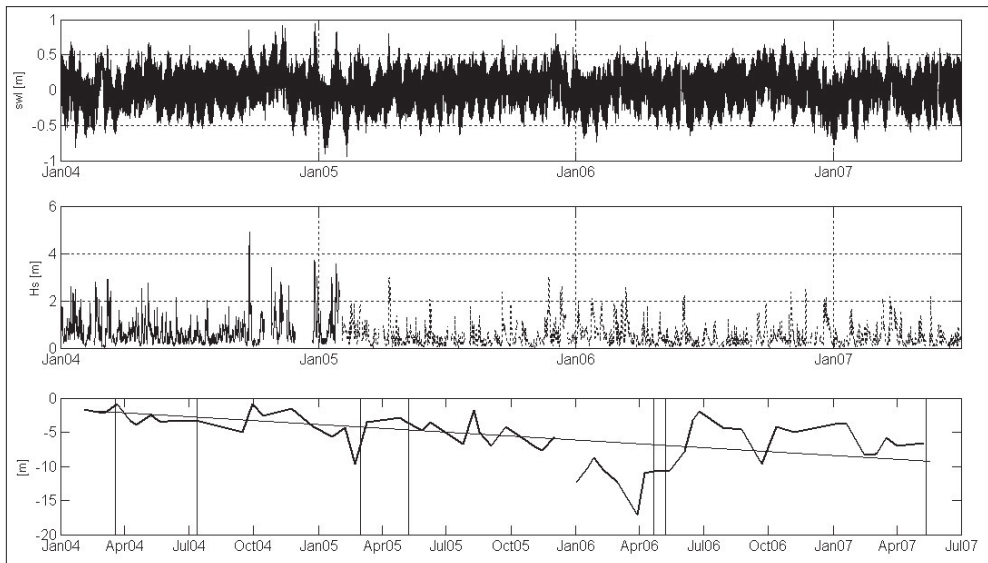
Figure 4 - Sea water level in Porto Corsini (top panel); Significant wave height (central panel): bold line from the buoy located in offshore in the Northern Adriatic Sea, and dot line from SWAN data. MIP in the protected part of Lido di Dante beach in respect to the initial bathymetry (bottom panel). Vertical lines in bottom panel are the nourishment events and rearrangement of the beach.

At the beginning of winter 2004, a series of storms occurred, causing an overall retreat of approximately 1.5 m within three months for the MIP (Figure 4). Following those events, the position of transects was relatively stable during spring and summer. A significant storm from the SE occurred on 24 September 2004 with an offshore wave height reaching 3.8 m, resulting in a momentary increase of the beach instead of the expected erosion. Storm surges from the SE are generally coupled with high sea levels; on this occasion, the LCS system was completely submerged. During intense storms, the overtopping and the wave transmission is considerable (Caceres et al., 2005), and the transmitted waves transport the sediment inside the protected zone of the beach, resulting in sediment deposition in the area. During the storm of 24 September 2004, wave run-up reached a very high level, and consequently the beach was completely flooded and sand bars were generated. Sediment transport from the upper part of the beach to the lower part is responsible for the increase in the beach slope and the short-term momentary accretion of the beach (Zanuttigh, 2007).

At the end of 2004, the total transect withdrawal results were on the order of 1.5 m ± 1.0 m (Kroon et al., 2007). This value is low considering that the beach was subjected to very strong storms in 2004. During the first weeks of 2005, the beach was subjected to several storms and reacted by regressing (in March 2005, the total positions had withdrawn 10 m with respect to their position at the beginning of January 2004.) After a nourishment in March-April 2005, beach enlargement was observed in the spring, and the beach was relatively stable in the summer. In 2006, the winter was characterised by a series of storms from the North (Hs = 3.5 m, Dir = 62°N), alternating with storms from the South (H_s = 2.5 m, Dir = 180°N). The storms caused a strong regression, and the beginning of March 2006 yielded the maximum beach regression since the beginning of the analysis (total regression was estimated as 12 m). This critical condition was observed in all transects, reaching in some sections a temporary regression of 20 m. This was the most critical situation observed over the four years. After sand nourishment in May 2006, a return to the previous situation was observed, and the beach was semi-stable in the spring and summer. The total MIP shows some fluctuations equal to ± 3.5 m in the winter period and ± 1 m in the summer period.

After three years and four months of observations, a seasonal pattern of behaviour is clear. Strong storms from the North occur in the winter and are responsible for a withdrawal of the beach, and nourishments are usually planned in spring (April – May) before the tourist season begins (except in 2004, when nourishment was carried out in the preceding autumn instead). In summer, the beach is stable due to mild conditions and recent nourishment. Based on the total data, we observe that the position of the beach in the intertidal zone (the total MIP) shows a regression trend of about 2.3 m/year.

Conclusions

This work has presented the results of 40 months of high-frequency video monitoring of the shoreline position of a beach protected by a system of breakwaters in Lido di Dante, Italy.

The error in the detection of the shorelines in Lido di Dante using the Argus video station was carefully estimated to a value of around 0.90 ± 0.74 m in the cross-shore direction. This value is completely acceptable, being on the same order of magnitude as the excursion of the swash-zone width during calm days.

The mean position of the intertidal zone (MIP) is an appropriate indicator to describe the state of the coast; in 40 months, a total of 72 MIP measurements were detected based on video analysis in several transects and for the whole beach (as an average of all transects). It was observed that the behaviour of the section in the middle of the cell is comparable to the behaviour of the total beach, so results are given in terms of the Mean Intertidal Position of the whole protected beach.

This study reveals that a sporadic coastline survey carried out with annual or bi-annual frequency can be misleading.

The time series of the MIP of the protected beach demonstrates a regression tendency equal to about 2.3 m/year. The instantaneous position of the intertidal bathymetry can vary within a range of about ± 3.5 m in winter and ± 1 m in summer. This trend is due in part to the strong subsidence at the site, based on the last published data on subsidence (Teatini et al., 2005) in the order of 1.8 cm/year.

Acknowledgements

References

Aarninkhof S.G.J and Roelvink J.A. (1999) - *Argus–based monitoring of intertial beach morphodimanics*. In Proc. Coastal sediment 1999, New York: ASCE pp.2429-2444.

Aarninkhof S.G.J. (2003) - *Nearshore bathymetry derived from Video Imagery*. PhD-Thesis, Delft University of Technology.

Aarninkhof S.G.J., Turner I.L., Dronkers T.D.T., Caljouw M. and Nipius L. (2003) - *A video-technique for mapping intertidal beach bathymetry*. Coastal Engineering 49: 275-289.

Archetti R. and Lamberti A. (2006) - *Study of hydrodynamic induced by low crested structures through image processing*. Proc. of the XXX ICCE2006. San Diego, 2-7 September 2006.

Armaroli C, Ciavola P., Balouin Y. and Gatti M. (2004) - *An integrated study of shoreline variability using GIS and ARGUS techniques*. Journal of Coastal Research. SI 39. Proceeding of the International Coastal Symposium.

Boak E. and Turner I. L. (2005) - *Shoreline definition and detection: A Review*. Journal of Coastal Research, 21: 688 – 703.

Cáceres I. M., Stive J.F., Sánchez-Arcilla A. and Hai Trung L. (2007) - *Quantification of changes in current intensities induced by wave overtopping around low-crested structures*. Coastal Engineering (in press).

Cáceres I., Sánchez-Arcilla A., Zanuttigh B., Lamberti A. and Franco L. (2005) - *Wave overtopping and induced currents at emergent low crested structures*. Coastal Engineering, 52: 931 – 947.

Kroon A., Aarninkhof S.G.J., Archetti R., Armaroli C., Gonzalez M., Medri S., Osorio A., Aagaard T., Davidson M.A., Holman R.A. and Spanhoff R. (2007) - *Application of remote sensing video systems for coastline management problems.* Coastal Engineering, 54: 493-505.

Lamberti A., Archetti R., M. Kramer, Paphitis D., Mosso C. and Di Risio M. (2005) - *European experience of low crested structures for coastal management.* Coastal Engineering, 52: 841 – 866.

Takewaka S. (2005) - *Measurements of shoreline positions and intertidal foreshore slopes with X band marine radar system.* Coastal Engineering Journal, 47: 91-107.

Teatini P, Ferronato M., Gambolati G., Bretoni W. and Gonnella M. (2005) - *A century of land subsidence in Ravenna, Italy.* Environ Geol, 47: 831846 .

Van der Meer J.W., Briganti R., Zanuttigh B. and Wang B. (2005) - *Wave transmission and reflection at low-crested structures: Design formulae, oblique wave attack and spectral change.* Coastal Engineering, 52: 915 - 929.

Van Koningsveld M. and Mulder J.P.M. (2004) - *Sustainable coastal policy developments in The Netherlands. A systematic approach revealed.* Journal of Coastal Research, 20: 375-385.

www.delos.unibo.it

www.TheCoastViewProject.org

Zanuttigh B. (2007) - *Numerical modelling of the morphological response induced by low-crested structures in Lido di Dante, Italy.* Coastal Engineering, 54: 31-47.

Zyserman J. A., Johnson h. K., Zanuttigh B. and Martinelli L. (2005) - *Analysis of far-field erosion induced by low-crested rubble-mound structures.* Coastal Engineering, 52: 977 – 994.

LiDAR technology and beach survey: history, experimentation and assessment

Hugues Heurtefeux

LiDAR (Light Detection And Ranging) is a technology that allows a large scale approach of beach survey. At the origin (mid-1960s) it was a military system used to detect submarines in the shallow water. Since the beginning of the 1990s this technology entered the civil industry and became operational in Australia (LADS), The United States (SHOALS) and Sweden (Hawk Eye) (Guenther et al., 2000).

The tool itself is constituted by a laser scanning system and an inertial navigation system (INS) tied to a differential GPS disposed on board of an aircraft or a helicopter (Liu et al., 2007). Two different wavelengths, infrared (1064 µm) and green (532 µm), operate at the same time in each laser pulse: the infrared one is returned by the water sea surface, whereas the green one is returned by the sea floor. Water depth is retrieved from the difference in return time of the two beams.

The main advantages of this technology are:

• data points over land and water collected at the same time, allowing a continuum between the submerged and the emerged beach.

• synoptic view over wide areas thanks to the high acquisition velocity (from 25 to 60 km≤/h).

• risk-free access to traditionally hazardous or difficult access areas.

The main disadvantage is that data outputs can be enormous and thus hard to process, moreover LiDAR files contain millions of X,Y,Z ASCII records and you have to define with the provider what is really needed in term of deliverables.

During the survey, at least 5 visible GPS satellites having elevations >10° must be available and the PDOP shall be <3.5. The distance to the fixed GPS stations used on land should not exceed 15 km.

During the survey, one 1600 x 1200 pixels image is stored every second and it is approximately 50% end lapped to the previous one. For nearshore monitoring, flight height is between 200 and 5000 m and standard ground resolution cell is approximately 15 x 15 cm. The images allow checking any objects that are source of artefact problem.

Within BEACHMED-e / OpTIMAL Project, ARPA "Ingegneria Ambientale" (Emilia-Romagna, Italy) and with EID MÈditerranÈe (HÈrault, France) have worked on a program to evaluate the capacity of Hydrographic LiDAR to monitor coastal evolution.

In France, the Gulf of Aigues-Mortes was chosen as the study site because it offers a wide variety of relief and thematic. It presents though some difficulties: flat sandy beach closed by a barrier island forming a lagoon, rocky formation in the seafloor with some *Posidonia oceanica* prairies, waterfront beach resort and natural space. The provider who answered EID's call was the Sweden Company Admiralty Coastal Surveys AB, who use LiDAR Hawk Eye II system.

In Italy, the coast located between Rimini and Marina di Ravenna was investigated along a linear strand of 50 km. This littoral stretch comprises a low, sandy coast defended by detached breakwaters. The provider in Italy was Tenix Lads Corporation ALB flight, an Australian company.

In the two cases, a comparative analysis was carried out between ALB bathymetric measurements and classical measurements (multibeam or single-beam) in order to evaluate the accuracy of the topo-bathymetric data obtained when using LiDAR technology.

Conclusions from the two campaigns are similar, even though they were carried by two different providers.

In both the experiments, the minimum water depth measured with LiDAR resulted to be 10 cm.
For the Italian group when water transparency conditions are good, the depth difference between measurements taken using each of the two methods can be calculated as Δ_{mean} = -0.17 ±0.09 m.
For the French group, the depth difference between measurements taken using each of the two methods can be estimated as 11 cm.
The conclusion is therefore that bathymetric LiDAR accuracy for vertical data is approximately 15 cm, which is not perfect but good enough for working on large-scale coastal sediment management.
Other opportunities begin to appear. At the moment we can also have an idea of the signal accuracy degradation induced by vegetation with a determination of species by classification of the standard deviation (Populus et al., 2001).
The research is still active and a promise future for bathymetric LiDAR could be the possibility to directly map areas by using the return of the local signal: we could define the bottom of sea floor with eelgrass, sand, algae, or rocky areas. Future programs shall try to explore these new aspects.

References

Guenther G.C., Grant Cunningham A., LaRocque P.E. and Reid D.J. (2000) - *Meeting the accuracy challenge in airborne LIDAR bathymetry*. Proceedings of EARSeL-SIG-Workshop LIDAR. Dresden/FRG. 27 pp.

Populus J., Barreau G., Fazilleau J., Kerdreux M. and L'Yavanc J. (2001) - *Assessment of the Lidar topographic technique over a coastal area*. CoastGIS'01, Second International Symposium on GIS and Computer Mapping. Halifax. 11 pp.

Liu H., Sherman D. and Gu S. (2007) - *Automated extraction of shorelines from Aiborne Light Detection and Ranging data and accuracy assessment based on Monte Carlo simulation*. Journal of Coastal Research, 23: 1359-1369.

Assesment, validation and further uses of LiDAR survey in the Western part of French Mediterranean sea

Hugues Heurtefeux, Audrey Lesaignoux, Cléa Denamiel

EID[1]-Mediterranee, DRE-LR[2] and Administrative Department of Hérault are currently developing a beach survey in the Gulf of Aigues-Mortes (Western part of the French Mediterranean sea) using Airborne hydrographic LiDAR. This technique has been widely used for coastal surveys in the United States of America but it's one of the first experimentations in South of France. This study presents an analysis of the results of this field testing to evaluate the capabilities of Hydrographic LiDAR to monitor coastal evolution. Altimetry precisions and density obtained are very encouraging and correspond fully to the existing needs.

Introduction

The topo-bathymetric campaign realised with the LiDAR technique on the Gulf of Aigues-Mortes coast is centred on new technologies as a purpose in order to realise an accurate and regular monitoring of the shoreline.

The provider of the LiDAR technology is the Sweden Company Blom Environment & Coastal Survey. The LiDAR pre-test flight (Mars 2006) and calibration (April 2007) were realised by this company.

The final flying LiDAR campaign took place between 24 and 26 April 2007 and covered most of the Gulf of Aigues-Mortes coast. The main aim of this campaign was to validate the use of LiDAR technology for the monitoring of the topography and the bathymetry of the nearshore area.

In a first part, the study area, flying campaign, data acquisition and results provided by the Blom Environment & Coastal Survey AB Company (BECS AB) are described. The analysis, checking and validation of the results carried by EID Méditerranée are then presented in the second part. Finally and to conclude, an assessment of the results obtained on the Gulf of Aigues-Mortes with the LiDAR procedure is realised. The future of the use of such a technology with the aim of describing the evolution of the coast is also discussed.

LiDAR mission: Flying campaign
Description of the study area

The study area covers 47 km² along the Gulf of Aigues-Mortes coast. This area is located between the Frontignan municipality (on the western part) and the Grande-Motte municipality (on the eastern part). Because of the convex form of the gulf, the survey area - represented in blue in Figure 1 - was cut into three parts: zones A, B and C. Indeed, the LiDAR data acquisition could only be done on rectilinear areas and in order to cover the entire area of the Gulf of Aigues-Mortes the cut-out in three rectilinear areas was the best technical solution. The coordinates of the three zones were given in Lambert III South system.

---

1   Ententende Interdépartementale de Démoustication
2   Direction Régionale de l'Equipement Languedoc-Roussillon
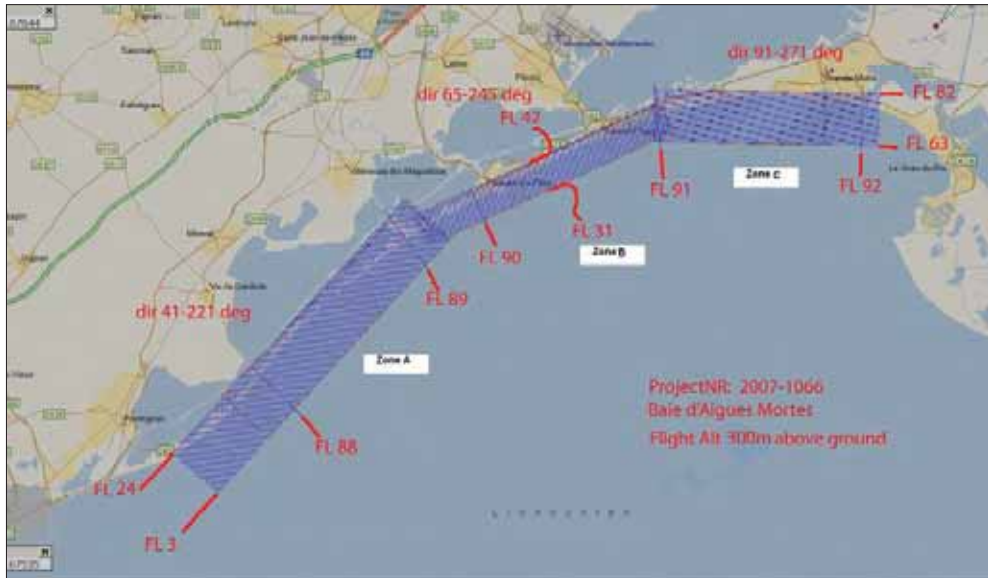
Figure 1 - Schematic representation of the 3 areas (zones A, B and C) covered by the flying LiDAR campaign on the Gulf of Aigues-Mortes.

Description of the final flying campaign and data acquisition

All the flying campaigns (pre-test, calibration and final flights) were realized by the BECS AB Company with the Hawk Eye II system (Figure 2). This technology allows acquiring topographic and bathymetric data. In the bathymetric mode, LiDAR emits green laser at 532 nm with a 4 kHz frequency. It is projected by a rotary mirror which sweeps water surface with swath width of 120 m and flight altitude of 300 m. Associated to the LiDAR system, navigation and position are provided by an integrated GPS and inertial reference system (Figure 2) which delivers accurate coordinates in all three dimensions. The data are referenced on WGS 84 UTM projection system and the acquisition is realised with a 1 Hz frequency.

Figure 2 - LiDAR Hawkeye II system (left) and GPS station (right).

After the calibration flight realised in Sweden in order to test the system, the "Air Commander" plane equipped with LiDAR technology was ready for the final flying campaign in the Gulf of Aigues-Mortes.

Between 24 and 26 April 2007, three flights with a total duration of 8h30 allowed acquiring all data. Meteorological conditions were perfect during the whole campaign: 1) water temperature was circa 18°C, 2) air temperature was circa 22°C, 3) wind velocity was circa 10 km/h and 4) turbidity measurements showed that water quality had no influence on LiDAR data acquisition with a visibility of circa 4 m.

Description of the results and the data

At the end of the campaign, the BECS AB Company provided two types of data: raw data (more than 80 million points and non geo-referenced orthophotos acquired each second during the whole campaign) and the post-process data (7 million points and geo-referenced orthophotos).

The raw data in LAS and ASCII format was not used by EID Méditerranée. In fact only the post-process data is really of interest for operational studies.

Data processing was realised in three steps:

1) WGS84 coordinates were transformed in Lambert III south coordinates;
2) the total area covered during the campaign was cut into 23 zones;
3) data were cleared (only 30% of the total data is useful) and two classifications were establish: ground points and high vegetation points.

Finally the post-process data provided by the company were:

1) the X, Y, Z points in ASCII format given in Lambert III South coordinates;
2) the classification of the ground and high vegetation points;
3) the regular grids (with a mesh resolution of 2 m, 5 m and 10 m) in ASCII and GeoTIFF format of the topography and the bathymetry: digital elevation model (DEM), digital terrain model (DTM) and digital slope model (DSM);
4) the geo-referenced orthophotos (in Lambert III south coordinates) with a resolution of 1m and 25 cm.

Assessment of the technical course of the LiDAR 2007 mission

Concerning the technical course of the campaign and the acquisition of data, the LiDAR 2007 mission was a success. Moreover the exchanges with the BECS AB Company were easy and data restitution took place only 1 month after the campaign. This experiment can be thus reproduced with the same company in the future.

But, with the aim to show that the LiDAR technology is available to describe the nearshore bathymetry and topography and to provide better results than others methods, all the post-process LiDAR data provided by the company had to be carefully analysed and checked.

LiDAR data analysis, checking and validation

Checking and validation of the orthophotos

The first step of the LiDAR data analysis, checking and validation was to compare the orthophotos provided by the company to those produced in 2005 by Gaia Mapping. The comparison consists in getting the roads, house roofs, vegetation, etc., of the two types of photos to coincide.

One example of this comparison done by the EID Méditerranée was realised with the orthophotos of the Frontignan municipality (Figure 3).

The two orthophotos are in natural colours and present the same aesthetic qualities. Moreover the house roofs, the vegetation and the beach coincide with a great precision (Puissant and Weber, 2006). Concerning the contrasts, the LiDAR ortophotos have a better quality than that of ortophotos provided by Gaia Mapping. The LiDAR technology is thus validated concerning the orthophotos.

Figure 3 - Comparison of the orthophotos obtained with the LiDAR technology in 2007 (top) and those provided by Gaia Mapping in 2005 (bottom) in the municipality of Frontignan.

Validation of the Delauney triangulation: problems of boundary artefacts

The regular grids (DTM, DEM and DSM) – delivered by the BECS AB Company and generated by EID Méditerranée - were obtained with Delauney triangulation (Figures 4 and 5). This kind of geostatistic is an interpolation with specific rules: three data points define one circle which not contain other data points (in 2D). This interpolation can also be transposed in 3D.
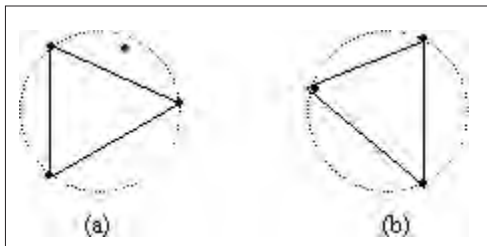
Figure 4 - Non-Delaunay triangle (a); Delaunay triangle (b).
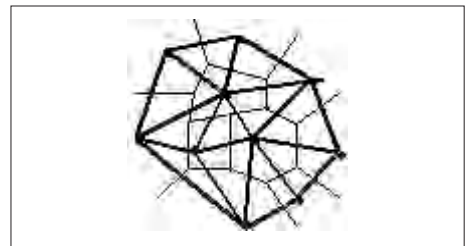
Figure 5 - Illustration of the Delaunay triangulation.

The TIN (Triangle Irregular Network) was chosen because it is naturally adapted to the slope restitution (Swales, 2002).

Generally, when data is interpolated some problems can appear at the boundaries. The second step of the data analysis, checking and validation was thus to know if the TIN generated some boundary artefacts.

The following procedure was used:

1)   two adjacent areas were interpolated separately;
2)   the two areas were put together;
3)   the coincidence of the two area boundaries and the profiles obtained at the junction were checked.

The profiles generated with this procedure were all continuous and thus the Delauney triangulation was verified not to produce artefacts at the boundaries (Populus, 2003).

The use of the Delauney triangulation to generate the DTM, DEM and DSM was validated.

Checking and validation of the X, Y, Z bathymetric data

In order to validate the X, Y, Z bathymetric data delivered by the BECS AB Company, EID Méditerranée compared these data with those obtained with the singlebeam technology in several distinct areas of the Gulf of Aigues-Mortes.

The comparison of the bathymetric data obtained with the two technologies requires the generation of DTM (Digital Terrain Model). EID Méditerranée chose to generate the LiDAR DTM with the X, Y, Z data delivered by the BECS AB Company and not to use the LiDAR DTM delivered by the Company.

The generation of the LiDAR and the singlebeam DTMs was realised with MapInfo using the Delauney triangulation method.

Concerning the singlebeam measurements, the depth data must be corrected - following water temperature and salinity - before the generation of the DTM. Indeed, the velocity of the singlebeam signal is directly linked to water temperature following the formula below [1]:

$$\text{Gap in meters} = (1/V_{T1} - 1/V_{T2}) * d_{10} * V_{T2} \qquad [1]$$

Where:
- T1 and T2 are the temperatures at 10m above the bottom of two profiles realised in the same location but not under the same conditions
- V_{T1} and V_{T2} are the sound velocities at temperatures T1 and T2
- $d_{10} = 10$ m

The sound velocity in the water following water temperature is given by the curve in Figure 6.
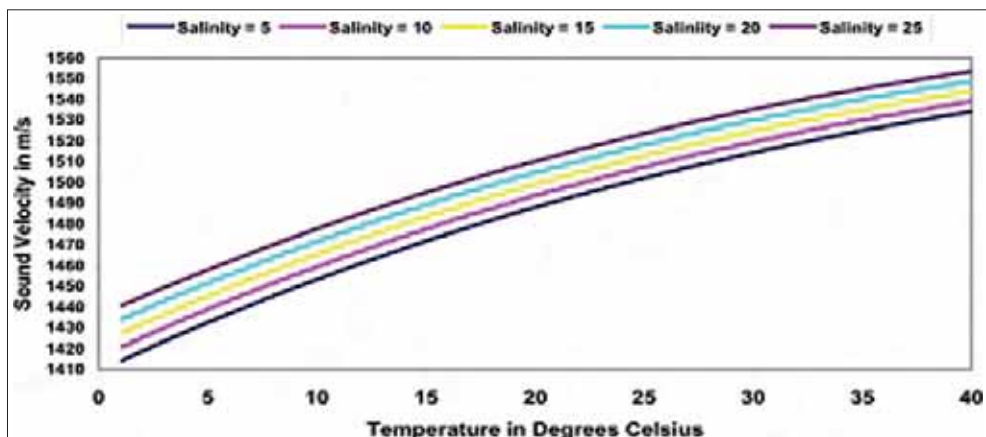
Figure 6 - Sound velocity in the water (m/s) following water temperature (°C).

The comparison between profiles measured at different temperatures had shown that the gap theory is well correlated to measurements. This gap increases with depth and profiles slowly change close to the extern bar. The measurement error in the depth near the closure depth thus results from the captor error due to the variations of temperature. Finally, the temperature correction can be applied on the singlebeam data and the DTM is generated with these corrected data.

The X, Y, Z LiDAR data used in this comparison are the post-processed data in Lambert III South coordinates.

Although several comparisons of the LiDAR and mono beam data were done, we just present one example here.

One of the areas where the validation of the bathymetric X, Y, Z LiDAR data was done is the Villeneuve-Lès-Maguelone zone (Figure 7, Table 1).

Figure 7 - Villeneuve-Lès-Maguelone zone.

Table 1 - Lambert III South Co-ordinates of the Villeneuve-Lès-Maguelone zone.

X1, Y1	723 780 m, 134 000 m
X2, Y2	723 920 m, 134 100 m
X3, Y3	724 740 m, 132 940 m
X4, Y4	724 590 m, 132 890 m

The generation of the DTM with MapInfo in this area using the two types of data and their 3D representations (Figure 8) allowed comparing and validating the LiDAR technology concerning bathymetric data. Indeed, the two DTMs (Figure 7) are similar.

Moreover the LiDAR DTM represents the littoral bars with precision while the singlebeam DTM gives a result with a smoother surface. The LiDAR technology characterised the bottom irregularities and relief better than singlebeam. It is thus a good tool for the morphologic description of the nearshore area.

In order to compare with more precision the two types of data, some bathymetric profiles were extracted from the LiDAR and the singlebeam DTMs (Figure 9).

After several comparisons it can be established that:

1) between 0 m and 4.5 m of depth the gap between the two types of data is lower than 10 cm;
2) after 4.5 m of depth this gap is between 10 cm and 60 cm.

The increase of the gap following depth between the two types of data can be explained by the increase of turbidity or by the nature of the bottom. The LiDAR precision thus depends on turbidity and the nature of the bottom. Indeed when the bottom roughness increases the reflectance and the amplitude decrease (Lesaignoux, 2006).

For example, in the zone of Villeneuve-Lès-Maguelone the presence of a rocky relief between 8 m and 11 m of depth can explain the large gap between the two types of data. The LiDAR data are thus less precise on this area than the singlebeam data.
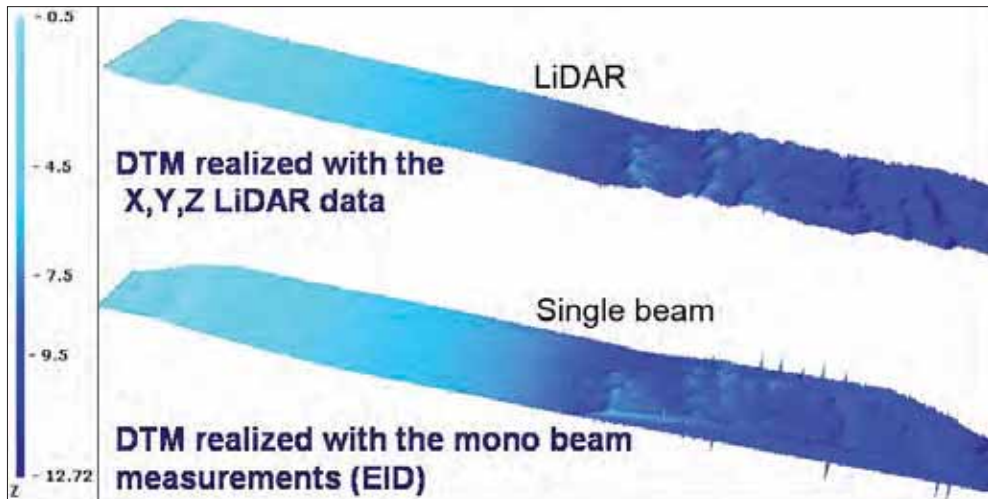
Figure 8 - 3D representation (with MapInfo) of the Maguelone MNT generated with the X, Y, Z LiDAR data and with the X, Y, Z singlebeam.
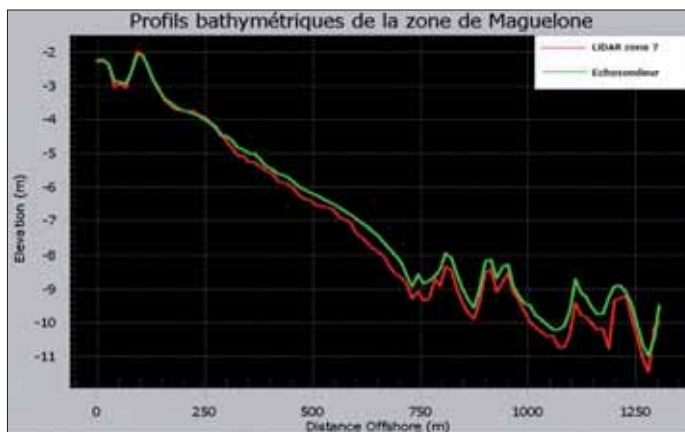
Figure 9 - Bathymetric profiles of the Maguelone zone generated with LiDAR data (red) and with singlebeam (green).

The LiDAR X, Y, Z bathymetric data are thus validated on the Gulf of Aigues-Mortes and although LiDAR precision decreases when the depth increases, the LiDAR technology provide good results concerning the bottom relief.

Checking and validation of the X, Y, Z topographic data

Validation of the LiDAR DTM generated with these data
In order to validate the X, Y, Z topographic data delivered by the BECS AB Company, EID Méditerranée compared these data to those obtained with D-GPS technology in several distinct areas of the Gulf of Aigues-Mortes.
Such as for the bathymetric data, the comparison of the topographic data obtained with the two technologies requires the generation of DTMs (Digital Terrain Model). EID Méditerranée chose to generate the LiDAR DTM with the X, Y, Z data delivered by the BECS AB Company and not to use the LiDAR DTM delivered by the Company.
The generation of the DTMs from LiDAR and D-GPS technologies was realised with MapInfo using

the Delauney triangulation method. Although several comparisons of the LiDAR and D-GPS data were done, we just present here one example.
One of the areas where the validation of the topographic X, Y, Z LiDAR data was done is the zone of Villeneuve-Lès-Maguelone (Figure 10, Table 2).

Figure 10 - Location of topographic measurements (in red) in the Villeneuve-lès-Maguelone zone.

Table 2 - Lambert III South coordinates of the area of topographic measurements.

X1	723 573 m	Y1	134 124 m
X2	723 616 m	Y2	134 254 m
X3	723 886 m	Y3	134 146 m
X4	723 723 m	Y4	134 011 m

The generation of the DTM with MapInfo in this area, using the two types of data and their 3D representations (Figure 11), allowed to compare and to validate the LiDAR technology concerning the topographic data. Indeed, the two DTMs (Figure 11) present similarities. Moreover the LiDAR DTM represents the dune relief with precision while the D-GPS DTM gives a result with a smoother surface. For example, the berm is well described by the LiDAR DTM while it does not appear on the D-GPS DTM.
Moreover the interpolation of the data measured with D-GPS generates a large area of artefacts (red circle on the right of Figure 11). In fact this area could not be covered by the measurements and the DTM is extrapolated.
With the same number of data (approximately 4.000 points for each method – see Figure 12 at the bottom) - but not the same repartition of the data - the quality of the two types of measurements is not the same. Indeed the regular distribution of the LiDAR data allows describing the bottom irregularities with precision. The irregular distribution of the D-GPS data described some areas with great precision (areas with numerous data) and did not describe some others areas (areas without data). Because of this lack of data in some areas, the interpolation needed for the generation of the DTM creates some artefacts and smoothes the data.
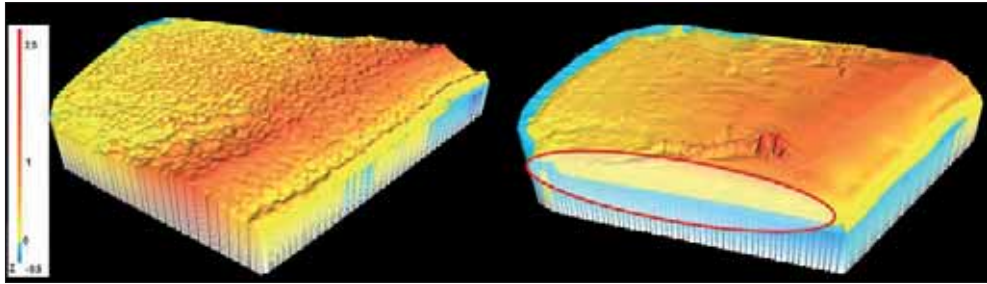
Figure 11 - 3D representation of the DTM (realised with MapInfo) measured in the Maguelone zone with LiDAR technology (left) and with D-GPS (right); red area: artefacts.
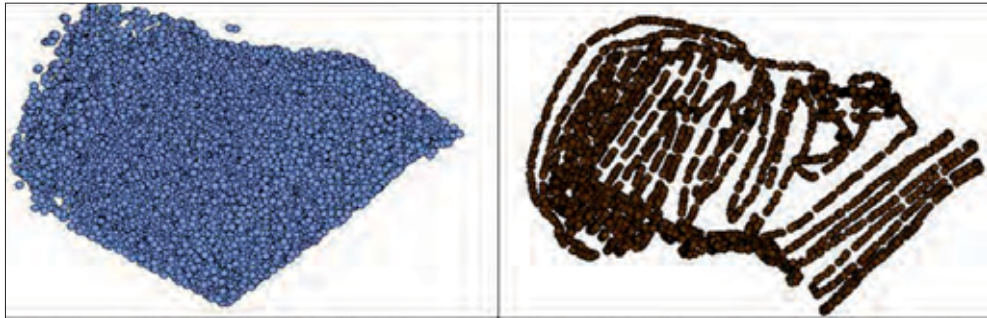
Figure 12 - Repartition of data (realised with MapInfo) measured in the Maguelone zone with the LiDAR technology (left) and with D-GPS (right).
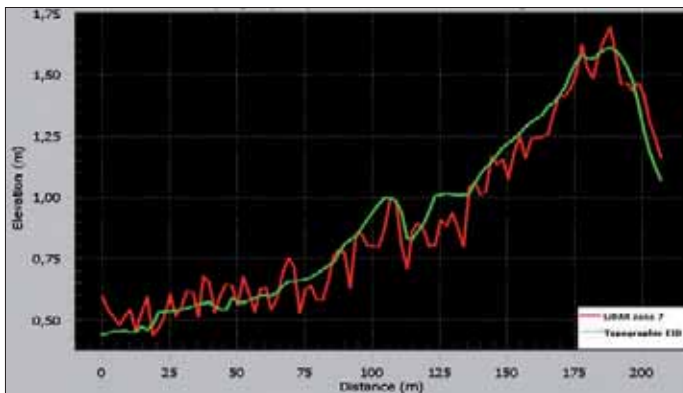
Figure 13 - Topographic profiles in the Maguelone zone measured with LiDAR technology (red) and with D-GPS (green).

The LiDAR technology characterised the bottom irregularities (Figure 13) and relief better than the D-GPS technology. It is thus a good tool for the topographic description of the nearshore area although the measurement error is circa 15 cm.

Results at the land-sea interface

EID Méditerranée was interested in validating the LiDAR DTM at the land-sea interface. Indeed the study of the shoreline is one of the main objectives in beach protection.

A shoreline area was selected in the Maguelone zone at the land-sea interface.

This area contains 156 data measurements (Z_{min} = - 0.276 m and Z_{max} = 0.635 m) and 128 data

measurements (Z_{min} = - 0.38 m and Z_{max} = 0.76 m) obtained respectively with D-GPS and LiDAR technology (Figure 13). The spatial repartition of data seems to be similar and the LiDAR data did not cover the full shoreline due to the laser imprecision in this area.

The generation of the DTM with MapInfo in the shoreline area using the two types of data and their 3D representations (Figure 14) allowed comparing and validating the LiDAR technology concerning the topographic data at the land-sea interface.
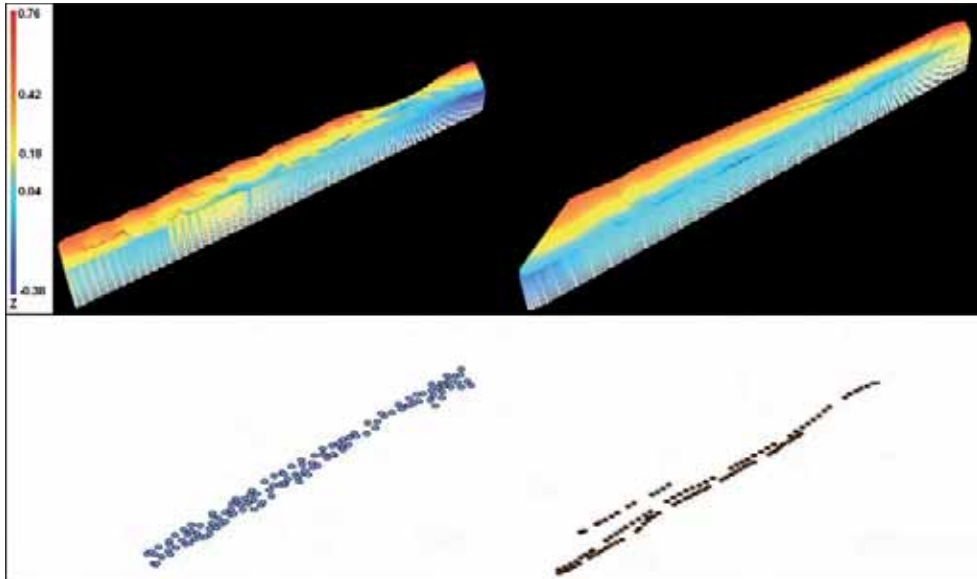
Figure 14 - 3D representation of the DTM (realised with MapInfo) of the Maguelone zone at the land –sea interface measured with the LiDAR technology (left) and with D-GPS (right). Repartition of points at the bottom.

The profiles extracted from the DTM (Figure 15) allow studying the location of the shoreline with the two types of measurements. The result of this comparison is that LiDAR technology cannot reproduce the shoreline. Indeed the error of measurements is close to 40 cm which is very relevant in this field (Figure 15, red line). D-GPS measurements (Figure 15, green line) are thus more precise concerning the shoreline.

Finally, the LiDAR X, Y, Z topographic data were validated in the Gulf of Aigues-Mortes and although LiDAR is not adapted for the description of the shoreline, LiDAR technology provide good results concerning the relief.
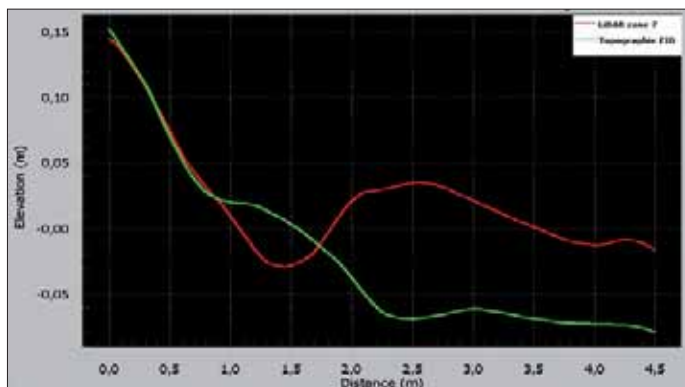
Figure 15 - Topographic profiles at the land-sea interface measured with LiDAR technology (red) and with D-GPS (green).

Checking and validation of the DTM LiDAR data

In 1982 SHOM[3] measured – with the traditional tools - the topo-bathymetry of an area of 160 km^2 located between the municipalities of Frontignan and Palavas-les-Flots. The number of data measured by SHOM was approximately 15.000 points in this area. The horizontal and vertical precisions are circa 30 cm for a depth greater than 30 m.

In the Villeneuve-lès-Maguelone zone, 5.000 data measurements were realised by SHOM and 3.000.000 data measurements were realised with LiDAR technology.

The comparison between the DTM provided by SHOM and the LiDAR DTM (Figure 16) shows that LiDAR technology allows to have a very good precision for the relief. Indeed the inner bar is well reproduced on the LiDAR DTM while it does not appear on the SHOM DTM. Moreover the rocky relief and the outer bar are better represented on the LiDAR DTM.

These differences are essentially due to the density of data measurements. Indeed the interpolation is always better for a large data set and LiDAR technology provides 600 times more points than SHOM in the area of Maguelone.
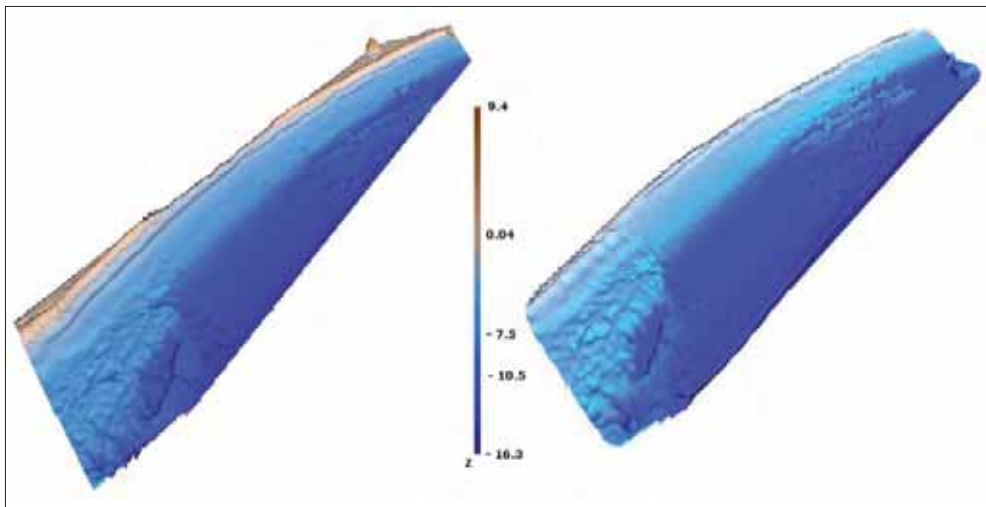
Figure 16 - 3D representation (realised with MapInfo) of the LiDAR 2007 DTM (left) and of the SHOM 1982 DTM (right).

Conclusion

The technical course of the campaign and the data acquisition as well as the analysis of the results of the LiDAR 2007 mission was a success. Indeed EID Méditerranée showed that LiDAR technology provides better results than the traditional methods for topo-bathymetric measurements. The precision of LiDAR data is always satisfying except concerning the shoreline description.

Concerning the use of LiDAR technology in the Gulf of Aigues-Mortes it is thus possible to conclude that:

- LiDAR technology allows to describe the topo-bathymetry of nearshore areas;
- acquisition of topo-bathymetric data and orthopohotos with LiDAR technology is 30% less expensive than by traditional ways;
- acquisition of a very large dataset by LiDAR technology allows to improve the quality and the precision of DTMs, DEMs and DSMs.

Concerning the prospects of the use of LiDAR data, many forms can be explored in the Gulf of Aigues-mortes.

First, the analysis of topo-bathymetric data allows describing the sedimentary structures with preci-

---

3   SHOM: Service Hydrographique et Océanographique de la Marine.

sion (Populus et al., 2001). The long-term acquisition of LiDAR data in the same area should be interesting in order to compare the evolution of these structures following the seasons and the years. Second, LiDAR data allows describing the submersion of the land due to sea level rise (because of storms or climate changes). Indeed, the analysis of static submersion maps (example in Figure 17) should provide a first assessment of the impact of sea level rise on the landscape.
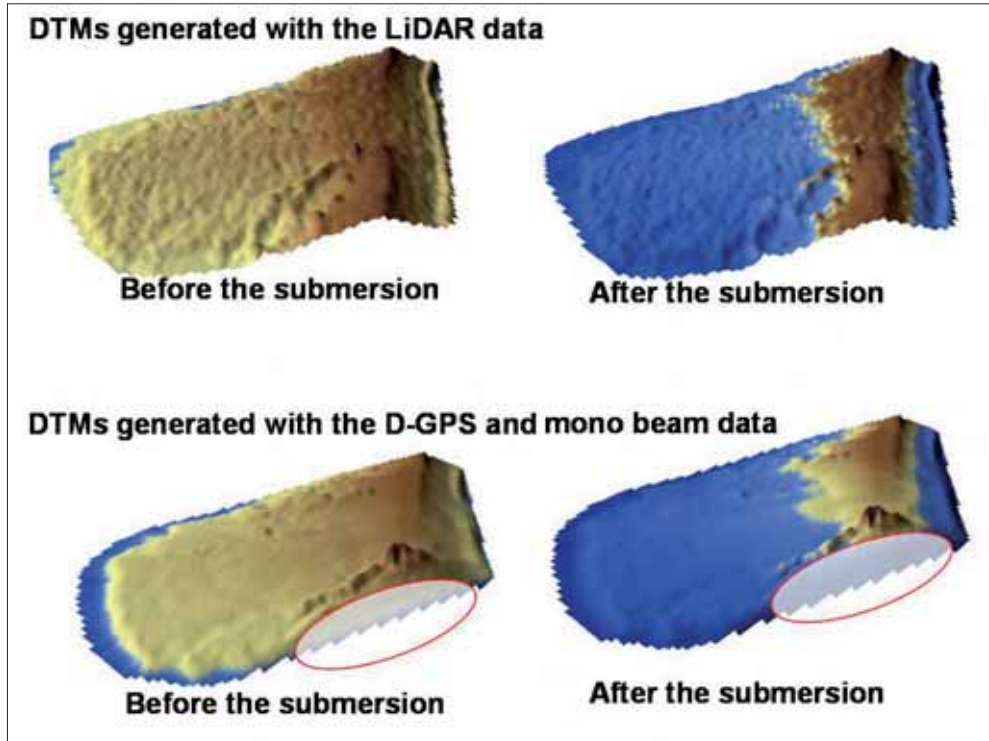
Figure 17 - Static submersion due to a sea level rise of 1m ("Surfer" 8 software) – DTMs of the Villeneuve-lès-Maguelone area before submersion (left) and after submersion (right), generated with LiDAR data (top) and D-GPS and singlebeam data (bottom). The red circles represent the numerical artefacts.

Third, the use of hydrodynamic models generating the currents following meteorological conditions, swell, submersion and topo-bathymetry (obtained with LiDAR technology) should provide a first assessment of the effects of currents on the sedimentary transport.

Fourth, LiDAR data can be post-processed with the aim to determine ecological units: for example to determine the presence and the concentration of some habitats or species.

And at last, a comparison among webcam images, satellite images and LiDAR data should be done with the scope of determining the best way to describe shoreline evolution.

References

Lesaignoux A. (2006) - *Modélisation et simulations de trains d'ondes LiDAR «vert»: application à la détection de faibles lames d'eau en rivière*. Master's Thesis, UMII.

Populus J., Barreau G., Fazilleau J., Kedreux M. and L'Yavanc J. (2001) - *Assessment of the LiDAR topographic technique over a coastal area*. CoastGIS 2001.

Populus J. (2003) - *Les modèles numériques de terrain en zone intertidale*. REBENT, Décembre 2003.

Puissant A. and Weber C. (2003) - *Les images à très haute résolution, une source d'information géographique en milieu urbain ? Etat des lieux et perspectives*. L'espace géographique, pp. 345-356.

Swales A. (2002) - *Geostatistical estimation of short-term changes in beach morphology and sand budget*. Journal of Coastal Research, 18 : 338-351.

Bathymetric survey: a comparison between Airborne LiDAR Bathymetry (ALB) and conventional methods of measure

**Mentino Preti, Matteo Monti,
Nunzio De Nigris, Maurizio Morelli**

The need to periodically acquire data along wide coastal stretches in order to monitor coastal evolution and the effectiveness of defence works led ARPA Ingegneria Ambientale to search for new technologies of topo-bathymetric survey.

The aim was to verify the existence of new survey methodologies that were able to combine reduced working time with accuracy and costs comparable to traditional systems.

Within the BEACHMED-e / OpTIMAL project, the functional principles and operative characteristics of the bathymetric LiDAR (ALB) were analysed, based on the survey performed by ENI in 2006 along 50 km of the Emilia–Romagna coast, from Rimini to Ravenna. This paper presents the results of the comparison among this survey and the ones acquired by ARPA, in the same area and in the same period, with single-beam and multibeam integrated systems (SBE and MBE). Moreover, a statistical analysis of the depth difference measured with ALB and with traditional systems was performed in order to detect possible systematic errors and to get information about the reliability of ALB data.

Introduction

The areas along the coast are subject to growing human pressure, and, as such, to growing economic, social and environmental interests. This strip of territory on the border between the sea and the land is marked by a dynamic and fragile morphological equilibrium, as can be seen by the considerable amount of erosion which affects the vast majority of beaches through the world. The continued decline of the beach is changing the environmental nature of this part of the territory and is placing the social-economic interests which depend on it in serious danger.

Monitoring the morphological evolution of the active beach takes on a key role in terms of our awareness of the phenomenon and its assessment - used to provide a scientific basis to support the definition of intervention policies to be implemented in order to protect the coastline.

In 1983, the Region of Emilia-Romagna - working in conjunction with Idroser's technical-scientific support (today ARPA Ingegneria Ambientale) – set up a network to monitor the subsidence of the coast and the morphology of the active beach (topobathymetric network) on 130 km of coastline in the region.

These nets were measured for the first time in 1984 and then, successively, another 4 -5 times. In particular, the topobathymetric network was monitored in 1993, 2000 and - more recently - in 2006.

Over time, individual tracts of the coast have also undergone monitoring, particularly in order to analyse the effects of beach nourishment and the efficacy of defence works. Throughout the 80[s] and 90[s], topobathymetric measurements were taken using a single-beam echosounder. Multibeam echosounders were introduced later.

In both cases, taking measurements is a fairly complicated procedure since various instruments are required for positioning as well as for measuring tides and correcting for waves, including one or more boats.

The time required to monitor a wide stretch of the coast - based on measuring of several cross-shore and long-shore profiles - is relatively long. Taking into account bad sea conditions, this can take anywhere between weeks to even a few months.

Objectives

The need to take increasingly frequent and more detailed bathymetric measurements over a short period of time is what led us to experiment new methods of measurement along the coast of the Emilia-Romagna region.

Within the scope of the BEACHMED-e / OpTIMAL Project, ARPA Ingegneria Ambientale set the objective of comparing bathymetric measurements taken using "conventional systems" (single-beam and multibeam) and airborne (ALB) measurements from a technical, operational and economic point of view in order to assess their applicability in terms of the Emilia-Romagna coast.

Phases of the project

The project can be broken-down into the following phases;
a) bibliographic research;
b) project design;
c) field work and data analysis.

The bibliographic research we carried out during phase A (see report AA. VV., 2007a) and our frequent contacts with different experts from the sector allowed us to identify the key features of the ALB system as well as its functions.

The system's most important element is a scanner which sends two laser impulses - one of which can penetrate water. The combination obtained with the two return times of signals is used to measure the depth of the sea bottom. This data allows us to measure the depth of the sea bottom when it is combined with a position reading obtained using a GPS navigation system.

The manufacturers of the system guarantee a planimetric and altimetric precision of IHO Order 1 in the hydrographical mode. A bathymetric precision of 15 cm was also obtained with some studies, even if the results were often influenced by much larger errors due to the many variables present when taking the measurements (AA.VV., 2005; Milli and Surace, 2006).

The maximum depth which can be measured using this system depends on the transparency of the water and is equal to 2-3 times the depth of the Secchi disk.

Given the cost of LiDAR measurements and the restricted BEACHMED-e budget available for this activity, Phase B of the project (see report AA. VV., 2007b) focused on the search for a partner wishing to invest in measurements taken using ALB.

As such, we were able to acquire data from the Tenix Lads Corporation ALB flight commissioned by ENI, who kindly allowed us to use the data for our analysis.

A detailed description of the work carried out by ARPA Ingegneria Ambientale during Phase C of the OpTIMAL project is found below, focusing in particular on the data we acquired, the instruments employed to take the measurements, the analyses which were carried out and final results.

Area of study

Initially, and according to the project, the study area was a tract of approximately 1800 m on the Igea Marina coast between Rimini and Cesenatico. In fact, this area has been the subject of another study since 2001 on low-crest structure behaviour and as such has undergone repeated monitoring.

Morphologically-speaking the area in question is comprised of a low, sandy coast defended by detached breakwaters.

Since ENI measured all of the coastal area from the port of Rimini to Marina di Ravenna - more than 50 km in length - we decided to extend our analysis for this project to include the entire area.

Instruments, methods and accuracy

Conventional measurements

Commissioned by ARPA Ingegneria Ambientale, Geosystem Parma s.r.l measured the entire topo-bathymetric network within the scope of the "IV measuring campaign for the regional coast" between the end of November 2005 and the first half of April 2006. This comprised 251 cross-shore profiles (average distance of 500 m) and several kilometres of long-shore profiles.

The cross-shore profiles begin in the highest part of the emerged beach and stretch up until the 6 – 8 m bathymetric. Furthermore, every 10 km of coast a cross-shore profile is stretched up to the 10 m bathymetric in order to identify any variations in the sea bottom in deeper waters.

Detailed measurements were taken on the Igea Marina tract - approximately 1.8 km in length - as described above. These measurements, which were taken using conventional technologies, provided for the acquisition of data on cross-shore profiles with a distance of 100 m between them, with the head of the section positioned on the highest part of the emerged beach and stretching up to a bathymetric of 6 m. The work was carried out during the first half of March 2006.

Each cross-shore profile was broken-down into three segments, based on the instruments necessary to carry out the operations as efficiently as possible given the different morphological configurations of the coast, and more precisely:

– emerged beach: between the head of the section and the 0.3 m bathymetric;
– submerged beach: between the 0.3 m bathymetric and the inner part of the breakwaters;
– submerged coast: from the outer part of the breakwaters until the end of the section.

Two double-frequency GPS receivers operating in RTK with OFT initialisation were employed to carry out level-altimetric positioning operations in all three areas.

Data were collected while maintaining a maximum distance of 10 km between the Reference Station and the Rover in order to minimise variable errors caused by the length of the base measured.

The altimetric frame was calibrated based on the plan defined by the ARPA levelling network of 2005, which was used to monitor subsidence in order to identify the exact configuration of the local geode. The subsidence network refers to the IGM bench mark of Sasso Marconi, which is deemed stable by IGM and which in turn refers to the Genoa 1943 mean sea level.

The GPS was associated with other equipment in accordance with the section being examined. As such, data was collected using the procedures described below.

Emerged beach

The Rover GPS - which was associated with the data collection, monitoring and management system supplied with the GPS equipment - was either installed on a jeep or carried by shoulder.

The accuracy of the data for this part of the section corresponds to that collected using GPS, since this was the only instrument employed, as such:

– Altimetric accuracy $\Delta H = \pm 0.03$ m;
– Planimetric accuracy $\Delta P = \pm 0.05$ m.

Submerged beach

The GPS was associated with a single-beam echosounder (SBE) so as that to render the offset between the antenna phase centre and the bathymetric transducer null. The echosounder releases a beam in an 8° cone at a frequency of 200 KHz. This is used to measure a point for every meter along the route with an instrumental precision of 0.5% of the depth measured.

The following instruments were also present on the boat:

– CTD probe to measure the speed of sound;
– a data collection system to monitor wave energy and rolling and pitching movements.

The final accuracy of the bathymetric data for the submerged beach was calculated by the company who carried out the work at $\Delta H = \pm 0.05$ m.

Submerged coast

The area beyond 1.5 m in depth or beyond the breakwater was monitored using the GPS system together with a multi-beam echosounder (MBE). Both were installed on a boat so that to minimise offset between the phase centre of the antenna and the bathymetric transducer. A system to measure wave energy and the CTD probe described above were also present on the boat together with a navigation system complete with data acquisition, monitoring and storage software.

The multi-beam echosounder was used to obtain bathymetric data with a width of 120° by means of 240 beams generated with a frequency of 455 kHz, each emitted in a cone with a width of 0.5°.

The accuracy of the data for the submerged coast was evaluated as:

−   Altimetric accuracy ΔH = ± 0.04 m;
−   Planimetric accuracy ΔP = ± 0.10 m.

ALB measurements

Tenix LADS Corporation - working in collaboration with Compagnia Generale Riprese aeree (CGR) - carried out twelve flights for ENI between May 22 and June 12 2006, using ALB technology to obtain a set of high-density bathymetric data in an area stretching from the port of Rimini to Marina di Ravenna.

Soundings in the LADS Mk II system are obtained by the transmission of laser pulses from the aircraft through a scanning system and detecting return signals from land, the sea surface, the water body and the seabed. The transmitting and receiving components are housed on a stabilised platform that compensates for aircraft pitch and roll.

The laser scanner is comprised of:

−   Laser: a Nd: Yag laser producing IR energy at a wavelength of 1064 nm at 990 pulses per second of which 900 pulses are used for sounding purposes;

−   optical coupler: used to split the ray of the laser. Part of it is sent vertically towards the sea surface while the other is doubled in frequency in order to obtain a green ray with a wavelength of 532 nm, which is then transmitted onto the mirror of scanner;

−   Scanning system: the scanning mirror is oscillated in both the major (across track) and minor (along track) axes. The required scan pattern is generated by controlling software (Tenix LADS Corporation, 2006).

−   A video recording system for nadir images - useful during the post-processing phase - and a GPS system with an antenna and two receivers were also installed on the plane. Specifically:

−   an Ashtech GG24 operating in DGPS mode with corrections received from the Fugro OmniStar Wide Area Differential GPS (WADGPS) through a Virtual Base Station System, employed to calculate the position of the plane in real time;

−   a double-frequency Ashtech Z12 to record data in KGPS (L1/L2) mode to be used later, during post processing. The receiver was associated with another, identical receiver which was used as a Reference Station and was located at the CGR in Parma, approximately 177 km away.

The measurements were taken by acquiring bathymetric data according to a grid with a square mesh of 5 m per side, a width of the strip equal to 240 m and a distance between two successive lines of 200 m; this distance was reduced to 100 m in areas where a greater amount of turbidity was registered.

The campaign scanned the "main lines". For the most part, these ran parallel to the coast and represented the actual line itself. Other routes were also measured in order to improve the accuracy of the final data and to provide constant controls on the correctness of the calibration of the instrument and the depth registered.

The alternative routes were:

−   14 lines transversal to the main lines (cross lines). Of these, 4 were unusable as a result of elevated turbidity. The cross lines were used to check the reliability of the data gathered. A comparison of 788,223 points of intersection with the primary lines led to an average difference between the depth registered in the two cases of 0.07 m (95% confidence);

–   3 depth benchmark areas, that is, areas marked by a flat sea bottom with an average depth of 8, 10 and 14 meters. These areas were measured during each flight to check the exact calibration of the instruments.
Lastly, in order to proceed to data post-processing, tides were measured by the tide gauge located at the Istituto Idrografico Italiano in Marina di Ravenna.

Planimetric accuracy
According to the Ashtech manual, the accuracy of the post-processing solution for the data obtained in KGPS (L1/L2) mode with a PDOP (Percent Dilution of Position) of less than 4 is:

$$\Delta_{KGPS}(L1/L2) = 0.3 \text{ m} + 1 \text{ ppm (worst case)} \qquad [1]$$

Therefore, since the distance between the Reference Station and Rover was of 177 km on average, expected accuracy was

$$\Delta_{KGPS}(L1/L2) = \pm 0.48 \text{ m} \qquad [2]$$

Other uncertainties must be added to this technical error when calculating the planimetric position, that is:
–   an error in positioning the points due to the fact that the position supplied by the GPS did not represent the centre of the acquisition equipment $\Delta frame = \pm 0.66$ m;
–   platform and laser position errors $\Delta plat = \pm 2.14$ m;
–   errors in identifying objects caused by the distance between the points measured. With a 5 x 5 grid, the worst case is $\Delta spot = \pm 2.5$ m;
– $\Delta surface$ errors caused by waves, depending on the angle of incidence for the laser with respect to the surface of the sea, the depth of the water and the conditions of the sea.
All these uncertainties were defined at a 95% confidence level. As such, total planimetric accuracy is equal to

$$\Delta_{PTOT} = \sqrt{11.4956 + \Delta_{surface}^{2}} \qquad [3]$$

As can be seen in Table 1, it always falls within the IHO of Order 1, where the maximum admissible planimetric value is given by

$$\Delta_{PIHO1} = 5 \text{ m} + 5 \text{ \% depth}$$

Table 1 - Planimetric Error for ALB data and IHO Order 1 accuracy.

Depth (m)	State of the sea				IHO Order 1
	1	2	3	4	
2	3.39	3.39	3.40	3.43	5.1
10	3.39	3.39	3.45	3.56	5.5
15	3.39	3.39	3.52	3.77	5.75
20	3.39	3.39	3.61	4.04	6
30	3.39	3.40	3.87	4.73	6.5

Altimetric accuracy
Measuring the depth benchmarks and based on our experiences during the previous campaign, the accuracy of the LADS MK II laser scanner was assessed at a 95% confidence level in

$$\Delta_{LADS} = \pm 0.15 \text{ m} \qquad [4]$$

The following must be added to instrumental error:
– tide evaluation errors, equal to $\Delta_{tide} = \pm\,0.10$ m (68% confidence level);
– errors induced by the wave energy, estimated at $\Delta_{swell} = \pm\,0.05$ m (68% confidence level);
– errors caused by turbidity. We noted a systematic error present in cases of elevated turbidity. The systematic error was slightly higher in areas most affected by turbidity, with a maximum difference of 0.3 m compared to measurements taken in clear waters. As such, corrections based on the level of turbidity and taking into account the remaining effects caused by turbidity and which could not be modelled were carried out and a further error equal to $\Delta_{turbidity} = 0.15$ m with a 68% confidence level was introduced.

As such and combining the various uncertainties in a Gaussian model, the total accuracy of the bathymetric data with a confidence level of 95% is equal to

$$\Delta_{HTOT} = 0.47 \text{ m} \qquad\qquad [5]$$

this is less than the limit provided by IHO Order 1, which is

$$\Delta_{HIHO1} = \sqrt{0.5^2 + (0.013 \text{x} h)^2} \qquad\qquad [6]$$

where h is equal to the depth of the sea bottom reading (IHO, 1998).

Available Data

15,564,000 points distributed over an area of approximately 540 km^2 were measured using the ALB system (Figure 1). This was comprised of a strip which stretched from the port of Rimini to Marina di Ravenna (approximately 50 km in length) and up to a bathymetric of 25 m. Of these, approximately 125,000 points were located in the Igea Marina area. Data were distributed homogeneously on a grid with a square mesh of 5 m. Nevertheless, this homogeneity is only theoretical since measurements were not taken in some areas as a result of elevated turbidity.

In 45 days, 4,657,000 points were measured on 128 cross-shore profiles (with an average distance of 500 m) and long-shore profiles for a total of more than 220 km using the conventional method (DGPS together with singlebeam and multibeam). Furthermore, detailed measurements were taken in the Igea Marina area which was comprised of 15 cross-shore profiles with a distance of 100 m between them and several long-shore profiles. In both cases, the limit on the side of the sea for measurements was of 6 m – 8 m bathymetries. Approximately 260,000 points were measured in this area.
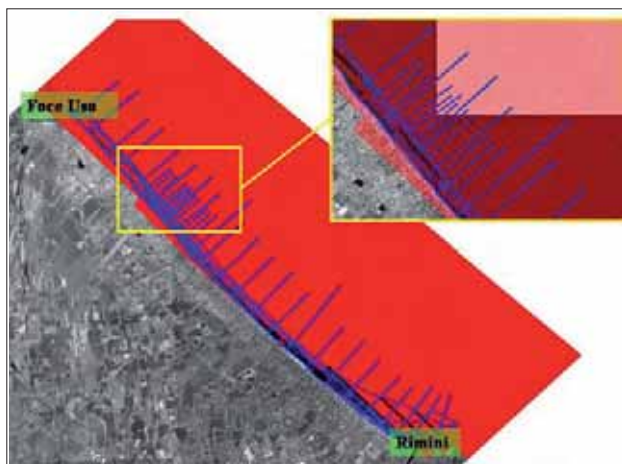
Figure 1 – Points measured with ALB (red) and points measured using the conventional method (blue) on the coast between Rimini and Foce Uso. A detail of the Igea Marina area subject to the study with detailed readings is contained in the box.

The Tenix LADS Corporation took a number of measurements before and during the monitoring period to check trends in turbidity (Table 2). In turn, ARPA Ingegneria Ambientale acquired transparency data collected by ARPA Daphne while monitoring water quality in the Adriatic in front of the Emilia Romagna coast.

Table 2 - Tenix LADS Corporation turbidity results.

Date	Secchi Depth		Note
	Minimum	Maximum	
05/04/2006	-1.5 m	-4.5 m	Could not be measured
28/04/2006	-1.8 m	-9.5 m	Good conditions
15/05/2006	-2.5 m	-11 m	Very good conditions: equipment sent to Italy
06/06/2006	-1.5 m	-3.5 m	Measurements suspended
09/06/2006	Increase		Measurements started again on the following day

Conditions were optimal at the beginning of the period of measurement, allowing for measurements to be taken at sea bottom up to a depth of 25 m. However, on May 29 a sea storm led to the suspension of all activities for 10 days as a result of the increase in turbidity.
Furthermore, persistent turbidity was recorded in the northern area, next to the port of Ravenna and the Po delta, causing noticeable difficulties.
This is reflected in the ARPA Daphne measurement results as well (Figure 2).
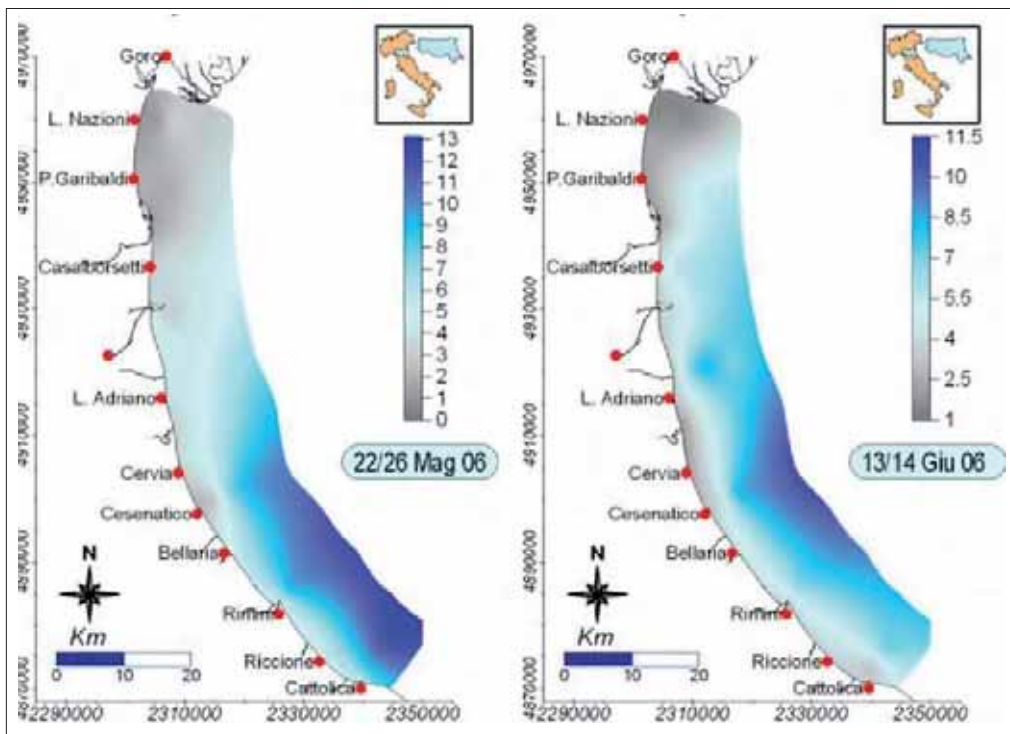
Figure 2 – Transparency maps measured using a Secchi disk on all of the Emilia Romagna coastline relative to - respectively - the start (left) and the end (right) of the data collection period, figures in meters (ARPA Daphne).

The comparative analysis carried out between ALB bathymetric measurements and multibeam measurements took into account the interval of time between the two readings, which went from March to June 2006.

In order to eliminate any influences due to possible bathymetric variations caused by wave energy - which had taken place during the interval of time between the two readings - a portion of the sea bottom not influenced by waves during that period was identified.

In other words a *closure depth*, that is the outer limit of the active section representing the strip of sea bottom directly affected by the waves, was identified along the coast between Rimini and Ravenna.

The *closure depth* was calculated using the Hallermeier (1981) and Birkemeier (1985) formulas, both of which are based on knowing the height of the wave (He) which presents an exceedance frequency of 0.137%, equal to 12 hours per year (Dean et al., 2002):

$$h_C = 2.28\,H_e - 68.5\left(\frac{H_e^2}{gT_e^2}\right) \quad \text{(Hallermeier, 1981)} \qquad [7]$$

$$h_C = 1.57\,H_e \qquad\qquad\qquad \text{(Birkemeier, 1985)} \qquad [8]$$

In the period in question, the buoy for wave measurement of Ancona (RON network), which was the reference for the study area, was not working. As such, the wave climate data necessary to calculate the wave height He was obtained using model reconstructions carried out by ARPA SIM employing the SWAN model.

The wave energy features elaborated with the SWAN model (significant wave height, wave direction, average period and peak) for the area surrounding the coast of the Region have been supplied with a calculation grid of approximately 800 m and with semi-hourly cadence.

With reference to the tract of the coast - 50 km - under study, reconstructions of the state of the sea were taken into account and analysed for 3 points situated in front of Rimini, Cesenatico and Ravenna. The reference period was 2005 - 2007.

Figure 3 shows a rose diagram for the waves – both overall and divided by height class – obtained based on the data reconstructed using the SWAN model for the 3 points described above and for the period in question.

In all three cases - albeit with dissimilarities caused by a different positioning of the calculation points - and at least for the three-year period in question, we can see that waves come from directions falling between the I and II quadrant and for the most part from the sector between NE and E, conventionally defined as the Bora and Levant sectors.

Analysing the historical series reconstructed in front of the 3 points described above, we obtained wave height values associated with wave energy events with an exceedance frequency of 12 hours a year. As such, the *closure depth* for the Rimini, Cesenatico and Ravenna coastlines was calculated applying the Hallermeier (1981) and Birkemeier (1985) formulas (Table 3).

Table 3 – Height and average wave period for an exceedance frequency of 12 hours per year and closure depths calculated using the Hallermeier and Birkemeier formulas.

Point of calculation	He (m)	Te (sec)	hc (Hallermeier) (m)	hc (Birkemeier) (m)
Rimini	2.56	5.8	4.49	4.02
Cesenatico	2.73	5.8	4.70	4.29
Ravenna	3.00	5.6	4.83	4.70
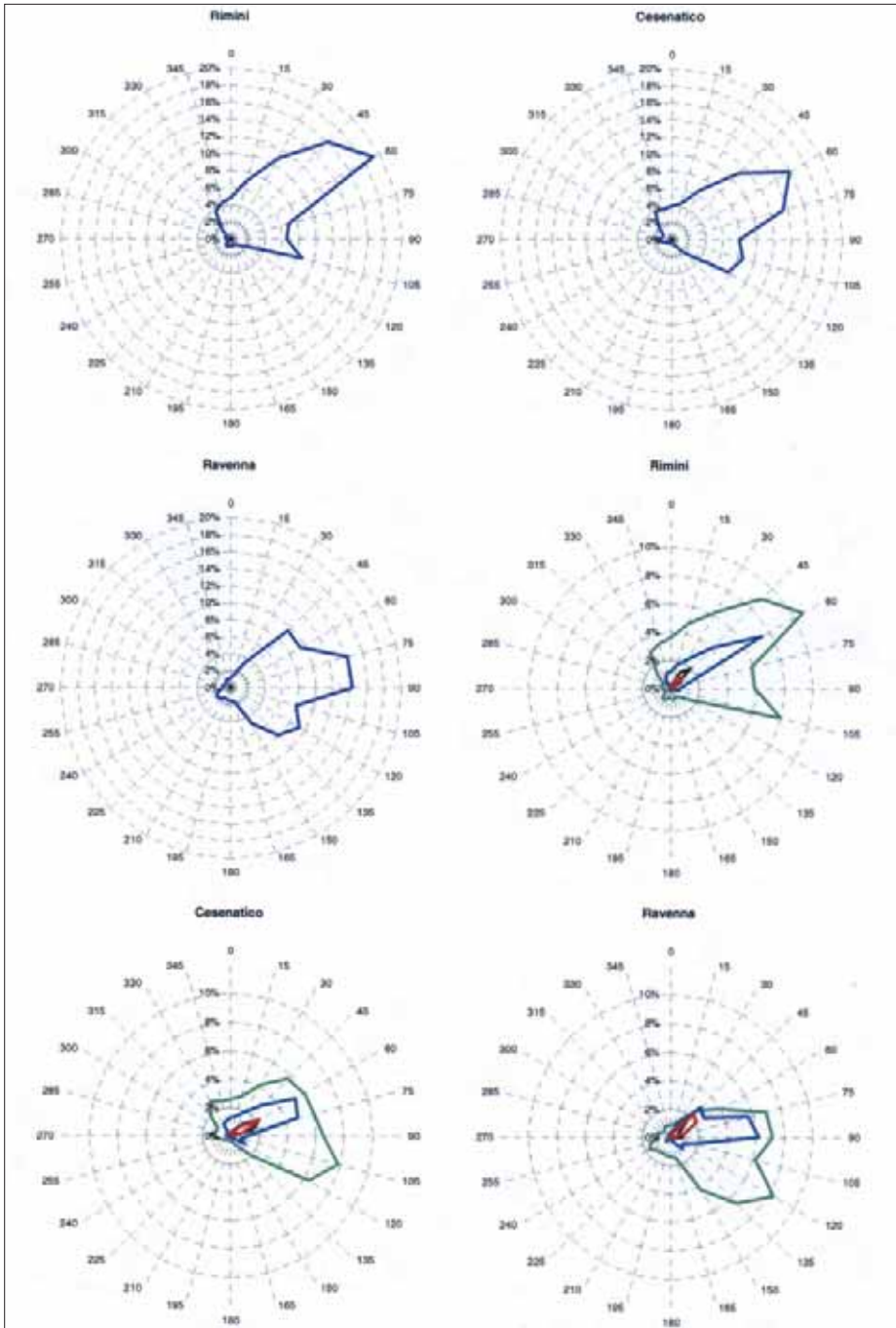
Figure 3 - Wave energy force in percentages, based on origin (overall and for interval in terms of wave height) reconstructed according to the SWAN model for the three points of interest in front of Rimini, Cesenatico and Ravenna during the 2005 - 2007 period.
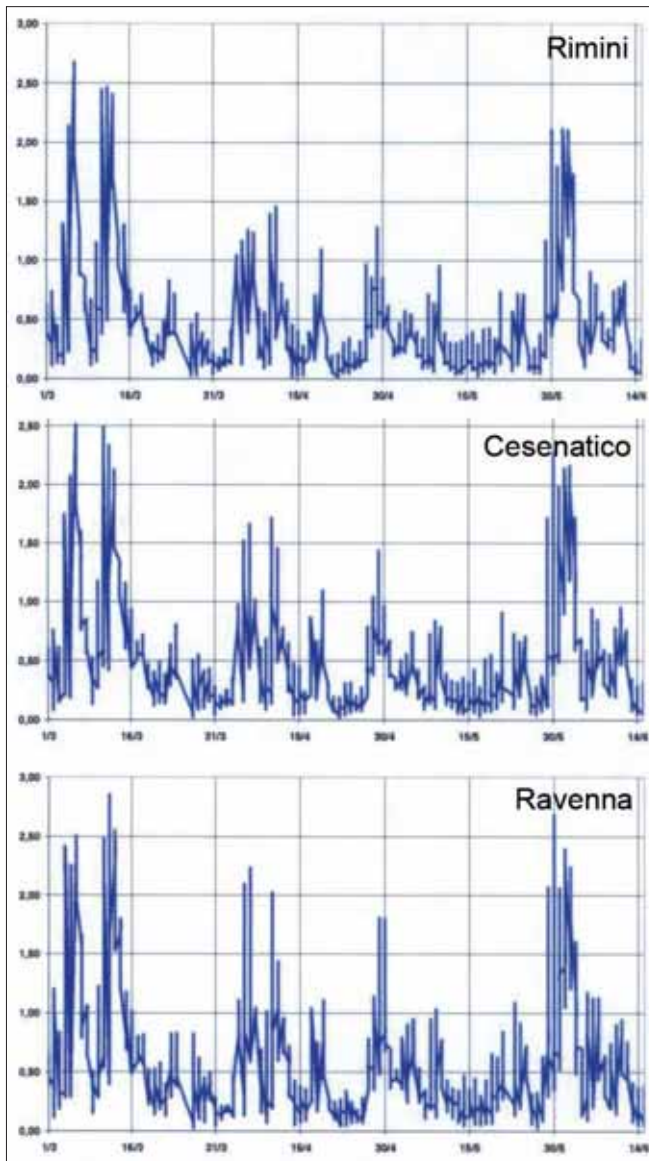
Furthermore, significant wave height trends for the period between March and June of 2006 - during which bathymetric measurements using ALB and multibeam technology were taken - were calculated using the three historical series supplied by the SWAN model.

The data illustrated in Figure 4 highlight how the height of the waves seen in this interval of time fall easily within the He values obtained for the three sites.

A single event with a significant wave height (Hs = 2.68 m) which was greater than the one registered in the 2005 - 2007 three-year period with an exceedance frequency of 12 hours a year (He$_{Rimini}$ = 2.56 m) was registered at sea in front of Rimini.

Based on the considerations described above, the depth beyond which no significant movements of materials on the sea bottom caused by waves took place was preliminarily set at 5 m along the entire tract of sea bottom between Rimini and Ravenna.

Figure 4 – Wave heights (m) at the points of interest in Rimini, Cesenatico and Ravenna, 1 March -15 June 2006.

Qualitative analysis

Two DTMs were generated using a triangulation method with a linear interpolation employing the Delaunay optimal triangular algorithm: one for the data collected using the conventional method and the other for the ALB data. These were in turn employed in various mathematical analysis and graphic elaboration, including the restitution of the bathymetric maps.

A comparison between the two bathymetric maps relative to the ALB data (Figure 5) and the conventional data (Figure 6) shows that:

– coastal structures can be identified using ALB technology. Nevertheless there are areas where data is not available due to elevated errors induced by water turbidity;
– bathymetric trends are indicatively the same for both maps.
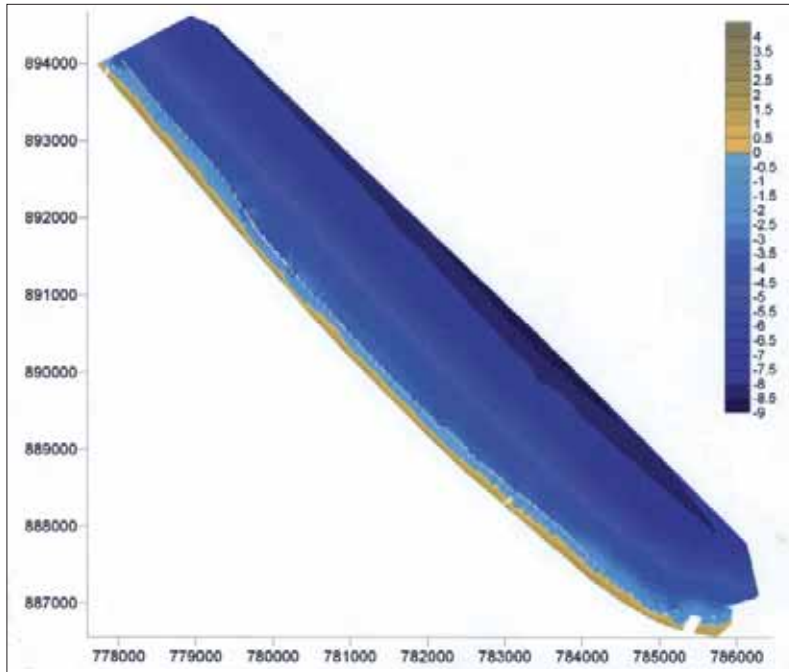
Figure 5 – Bathymetric map of the Rimini – Foce Uso coast obtained using ALB data and limited to the area covered using conventional data collection methods (figures in m).
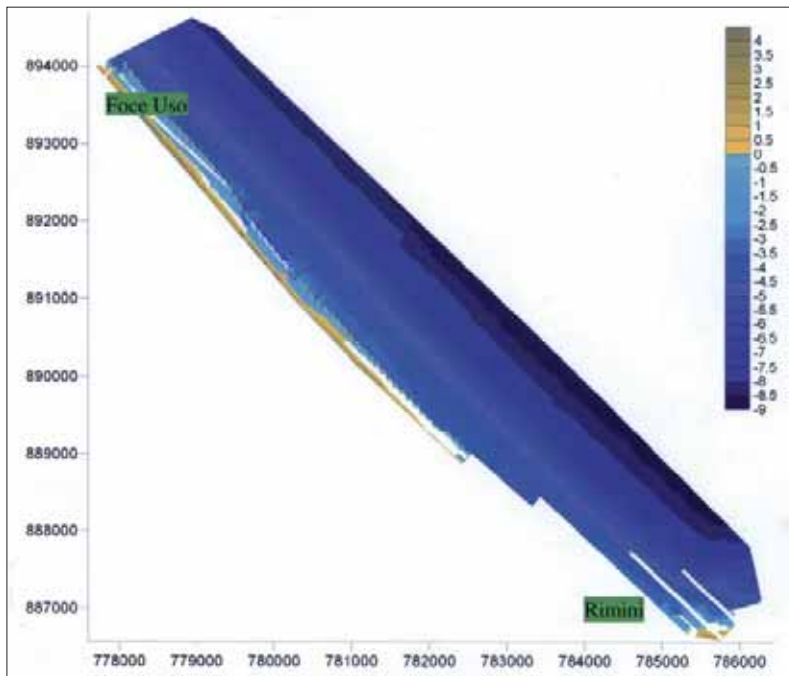
Figure 6 – Bathymetric map of the Rimini – Foce Uso coast obtained using the echo scanner (figures in m).

Figure 7 shows a detail of the area south of Foce Uso protected by detached breakwaters. Conventional data collection methods were used outside the detailed area. As such, the cross-shore profiles are approximately 500 m distant between them. However, thanks to the presence of long-shore profiles which run internal and external to the breakwaters, we can interpret the erosion found at the gaps and their diffusion within the protected area in a fairly realistic manner. This is something which is not fully possible using ALB data alone because of the absence of figures due to turbidity.

What we can see in the remaining areas is how, in general, the product of interpolations between the two sets of data are similar, even if it is obvious that the ALB data provides better circumscribed and more defined forms, given its great density.

Figure 8 instead contains a detail of the Igea Marina area marked by the presence of low-crested structures employing the data collected using conventional methods, with cross-shore profiles every 100 m and several long-shore profiles.

At a first glance, the maps appear very similar, even near the breakwater where both methods of measurement allow erosion present at the gap and at the head of the defence works to be described in a precise and defined manner.
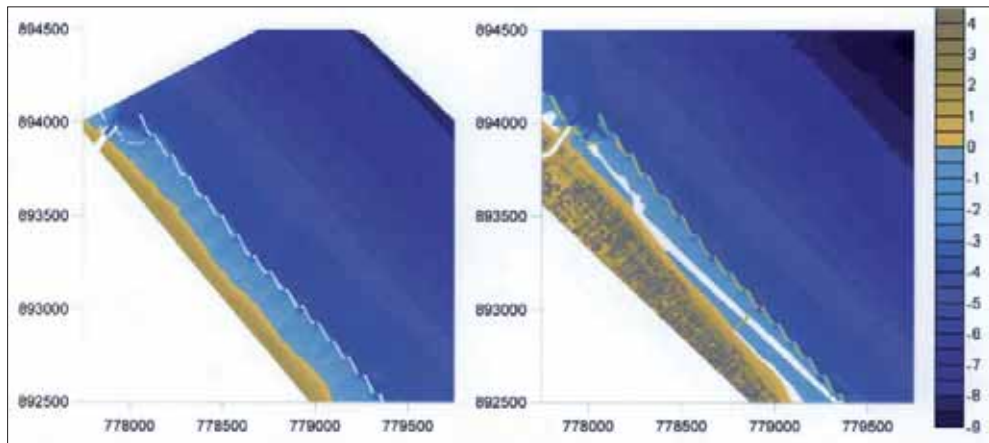
Figure 7 – Detail of the bathymetry in the area south of Foce Uso obtained using ALB data on the right, and using data collected by conventional method on the left (figures in m).
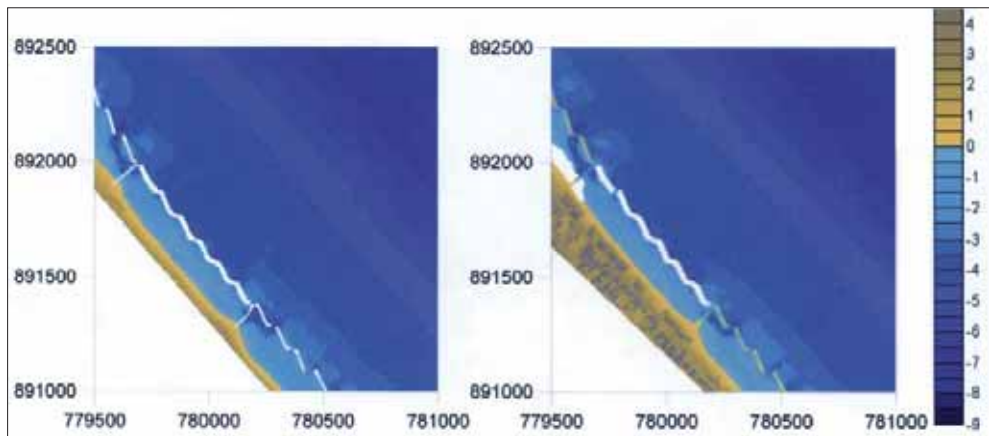
Figure 8 – Detail of the bathymetry in the Igea Marina area protected by low-crested structure obtained using ALB data on the right, and using data collected by conventional method on the left (figures in m).

This provides very important information when planning a bathymetric data collection campaign. Cross-shore profiles, measured using single-beam and multibeam echosounders, with a distance of 100 m between them and associated with longshore profiles allow for erosion to be measured with a detail very near to that which can be obtained using points positioned in a regular manner on a grid with a square 5 m mesh.

In order to compare the measurements obtained for the sea bottom using each of the technologies, two cross-shore profiles located within the area subjected to detailed measurements are illustrated in the graph below (Figure 9). What can be noted is that the sea bottom measured using the two methods is almost identical and that this concordance can be found in areas with greater depth as well, even if the differences are more marked here.
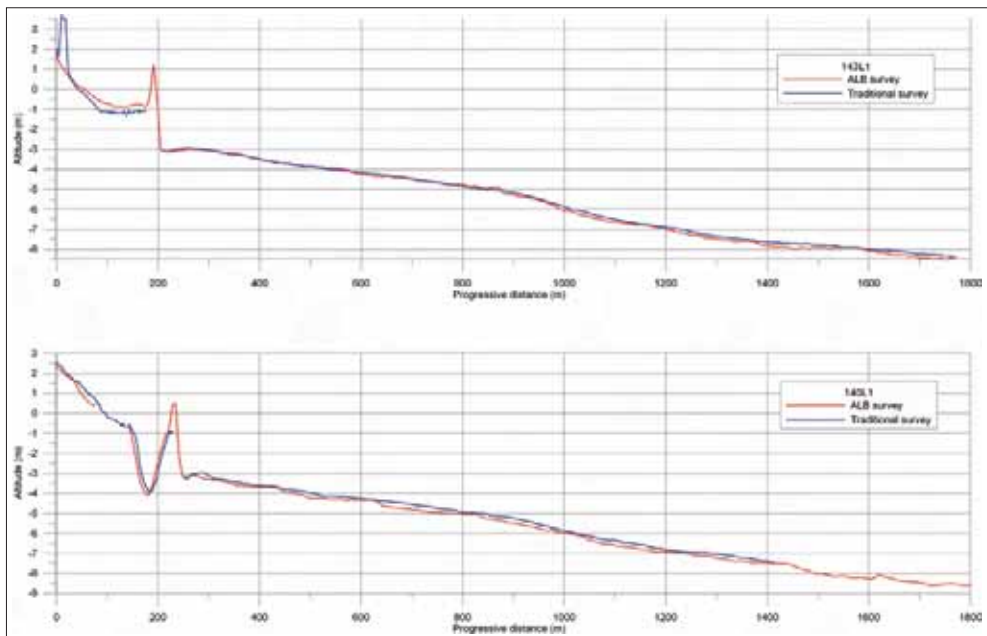
Figure 9 – Igea Marina. Comparison between the measurements taken for the cross-shore profiles using the ALB system (red line) and the conventional system (blue line). Cross-shore profiles 143L1 (top) and 140L1 (bottom) of the Emilia-Romagna topobathymetric network.

Figure 10 shows a map of the depth difference between the points measured using ALB and the measurements taken using the conventional method. The colour scale has the following meaning:
–   warm colours (from yellow to red): areas marked by depth measured using ALB lesser than those obtained using the conventional method;
–   cold colours (from sky blue to dark blue): areas with depth measured using ALB greater than those obtained using the conventional method;
–   white: areas where the depth difference in absolute values is less than or equal to 15 cm.

Looking at the map of depth differences measured using ALB and the echosounder (Figure 10) we can see that the measurements taken using conventional topobathymetric methods in the area between the shoreline and the inner limit of the breakwater records a greater depth compared to the measure obtained using ALB.

The conventional method instead records a less deep sea bottom in the area beyond the coastal defence system when compared to the one measured using ALB.

Taking into account the fact that both areas were measured using different tools, the results find confirmation in the studies carried out by Milli and Surace (2006) and Intelmann (2006), which show that measurements taken using single-beam and multibeam are respectively deeper and less deep than those obtained with ALB.

Nevertheless, what must also be remembered is that an interval of two and a half months passed between the times when the two measurements were taken. Materials could have been deposited on the back of the defence works during this time which may have been the cause of the rise in the sea bottom registered by LiDAR.

The situation is instead different when looking at the data acquired using multibeam, since the progressive decrease of the areas marked in yellow and the preponderance of cold colours recorded while moving towards the 5 m isobath - and therefore beyond the closure depth of the period between the two measurements – validate the hypothesis that ALB data is systematically deeper than data measured with an MBE.
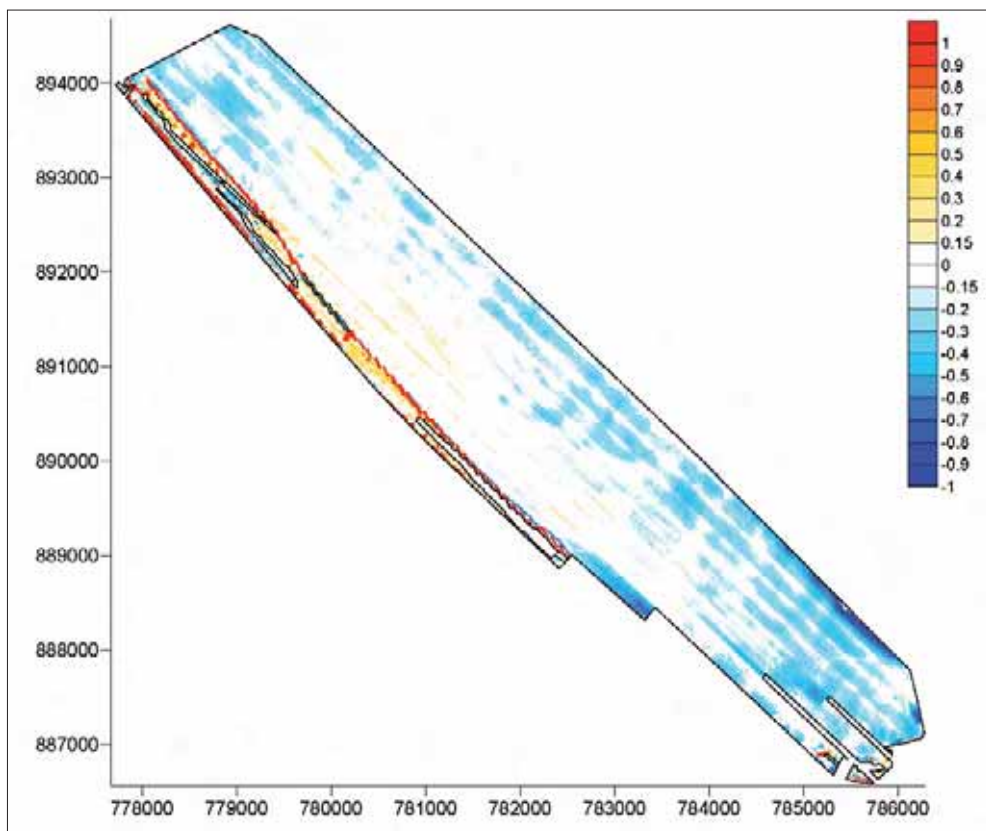
Figure 10 – Rimini - Foce Uso. Map of the differences depth when comparing ALB data with conventional data.

Statistical analysis

After a qualitative analysis of the sea bottom using the two data sets was carried out, a statistical analysis was also performed on the difference in depth between points measured with ALB and those measured using the conventional method.

The data collected using the conventional method was projected on a grid obtained by interpolating ALB points.

Subtracting the depth measured using the conventional method for a depth referring to the ALB map, we obtained the random variable $\Delta_{(ALB-Trad)}$, which was subjected to statistical analysis.

As such, all points belonging to the emerged beach were eliminated, since normal maintenance operations for the beach nourishment can lead to changes in the morphology of this part of the coast and therefore render a comparison between ALB measurements and measurements taken using conventional instruments - in this case GPS only - meaningless.

To carry out a statistical analysis, the data was subdivided into the following areas:

–   submerged beach, from a bathymetry of 0 m to the inner limit of the breakwater;
–   submerged coast, from the breakwater on the side of the sea to the end of the cross-shore profile (bathymetry of 6 m – 10 m), which was in turn broken down into:
    –   area 1: from the bathymetry of 5 m to the end of the profile;
    –   area 2: from the bathymetry of 6 m to the end of the profile;
    –   area 3: from the bathymetry of 7 m to the end of the profile;
    –   area 4: from the bathymetry of 8 m to the end of the profile.

Using a Matlab7 script created especially for this purpose, the mean difference Δ_{mean} between depth measured using LiDAR and that measured using the conventional system was calculated for each area. The number of points with values $\Delta_{(ALB-Trad)}$ falling within each single depth difference class was also counted. Classes have a depth of 2.5 cm and are distributed inside a [-100 ÷ 100] cm interval. The classes which mark the passage from negative to positive values correspond respectively to 41 [-2.5 ÷ 0] cm and 42 [0 ÷ 2.5] cm.

Furthermore and still using the Matlab7 script, we also subtracted Δ_{mean} from each single value $\Delta_{(ALB-Trad)}$, obtaining a residual vector r.

This variable is not disturbed by systematic effects, and therefore has a null average distribution r_{mean} from which quadratic mean deviation δ can be calculated as

$$\delta = \sqrt{\frac{\sum_{i=1}^{n}(r_i - r_{mean})^2}{n}} \qquad [9]$$

As such, using this procedure we were able to calculate probability distribution parameters for each area, that is the average Δ_{mean} and the standard deviation δ.

We then evaluated these results and identified and positioned any outliers - in other words, any points where the absolute value was $|r| = |\Delta_{(ALB-Trad)} - \Delta_{mean}|$ greater than 3δ.

The procedure described above was applied to the data obtained for the area defined submerged beach of Igea Marina and led to the development of the histogram in Figure 11. The probability distribution for this area is not comparable to a Gaussian distribution and is proof that the difference in depth is affected by a non random error, which cannot be eliminated.
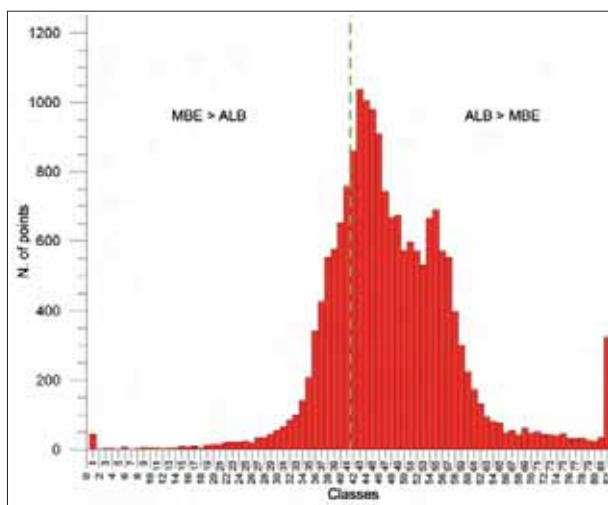
The mean of the depth difference measured in this area is of Δ_{mean} = 0.17 ± 0.30 m.

Figure 11 – Histogram of the number of points on the submerged beach in the Igea Marina area falling within the various classes with widths of 2.5 cm.

Two-hundred-sixty-four outliers were identified. Taken with their position, these were used to iden-
tify any localised systematic errors. In fact, the presence of anomalous points - physiological in a
turbid and complex area such as the one in question - can be the sign of a systematic effect if the
points are concentrated in certain areas.

As can be evinced from Figure 12, the outliers are located in the gaps between the breakwaters
and next to the groins. The simplest explanation for this could be either measurement errors due to
increased turbidity - which may be present in such areas – or caused by the presence of rocks which
may interfere both with LiDAR laser beams and acoustic MBE beams.
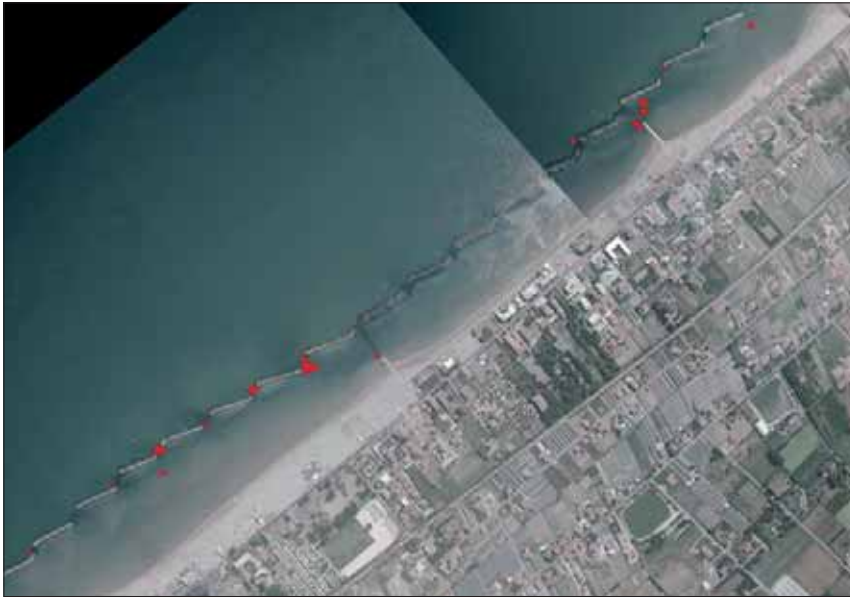
Figure 12 – Location of the outliers.

As such and for the reasons described above - that is because of the presence of a systematic error
which cannot be modelled and because of the interval of time which elapsed between when the two
measurements were taken - we decided not to take the statistical analysis of the points within the
area protected by the breakwaters into account, since the presence of this data would completely
change the trend in mean differences seen for the two measurements.

Therefore, having eliminated the points belonging to the submerged and emerged beach from our
statistical analysis, the comparison becomes between ALB measurements and MBE measurements
taken using the points within the area so-called submerged coast.

Looking at the values assumed by $\Delta_{(ALB-Trad)}$ in histograms representing the number of points within
each class for depth differences (Figure 13) in each area of the submerged coast on the Igea Marina
area where detailed measurements were taken using conventional methods, we can immediately
see that:

– the probability distribution followed by the variable is more easily comparable to a Gaussian
distribution;

– the bell curves are not centred on zero, but on classes 35 to 40. That is, they are always below
the transition classes between positive and negative numbers, i.e. classes 41 - 42.

This first analysis leads us to conclude that $\Delta_{(ALB-Trad)}$ is affected by a systematic error, since the mean
is not zero. However, once this systematic error is removed, the residual error is random since the
histograms reflect a normal distribution.

Furthermore, constant negative modal values for $\Delta_{(ALB - Trad)}$ can once again be taken as proof in support of the hypothesis that MBE data is systematically less deep than ALB data. It confirms the correctness of excluding negative data from the submerged beach from the analysis in question, where the opposite can be seen.

Analysing the way the histograms evolve as depth increases, we can also note that as we move towards deeper waters - that is as we progressively eliminate the points closest to the shore from our analysis - the Gaussian tail disappears, reflecting a fall in the number of outliers. Furthermore, the bell curves also become smaller, prooving that the values are marked by lesser dispersion around the mean.

Nevertheless, the most interesting result remains the progressive concentration of means from classes 35 - 39 recorded for the entire submerged coastline to classes 35 - 36 for measurements taken for the bathymetry from 5 m onwards.
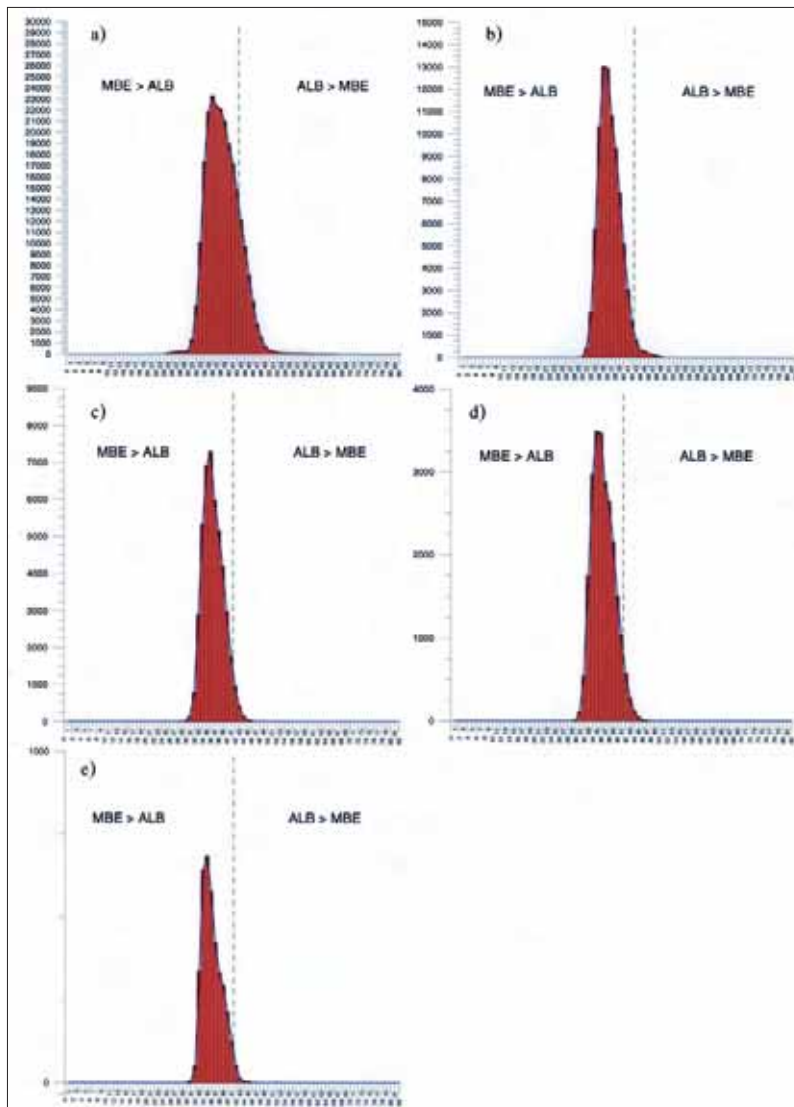
Figure 13 – Histograms of the number of points in the Igea Marina area subject to the study falling within the classes widths of 2.5 cm. a) submerged coast; b) area 1; c) area 2; d) area 3; e) area 4.

The plot which can be seen in a visual analysis of the histograms is confirmed by an analytic calculation, where Δ_{mean} takes the following values:

−   submerged coast: Δ_{mean} = -0.07± 0.11 m;
−   area 1: Δ_{mean} = -0.12 ± 0.07 m;
−   area 2: Δ_{mean} = -0.12 ± 0.06 m;
−   area 3: Δ_{mean} = -0.12 ± 0.07 m;
−   area 4: Δ_{mean} = -0.13 ± 0.06 m.

For the entire submerged coast, once the points located immediately next to the breakwaters are excluded, we can see that the value of Δ_{mean} remains - for the most part - constant.

Extending this statistical analysis to all of the Rimini - Foce Uso coastline, starting from a depth of 5 m and therefore increasing the number of points and - above all - the area under examination, we can see that the variable depth difference is still distributed according to a Gaussian distribution, but that it is marked by greater dispersion, given the 830 outliers defied, and by a mean of Δ_{mean} = -0.17 ± 0.09 m.

Nevertheless, when the area subject of the study is increased to include all of the area covered using both types of measurements (Rimini - Marina di Ravenna), we are faced with the problem of the value of the variable being dependent on the transparency of the sea for the area in question.

In fact and keeping in mind that ALB data remains systematically deeper than data collected using MBE, we can see that - starting from Rimini and moving North towards Marina di Ravenna - the value of Δ_{mean} is highly variable, both long-shore and cross-shore, as shown in Figure 14.
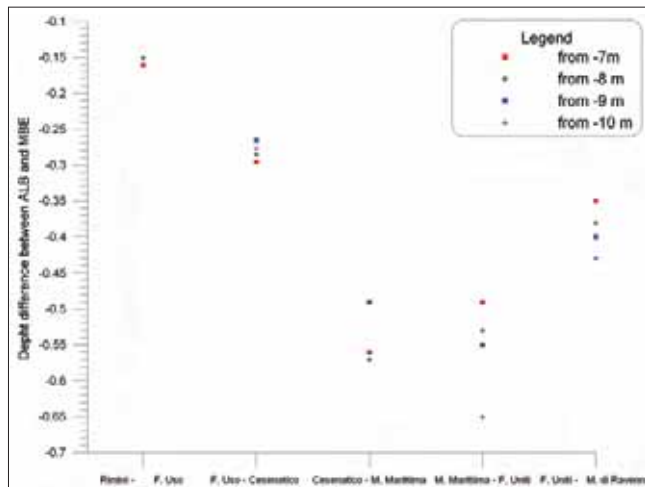
Figure 14 – Mean depth differences calculated starting from different depth for the entire coastline measured using ALB.

Three elements can be seen:

−   the mean calculated starting from the same depth differs greatly from area to area;
−   there is no regular trend for means calculated from increasing depth within each given area;
−   mean differences diminish as we move between Rimini and the mouth of the Fiumi Uniti, before starting to increase again up until the port of Ravenna.

This phenomenon leads us to question the possibility of the existence of a systematic effect in the area in question. Taking into account the fact that water transparency appears to be the single most influential factor in obtaining good results with ALB, we immediately tried to connect the dispersion of the data to the presence of turbidity.

In truth, the turbidity plotted along the coast of Romagna may explain both the cross and long shore trend for the size taken into consideration. As shown in the graph above - starting from

Rimini - the absolute value of the differences and the distance between means calculated from different depth increase rapidly, reaching their peak between Cesenatico and the mouth of Fiumi Uniti. That is, it is at a maximum in areas with the greatest turbidity, before diminishing again as we move towards the port of Ravenna, where the waters are marked by greater transparency. This is probably caused by the screening effect that offshore dams have on the sediments transported.

In fact, when calculating an estimated mean of the depth difference of each area - while taking into account only points beyond the closure depth from sediment movements – we obtain the following results:

– Foce Uso – Cesenatico: -0.28 m $< \Delta_{mean} <$ -0.30 m;
– Cesenatico – Milano Marittima: -0.49 m $< \Delta_{mean} <$ -0.57 m;
– M. Marittima – Foce F. Uniti: -0.53 m $< \Delta_{mean} <$ -0.65 m;
– Foce F. Uniti – M. di Ravenna: -0.38 m $< \Delta_{mean} <$ -0.43 m.

Looking at these parameters, we can see that the depth difference between the data collected using ALB and the data collected with MBE is affected by a systematic effect which survives both the correlations made during post-processing and when calibrating the instruments and which is difficult to model and eliminate. This effect is probably connected to the turbidity of the water when the measurements were taken.

Conclusions

A statistical analysis carried out based on a comparison between data collected using ALB and data collected using a multibeam system allowed us to reach the following conclusions:

– depth measured with ALB are systematically deeper than those measured using the multibeam;
– when water transparency conditions are good, the depth difference between measurements taken using each of the two methods can be calculated as Δ_{mean} = -0.17 ± 0.09 m;
– the quality of measurements taken using ALB is strongly dependent on water transparency. In fact, in areas with greater turbidity, measurements are invalidated by the presence of an elevated number of errors which are difficult to eliminate.

From an operative point of view, we saw that:

– the amount of time necessary to take measurements using ALB is less than that required with conventional methods;
– the ALB system allows operators to take measurements of the beach and coastal structure as well as the sea bottom.

In terms of costs, we estimated that ALB measurements oscillate around 1.000 and 2.000 €/km², for areas with minimum surface areas of around 50 - 100 km². As such, they are competitive when compared to measurements taken using conventional methods.

Lastly, taking bathymetric measurements on coasts with features similar to those seen in Emilia Romagna region using the ALB system is surely - under certain conditions – a valid system. Nevertheless, it cannot as yet be considered to be an alternative to measurements taken using an echosounder.

Firstly, because these coasts are marked by a high number of river mouths which dump the sediment loads they transport into the sea. They also have a sandy sea floor, which is easily suspended by waves, causing high water turbidity.

Secondly, many of the areas monitored are small. As such, the high initial cost of using ALB does not render it cost effective.

Acknowledgements

References

AA. VV. (2005) - *Le projet Beachmed: Récupération environnementale et entretien des littoraux en érosion avec l'utilisation des depots sablonneux marins* (Convention 2002-01-4.3-I-028). 3ème cahier technique (phase C). Roma. pp 81.

AA. VV. (2007a) - *Le projet BeachMED-e: La gestion stratégique de la défense des littoraux pour un développement soutenable des zones côtières de la Méditerranée.* 1er cahier technique (phase A). Roma. pp. 40-41.

AA. VV. (2007b) - *Le projet BeachMED-e: La gestion stratégique de la défense des littoraux pour un développement soutenable des zones côtières de la Méditerranée.* 2éme cahier technique (phase B). Roma. pp. 38-39.

Dean R., Kriebel D. and Walton T. (2002) – *Cross-shore sediment transport processes*, USACE Coastal Engeneering Manual, part III: coastal sediment processes. Available at http://chl.erdc.usace. army.mil/cemtoc.

Intelmann S. (2006) - *Comments on Hydrographic and Topographic LIDAR Acquisition and Merging with Multibeam Sounding Data Acquired in the Olympic Coast National Marine Sanctuary.* Marine Sanctuary Conservation Series ONMS-06-05. Silver Spring, Maryland. pp. 1-16.

IHO-International Hydrographic Organisation (1998) – *IHO standards for Hydrographic Surveys.* Special Publication No 44, 4th Edition.

Milli M. and Surace L. (2006) - *Tecniche innovative e tradizionali a confronto nella realizzazione di rilievi batimetrici costieri: un caso di studio.* Bollettino SIFET 2: 11-31.

Tenix LADS Corporation (2006) – *Report of survey: Ravenna Coast, Italy 2006.*

High-resolution seismic technology: application to coastal zone management

Belén Alonso

The seismic reflection method is based on the transmission of a seismic wave and the recording of the arrival time of reflected waves at a series of detectors (hydrophones) located at a given distance from the transmission source. These waves travel downward until they reflect off an interface that has varying properties (Blondel and Murton, 1997).

High-resolution single-channel seismic reflection is a methodology mostly used in the study of continental margins and deepsea areas. Studies using this seismic method in coastal zones demonstrate how employing it in submerged coastal environments provides also extensive information about the subsoil and the accumulation of sedimentary bodies deposited in coastal areas (Saito et al., 1998; Lobo et al., 2005; Certain et al., 2005).

Changes in the coastal system mainly depend on the balance between the amounts of sediment and mixing caused by swells. These two factors mostly determine the surface area, shape, volume, and extent of sedimentary bodies that develop in the infralittoral zone. The study of these sedimentary bodies using seismic reflection allow to recognise the historical evolution of the coastal environment, estimate the perpendicular transport to the coast, and assess the effects of the longshore transport. Overall, morpho-sedimentary information on the coastal zone can be an effective tool in coastal management.

Within the framework of BEACHMED-e/OpTIMAL project, which performed a quantitative analysis of the morphological and sedimentological evolution of coastal zones as a vital step in the integrated management of coastal areas, the continental margin group from Institute of Marine Sciences of Barcelona (ICM-CSIC) has concentrated on assessing the application of high-resolution seismic reflection in combination with multibeam bathymetry as a tool for coastal zone management.

In March 2007, during the seismic testing phase, researchers of ICM of Barcelona used a GeoPulse Boomer (350 KJ) to test several *in situ* configurations, determining the best configurations for obtaining satisfactory results in terms of resolution, penetration, and efficacy. The chosen configurations given a resolution between 0.75 m and 1 m and a penetration of about 20 m were achieved.

The assessment of the application of high-resolution, single-channel seismic reflection to coastal zone management was brought to a successful conclusion thanks to the geological study that identified and characterised the infralittoral prism in an area of the Catalonian coast (between Premià de Mar and El Masnou). For this project, the following tasks were carried out in the infralittoral sedimentary bodies: i) distribution and definition of geometry; ii) characterisation of seismic facies; iii) determination of sediment structure.

The results of this study show how high-resolution seismic technology was able to provide the penetration and vertical resolution necessary to: i) Locate and delimit the sedimentary bodies that participate in the construction of the submerged coastal zones, and study their space-time relationships; ii) Establish the hierarchization of the infralittoral environment; and iii) Reconstruct the paleo-topographies to determine the thicknesses and spatial variations in the present infralittoral prism; iv) Determine the shallow pattern as well as the types of sedimentation in the infralittoral zone; and v) Define sedimentation cyclicity and its relationship to climate change and sea levels of centennial and millennium scales,

to compare the results to the present status with respect to the historical evolution of the coast, and to evaluate possible horizontal transport to the coast and the effects of longshore transport.

The results of this pilot study indicate that high-resolution seismic reflection is a useful tool in the study of coastal deposits and can be effectively applied to coastal management studies. Moreover, seismic technology is easy to operate and install and can be used in the future in other regions. In conclusion, its use provides detailed information on the coastal sedimentary system and its current status with respect to historical trends; this information is central to develop a *coastal management strategy*. Among the applications of high-resolution seismic methods in monitoring coastal zones, we note the following:

- Identification of anthropogenic impact areas, such as dredging sites;
- Localisation and delimitation of sedimentary bodies in the coastal prism as potential sources of sediment of beaches;
- Deep delimitation of the thickness of moving sand and sandbars that can potentially be reworked and considered in future recovery projects, both natural and artificial. The internal structure of sandbars makes it possible to increase our understanding of the current dynamics involved in the construction and destruction of sandbars;
- Determination of the architecture of the coastal prism, expanding our knowledge of the current morphological and sedimentological changes in the coastal system.

References

Blondel P.H. and Murton B.J. (1997) - *Handbook of seafloor sonar imagery*. PRAXIS-Willey and Sons Ed., Chichester. pp. 314.

Certain R., Tessier B., Barusseau J-P., Courp T. and Pauc H. (2005) - *Sedimentary balance and sand stock availability along a littoral system. The case of the Western Gulf of Lions littoral prism (France) investigated by high resolution seismic*. Marine and Petroleum Geology, 22: 889-900.

Lobo F.J., Fernández-Salas L.M., Hernández-Molina F.J., González R., Dias J.M.A., Díaz Del Río V. and Somoza L. (2005) - *Holocene highstand deposits in the Gulf of Cadiz, SW Iberian Peninsula: A high-resolution record of hierarchical environmental changes*. Marine Geology, 219: 109-131.

Saito Y., Katayama H., Ikehara K., Kato Y., Matsumoto E., Oguri K., Oda M. and Yumoto M. (1998) - *Transgressive and highstand systems tracts and post-glacial transgression, the East China Sea*. Sedimentary Geology, 122: 217-232.

The Masnou infralittoral sedimentary environment (Barcelona province)

David Casas, Gemma Ercilla, Ferran Estrada, Ruth Durán, Marta Nuez, Belén Alonso, Marcel-lì Farrán

This study was undertaken using shallow-water multibeam echosounder and a Geo-Pulse system. Five groups of morphosedimentary features are identified regarding their genesis. In the infralittoral environment of the El Masnou coast, four of them represent sedimentary features (depositional, erosive, instability and hydrodynamic features) and the fifth one is an anthropogenic feature. The depositional features comprise infralittoral wedges; the erosive features include furrows and terraces; the instability features are characterized by slides; the hydrodynamic features refer to fields of large- (hundreds of meters long) and small- (tens of meters long) scale wavy bedforms; and the anthropogenic features comprise trenches and pits related to successive dredges. The late Holocene stratigraphy of the infralittoral environment is defined by two major seismic sequences, lower and upper, each one formed by internal seismic units. The development of this stratigraphy and stacking patterns has been governed by sea-level changes. The stratigraphic division represents the coastal response to the last 4th order transgressive and highstand conditions, modulated by small-scale sea level oscillations ($\approx$1 m - 2 m) of 5th to 6th order.

Introduction

The present study has been carried out in the framework of INTERREG European Project Beachmed-e / OpTIMAL. A special target of this project is to study the vulnerability to coastal infrastructures (ports, piers, dams, breakwaters, reefs, etc.) affecting sediment transport along the Mediterranean coastline. The present study was carried out in the framework of this target, to asses the vulnerability of the El Masnou harbour, in the Barcelona province (Figure 1). This infrastructure interrupts the longshore transport of sediment, which causes two unwanted effects in the El Masnou coast: i) sediment accumulation off the breakwater, resulting in harbour infilling that blocks its entrance, and ii) erosion of the coast in the neighbouring areas, with the resulting loss of beach for tourist amenities. A study of the infralittoral environment of the El Masnou coast has been carried out, in order to assess the vulnerability of the El Masnou harbour. The length of the coast under investigation is about 10 km and the water depth extends from the interlittoral down to about 34 m of water depth. The present article defines and characterises the late Holocene sedimentary infralittoral environment of the El Masnou coast. We present a detailed description of the morphosedimentary features, seismic and sequence stratigraphies, and also the depositional model of the infralittoral environment.
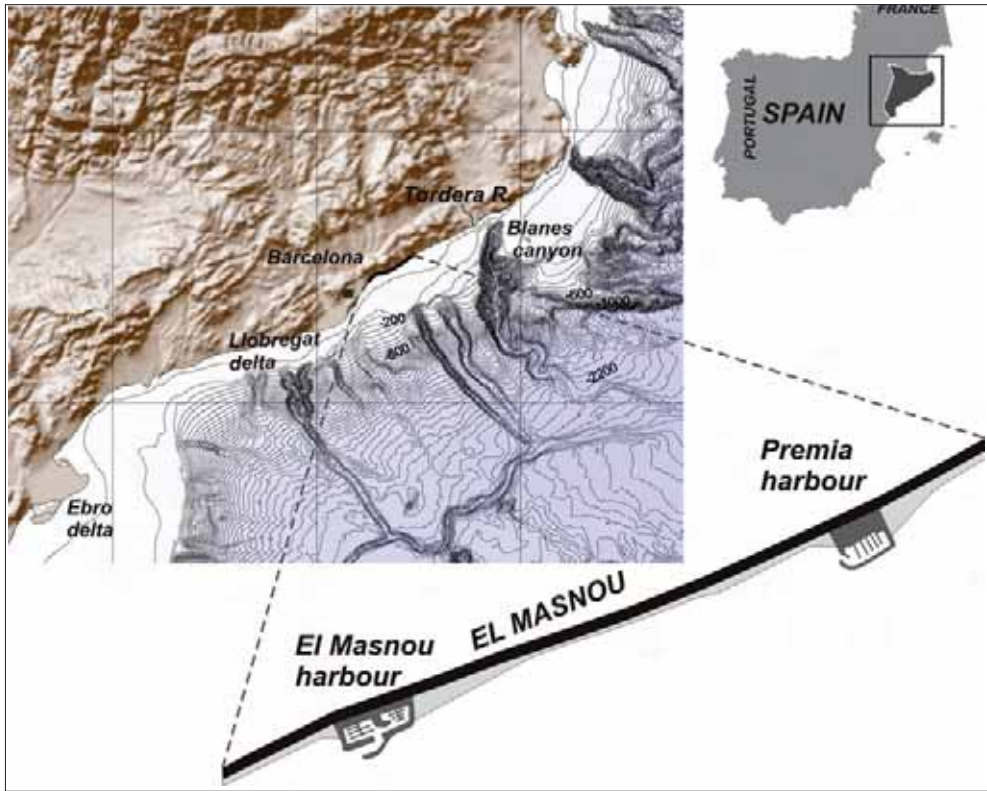
Figure 1 – The study area is located in the Masnou coast, Barcelona Province, Spain.

Methodology

The present study was carried using methods as shallow-water multibeam echosounder and a 350KJ Geo-Pulse system (Figure 2). Two multibeam bathymetric surveys were carried out in November 2006 and May 2007. The comparison between the bathymetric maps was used to monitor the temporal variability of the morphologic features. High-resolution seismic reflection profiles were collected along 136 km with a Geo-Pulse system. These profiles vary in quality according to
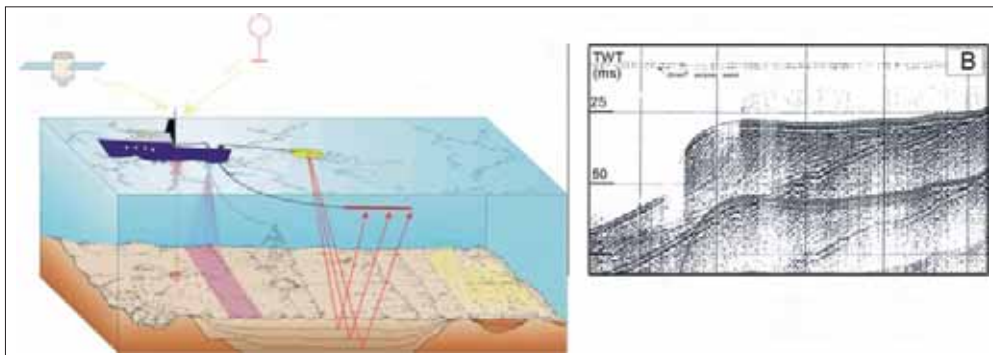
Figure 2 – (A) high resolution seismic sketch, with an acoustic source plate mounted on a Catamaran and (B) example of high resolution profile.

sea conditions, but the major regional reflectors and stratal patterns can be correlated and recognised over most of the area to characterise the existing sedimentary bodies such as littoral prisms, their thickness, extension, lateral variability and morphosedimentary evolution.

The GeoPulse Boomer (Figure 2) is a seismic system widely used for high resolution, deep penetration profiling both in proximal margin and shallow coastal environments. The system has an average resolution between 0.75 m and 1 m and a penetration of about 20 m. The discontinuity surfaces plus seismic facies were used to define the seismic sequences and units, the two hierarchies of depositional units that we used to define the stratigraphy of the infralittoral environment. The natures of the bounding reflectors, the reflector configuration, and the architecture pattern were used to interpret the depositional events at two different scales: seismic sequences and units.

Geological Setting

The Masnou coast is located in the mid Catalan Sea and displays a NE-SW trend. It is a sandy, wave-dominated coast. The sediment source comprises short (few kilometres long), ephemeral streams. The Holocene littoral prism of this area displays a wedge-shaped geometry whose thickness decreases seaward to disappear at about 30 m water depth (Medialdea et al., 1989). The Pleistocene-Holocene continental shelf of the Masnou region is made up of the vertical stacking of downlapping regressive deposits (Medialdea et al., 1989; Díaz and Maldonado, 1990).

Morphology

Five groups of morphosedimentary features are identified regarding their genesis (Figure 3). Four of them represent sedimentary features, and they are the following: depositional, erosive, instability and hydrodynamic features. The fifth one is a man-made feature. The depositional features are the largest ones (tens of kilometres) and their seafloor is affected by the rest of them that are of minor scale (tens and hundreds of meters, and kilometric).

The depositional features comprise infralittoral wedges; they are shore-subparallel and seaward bodies that extend from the distal edge of the shoreface. At least two superimposed infralittoral wedges extending down to different water depths are found between the interlittoral domains down to 32 m water depth. The lower or older infralittoral wedge extends down to 26 m - 32 m; the younger one reaches variable water depths, down to 7 m and 15 m.

The erosive features include furrows and terraces. The furrows comprise series of negative irregular lineations of tens and hundreds of meters of length and metric relief. They mostly appear in the proximal areas, down to 10 m water depth, affecting the seafloor of the youngest infralittoral wedge, although one series is also identified between 14 m and 30 m water depth, affecting the older one. The terraces define striking kilometric long scarps of metric relief with the steep side oriented seaward. At least four series of terraces, parallel to the bathymetric lines are identified at different water depths, all of them seaward of the older depositional wedge, where the transition to the inner shelf occurs.

The instability features are characterised by slides that are easily recognisable on the surface by their scarp (125 m to 325 m wide) and the sliding sediment resting at the base of the scarp. At least four slides are mapped. They affect the near-surface of the older and younger infralittoral wedges.

The hydrodynamic features refer to fields of large- and small-scale wavy bedforms. The larger-scale wavy bedforms comprise at least 13 large WNW-ESE and NW-SE ridges (hundreds of meters long), on the proximal part of the older infralittoral wedge. The smaller-scale wavy bedforms (tens of meters long) are characterised by sinuous- and straight-crested features with a NNE-SSW and NE-SW, and some are linear and other display bifurcations. The several multibeam bathymetries obtained in the study area along the years 2006-2007, indicate that only the small-scale wavy bedforms located at shallower water depths (< 10 m) off the El Masnou breakwater changed their shape, whereas the rest seems to remain invariable.

The anthropogenic features comprise trenches and pits, formed by the action of the successive dredges that are used for the nourishment of the eroded El Masnou beach and to avoid the infilling of the harbour entrance.
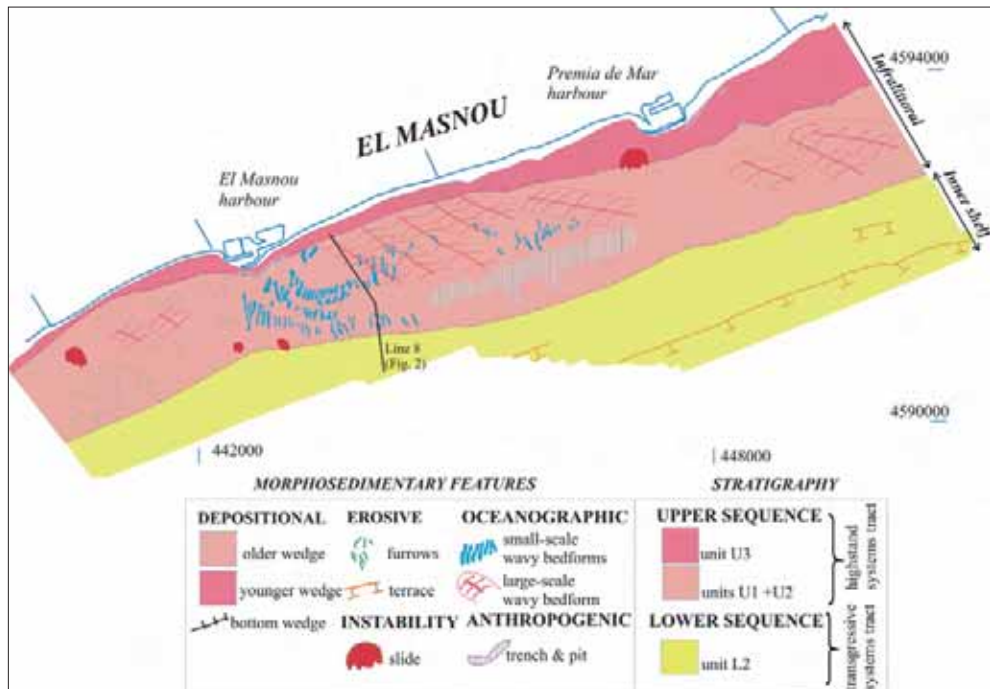
Figure 3– Morphosedimentary map displaying the main features and the surficial distribution of the seismic sequences and units in the El Masnou infralittoral environment.

Seismic stratigraphy

The high resolution seismic stratigraphy analysis of the El Masnou infralittoral environment allows us to differentiate two major seismic sequences, lower (L) and upper (U), each one formed by internal units (Figure 4). The thickness of both sequences is at least > 65 m (twtt). These sequences rest unconformably onto an erosive surface that is regionally traceable throughout the continental shelf (Medialdea et al., 1989; Díaz and Maldonado, 1990). The lower seismic sequence comprises two subtabular units (L1 and L2, from older to younger) separated by a discontinuity surface that onlaps onto the mentioned regional erosive surface. The lower boundary of L1 and L2 is a discontinuity surface defined by a coastal onlap surface; in the L2 unit this surface evolves seaward to a downlap surface. The upper boundary seems to be a toplap and/or an erosive surface, and that one of the L2 unit represents the seafloor surface, seaward from 26 m - 32 m water depth. Internally, both units are formed by clinoforms with oblique and backsteeping aggrading configurations, and also by amalgamated concave reflectors. The distal ends of both units extend toward the inner shelf, far away from the limits of the study area. All these reflectors define an aggrading-prograding stratal pattern in each unit. The vertical stacking of both units lends a retrogradational or backsteeping pattern to the lower sequence.

The upper seismic sequence rests unconformably over the lower sequence and the erosive surface in the most proximal areas. It comprises at least three units, U1, U2 and U3, from older to younger. These units are parallel to the coast and display a wedge shaped geometry internally defined by seaward downlapping clinoforms. Their development and distribution are different.
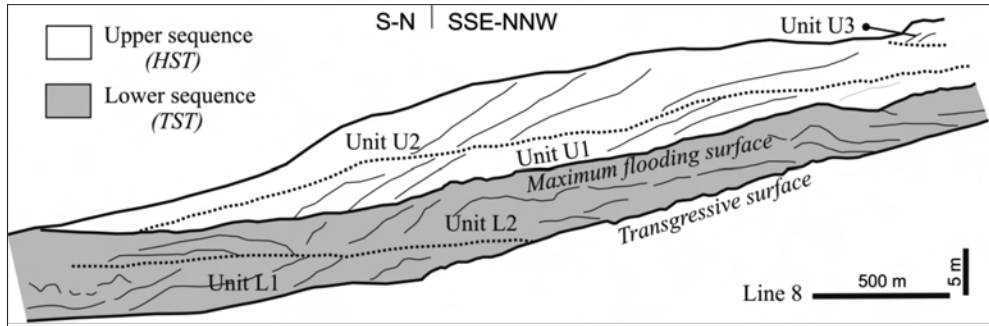
Figure 4 – Line drawing of Geo-Pulse seismic line displaying the defined seismic and sequence stratigraphy. Location of line in Figure 3.

The vertical stacking of U1 to U3 deposits shows a retrogradational pattern. These units corre-spond to the depositional wedges defined on the morphology. The U1 and U2 units have been studied in detail. Their lower boundary is a downlap surface and the upper boundary seems to be a toplap surface. Internally, they are defined by seaward prograding reflectors. These units have an unequal alongshore development, being better developed to the north where both units add up to 20 m thick and extend down to 32 m water depth, than to the south where add up to 7 m thick and extend down to 26 m water depth (Figure 5). With respect to U3, only the most distal part of the wedge was surveyed. This part is characterised by a seaward downlapping pattern.
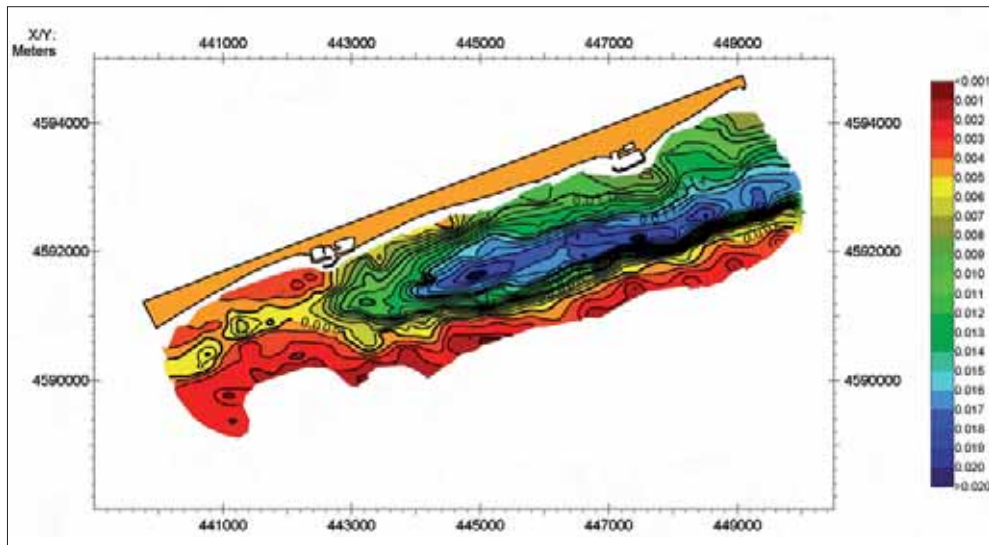
Figure 5– Upper seismic sequence isopach map showing its development alongshore. Vertical scale in seconds.

Sequence stratigraphy age model

The development of this stratigraphy and stacking patterns has been governed by late Holocene sea-level changes (Figure 6). The basal erosive surface underlying the lower and upper seismic se-quences represents the transgressive surface developed during the last 4th order-Versilian trans-gression (18.000 to ca. 6.900/65.000 yr BP - Hernández-Molina et al., 2000). Consequently, the basal erosive surface in our study area developed during the last stages of this interval. The onlapping

seismic facies and backsteeping stratal pattern that characterise the lower sequence indicate that it is formed by transgressive sediments deposited during that transgression. Thus, the lower sequence is a transgressive system tract and its upper boundary represents the maximum flooding surface (Figure 4). The two seismic units, L1 and L2, that define the internal structure of this sequence would be related with two smaller amplitude ($\approx$ 1 m - 2 m) and higher frequency see-level changes (5th to 6th order) that produce stillstands or reduce sea-level rises in the 4th order sea-level change (e.g., Somoza et al., 1998; Fernández-Salas et al., 2003).

The seismic facies and distribution of the upper seismic sequence indicate that it comprises sediments deposited during the last highstand, that in this area was reached at approximately ca. 6.900/6.500 yr BP (Medialdea et al., 1989; Ercilla et al., 1995), being sea level about 1 m - 2 m above the present (e.g. Chappell, 1983; Fernández-Salas et al., 2003). Thus, the upper sequence forms a highstand systems tract (Figure 4). Its internal structure and stacking pattern could be related to the influence of sea-level changes of minor order ($\approx$1 m - 2 m, 6th order, Somoza et al., 1998; Hernández-Molina et al., 2000). In that time, climatic changes produced small-scale variations of amplitude of the sea-level (few meters), conditioning the formation of discontinuities and then changes in the sediment transport and deposition of the prograding wedges. These changes conditioned the formation of U1 to U3 units. In this sense and taking into account the relative magnitude of U1 to U3 units, we consider U1 and U2 units could be related to the two main Holocene progradational phases reported in the Iberian coastal deposits, and also around the world (e.g. Fernández-Salas et al., 2003). With respect to the age model for the U3 unit, we propose it is probably of centennial scale, and/or a more local control in its development, as the topography, wave regime, stream regimes, etc.
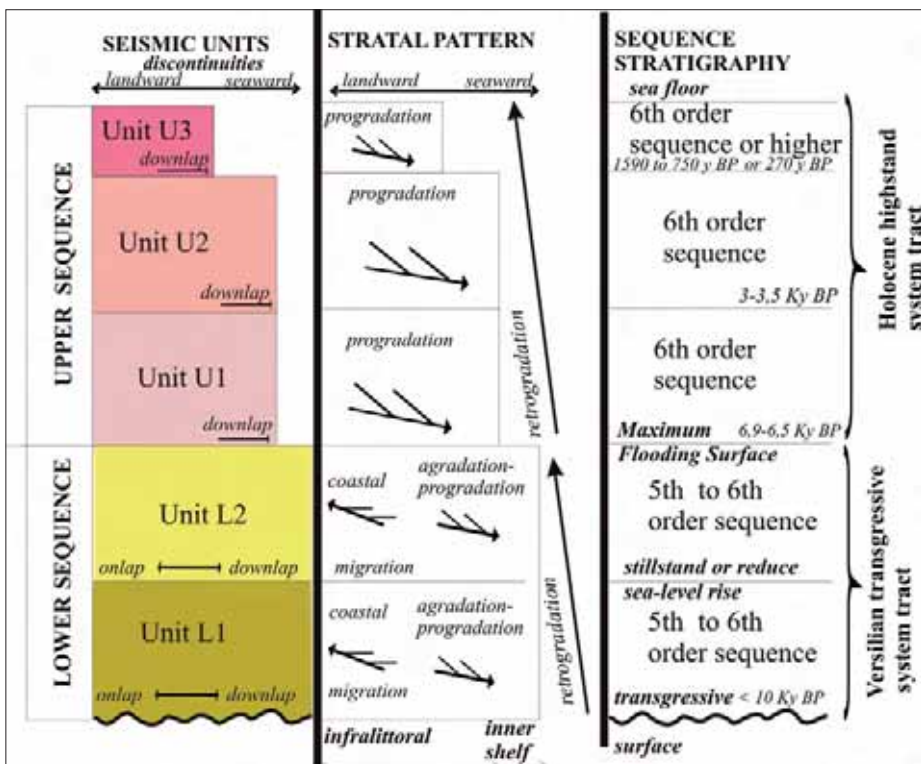
Figure 6 – Schematic diagram showing type of boundaries, strata pattern and sequence stratigraphy age model of the stratigraphy defined in the infralittoral environment

Conclusion: depositional model

Deposits that form the Masnou infralittoral environment are a unique depositional system, named the infralittoral wedge (Medialdea et al., 1989) or the infralittoral prograding wedge (Hernández-Molina et al., 2000). Its deposition has been controlled specially by storm processes. The storm conditions produce rip and undertow currents that transport the sediment in a seaward direction, and deposit down to the storm wave base. The effectiveness of these processes is conditioned by the intensity/energy of the storms, the coast orientation with respect to the direction of wave propagation and the resulting longshore currents, amount and type of sediment, topography, and water depth (e.g. Díaz and Maldonado, 1990). This sedimentary environment is made up of deposits formed by progradation of coastal lithosomes. The progradation occurred during different conditions of sea-level. They represent the coastal response to the last 4th order transgressive and highstand conditions, modulated by small-scale (≈1 m - 2 m) sea level oscillations of 5th to 6th order. In other words, the transgressive systems tract represents ancient infralittoral prograding wedges, and the highstand systems tract the present-day infralittoral wedge.

The El Masnou infralittoral environment is a combination of large depositional features governed by sea-level changes that operate at millennia scales, upon which the processes forming the small scale features contribute to rework, redistribute the infralittoral seafloor sediments. The small scale features (furrows, slides, and large- and small-scale wavy bedforms) are formed by processes acting at different time scales, from seasonal to daily.

Acknowledgements

References

Chappell J. (1983) - *Evidence for a smoothly falling sea level relative to north Queesland*. Nature, 302: 406-408.

Díaz J.I. and Maldonado A. (1990) - *Transgressive sand bodies on the Maresme continental shelf, western Mediterranean*. Marine Geology, 91: 53-72.

Ercilla G., Díaz J.I., Alonso B. and Farran M. (1995) - Late Pleistocene-Holocene sedimentary evolution of the northern Catalonia continental shelf (northwestern Mediterranean Sea). *Continental Shelf Research*, 15: 1435-1451.

Fernández-Salas L.M., Lobo F. J., Hernández-Molina F. J., Somoza L., Rodero J., Díaz del Río V. and Maldonado A. (2003) - *High-resolution architecture of late Holocene highstand prodeltaic deposits from southern Spain: the imprint of high-frequency climatic and relative sea-level changes.* Continental Shelf Research, 3: 1037-1237.

Hernández-Molina F.J., Fernández-Salas L.M., Lobo F.J., Somoza L. and Díaz del Río V. (2000) - *The infralittoral prograding wedge: a new large-scale progradational sedimentary body in shallow marine environments*. Geo-Marine Letters, 20: 109-117.

Medialdea J., Maldonado A., Díaz J.I., Escutia C., Farrán M., Giró S., Medialdea T., Serra M. and Vázquez J.T. (1989) - *Mapa Geológico Plataforma de Barcelona*. IGME, Madrid.

Somoza L., Barnolas A., Arasa A., Maestro A., Rees J. and Hernández-Molina F.J. (1998) - *Architectural stacking patterns of the Ebro Delta controlled by Holocene high-frequency eustatic fluctuations, delta-lobe switching and subsidence processes.* Sedimentary Geology, 117, 1-2: 11-3.

Coastal Modelling

Vassilios Th. Karambas, Paolo Tortora

Coastal models reproduce, in a "virtual laboratory", natural processes at different time and spatial scales and their effects on coastal evolution. Today models represent one of the most sophisticated tools to comprehend how the coastal system works, to manage coastal areas and to design different types of intervention. Within this broad discipline of investigation, the activity of OpTIMAL has concentrated on two themes. One regards the development of numerical models, with an application of the model ALS to the region of Kokkinos Pirgos, in South Crete, in order to determine the wave climate, the current pattern and the shoreline evolution trend. The other concerns the development of a sedimentological model for beach nourishment interventions and its experimentation to theoretical and real cases, the latter regarding two sectors of the Latium coast (central Italy).

Shoreline change models (first theme) are used to predict shoreline changes associated with coastal structures or storm effects over the long term. These models are based on the single line or multiple line theories, where the potential longshore and cross-shore sediment transport components are calculated empirically for the open shore case. These models have the advantage of being very fast, and can predict long-term shoreline changes very well after suitable calibration. However, they cannot accurately predict the impact of morphological changes in the vicinity of coastal structures that are due to short-term storms. An alternative approach involves the modelling of the whole suite of elementary processes responsible for the local morphological changes in a given area (Leont'yev, 1999). A typical coastal area model consists of several modules describing the wave field, the spatial distribution of wave-induced currents, the associated sediment transport fluxes, and finally the resulting spatial and temporal changes of the bed level. Such an approach is employed in the models developed by Delft Hydraulics (De Vriend et al., 1993; Roelvink et al., 1995; Broker et al., 1995; Price et al., 1995). The attempts to evaluate the short-term morphological impacts of coastal structures using these models are not yet numerous, but the results obtained are encouraging. Although these models can be used to predict medium-term morphological impacts on coastal structures, the long-term morphological impacts are still predicted solely by the shoreline models.

Accurate numerical modelling of water wave propagation from offshore to coastal regions is of paramount importance to coastal, port and environmental engineers. Such models can greatly simplify and expedite the design of coastal structures and the evaluation of their influence on the surrounding environment. An integrated approach includes also the estimation of the wave-induced current field, the sediment transport and the bottom topography changes in the coastal areas due to the action of waves. Basic to the description of these processes is the incorporation of wave breaking (into the wave model) and the formulation of the driving forces (radiation stress) from the wave model results. Thus a circulation model is able to simulate wave-induced nearshore currents and, together with the wave model, to provide a sediment transport model and morphology evolution with the required wave and current information. An integrated coastal engineering model consists of several modules describing the wave field, the spatial distribution of wave-induced currents, the associated sediment transport fluxes, and finally the resulting spatial and temporal changes of the bed level.

Within OpTIMAL Project, model sensitivity to morphological data changes was analysed as well, in order to assess the confidence level of results obtained when different accuracy/scale data are used as models' input.

Models for beach nourishment projects (second theme) address different tasks: (1) to describe the morphodynamic context in which the intervention will occur; (2) to design the appropriate intervention; (3) to

correct eventual inconveniences following nourishment; (4) to plan the maintenance of the reconstructed beach by periodic sand refills.

Nourishment design is the most important point and typically involves an optimisation process in order to establish the correct beach enlargement in terms of cost-benefits and the elements in the project that guarantee such enlargement and its persistence in time. These elements are the volume of nourished sand, its grain size characteristics and eventual structures realised in order to restrict the dispersion of sand from the littoral zone under work. The route for reaching an optimised nourishment project is very rich in complexities due to the interactions between the various coastal engineering aspects, with further complications deriving from economic implications. A life nourishment project must include solutions with low risk of failure and that implement the quality of the recreational areas and more in general satisfy the local community.

The question is how coastal models support the optimisation of the project. They provide "material" for different levels of decision-making and this material consists of predictions on the morphological effects deriving from nourishment. In this way many preliminary hypotheses of intervention can be tested and evaluated with the purpose of progressively reaching the best forecasting reproduction, on which the life of the project can be based. Elements of evaluation, in terms of advantages and disadvantages, are the shoreline position, the nourished sand volume, the quality and duration in time of the beach for the available borrow sands, the topography of the beach-shoreface profiles, and the economic aspects linked to the above set of elements. In a broad sense, predictions depart from parameters that objectively describe the littoral zone and from parameters that the model assumes to control the coastal dynamics. Different types of numerical models can be used for these predictions (Capobianco et al., 2002), even if many of them have not been originally developed for beach nourishment purposes.

In terms of realism, a good prediction always contains approximations and a wrong prediction leads to wrong decisions. Approximations derive first from difficulties in replicating an event (nourishment) that does not exit in nature and that produces a strong perturbation on the coastal environment. A priori, how much this perturbation is prolonged in time and which processes it generates is difficult to be established. There are other approximations within the models, and these often depend on the contrast between model over-simplifications and complexities existing in nature. In any case models must pass through verification, calibration, validation and sensitivity analysis processes (Capobianco et al., 2002). Further approximations derive from the uncertainty estimate of the data input (depth of closure, wave parameters, rate of erosion, etc.). Model outputs must show transparency with this regard. Some model use stochastic analysis furnishing probabilistic predictions that contemplate these uncertainties.

Post-intervention monitoring is not a separate part of coastal modelling. In general, no model is capable of describing reality as monitoring data does. In particular, these data are used to calibrate the model used making it more efficient regarding forecasts on the maintenance of the beach through periodic refills.

References

Broker I., Johnson H.K., Zyserman J.A., Ronberg J.K., Pedersen C., Deigaard R. and Fredsoe J. (1995) - *Coastal profile and coastal area morphodynamic modelling*. MAST 68-M Final Workshop, Gdansk, Poland. pp. 7-12 to 7-16.

Capobianco M., Hanson H., Larson M., Steetzel H., Stive M.J.F., Chatelus Y., Aarninkof S. and Karambas T. (2002) - *Nourishment design and evaluation: applicability of model concepts*. Coastal Engineering, 47: 113- 135.

De Vriend H.J., Zyserman J., Nicholson J., Roelvink J.A., Pechon P. and Southgate H.N. (1993) - *Medium-term 2DH coastal area modelling*. Coastal Engineering, 21: 193-224.

Leont'yev I.O. (1999) - *Modelling of morphological changes due to coastal structures*. Coastal Engneering, 38: 143-166.

Price D.M., Chesher T.J. and Southgate H.N. (1995) - *PISCES: A Morphological Coastal Area Model*. Report SR 411. Wallingford, U.K. HR Wallingford.

Roelvink J.A., Reniers A.J.H.M. and Walstra D.J.R. (1995) - *Medium term morphodynamic modelling*. MAST 68-M Final Workshop, Gdansk, Poland. pp. 7-3 to 7-6.

Application of numerical models in the region of Kokkinos Pirgos and their sensitivity to sea-bed level data

**Vassilios Th. Karambas,
Nikolaos A. Kampanis, Alexandos Pantazis**

Project Optimal is approaching the quantitative analysis of the morphological and sedimentolog-ical evolution of the littoral that is essential for the integrated management of the coastal zone. IACM's contribution is focused on the development of numerical models for the description: i) of the propagation of the waves, ii) of the littoral surging movements, iii) of the tree-dimensional littoral transport of the sedimentary matters and iv) of morphodynamics of sea-bed. For this pur-pose a bibliography research was done based on the above main ideas. Then the model ALS has been presented and applied in the region of Kokkinos Pirgos in South Crete, in order to deter-mine the wave climate, the current pattern and the shoreline evolution trend which could be compared with the future monitoring data. The sensitivity of the model results to sea-bed level fluctuations is observed.

Introduction

At both conceptual level and numerical implementation level, multidimensional coastal evolution models usually start from a number of the constituent physical processes (waves, currents, sediment transport), which are coupled via a bottom evolution module based on sediment conservation. We have three basic model concepts (Figure 1):

i) ISE (Initial Sedimentation/Erosion)-models, which go only once through the sequence of constituent models, in fact, the hydrodynamics and sediment transport computation is based on the assumption of invariant bed topography and only the rate of sedimentation or erosion for that topography is computed at every location. The composition of this series is far from trivial and determines to a high extent the quality of the final result (De Vriend, 1987).

ii) MTM (Medium Term Morphodynamic)-models, in which the new bottom topography is fed back into the hydrodynamic and sediment transport computations. This yields a looped system which describes the dynamic time-evolution of the bed. The timescale of this essentially deterministic mor-phodynamic simulation (De Vriend, 1991) cannot be substantially larger than the hydrodynamic time scale, even allowing for future improvements of the efficiency of time-stepping techniques. In con-trast to ISE-models, MTM-models describe the dynamic behavior of the morphological system. One very prominent category of these models is the 2DH-MTM models (De Vriend et al, 1993).

iii) LTM (Long-Term Morphological)-models.

The 2DH approach fails where cross-shore transport mechanisms are important. In order to model these situations, the 3D flow structure has to be described. One way to achieve this is to include a flow module which solves the hydrodynamic equations on a 3D grid, usually under the assumption of hy-drostaticity. In a wide range of practical applications we can make use of the difference in scale of the

predominant flow processes in the horizontal plane and in the vertical, and often also between those in the longshore and the cross-shore direction. This opens the way to quasi-3D concepts such as: i) n-profile models, ii) 2DH models with 1DV postprocessing.

Methodology analysis

The model ALS comprises different submodels. The wave submodel WAVE-L, based on the hyperbolic type mild slope equation, valid for a compound wave, after the incorporation of breaking and the evaluation of the radiation stress, drives the depth-averaged circulation and sediment transport submodel CIRC-L for the description of the nearshore currents and beach deformation. A new one-line model, 1L-L, with additional terms, is proposed in order to calculate shoreline position taking into account the cross-shore related seasonal shoreline variation.

Wave submodel -wave-l-

The breaking and non breaking wave model is based on the hyperbolic type mild slope equation without using the progressive wave assumption. The model consists of the following pair of equations (Copeland, 1985a):

$$\frac{\partial \zeta_w}{\partial t} + \frac{c}{c_g} \nabla \frac{c_g}{c} Q_w = 0$$

$$\frac{\partial U_w}{\partial t} + \frac{c^2}{d} \nabla \zeta_w = 0$$

[1]

where ζ_w is the surface elevation, U_w the mean velocity vector $U_w = (U, V)$, d the depth, $Q_w = U_w h_w = (Q_w, P_w)$, h_w the total depth ($h_w = \zeta + s_w$), c the celerity and c_g the group velocity.
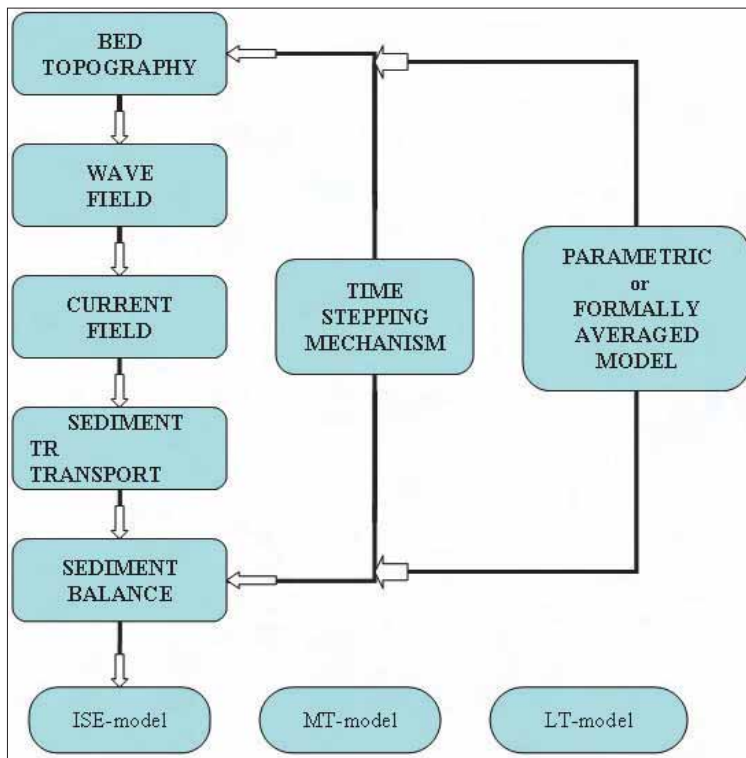
The above equations, derived by Copeland (1985a), are able to compute the combination of wave refraction, diffraction and reflection (total or partial). The model is extended in the surf zone in order to include breaking effects providing the equations with a suitable dissipation mechanism by the introduction of a dispersion term in the right-hand side of momentum Eqn [1]:

Figure 1 – Compound morphological model concepts.

$$\nu_h = \nabla^2 U_w \qquad [2]$$

where ν_h is an horizontal eddy viscosity coefficient estimated from Battjes (1995):

$$\nu_h = 2d \left(\frac{D}{\rho} \right)^{1/3} \qquad [3]$$

in which ρ is the water density and D is the energy dissipation given by Battjes and Janssen (1978):

$$D = \frac{1}{4} Q_b f \rho g H_m^2 \qquad [4]$$

with f the mean frequency, H_m the maximum possible wave height and Q_b the probability that at a given point the wave height is associated with the a breaking or broken wave. For a Rayleigh type probability distribution (Battjes and Janssen, 1978):

$$\frac{1 - Q_b}{\ln Q_b} = \left(\frac{H_{rms}}{H_m} \right)^2 \qquad [4b]$$

in which H_{rms} is the mean square wave height: $H_{rms} = 2(<2\zeta_w{}^2>)^{1/2}$ and the brackets <> denote a time mean quantity.

Wave-induced circulation submodel - circ-l-

Radiation stress and wave-induced current submodel
Taking the horizontal axes x1 and x2 on the still water surface, and the z axis upward from the surface, the definition of the radiation stress Sij component is:

$$S_{ij} = < \int_{-d}^{\zeta_w} \left(p\delta_{ij} + \rho u_i u_j \right) dz > -0.5\rho g (d + <\zeta>)^2 \delta_{ij} \qquad [5]$$

where δ_{ij} is the Kroneker's delta, $u_i(z)$ is the wave horizontal velocity component in direction x_i, ζ is the mean sea level, p the pressure and < > denotes a time average.
The total pressure p is obtained from the vertical momentum equation:

$$p = \rho g (\zeta - z) - \rho u_3^2 + \frac{\partial}{\partial x_1} \int_z^0 \rho u_1 u_3 dz + \frac{\partial}{\partial x_2} \int_z^0 \rho u_2 u_3 dz + \frac{\partial}{\partial t} \int_z^\zeta \rho u_3 dz \qquad [6]$$

where u_3 is the z-velocity component.
Based on the above Eqn [6] and after the substitution of u_i and p, from model results (Eqn 1) using linear wave theory, Copeland (1985b) derived the expressions for S_{ij} without the assumption of progressive waves. Those expressions are used in the present model.
The radiation stresses are the driving forces of a 2D horizontal wave-induced current model:

$$\frac{\partial \zeta}{\partial t} + \frac{\partial (Uh)}{\partial x} + \frac{\partial (Vh)}{\partial y} = 0$$

$$\frac{\partial U}{\partial t} + U \frac{\partial U}{\partial x} + V \frac{\partial U}{\partial y} + g \frac{\partial \zeta}{\partial x} =$$

$$-\frac{1}{\rho h} \left(\frac{\partial S_{xx}}{\partial x} + \frac{\partial S_{xy}}{\partial y} \right) + \frac{1}{h} \frac{\partial}{\partial x} \left(\nu_h h \frac{\partial U}{\partial x} \right) + \frac{1}{h} \frac{\partial}{\partial y} \left(\nu_h h \frac{\partial U}{\partial y} \right) - \frac{\tau_{bx}}{\rho h} \qquad [7]$$

$$\frac{\partial V}{\partial t} + U \frac{\partial V}{\partial x} + V \frac{\partial V}{\partial y} + g \frac{\partial \zeta}{\partial y} =$$

$$-\frac{1}{\rho h} \left(\frac{\partial S_{xy}}{\partial x} + \frac{\partial S_{yy}}{\partial y} \right) + \frac{1}{h} \frac{\partial}{\partial x} \left(\nu_h h \frac{\partial V}{\partial x} \right) + \frac{1}{h} \frac{\partial}{\partial y} \left(\nu_h h \frac{\partial V}{\partial y} \right) - \frac{\tau_{by}}{\rho h}$$

where h is the total depth h = d + ζ, U, V are the current horizontal velocities and τ_{bx} and τ_{by} are the bottom shear stresses.

In the current model the treatment of the bottom stress is critical (all longshore current models employing radiation stress solve for the mean current velocity through its role in the bottom friction term). The general expression for the time-average bottom shear stress in the current model is written:

$$\tau_{bx} = \rho C_f < (U + u_b)\sqrt{(U + u_b)^2 + (V + v_b)^2} >$$

[8]

$$\tau_{bx} = \rho C_f < (V + v_b)\sqrt{(U + u_b)^2 + (V + v_b)^2} >$$

where C_f is the friction coefficient which depends on the bottom roughness and on the orbital amplitude at the bed (Karambas, 1998), and u_b and v_b are the wave velocities at the bottom.
Inside the surf zone the existence of the undertow current that is directed offshore on the bottom cannot be predicted by a depth averaged model. However, representing the cross-shore flow is essential for a realistic description of the sediment transport processes. The present model calculates local vertical distribution of the horizontal velocity using the analytical expression for the cross-shore flow below wave trough level proposed by Stive and Wind (1986):

$$v_u = \frac{1}{2}\left[(\xi - 1)^2 - \frac{1}{3}\right]\frac{h - \zeta_t}{\rho \, v_\tau}\frac{dR}{dy} + \left(\xi - \frac{1}{2}\right)\frac{(h - \zeta_t)\tau_s}{\tilde{n} v_\tau} - \frac{M\cos\Theta}{h - \zeta_t}$$

[9]

where v_u is the undertow velocity in the y (shore-normal) direction, $\zeta = z/(h-\zeta)$, ζ_t is the wave trough level, $dR/dy = 0.14\rho \, gdh/dy$, τ_s is the shear stress at the wave trough level, M is the wave mass flux above trough level, Θ is the direction of the wave propagation and v_τ the eddy viscosity coefficient given by equation (1).

The value of the coefficient in Eqn [3] is now taken equal to 0.03 (instead of 2). The direction of the wave propagation Θ is given by:

$$\Theta = \arctan\left[(<Q_w^2>/<P_w^2>)^{1/2}\right]$$

[10]

Sediment transport submodel -sed-I-

Sediment transport in the surf zone
The prediction of the sediment transport is based on the energetics approach, in which the submerged weight transport rates, i_{xt} in the x direction and i_{yt} in the y direction, are given by Karambas (1998):

$$i_{xt} = <\left[\frac{\varepsilon_b}{\tan\phi}\left(\frac{u_o}{u_{ot}} + \frac{d_x}{\tan\phi}\right)\omega_b + \varepsilon_s\frac{u_{ot}}{w}\left(\frac{u_o}{u_{ot}} + \varepsilon_s d_x\frac{u_{ot}}{w}\right)\omega_t\right]>$$

[11]

$$i_{yt} = <\left[\frac{\varepsilon_b}{\tan\varphi}\left(\frac{v_o}{u_{ot}} + \frac{d_y}{\tan\phi}\right)\omega_b + \varepsilon_s\frac{u_{ot}}{w}\left(\frac{v_o}{u_{ot}} + \varepsilon_s d_y\frac{u_{ot}}{w}\right)\omega_t\right]>$$

where w is the sediment fall velocity, ϕ is the angle of internal friction, ε_b and ε_s are the bed and suspended load efficiency factors respectively (ε_b=0.13, ε_s=0.01), $u_{ot} = \sqrt{u_o^2 + v_o^2}$ (u_o, v_o are the total flow velocities at the bottom), d_x and d_y are the bottom slopes $\omega_b = C_f\rho u_{ot}^3$, and ω_t is the total rate of energy dissipation given by Leont'yev (1996, 1997):

$$\omega_t = \omega_b + De^{3/2(1-h/H)} \qquad [12]$$

in which H is the wave height (H=H_{rms}), D is the mean rate of breaking wave energy dissipation per unit area given by Eqn [4].

In Eqn [12] the first term express the power expenditures due to bed friction while the second due to excess turbulence penetrating into the bottom layer from breaking waves.

The above method had been applied using a non linear dispersive wave model based on the Boussinesq equations (Karambas et al., 1995; Karambas, 1998). A Boussinesq model automatically includes the existence of the mean wave-induced current and consequently there is no need to separate the bottom velocities into a mean and an oscillatory part. However, since the present model is a linear one, the total flow velocity at the bottom is considered as a sum of the steady U, V, v_u and the oscillatory u_b, v_b components which include two harmonics:

$$u_o = U + u_{bm}\cos(\omega t) + u_{b2m}\cos(2\omega t)$$
$$v_o = V + v_u + v_{bm}\cos(\omega t) + v_{b2m}\cos(2\omega t + a) \qquad [13]$$

in which ω is the wave frequency, a is the phase shift and u_{bm}, u_{b2m}, v_{bm} and v_{b2m} are the velocity amplitudes given by Leont'yev (1996, 1997) .

The above sediment transport formula has been derived directly form the Bailard primitive equations without the assumption that the only dissipation mechanism is the bed friction. This is the most important limitation of the Bailard theory and precludes the use of the original formula within the surf zone, where the dissipation of energy associated with the process of wave breaking is largely dominant.

Sediment transport in the swash zone

Adopting the procedure proposed by Leont'yev (1996), the submerged weight transport rates i_{ys} near the shoreline, in the y (shore-normal) direction, is given by:

$$i_{ys} = \frac{\varepsilon_b f_R}{2\tan^2 \phi} \rho \left| < u_R^3 > \right| \left(\tan \beta_{eq} - \tan \beta \right) \qquad [14]$$

where f_R is the run-up friction coefficient (of order 10^{-1}-10^{-3}), u_R is the flow velocity in the swash zone, tanβ is the actual slope gradient and tanβ_{eq} is the slope under equilibrium state approximated by Yamamoto et al. (1996):

$$\tan \beta_{eq} = \left(\frac{0.0864 s\, g\, d_{50} T^2}{H_b^2} \right)^{2/3} \qquad [15]$$

where s is the specific gravity of sediment in water, d_{50} is the median grain size, H_b is the breaker height and T the wave period.

The flow velocity in the swash zone u_R is parameterised in terms of the run-up height R according to Leont'yev (1996): $u_R = (2g (R-z_c))$, where z_c is the height of water mass above the water level which increases proportionally to the distance from the upper run-up boundary.

If the bottom gradient exceeds the equilibrium value then $i_{ys} < 0$ (erosion). In opposite case $i_{ys} > 0$ (accretion).

The longshore (x direction) total swash sediment transport i_{xs} is calculated by the global expression proposed by Briad and Kamphuis (1993).

3D bed evolution and one-line models

The submodel CIRC-L is coupled with a 3D bed evolution model or with a one-line model to provide bathymetry or shoreline changes.

The nearshore morphological changes are calculated by solving the conservation of sediment transport equation:

$$\frac{\partial d}{\partial t} = \frac{\partial q_x}{\partial x} + \frac{\partial q_y}{\partial y}$$ [16]

where d is the still water depth and q_x, q_y are the volumetric longshore and cross-shore sediment transport rates, related to the immersed weight sediment transport through:

$$q_{x,y} = \frac{i_{x,y}}{(\rho_s - \rho)gN}$$ [17]

in which N is the volume concentration of solids of the sediment (N= 0.6) and ρ_s and ρ are the sediment and fluid densities.

Under certain assumptions Eqn [16] can be transformed into a 1D equation (one-line model). The one-line models find wider engineering use as they are much less costly to run.

Let us define the total longshore sediment transport Q and the mean (cross-shore) water depth $\overline{d}$ by the equations:

$$Q = \int_0^{y_s} q_x dy \qquad \overline{d} = \frac{1}{y_s} \int_0^{y_s} d\,dy$$ [18]

where y_s is the width of the nearshore zone.

The integration of Eqn [17] over the width of the nearshore zone from its outer boundary (y=0) to the shoreline (y=y_s), using the Leibnitz relation, leads to the following equation:

$$\frac{\partial(y_s \overline{d})}{\partial t} = \frac{\partial Q}{\partial x} - q_x(y_s)\frac{\partial y_s}{\partial x} + q_y(y_s)$$ [19]

where we have supposed that the following conditions are valid: d=0 at shoreline (y=y_s) and the transport rates $q_x(0)$=0, $q_y(0)$=0 at the outer boundary (y=0) are zero.
Eqn [19] differs from a standard one-line model in the last two terms. The second term of the right hand side of the equation is related to the longshore transport rate near the shoreline while the last term incorporates the cross-shore related seasonal shoreline variation.
The cross-shore transport rate near the shoreline $q_y(y_s)$ is given by the Sunamura formula (Yamamoto et al., 1996):

$$q_y(y_s)=K\, U_r^{0.2}\, \Phi\, (\, \Phi -0.13\, U_r)\, w\, d_{50}$$ [20]

where U_r is the Ursell parameter $U_r=gHT^2/h^2$ (H is the wave height and h is the wave set-up at shoreline), $\Phi=H^2/shd_{50}$ (s is the specific gravity of sediment) and K is a coefficient of sediment transport rate:

$$K=Ae^{-Bt/T}$$ [21]

where the coefficient A and B are given by Yamamoto et al. (1996):

$$A = 1.61 \cdot 10^{-10} \, (d_{50}/H_o)^{-1.31}$$

[22]

$$B = 4.2 \cdot 10^{-3} \, (\tan \beta)^{1.57}$$

where H_o is the deep water wave height.

The coefficient K of Eqn [21] is a function of time since the rate of cross-shore sediment transport decreases with the lapse of time and the beach profile approaches the equilibrium state.

It can also be expected that the mean depth $\overline{d}$ is relatively conservative characteristic in comparison with the local shoreline position y_s, and consequently, it can be considered as a constant in Eqn [19].

Application of the numerical models in the region of Kokkinos Pirgos

The above methodology is applied in the region of Kokinos Pirgos near Timbaki in South Crete in order to determine the wave climate (Figures 3, 4, 5), the current pattern (Figures 6, 7, 8), the sediment transport pattern and finally the shoreline evolution trend (Figure 9).

The sediment balance of the coast has been significantly influenced by the construction of a small harbor in the west corner of the beach. As a result of these, erosion phenomena have been observed in the south-east coast of Kokkinos Pirgos. In Figure 2 a satellite image of the area of Kokkinos Pirgos near Timbaki in South Crete is presented.

The results of the models were calculated for winds blowing from the three most frequent directions in the study area (West, South-West and South sector) using wind data from Station 759 of the Greek Meteorological Service and the bottom topography collected.
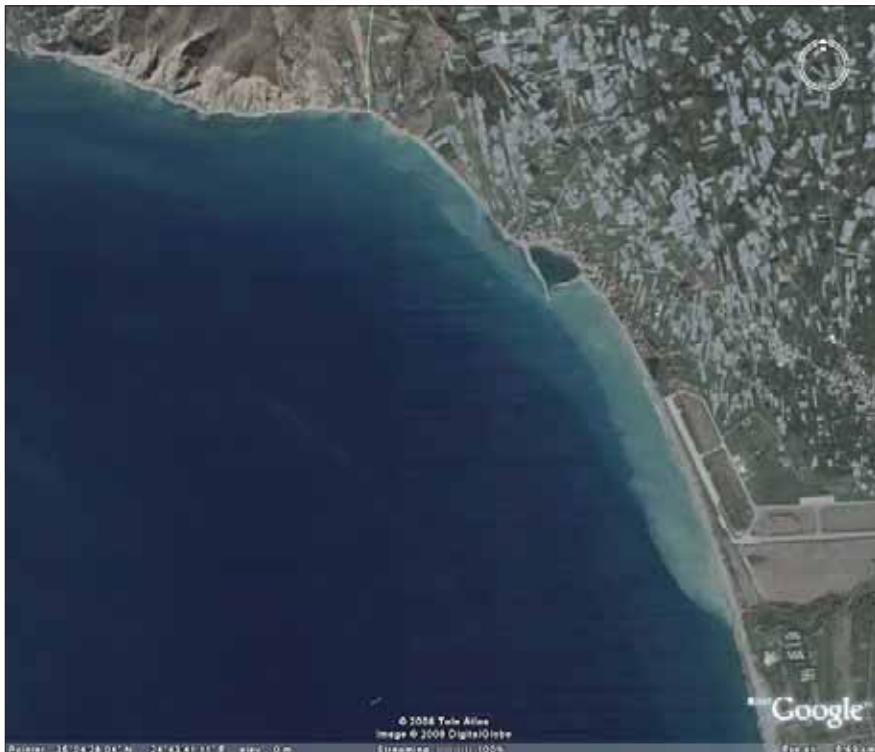
Figure 2 – Satellite image of the area of Kokkinos Pirgos near Timbaki in South Crete.
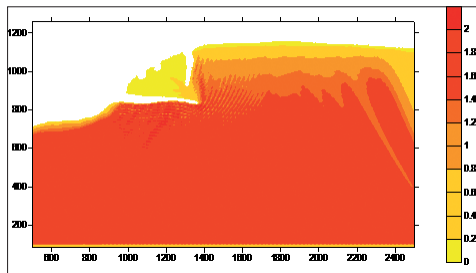
Figure 3 – Hs contours for South direction winds.
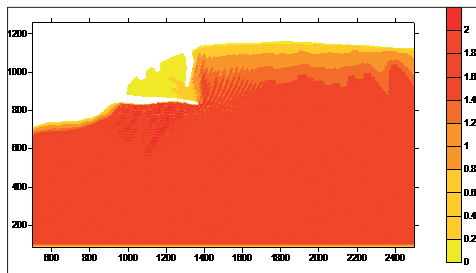
Figure 4 – Hs contours for South-West direction winds.
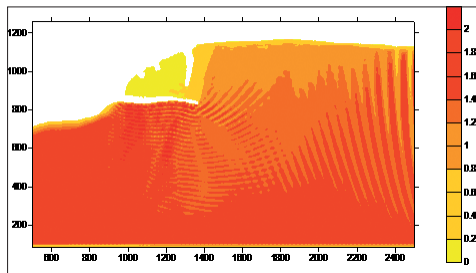
Figure 5 – Hs contours for West direction winds.
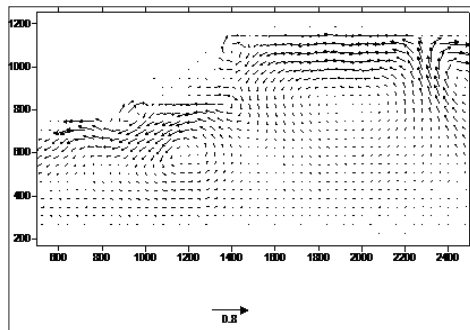
Figure 6 – Wave-induced current velocities for South direction winds.
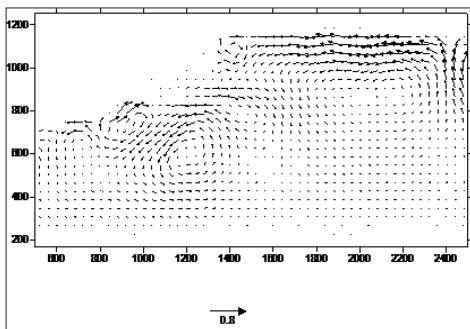
Figure 7 – Wave-induced current velocities for South-West direction winds.
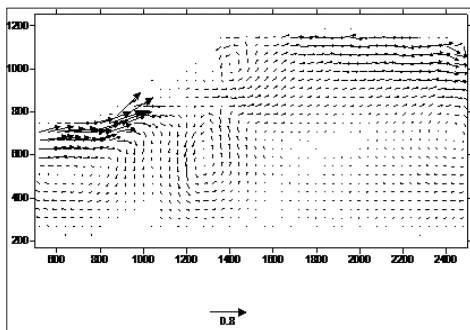
Figure 8 – Wave-induced current velocities for West direction winds.

The following conclusions have been derived:

- H_s contours reveal the wave propagation pattern for each wind direction.
- Wave refraction and breaking phenomena due to the existence of the coast and the harbour works are revealed.
- Wave induced currents calculations reveal the existence of an alongshore current in the breaker zone with a mean value of 1 m/s.
- South and South-West winds produce currents of North-West direction while West winds currents of South-East direction.
- For West winds the wave induced current in the leeside of the east seawall changes in direction and reformulates, a phenomenon that will lead to sediment accretion in the region of the breakwater and erosion in the South-East part of the coast.
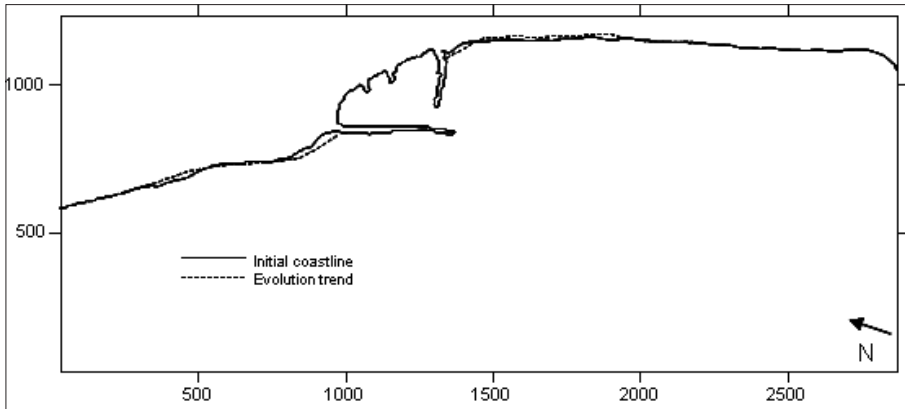
Figure 9 – Coast evolution trend (sequence of S, SW and W waves).

The realisation of beach nourishment is the proposition for the solution to the erosion problems. In addition, submerged breakwaters are proposed for the stabilisation of the coast as well as to avoid the repetition of unwanted erosion phenomena.

Numerous solutions have been tested. Three of them are listed in Table 1 and Figures 10 to 12. The solution considered to be the best is Solution 3 (Figure 12) which proposes the placement of 3 break-waters with 100 m of length and 90 m of distance between them, with high rising up to the mean sea level and placed at 180 m parallel to the coast.

With this solution a better erosion trend control is observed in the majority of the coastline in comparison with the results of the other solutions tested.

The sand for the beach nourishment will be taken from the west accumulation points outside of the port and put in the area of erosion.

Table 1 - Recommended sizes of breakwaters.

Current situation	Number of breakwaters	Breakwater length (m)	Distance from the coast (m)	Distance between breakwaters (m)
Solution 1[1*]	2	100	180	110
Solution 2	2	100	180	80
Solution 3	3	100	180	90

1   *Solution 1 breakwaters are not parallel to the coast, but have a slight declination for better protection from West waves.
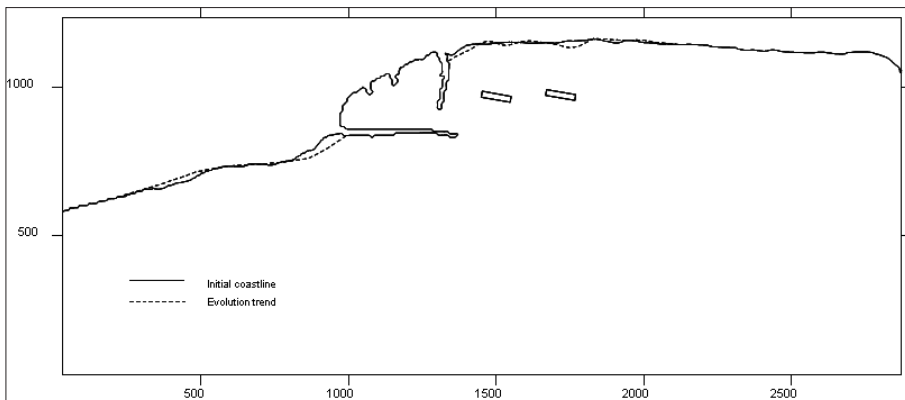
Figure 10 – Solution 1 – Coast evolution trend (sequence of S, SW and W waves).
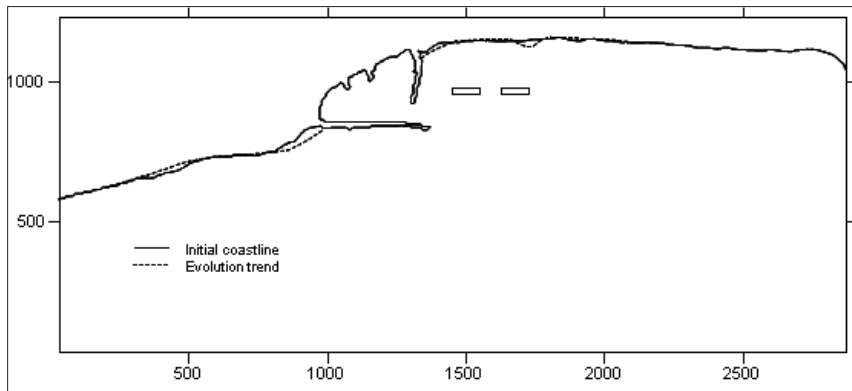
Figure 11 – Solution 2 – Coast evolution trend (sequence of S, SW and W waves).
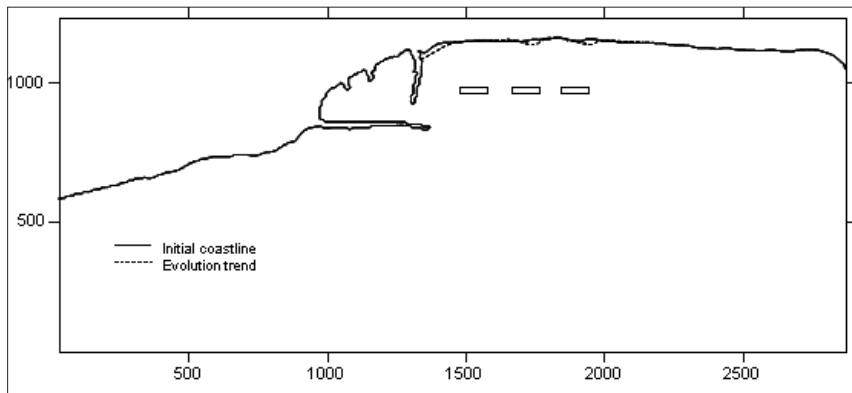
Figure 12 – Solution 3 – Coast evolution trend (sequence of S, SW and W waves).

Sea-bed level fluctuations

Current wave propagation and wave-induced numerical models are quite sensitive to bed level fluctuations, since the phenomena of refraction and reflection are mainly influenced by bed morphology. A change in bed morphology can increase (or decrease) wave reflection, change wave direction (refraction) and consequently change wave and wave-induced current field. Wave propagation models incorporate water depth in their governing equations and consequently are sensitive to bed level changes and the quality of bed level description data.

References

Battjes J.A. (1995) - *Modelling of turbulence in the surf zone.* Proc. Symp. Modelling Techniques, California, ASCE. pp. 1050-1061.

Battjes J.A. and Janssen J.P.F.M. (1978) - *Energy Loss and set-up due to breaking of random waves.* Int. Conf. on Coastal Engineering '78, ASCE, 569-587.

Briad M-H.G. and Kamphuis J.W. (1993) - *Sediment transport in the surf zone: a quasi 3-D numerical model.* Coastal Engineering, 20: 135-156.

Copeland G.J.M. (1985a) - *A practical alternative to the «mild-slope» wave equation.* Coastal Engineering, 9: 125-149.

Copeland G.J.M. (1985b) - *Practical radiation stress calculations connected with equations of wave propagation.* Coastal Engineering, 9: 195-219.

De Vriend H.J. (1987) – *2DH mathematical modeling of morphological evolutions in shallow water*. Coastal Engineering, 11: 1-27.

De Vriend H.J. (1991) – G6 *Coastal Morphodynamics.* In: N.C. Kraus, K.J. Gingerich and D.L.Kreibel, Proc. Coastal Sediments '91, Seattle, WA., ASCE, New York. pp. 356-370.

De Vriend H.J., Zyserman J., Nicholson J., Roelvink J.A., Pechon P. and Southgate H.N. (1993) – *Medium-term 2DH coastal area modelling*. Coastal Engineering, 21: 193-224

Karambas Th. V. (1998) - *2DH non-linear dispersive wave modelling and sediment transport in the near-shore zone*. Int. Conf. on Coastal Engineering, ASCE, Copenhagen.

Karambas Th. V., Southgate H.N. and Koutitas C. (1995) - *A Boussinesq model for inshore zone sediment transport using an energetics approach*. Coastal Dynamics '95, Gdansk. pp. 841-849.

Leont'yev I.O. (1996) - *Numerical modelling of beach erosion during storm event*. Coastal Engineering, 29: 187-200.

Leont'yev I.O. (1997) - *Short-term changes due to cross-shore structures: a one-line numerical model*. Coastal Engineering, 31: 59-75.

Stive M. J. F and Wind H. G. (1986) - *Cross-shore flow in the surf zone.* Coastal Engineering, 10: 325-340.

Wright L.D. and Thom B.G. (1977) – *Coastal depositional landforms: a morphodynamic approach*. Prog. Phys. Geogr., 1: 412-459.

Yamamoto Y., Horikawa K. and Tanimoto K. (1996) - *Prediction of shoreline change considering cross-shore sediment transport.* Int. Conf. on Coastal Engineering 1996, ASCE. pp. 3405-3418.

A new model for beach nourishment interventions: theory and applications

Paolo Tortora

The characteristics of the *Grain-size Nourishment Model* together with some tests and applications are here presented. This model operates in three distinct ways (module A, B and C): one predicts the effects of the nourishment; one manages post-intervention monitoring data; and the other furnishes predictions, calibrated with real data (monitoring), for beach-maintenance refills. All modules run separately but are open to data inter-exchanges. Moreover they work in three-dimensions using data organized into grid matrices covering the coast that is being studied. Inputs for the model (for each module) are the topo-bathymetric and grain size data collected on the active morphological surface (dry beach and shoreface). The output is a numerical description of the artificial deposit, i.e. the sedimentary body comprises between the pre and post-intervention surface. This description aggregates: in module-A, real (pre-nourishment surface) and predicted (post-nourishment) data; in module-B, only real data (for both surfaces); in module-C, real (pre-refill surface) and predicted (post-refill) data. Description in modules A and C forecasts the following elements: a) beach and shoreface topography; b) shoreline position; c) geometry of the artificial deposit; d) sediment amount for the intervention; e) geographic distribution of sediment grain-size parameters (mean size, sorting, percentage of sand and mud). The nourishment simulations (modules A and C) are manoeuvred by three variables: the grainsize frequency distribution of the available borrow material; the depth of closure; the shoreline advance requested in the project. Theory and procedures of the model are reported in this paper together with some applications and final results deriving from the experimentation of the model.

Introduction

This paper presents the characteristics of a new numerical model, the *Grain-size Nourishment Model* (GNM), which has been developed and experimented during the course of the BeachMed project. This model operates in three dimensions through three distinct computational phases, each dedicated to a specific task in the overall beach-recovery project. Two of these predict morpho-geometric scenarios for the effects of artificial beach nourishment and maintenance refills, whilst the other manages the post-intervention monitoring data. The two predictive elements of the model are particularly innovative. Predictions are based on sedimentological criteria to evaluate the control of the borrow material's grainsize characteristics over the cross-shore morphodynamic profile. Shoreline advance and nourishment volumes are particularly dependent on the profile form (NRC, 1995; Dean, 2002). The predictive calculations ignore the widely used concept of equilibrium profile and, rather than borrowing from other techniques (Dean, 1991; Dean and Yoo, 1992; Pilkey et al, 1993; Larson et al, 1999; Capobianco et al, 2002), approach the nourishment in a new way. During the model's development, the following issues were taken into consideration in an attempt to resolve them: i) few models operate in 3D, and 3D methodologies represent the future frontier for coastal modelling; ii) many models used for beach nourishment are not fully adequate because they were in origin designed for other purposes;

iii) the division of processes in nourishment studies (nourishment design, monitoring of reconstructed beach, plan for beach maintenance) typically requires different methodologies rather than an integrated method.

Model characteristics

General features

The model has its main reference in the natural process of progradation that produces the seaward translation of the beach-shoreface profile through the deposition of sedimentary bodies juxtaposed in sequence. A single sedimentary body is taken to represent the attributes of the "artificial deposit" which is therefore comprised between the natural morphological surface and that following the intervention, and closed at a depth which may or may not exceed the wave base level depending on the dimension and amount of the nourished sands (Van De Graav et al, 1991; Houston, 1994; USACE, 2002). This deposit is the physical object taken into consideration and described in 3D using data organized into grid matrices (46x40 nodes) covering the coast that is being studied.
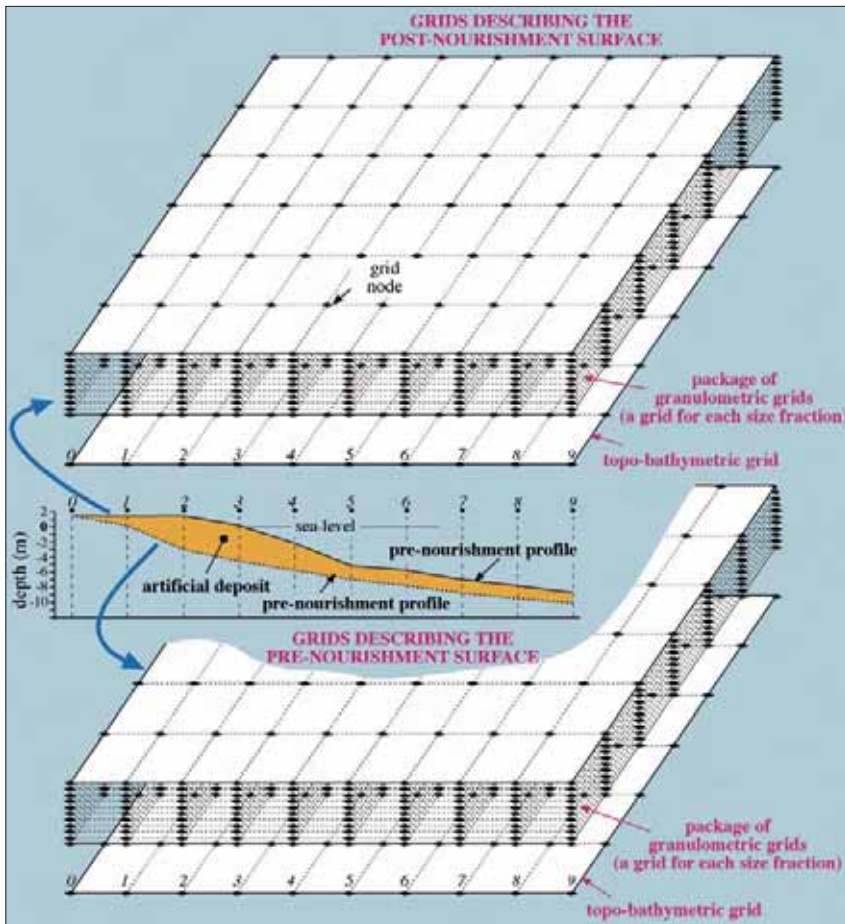
Figure 1 - Data used in the model to describe topography (beach-shoreface) and grain size characteristics of the lower and upper surfaces bounding the artificial deposit. Each surface is described by a grid matrix with elevation data and by a package of granulometric grids, one grid for each size fraction. Additional calculations extend the description to the internal characteristics of the artificial deposit (thickness and average sediment).

Inputs for the model are topo-bathymetric and grain size data collected on the active morphological surface (dry beach and shoreface). These data must be previously submitted to a process of gridding with an external software in order to obtain the numerical format accepted in GNM: one grid matrix (topo-bathymetry), and one package of 25 grids maximum (a grid for each grain size fraction) which together reconstruct on each grid node a grain size frequency distribution. The GNM operates in three distinct ways (module A, B and C: one forecasts results, one manages monitoring data and the other provides predictions calibrated with real data (monitoring). Each module is applied to specific require-
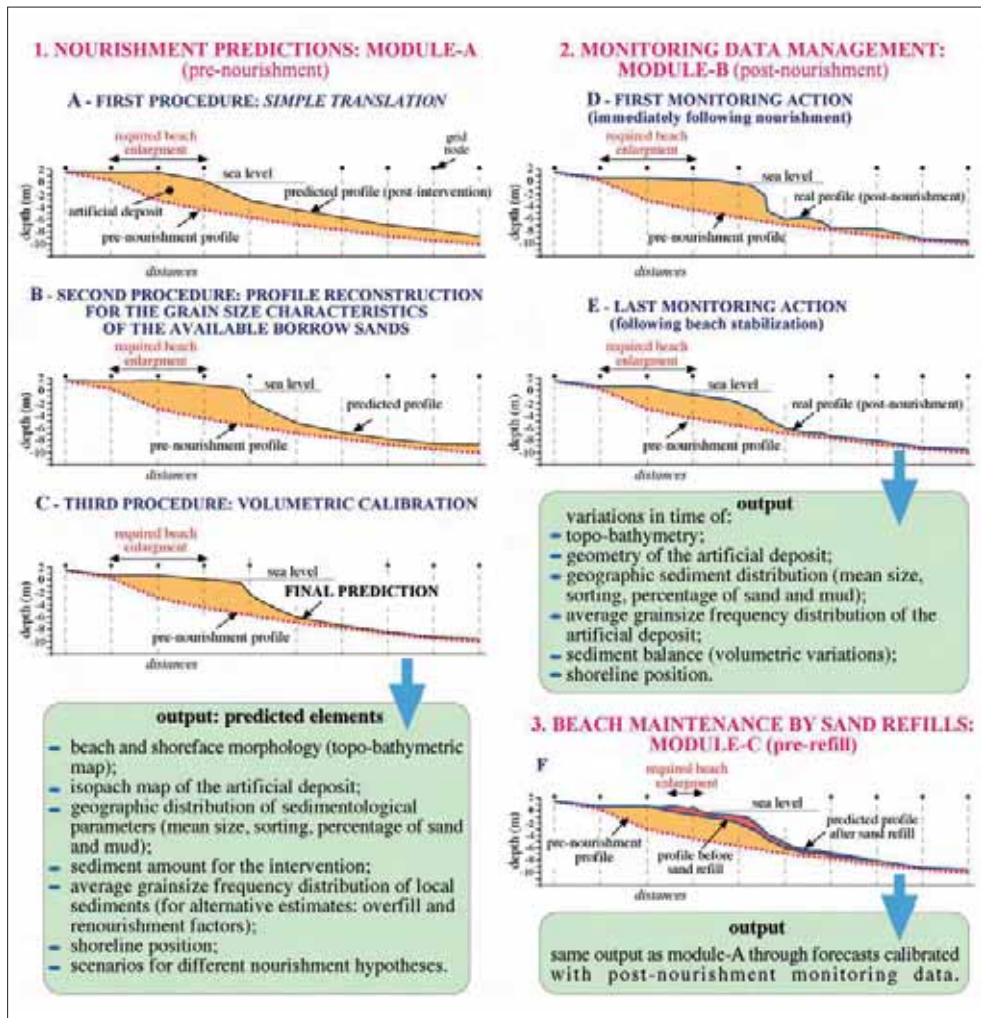
Figure 2 – Schematisation of the three calculation modules in the model. Module-A gives predictions using three procedures. The first (in A) translates the pre-nourishment profile (and the sediment distributed along it) by a distance equal to the required shoreline advance; the invariant form (and sediment distribution) of the two profiles is based on the assumption that the nourished material (B) and local sediment (L) have same grain size characteristics. The second procedure (in B) modifies the translated profile (and its sediment) as a function of grain size characteristics of the available borrow sand (B≠L). From this, an excess (as in B) or defect in shoreline advance may arise in respect to the position in A. The third procedure (in C) allows the correct position of the shoreline to be re-established through calibrated additions or subtractions of sediment to/from the artificial deposit. The model treats the monitoring data, generating a description of the deposit based on real data (in D, E). This description is also used to calibrate the model which, in Module C, gives estimates and predictions for beach maintenance with periodic refills (in F)

ments within the beach recovery project, which generally includes pre-intervention surveys in order to design the nourishment (module-A), and post-intervention surveys to ascertain the performance of the reconstructed beach (module-B) and to plan for its future maintenance by sand refills (module-C).

Each module furnishes in output the numerical description of the artificial deposit through matrices (grid data). The basic description regards the lower and upper boundary surface of the deposit (pre and post-nourishment surfaces), each defined by one topo-bathymetric grid and one package of 25 grids (Figure 1). Further data and grids derive from the above-mentioned information. The description includes in module-A real (pre-nourishment surface) and predicted (post-nourishment) data, in module-B only real data, and in module-C real (pre-refill surface) and predicted (post-refill) data. For mapping the individual attributes of the deposit, grid values must be contoured using a commercial software.

Module-A uses topo-bathymetric and grain size data from pre-intervention surveys to forecast the elements of artificial deposit. Three variables govern the nourishment simulations: the grain size frequency distribution of the available borrow material, the depth of closure, the shoreline advance requested in the project. Processing occurs by three distinct procedures of calculation based on the relationship between grain size characteristics, volumes, and geometric elements of the deposit. The first procedure results in a "simple translation" of the pre-intervention surface, by a distance equal to the required shoreline advance (Figure 2A). The second modifies the translated surface based on the characteristics of borrow material (Figure 2B). The third further varies it by increasing or decreasing volumes in order to re-establish the correct position of the shoreline (Figure 2C). The prediction may be completed with the first procedure if borrow (B) and the local (L) sediments have the same grain size frequency distribution (rare case), or with the second if B is different from L and the predicted shoreline satisfies project requirements, or with the third if it does not. Scenarios for more than one preliminary nourishment hypothesis (with different material and/or volumes) can be compared to choose the best solution for the live project. The outputs from module-A (as well from the other modules) are listed in Figure 2.
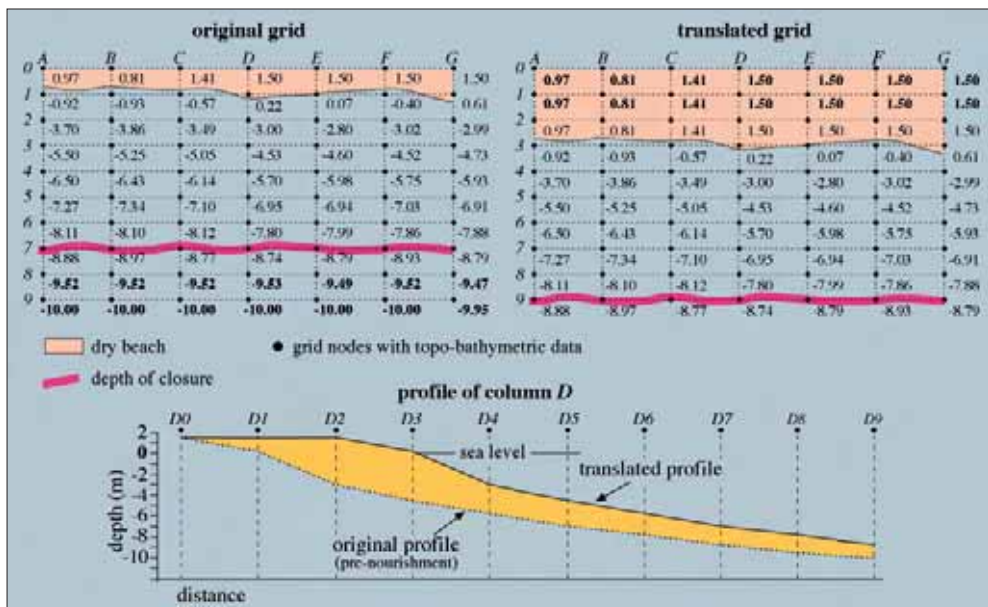
Figure 3 - Technique employed in the first procedure to reproduce an idealized nourishment scenario in the assumption that borrow material and local sediment have the same grain size characteristics. The translated matrix (post-intervention) is obtained from the original (pre-intervention) matrix by a seawards shift of the data from the latter by a number of nodes equal to the required shoreline advance (in this example 2 nodes). The translational process, in the example applied to topographic data, does not vary the original closure depth. The profiles underneath derive from data of column D of both the matrices. The technique, defined simple translation, must be similarly applied to the pre-intervention granulometric grid package (Figure 1).

Module-B manages post-intervention monitoring data which, together with pre-nourishment data, give a real morphogeometric and sedimentological picture of the artificial deposit for each monitoring phase (Figure 2D, E). Comparing data of these pictures, changes in sedimentary balance, morphology, geometry and others aspects can be rapidly obtained. Comparing real and forecasted (module-A) pictures, the errors in predictions can be highlighted and used for calibrating the model for its subsequent task (module-C)

Module-C, dedicated to the beach maintenance by sand refills, includes the same three procedures (and outputs) of module-A with possible calibrations using data of the surface really produced by the nourishment (Figure 2F). Even in this case various hypothetical scenarios can be assessed before choosing the right intervention.

Prediction process

As already discussed, GNM predictions (modules A and C) derive from three sequential procedures. The first is based on the assumption that a "simple translation" occurs (Figure 2A) when borrow (B) and local (L) sediments have same grainsize characteristics. The simple translation process is obtained by translating seawards the pre-intervention grid data by a number of nodes equal to the desired widening of the beach (Figure 3). The resulting artificial deposit is therefore described by two combined group of matrices (as in Figure 1) which identify the granulometric and topo-bathymetric characteristics of the translated and original surfaces. The data in these matrices are used in final calculations intended to create a numerical structure which can then be modified (second procedure) according to the type of borrow material available (B≠L). These calculations follow the principles synthesised in equations (1) through (5).

At any node, the thickness (S_L) of the deposit following a simple translation is defined by equation (1) where qt_L and qo mark the measured height of the translated and original surface, respectively. The average percentage of a given size fraction (f_L) is computed using equation (2) from corresponding values of ft_L and fo on each of the two surfaces. The volumetric contribution of f_L (Vc_L) around the node (i.e. in the cell) is given by equation (3), where A is the area of the cell. This contribution is extrapolated to the entire grid (Vg_L) using equation (4), as the sum of Vc_L in each cell. Finally, equation (5) computes the percentage (FL) of the size fraction f_L representing the average grainsize frequency distribution of the artificial deposit. This frequency distribution – whose entire spectrum is defined by extending equations (1) through (5) to other size fractions – corresponds to that of the material which would generate a simple translation and therefore, given the initial assumption of B=L, to that of the representative sample of the local sediment.

This sample may also be useful in alternative methods of volumetric calculations (overfill and renourishment factors: Krumben and James, 1965; Dean, 1974; James, 1975). Its calculation in the GNM, based on geographically equally spaced 3D data, points out some uncertainties in classical methods (Hobson, 1977) which ignore the different concentration of samples on the studied area (the sediment in the most appropriately sampled zones have a greater weight when compared to the final composition).

$$S_L = qt_L - qo \tag{1}$$

$$f_L = \frac{(fo + ft_L)}{2} \tag{2}$$

$$Vc_L = A \cdot S_L \cdot f_L \tag{3}$$

$$Vg_L = \sum_{C1}^{Cn} Vc_L \tag{4}$$

$$FL = \frac{Vg_L}{Vtot} \tag{5}$$

Depending on the available material, the second procedure modifies the surface of the simple translation (its elevation and sediment characteristics) along with the geometry of the deposit, without affecting its volume. This occurs through modifications to the results from equations (1) to (5) in their inverse order, and calculations which take into account the grain size characteristics of the borrow sand.

The process of calculation is based on the links defined by the inverse progression from (5) to (1), by which from the percentage of FL (5), followed by (4) and (3), the solutions (1) and (2) are obtained which define the characteristics of the deposit (B=L). Moreover this process is based on the fact that the computational progression can be repeated for a fraction FB of the available borrow material, whose percentage (and that of other fractions) also identifies the characteristics of the deposit, but this time for the available material (B≠L). Following this progression, the issue to be resolved is the volumetric contribution of FB (steps 5, 4 and 3).

Amongst the following calculations, equation (6) gives the previously existing conditions in order to resolve the issue, equation (7) solves it, (8) extends the solution to the single cells and (9), (10) and (11) define the characteristics of the deposit for the available material. Each of these equations is equal to or derived from the original (5) through (1).

Equation (6) is a simple repetition of (5) except that it is intended for the borrow size fraction FB analogous to FL. The two equations imply that, for equal V_{tot}, the volumetric contribution on the grid of Vg_L (known) and Vg_B (unknown) depend respectively on the known percentage of FL and FB. Equation (7) computes the unknown volume as a proportion, by varying Vg_L in the relation FB/FL (factor K), which is then employed in (8) to modify the original volumetric contribution (in Vc_B) in each cell. Finally the thickness at each (S_B) is given by equation (10) and the elevation of the translated surface (qt_B) by (11). Equations (9), (10) and (11) essentially assign new characteristics to the deposit derived from the simple translation in the first procedure, according to the available material. In Figure 4 an example application of these calculations is shown for a range of borrow material.

$$FB = \frac{Vg_B}{Vtot} \tag{6}$$

$$\frac{FB}{FL} = \frac{\dfrac{Vg_B}{Vtot}}{\dfrac{Vg_L}{Vtot}} \tag{7}$$

from which

$$Vg_B = K \cdot Vg_L$$

where

$$K = \frac{FB}{FL}$$

$$Vc_B = K \cdot (A \cdot S_L \cdot f_L) \tag{8}$$

$$f_B = \frac{Vc_B}{\sum_{f1}^{fn} Vc_B} \tag{9}$$

$$S_B = \frac{\sum_{f1}^{fn} Vc_B}{A} \tag{10}$$

$$qt_B = qo_L + S_B \tag{11}$$
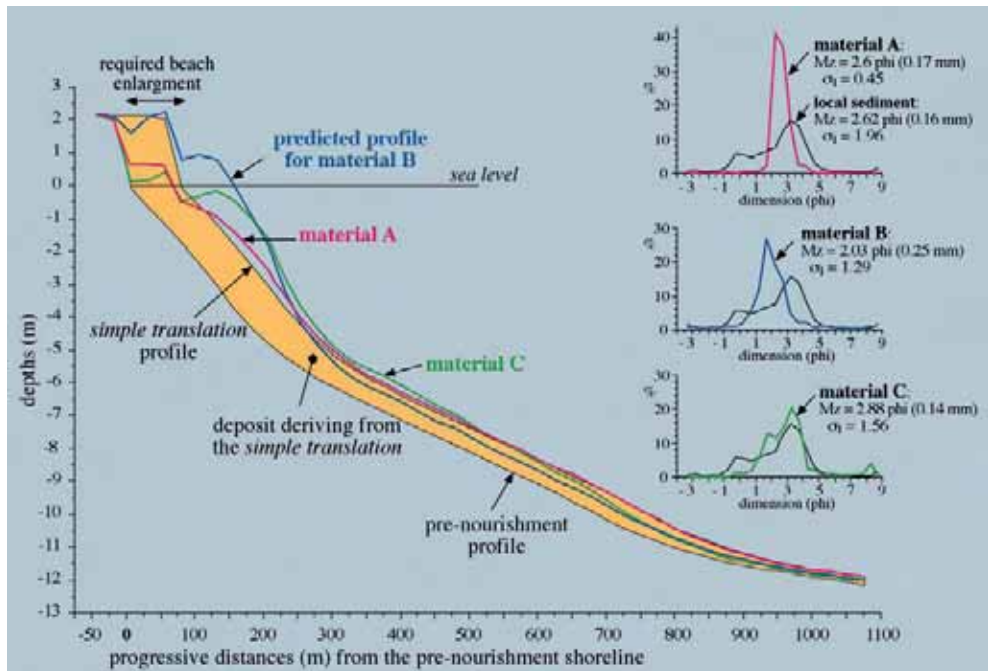
Figure 4 - Application (2D) of the model along a transept near Ladispoli beach. The first procedure used a simple translation of 75m, and the second one was repeated for three different types of borrow material derived from different marine sand reserves (Tortora, 1994; Chiocci and La Monica, 2003): one offshore Anzio (material A) and two near the Argentario promontory (B and C). The grain size distribution of the marine sands is shown on the right, over that of the local sediment. The section shows the deposit derived from the simple translation (first proc.) in orange, as well as the modifications of its upper boundary profile for each of the three materials (second proc.). Material B, the most coarse, gives the best results producing a shoreline advance which exceeds the desired distance (75 m). Of the other two types of material, type C causes the shoreline to advance considerably because, despite being the finer in average size, it is richer in coarse fractions (GNM considers the entire grainsize frequency distribution). In the example, the 3rd procedure is not applied (deposits A, B, C are equal in volume). Had it been applied, deposit B would be reduced by the appropriate volume to generate the required shoreline position, with consequent decrease in sediment amounts and costs for the intervention (the opposite for the other two cases).

The third procedure is applied in cases in which the available material is of a very different size compared to the local sediment, causing deposition to be concentrated on the upper (B>L) or lower (B<L) portion of the morphodynamic profile in the second procedure. This is manifest as deviations from the shoreline advance (Figure 4) as specified for the simple translation (B=L). This procedure therefore correctly repositions the shoreline through calibrated addition of subtraction of sediment to or from the deposit in the second procedure.

The volumetric corrections use two alternative methods. The first involves further applications of the first and second procedures: imposing different simple translations (first procedure) and observing the average shoreline advance obtained from each application (second procedure). The simple translation value which satisfies the required shoreline advance is extrapolated from a regression line which best fits these pairs of data (translation and shoreline advance). This value is used to repeat the first and second procedure in a definitive manner. The other method deals with the volume of the deposit by varying its thickness (in the second procedure) via the parameter Δ, where values of Δ>1 increase the volume and 0< Δ<1 decrease it. The parameter Δ which yields the correct shoreline position is similarly deduced using calibration techniques (given in Tortora, in press).

Each of the three procedures of calculation generates an output file which describes the artificial deposit. The three files have the same numerical structure (also identical to the output of module-B), so that the characteristics of the deposit at the various stages of the prediction process can be readily compared; for example, by subtracting the matrices of the first procedure form the second the effects of the available material on the prediction can be isolated. The output file of the final procedure contains the definitive prediction.

Each final consists mainly of data matrices (grids of 46x40 nodes) which describe:

a) the topography of the two surfaces (pre- and post-intervention) bordering the deposit; the two respective shorelines are defined by a zero value;

b) the geometry and volume of the deposit from thickness data (volumetric if multiplied by the cell area);

c) the spatial distribution of each grain size fraction (%), or of aggregated fractions, referred to both the upper and lower surfaces and the internal sediment of the deposit;

d) the spatial distribution of sedimentological parameters including mean size, sorting and sand/mud percentages, again referred to the upper and lower surfaces and internal sediment of the deposit, whilst all other granulometric parameters may be extracted from point (c).

Each file also contains three average grainsize frequency distributions referred to the entire mass of the deposit, to that eventually removed from the pre-intervention surface (generally through translation of trough zones), and to the net difference between the two. In the output file of the first procedure, this latter mass and its average grainsize frequency distribution correspond to the volume required for the nourishment (if the third procedure is not applied) and the local sediment composite, assuming the mass removed from the pre-intervention surface is incorporated in the artificial deposit.

Model application

Theoretical case: model outputs versus borrow sand grainsize characteristics

The model was applied to the coast of Marina di Tarquinia (northern Lazio), whose topo-bathymetric and granulometric characteristics were reconstructed using data in Tortora (1992). Further samples and sedimentological irregularities were then arbitrarily introduced to be verified by the model results in more complex cases. The bathymetry was varied and kept mostly free of irregularities. The characteristics of this (virtual) coastal area (Figure 5A) derive from 2071 elevation points and 108 surface sediment samples.

The subaerial beach is elevated 1-2 m above the sea level and the submarine beach is characterised by a concave profile in the lower depths (to -4 m) which becomes almost linear until the closure depth, placed arbitrarily at -9 m. The mean size values (Folk and Ward, 1957) indicate a progressive decrease in sediment size with distance from the shoreline (medium sands) to the extreme margins of the area (coarse silt). Certain anomalies (created ad-hoc) due to fairly coarse sediment (Mz<2 phi) are found on the western tract of the dry beach and on the far east at approximately -7 m.

For this area, a nourishment intended to widen the beach by 50 m was hypothesised, assuming the availability of 5 different types of borrow material from which to choose the best suited. For each material, a nourishment intervention was simulated (module-A) with predictions regarding: beach and shoreface topography; shoreline position; geometry of the artificial deposit; volume of this deposit (i.e. the amount required for intervention); spatial sediment distribution (mean size parameter). The five hypothetical types of material have grain size frequency distributions which are equal in shape but shifted by 1 phi towards finer classes progressively from material A to E (see Figure 6).

The first calculation procedure (simple translation), common to all five cases, produced the required shoreline advance (50 m) by a two nodes shift of the pre-nourishment grid data (method in Figure 3), thus simulating an intervention which, ideally, uses material identical to the local sediment (B=L). The resulting spatial distribution of the sediment is reported in Figure 5B, while Figure 5C shows the prismatic geometry of the artificial deposit, which encloses 1260000 m³, the quantity required for nourishment (assuming B=L).
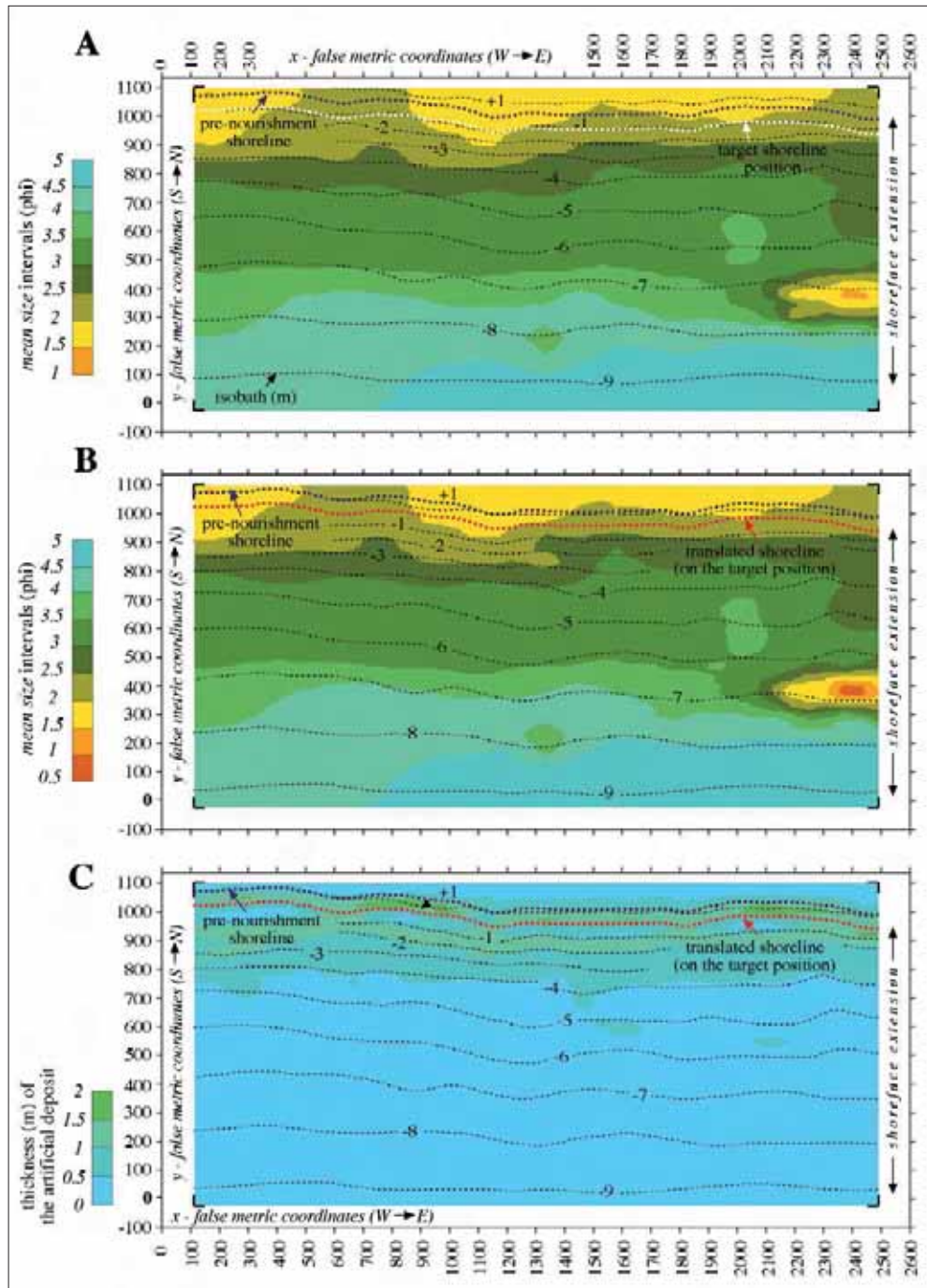
Figure 5 - Theoretical application of the model mostly based on data from Marina di Tarquinia beach. In A, bathymetry and grainsize characteristics (mean size parameter) of the beach prior the hypothetical nourishment intervention. In the others maps, the transitional outputs of the first step (simple translation) of the prediction process: B, mean size spatial distribution; C, morpho-geometry of the artificial deposit. Final predictions in the subsequent two figures.

The second procedure, which modifies the previous deposit (without altering its volume), was repeated for each of the five material types, generating as many morpho-geometric (Figure 6) and sedimentological (Figure 7) scenarios. The former show how the model outputs depend strongly on the grainsize characteristics of the borrow material. Proceeding from coarse to fine material (from A to E in Figure 6), the virtual mass deposited on the beach and upper shoreface decreases, and increases on the lower shoreface. This influences the shoreline advance which exceeds (materials A and B) or corresponds to (C) the desired amount (50 m), or falls short in the cases of the finer materials (D and E). The profile in Figure 6F summarises these issues, demonstrating further than the five morphological predictions agree with the three possible types of profile evolution described by Dean (1991): intersecting (materials A and B), nonintersecting (material C) and submerged (materials C and D) profiles. The eventual use of the coarser materials (type A and B) would reduced the volume originally calculated for the nourishment (1260000 m³). The inverse would occur for the finer materials (D and E), but only in theory - they are rejected as they are assumed incapable of widening the beach.
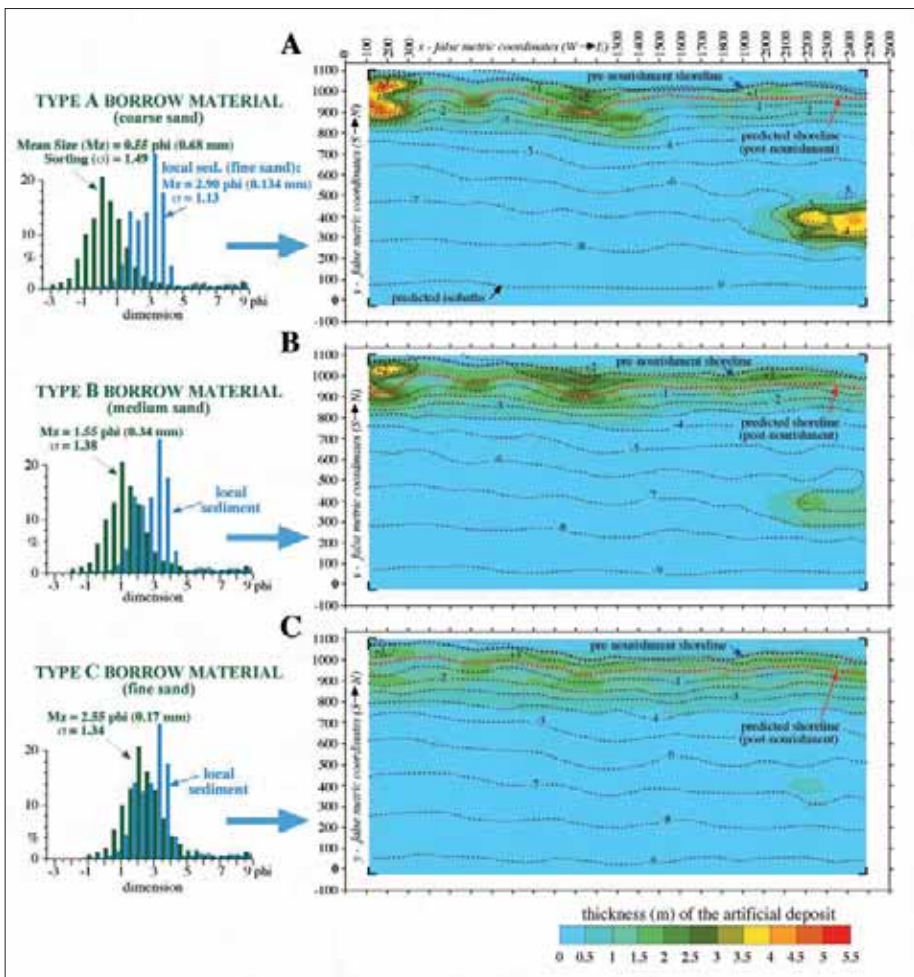
Figure 6 (continues on the following page) – In A-E, morpho-geometric predictions of five nourishments (1260000 m³ each) which use borrow materials with different grain size characteristics. The predictions concern the geometry of the artificial deposit (its thickness variability), the bathymetry and the shoreline position. As the size of the material decreases (progressing from A to E), the quantity of material deposited on the beach and upper shoreface decreases and this reduces the shoreline advance. Profile F summarises the differences between the 5 cases.

Sedimentological predictions (Figure 7) are also notably distinguished according to the type of material used. The coarsest and finest materials (type A, B and E) generate strong changes in the local sediment, respectively increasing and decreasing the mean size (mm) almost everywhere. These changes are generally of relevance due to their impact on the benthic community, marine activities and on the natural sediment balance. Of these, the latter would most benefit from the coarsest types of material (A and B) which are respectively 10 and 4 times more stable than the local sediment (according to the renourishment factor of James, 1975).

The choice of the material most suited to the intervention is based on a careful comparison amongst the model scenarios and their associated advantages and disadvantages (Figure 8). From the types of material considered, type C appears the best, providing the desired widening of the beach without altering the original quality of the coastal sediment too much.
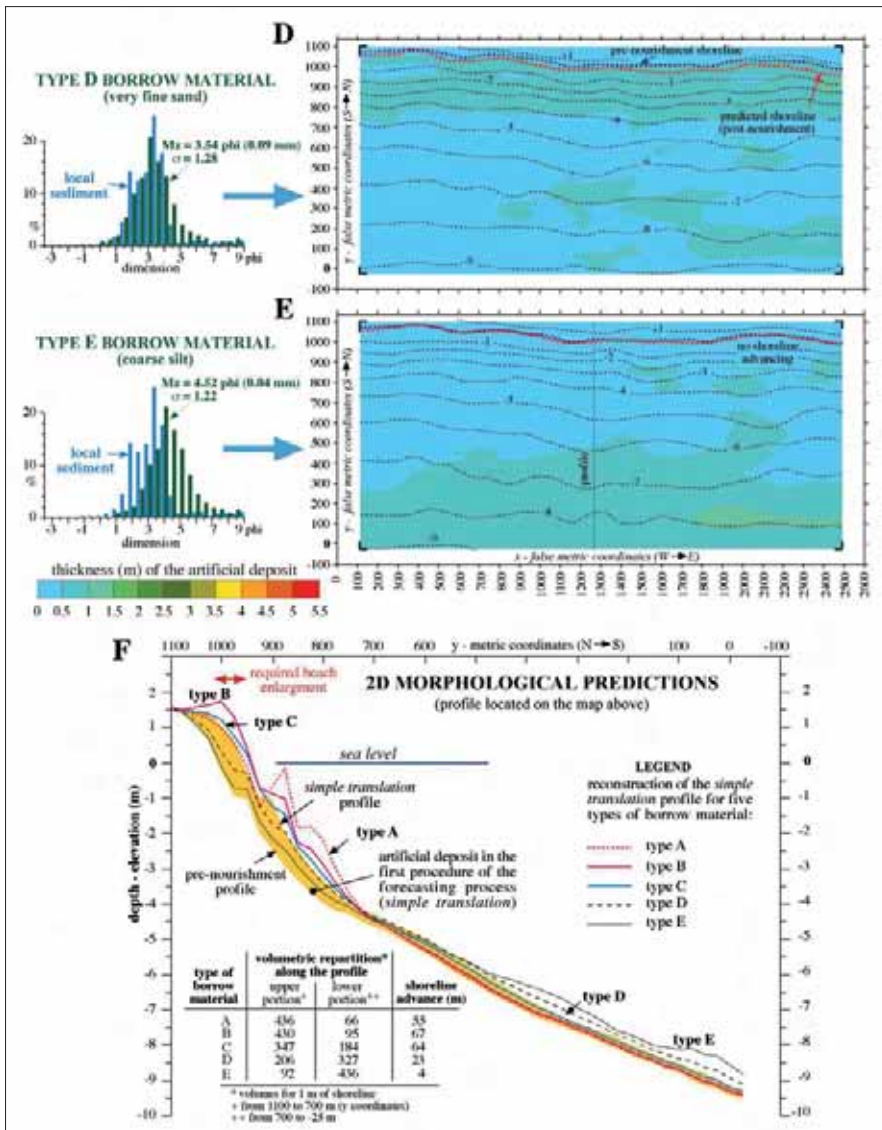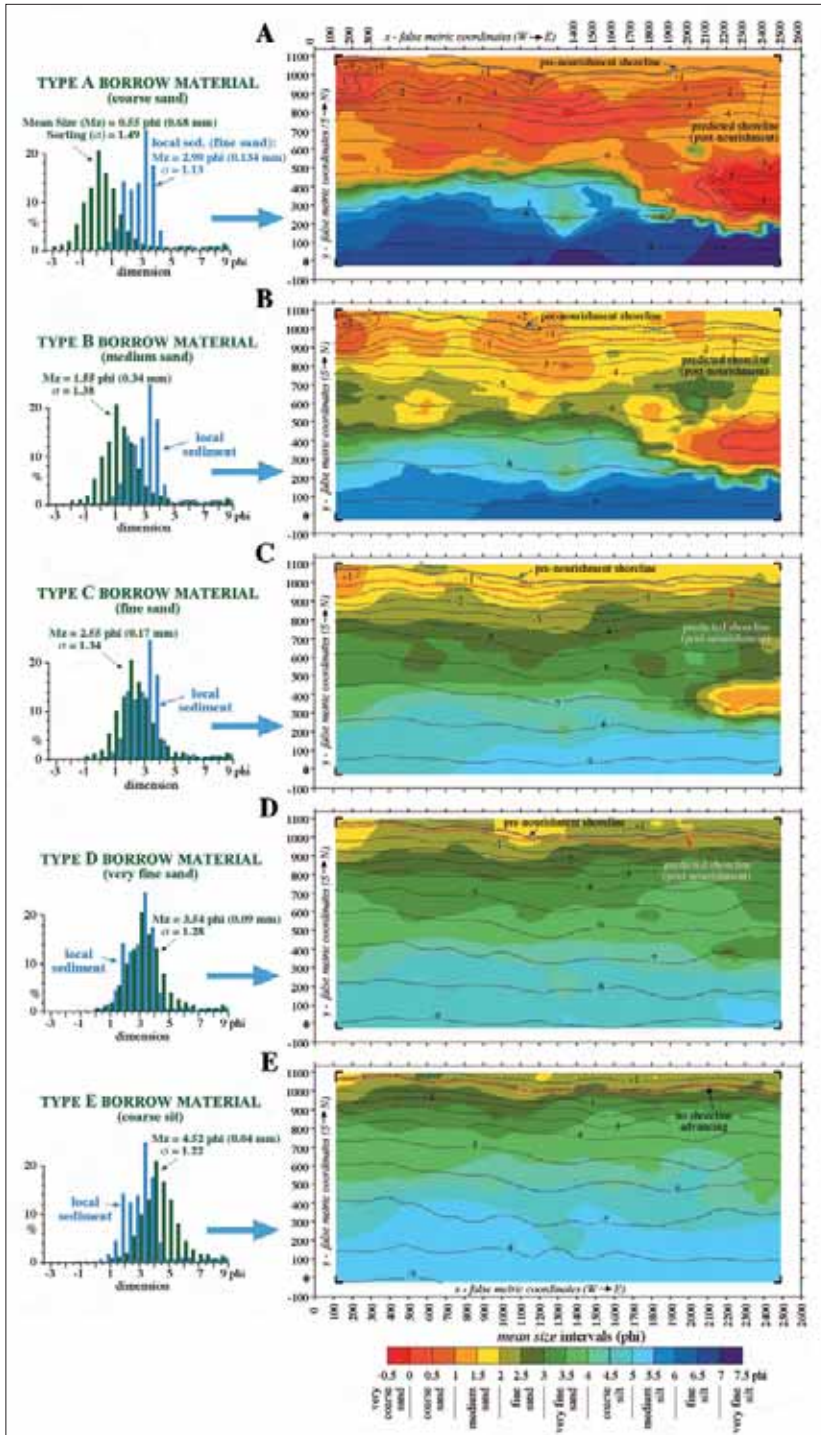
Figure 7 – Predictions of the spatial distribution of sediment for each of the five cases in the preceding figure.

Ladispoli Beach
Studies at Ladispoli beach (approximately 30 km north-west of Rome) aimed to: 1) identify the effects of the nourishment carried out there in 2003; 2) compare the model predictions with the real outcome for the nourishment; 3) understand the reasons for the partial failure of this intervention using the model as an investigatory tool; 4) propose a solution to restore the beach at Ladispoli.

Coastal changes due to the 2003 intervention
In order to ascertain the coastal changes following the nourishment, module-B procedures have been applied on topo-bathymetric (source: Regione Lazio) and grain size monitoring data collected at different times: before the intervention (topo-bathymetry 02-2002; samples 2001); at its conclusion (topo-bathymetry 04-2003) and successively (topo-bathymetry 04-2004; samples 2005). For these surveys, single-beam (only the 04-2003 survey), multi-beam e RTK instruments were used. A total of 160 seafloor samples was collected internally and externally to the nourishment area. The data above were processed via automated gridding and contouring techniques obtaining two sets of maps, respectively referred to the individual survey periods and to the variations between pairings of data from different periods (by subtracting grid matrices).
The nourishment action filled the emerged beach and was followed by levelling work which artificially widened it by about 40-70 m and lifted it by 1-2 m (figs. 9A and 10A). The added sand had an average diameter of 0.164 mm (grain size frequency distribution in Figure 12) and came from Lazio's continental shelf. At completion of the intervention, the artificial deposit included 367000 m^3 of sand, 229550 located on the emerged beach and 137450 m^3 on the seafloor very close to the shoreline.
One year after the nourishment (figs. 9B and 10B), the artificial deposit was reduced to 287000 m^3 of which 39000 m^3 were located on the beach (previously 229550 m^3), 208000 m^3 within the first 4 m depth, 40000 m^3 deeper than -4 m, while 80000 m3 of materials were transported to adjacent coastal zones (lateral spreading effect).
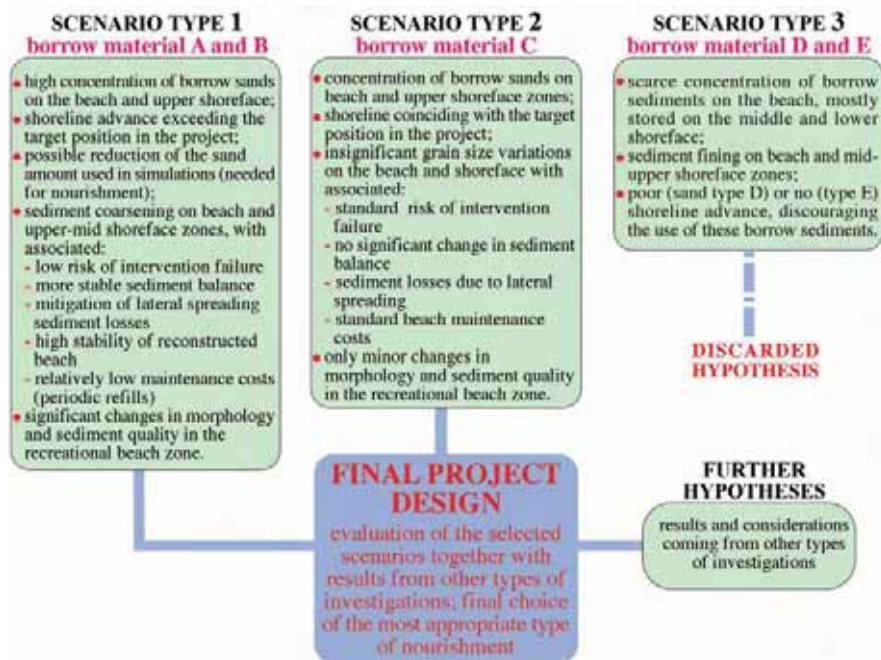
Figure 8 – Comparison of the scenarios predicted by the model aimed at choosing the best material for the intervention.

In one year the artificial deposit was drastically reshaped by waves through the erosion of the emerged beach, having retreated by 30-50 m (figs. 9C and 10C). A large part of the eroded material was re-deposited on the middle shoreface. The zones of erosion and re-deposition are aligned parallel to the shoreline forming a trough-bar system (even present today).
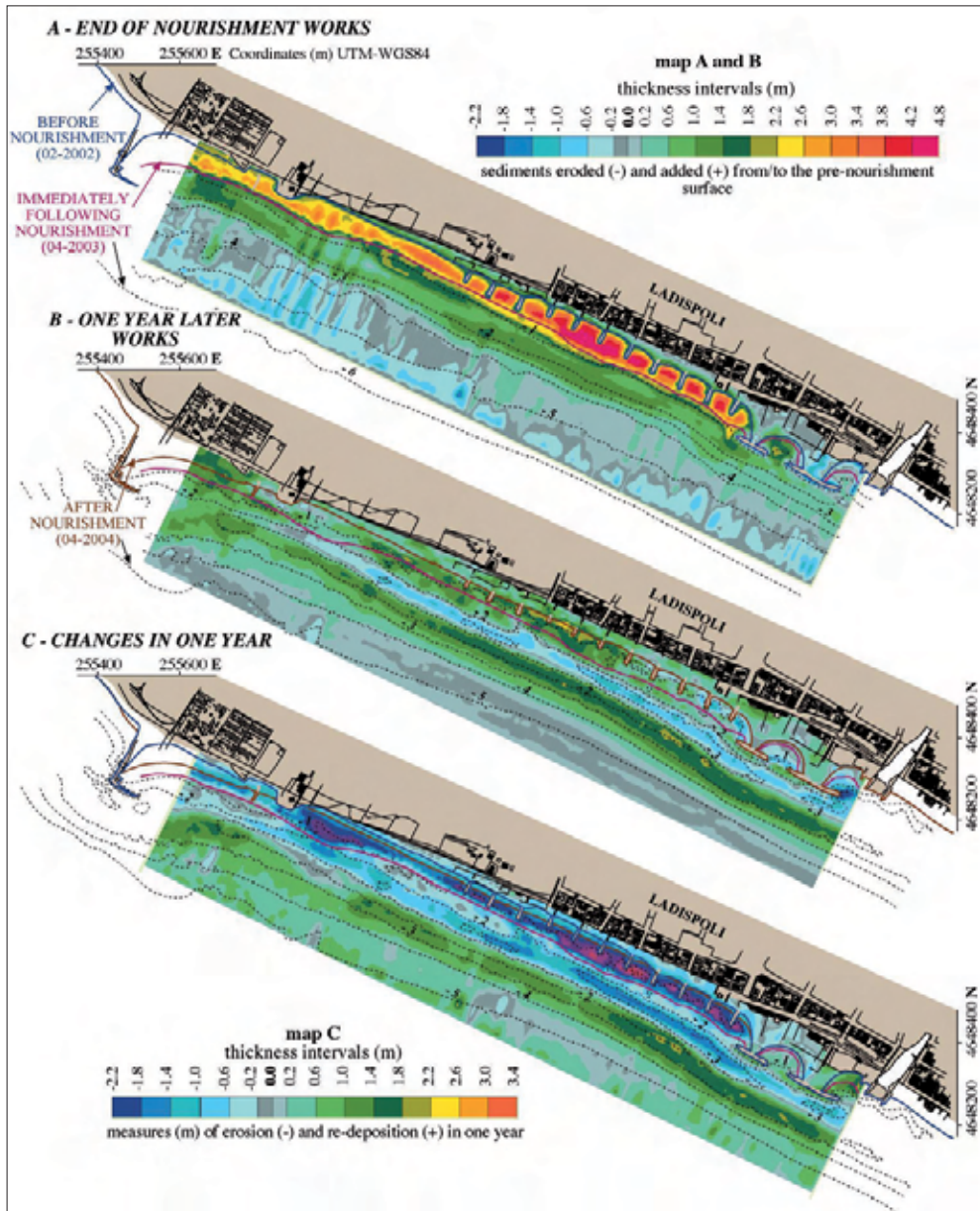
Figure 9 - The nourishment at Ladispoli beach. The first two maps show the geometry of the artificial deposit (its thicknesses), the topo-bathymetry and the shoreline position, at the end of the nourishment works (map A) and one year later (B). In C, the topo-bathymetric changes between these two periods. The maps are obtained by subtracting topo-bathymetric grids of different periods: survey 04-2003 and 02-2002 (map A); 04-2004 and 02-2002 (map B); 04-2004 and 04-2003 (map C). The morphological evolution is synthesized in the next figure.

The maps A, B, C in Figure 11 show respectively the spatial sediment distribution before and after the nourishment as well the granulometric variations between these two periods. These variations indicate a remarkable decrease in sediment size on the beach and upper shoreface zones. Therefore, two years after the intervention, the borrow materials were still present in these zones indicating that the mechanism determining the shoreline retreat (erosion and sediment re-distribution: Figure 10C) was still in action.

Simulation of the 2003 nourishment

The nourishment at Ladispoli was simulated in order to evaluate the quality of the model output through comparison of predicted outcomes with what actually resulted from the intervention. The simulation was carried out according to the three calculation procedures of module-A, calibrating the shoreline advance (simple translation: 33 m) in order to obtain an artificial deposit which is equal in volume to the remaining artificial deposit one year after the nourishment (287000 m^3). Inputs for the forecasting process are the pre-nourishment topo-bathymetric and grain size data (survey 02-2002; samples 2001) of the beach-shoreface zone, as well the grain size frequency distribution of the borrow material used for the 2003 intervention. The depth of closure is placed at -5 m that the influence of the 2003 nourishment was confined to the seafloor shallower than this depth. The GNM simulation predicted the following aspects: beach and shoreface topography; shoreline position; geometry of the artificial deposit; spatial sediment distribution (mean size parameter). The resulting scenario is shown in maps A and B of Figure 12. Comparing these maps respectively to the evidence in figs. 9B and 11B, it appears that real and predicted features have many aspects in common.

Use of the model as an investigatory tool

Three different types of nourishment have been simulated (module-A) in order to identify the cause of the rapid shoreline retreat that occurred after the 2003 intervention. Specifically the question is why the sands placed on the beach moved rapidly onto the middle shoreface (Figure 10C). The clarification of this point is considered by both local municipality and Regione Lazio as a prerequisite before proceeding to a second nourishment. The three GNM simulations (Figure 13) are based on the same sediment amount remaining in the area one year after the past intervention (287000 m^3) and on a borrow sediment respectively equal, coarser and finer than the sand adopted for the nourishment in
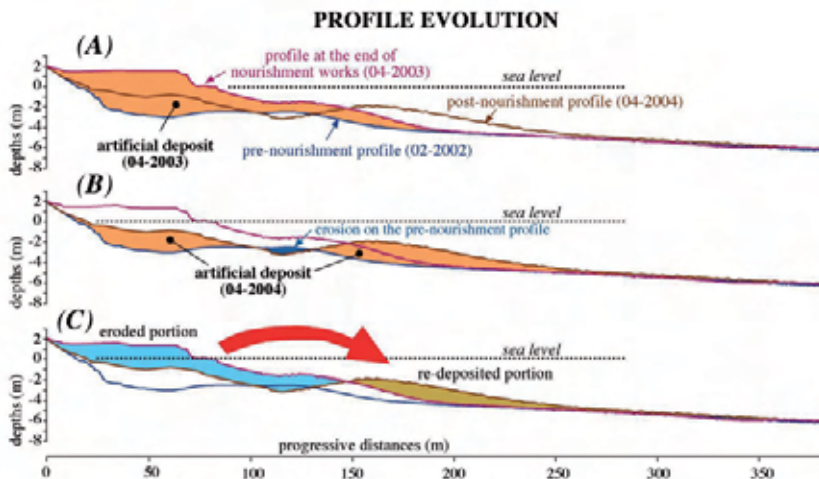
Figure 10 - Transect right to the central sector of Ladispoli beach with profiles surveyed in different periods. Reconstructions (A) and (B) highlight the shape of the artificial deposit, respectively at the end of nourishment works and one years later. This deposit was re-shaped by waves (C) through erosion (beach and upper shoreface) and sediment re-deposition (middle shoreface). Features in (A), (B), and (C) are reproduced in 3D in Figure 9.

Ladispoli. Comparison of the three simulations shows that the size of the borrow sands controls their final destination along and across the shoreface as well as the resulting shoreline advance. This suggests that the cause of the inconveniences of the 2003 intervention was in the sands used, which were too fine for the equilibrium on the beach and near seafloor (Figure 13A). Much better results would have been obtained using coarser sands (Figure 13B) and worse with finer sands (Figure 13C). These GNM experiments suggest attention must be given to the size of material devoted to an eventual second nourishment.
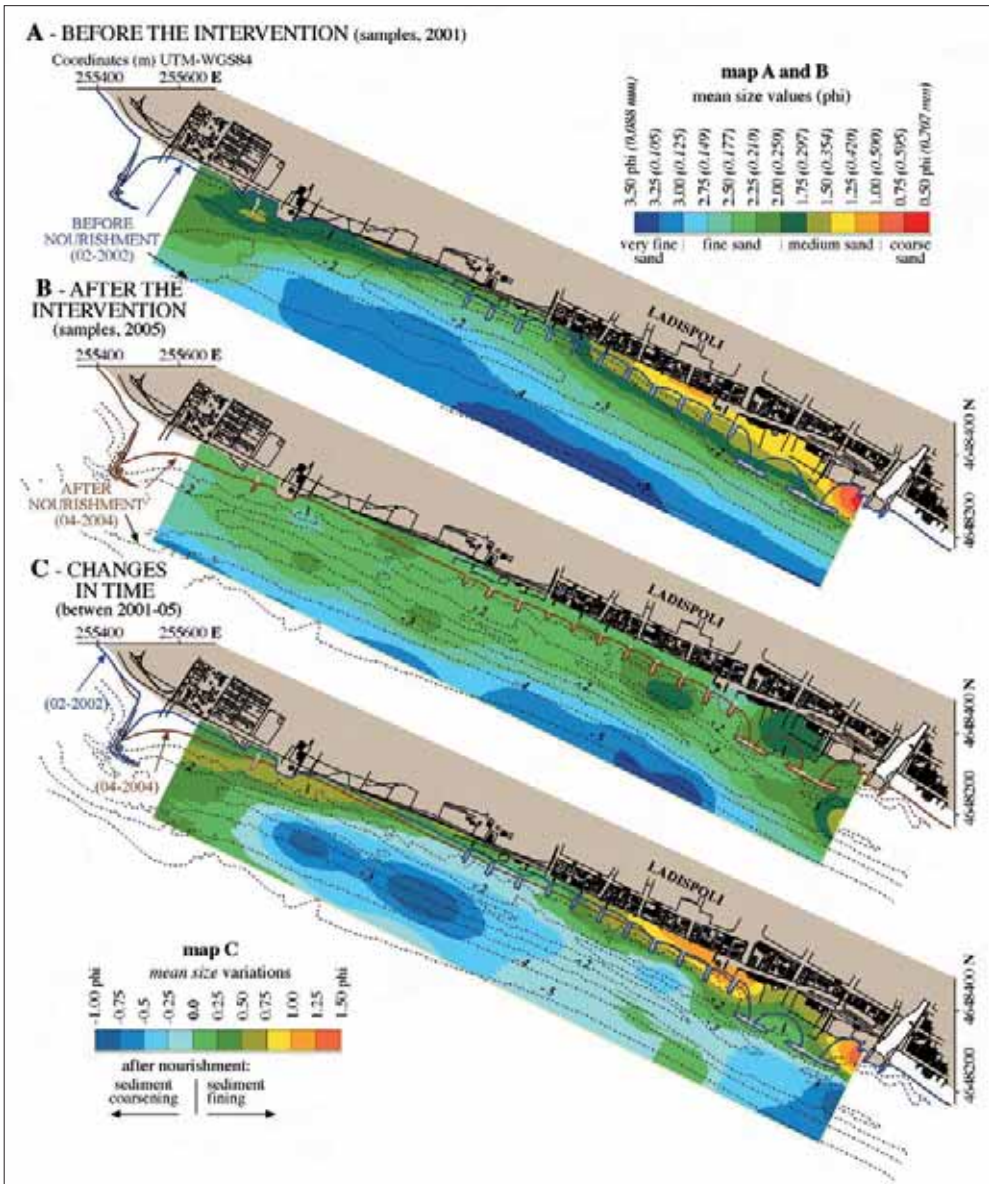
Figure 11 - Distribution along the coast of the sediment mean size before (A) and two year after (B) the nourishment of Ladispoli beach. In C, the mean size variations between these periods are reported.

Recovery of Ladispoli beach

Two hypotheses of re-nourishment have been evaluated in order to correct the problems following the 2003 intervention. In this case the procedure for beach maintenance (module-C) has been applied, which includes calibrations with some of the data of the post-intervention surveys. These hypotheses both looked at volumes of 152700 m³, using two borrow materials with different characteristics, one quarried from the Tuscany shelf while the other is the same sand as used for the 2003 intervention. Their average sizes are 0.25 mm and 0.17 mm respectively, compared with 0.19 mm of the local sediment. The model outputs - regarding the geometry of the artificial deposit, topobathymetry and shoreline position (Figure 14) - show that material measuring 0.25 mm gives much better results, providing a higher concentration of sand on and near the beach with a shoreline advance between 10 and 20 m (Figure 14A). The Rj renourishment factor (James, 1975) indicates that this material is eight times more stable than the other.

Limits of the model

The critical issues relating to GNM predictions (modules A and B), which emerged during the development and experimentation phases, are listed below.
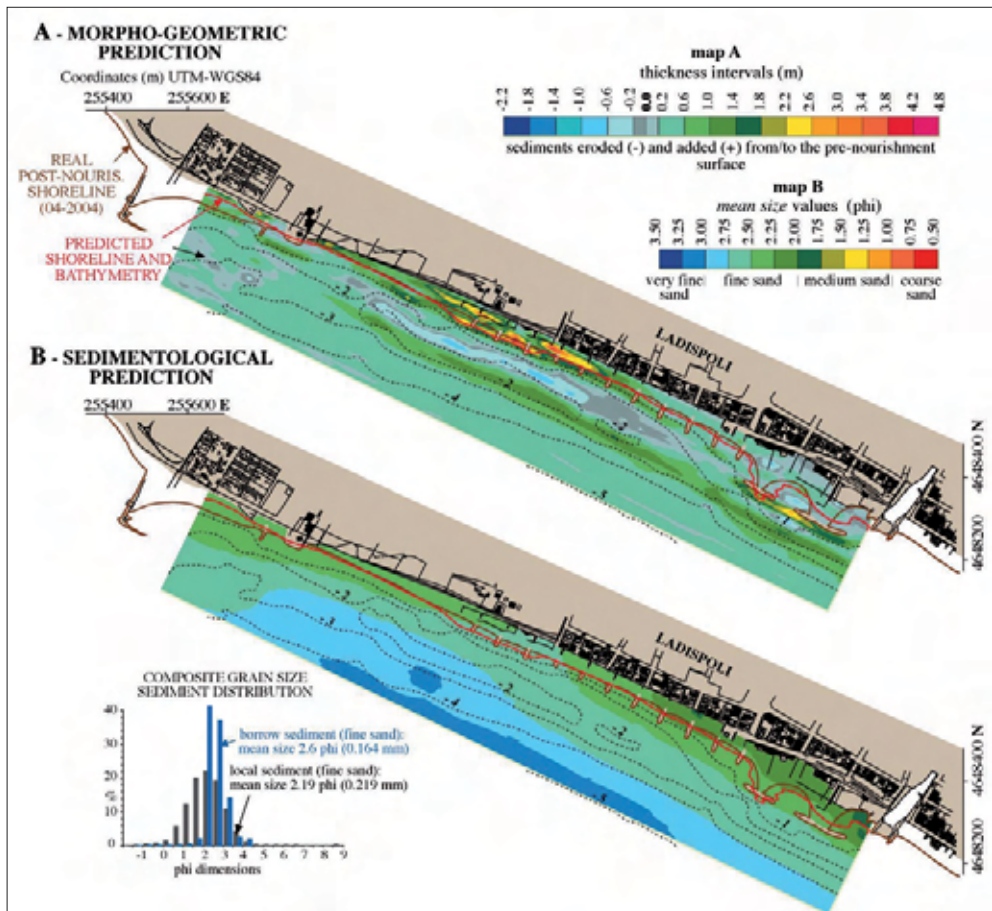
Figure 12 - Simulation by the model of the nourishment occurred in Ladispoli beach. The maps show morpho-geometric (A) and sedimentological predictions (B). Comparing these maps respectively to the evidence in Figure 9B and 11B, it appears that real and predicted features have many aspects in common.

1) The two modules are only applicable if all the grainsize fractions that make up the borrow material are present in the beach sediment for the site in question. In such a case the procedure, lacking in spatial reference, would not know where to deposit the borrow sand mass relative to the critical fractions (those not present on the beach). This limitation can be artificially overcome: for example if the critical fraction has a very low percentage, it can be cumulated into the dimensionally closest fraction, always
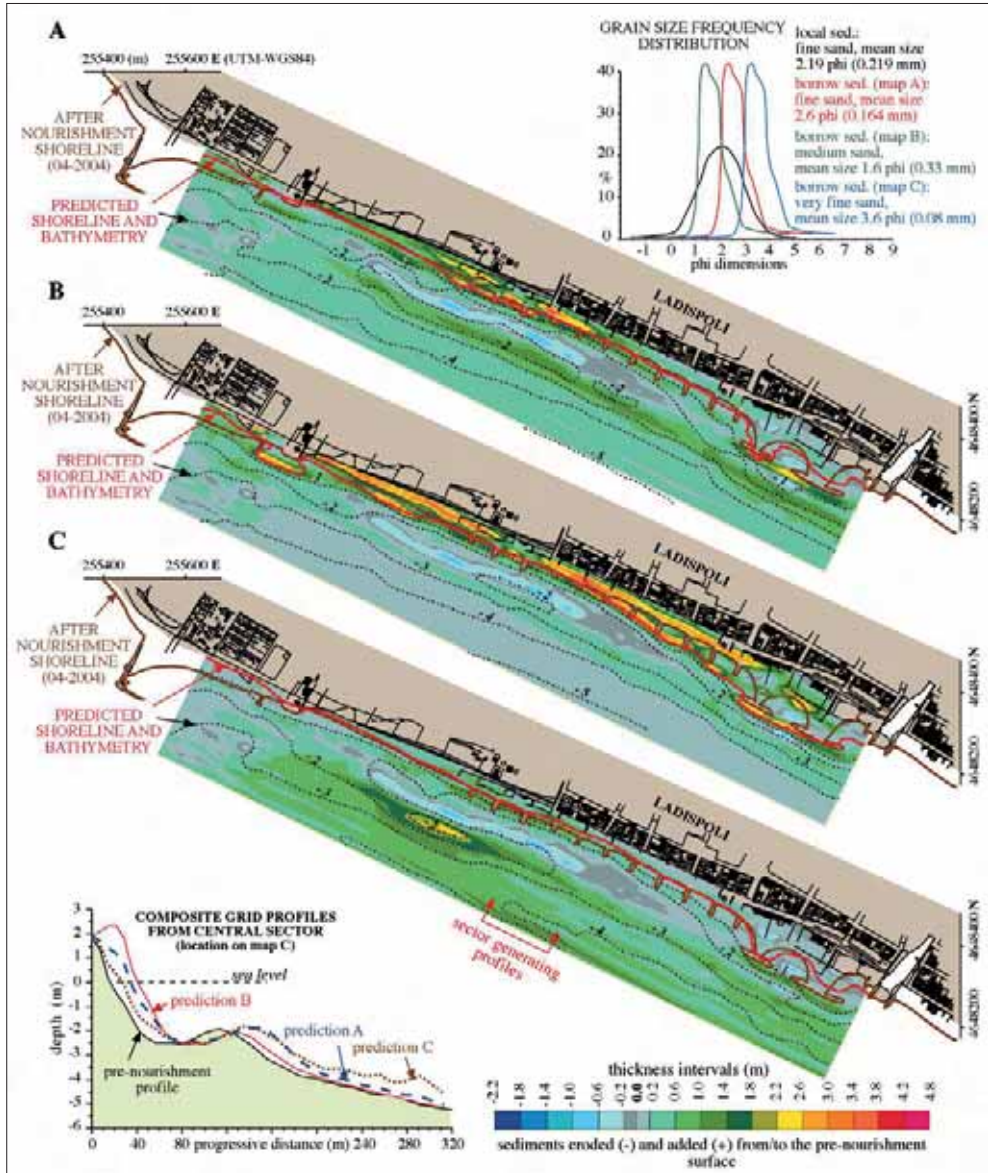
Figure 13 - Use of the model in order to explain the very fast shoreline retreat after nourishment. Model outputs A, B and C forecast the geometry of the artificial deposit as it is shaped by a borrow sediment equal (A), coarser (B) and finer (C) than the sand really used for the intervention. These simulations suggest that beach erosion was due to the grain size of the nourished sands, which was too much fine (A). In terms of shoreline advancing and stability a better result would have been obtained with sand of prediction B, a worse result with sand of prediction C.

assuming it is also present. Inapplicability of the predictive modules should be rare, since even the borrow fractions which differ most considerably from the local sedimentological context generally have counterpart, at worst with negligible percentages and distributed over very restricted areas.

2) Apart from the granulometry, the model ignores other sedimentological issues, particularly the specific weight of particles, which in some cases can be important. Furthermore, the quantity required for the intervention is calculates as the volume of the deposit with zero porosity.

3) GNM predictions do not make use of hydraulic parameters; these are rather assumed to be implicitly contained in the granulometric and topo-bathymetric characteristics of the original coast. Such characteristics generally give a much better indication of cross-shore hydraulic processes than of those parallel to the coast. As such, predictions which underestimate the effects of lateral transport of the borrow material may arise.

4) The simple translation technique (first procedure) lends itself to a (re)nourishment (B=L) of a stable or prograding beach rather than a beach undergoing strong erosion. In the latter case it is unlikely
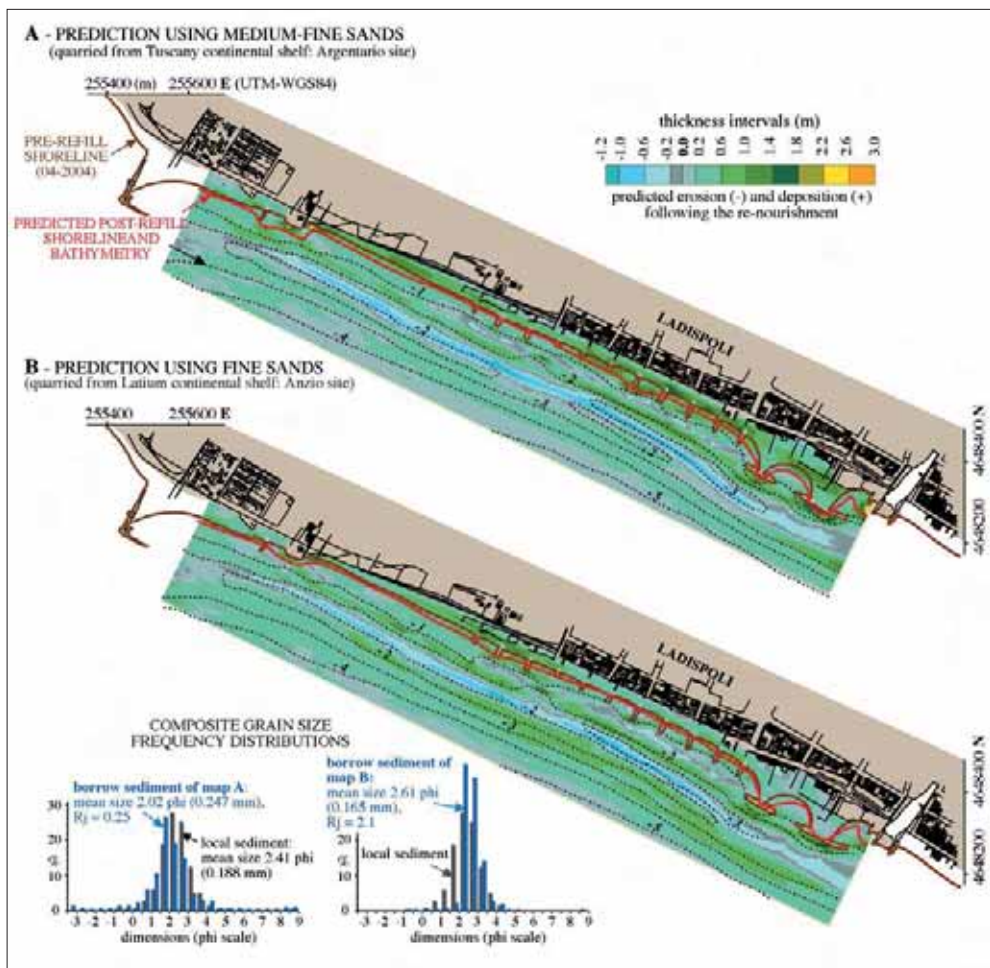
Figure 14 - Use of the model for decision making to choose the borrow sediment for the Ladispoli beach re-nourishment. Maps A and B predict the geometry of the artificial deposit and the shoreline position if the same amount of different borrow sands is used. Comparing these maps, the hypothesis A appears better than B. Forecasting results have been obtained calibrating the model with data collected after the first nourishment.

that the post-intervention surface would replicate the original erosive surface. The technique is therefore affected by approximations which are also transferred in the successive calculations, right up to the final prediction. Even other techniques of profile evolution are affected by the same errors which have been discussed (CUR, 1987; USACE, 2002. These approximations are less relevant to predictions of beach maintenance by sand refills (module-C), as these concern a coastal environment which has reached a quasi-stable condition.

5) The model controls deposition of the borrow sands in each grid cell ignoring the existing accommodation space. The result is that aggradation can exceed the accommodation threshold beyond which progradation could occur in nature. Thus, in the limiting case of a material consisting of fractions which are present only on a single cell of the coastal environment (pre-intervention), all the material would be placed on that cell, giving a thickness of thousands of metres. Effects of moderate over-aggradation have been noted in some tests dedicated to this issue, but these have not been observed in the experiments at Ladispoli. When present, this over-aggradation occurs in restricted areas on the original coast corresponding to zones with granulometric anomalies, where high percentages of certain fractions constrain deposition of relevant quantities of borrow material. Such anomalies, and their undesired effects, can be contained by subjecting the granulometric grids (pre-intervention) to a smoothing process.

6) The predictions depend on the closure depth parameter, since this controls the potential depositional area by marking its external limit. For calculation of this parameter requires consideration must be given to the methods employed and to the timescale of operation (Hallermeier, 1981; Kraus et al, 1999; Hanson et al, 2003). Overestimations (and vice versa for underestimation) lead to predictions in which the artificial deposit is distributed further offshore and the quantity required for the nourishment intervention is overestimated (Jenkins and Keehn, 2001).

Conclusions

The *Grain-size Nourishment Model* is characterised by the following features: (1) it is a 3D sedimentological model which does not borrow from existing techniques and which has been developed specifically for nourishment interventions, unlike numerous models created for other purposes; (2) the model aggregates methods (modules) which adopt common criteria and data exchanges, and as such supports the most important phases of nourishment intervention (nourishment design, post-nourishment monitoring, beach maintenance); data from nourishment interventions are readily recycled in future interventions; (3) the input data required may seem costly to acquire, however any nourishment project would, as a matter of course, foresee the acquisition of topo-bathymetric and sedimentological data; (4) the numerous predicted aspects are derived not from as many individual prediction processes but from a single deterministic process concerning the artificial deposit in its entirety; (5) the calculations from this process assume that the borrow material is mostly deposited in the zones where the sediment is most similar to the borrow material itself; (6) of the three variables that guide the simulations, two are objectively defined (simple translation and type of borrow material) and one (depth of closure) is affected by estimation uncertainty which can affect the validity of predictions; (7) the first two variables allow the model to be "manoeuvred" to elaborate a number of scenarios and evaluate several nourishment hypotheses; (8) GNM also generates 2D predictions and presents an alternative to methods based on equilibrium profiles (Dean, 1991; Larson et al, 1999) and, unlike these, provides morphological details for the profile (bars, troughs etc) which often have volumetric significance; (9) numerous tests and application to the case of Ladispoli beach have not highlighted any inconsistencies in predictions, even though the model is not free from approximations and operational limits, which are normal for methods of prediction.

References

Capobianco M., Hanson H., Larson M., Steetzel H., Stive M.J.F., Chatelus Y., Aarninkof S. and Karambas T. (2002) - *Nourishment design and evaluation: applicability of model concepts*. Coastal Engineering, 47: 113- 135.

Chiocci F.L. and La Monica G.B. (2003) - *Individuazione e caratterizzazione dei depositi sabbiosi presenti sulla piattaforma continentale della regione Lazio e valutazione di un loro utilizzo ai fini del ripascimento artificiale dei litorali in erosione.* Rapporto finale della seconda fase, Vol. 1, 2, 3 e 4, Università degli Studi di Roma "La Sapienza" Dipartimento di Scienze della Terra, Regione Lazio Assessorato Ambiente e Protezione Civile.

CUR (1987) - *Manual on Artificial Beach Nourishment*. Centre for Civil Research Codes and Specifications, Recommendation, report 130, Rijkswaterstaat/Delft Hydraulics (The Netherlands), pp. 1995.

Dean R.G. (1991) - *Equilibrium Beach Profiles: Characteristics and Applications*. Journal of Coastal Research, 7**:** 53-84.

Dean R.G. (2002) - *Beach Nourishment: Theory and Practice*. World Scientific Publishing Co. New Jersey, pp. 399.

Dean R.G. and Yoo C.H. (1992) - *Beach-Nourishment Performance Predictions*. Journal of Waterway, Port, Coastal and Ocean Engineering, 118: 567-585.

Dean R.J. (1974) - *Compatibility of borrow materials for beachfill*. Proceedings 14th International Coastal Engeneering Conference, ASCE, 1319-1333.

Folk R.L. and Ward W.C. (1957) - *Brazos river bar: a study in the significance of grain size parameters*. Jour. Sed. Petrol., 27: 3-36.

Hallermeier R.J. (1981) - *A profile zonation for seasonal sand beaches from wave climate*. Coastal Engineering, 4: 253-277.

Hanson H., Aarninkof S., Capobianco M., Jime´nez J.A., Larson M., Nicholls R.J., Plant N.G., Southgate H.N., Steetzel H.J., Stive M.J.F. and De Vriend H.J. (2003) - *Modelling of coastal evolution on yearly to decadal timescales*. Journal of Coastal Research, 19: 790-811.

Hobson R.D. (1977) - *Review of design elements for beach fill evaluetion*. U.S. Army Coastal Engineering Research Center, Techical Memorandum, TM-77-6: 1-51.

Houston J.R. (1994) - *Beach-fill volume required to produce specified dry beach width*. Coastal Engineering Technical Note 11-32, U.S. Army Engineer Waterways Experiment Station, Coastal Engineering Research Center, Vicksburg, MS.

James J.R. (1975) - *Techniques in Evaluating Suitability of Borrow Material for Beach Nourishment*. U.S. Army Coastal Engineering Research Center, Technical Memorandum, 60, Vicksburg, MS.

Jenkins M. and Keehn S. (2001) - *Effects of beach nourishment on equilibrium profile and closure depth*. Proceedings of Coastal Dynamics V01, Lund, Sweden, 888- 897.

Kraus N.C., Larson M. and Wise R.A. (1999) - *Depth of closure in beach-fill design*. Proceedings 12th Annual National Conference on Beach Preservation Technology, Florida Shore and Beach Preservation Association, Tallahassee, FL, 271-286.

Krumbein W.C. and James W.R. (1965) - *A lognormal size distribution model for estimating stability of beach fill material*. U.S. Army Coastal Engineering Research Center, Technical Memorandum, 16: 1-17.

Larson M., Capobianco M. and Wise R.A. (1999). *Modelling crossshore sediment transport at different scales using equilibrium beach profile theory*. Proc. 4th Int. Symp. On Coastal Engineering and Science of Coastal Sediment Processes (Coastal Sediments '99), Hauppauge, Long Island (NY, USA), ASCE, Reston, 1371–1387.

NRC (1995) - *Beach Nourishment and Protection*. National Research Council, Committee on Beach Nourishment and Protection, National Academic Press, Washington, DC, USA, pp. 334.

Pilkey O.H., Young R.S., Riggs S.R., Smith A.W., Wu H. and Pilkey W.D. (1993) - *The concept of shoreface profile equilibrium: A critical review*. Journal of Coastal Research, 9: 255-278.

Tortora P. (1991) - *Calcolo del volume di inerti nel ripascimento artificiale delle spiagge*. Rend. Soc. Geol. It., 14: 181-184.

Tortora P. (1992) - *Contributo dell'indagine sedimentologica al ripascimento dei litorali in erosione: ipotesi di ricostruzione della spiaggia di Marina di Tarquinia (Lazio settentrionale)*. Boll. Soc. Geol. It., 111: 315-333.

Tortora P. (1994) - *Sandy shelf deposits as source material for artificial nourishment of modern erosive beaches: an integrated approach using high resolution seismic and sedimentological analysis*. Giornale di Geologia, ser. 3a, 56: 275-277.

Tortora P. (in press) - *Un modello sedimentologico per gli interventi di pascimento artificiale delle spiagge*. Boll. Soc. Geol. It.

USACE (2002) - *Beach Fill Design*. In: Coastal Engineering Manual, US Army Corps of Engineers, EM 1110-2-1100 (Part V, chapter 4), pp 109.

Van De Graav J., Niemeyer H.D. and Van Overeem J. (1991) - *Artificial Beach Nourishments*. Coastal Engineering (special issue), 16**:** pp. 164.

Index